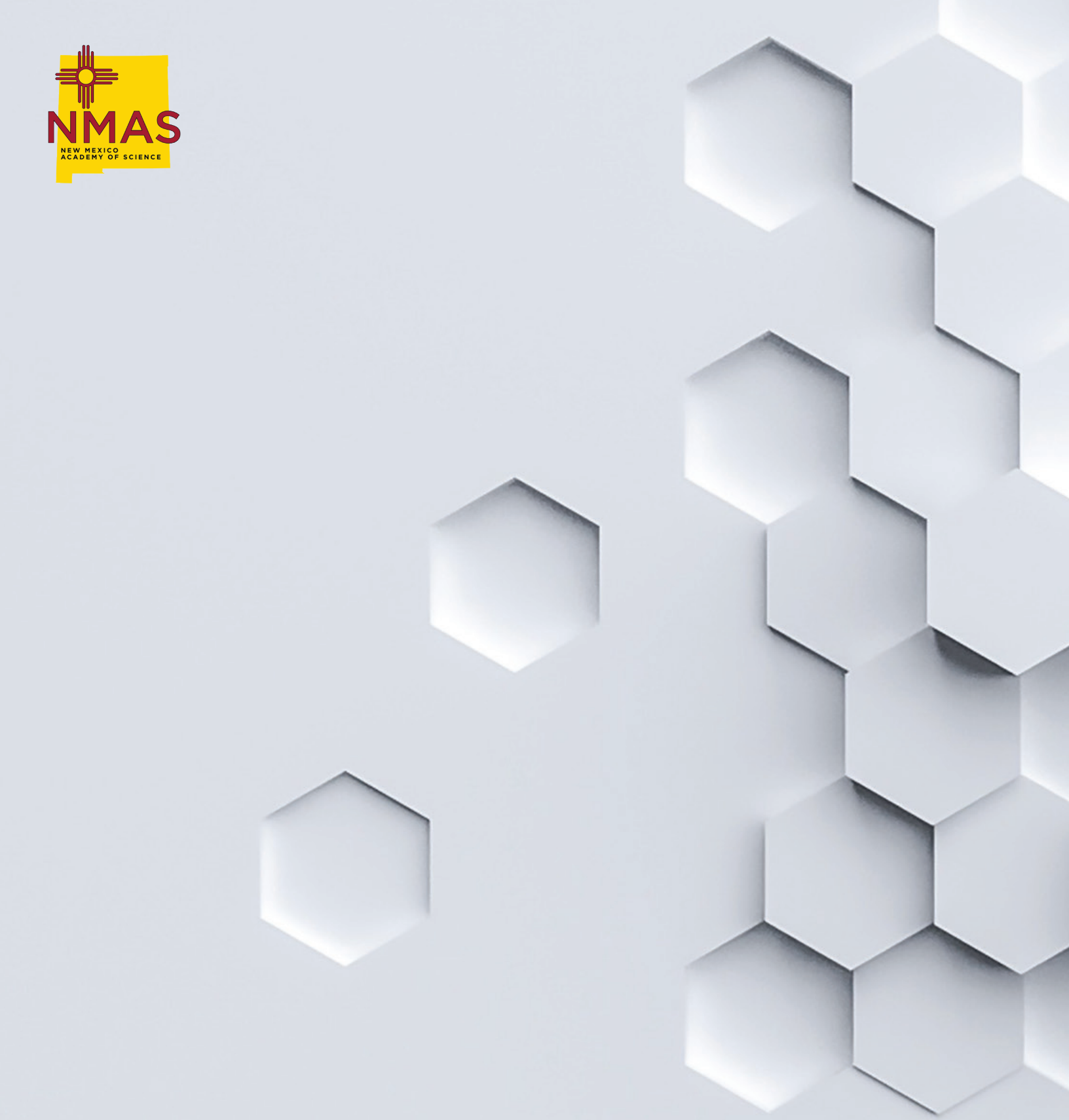

THE NEW MEXICO **JOURNAL OF SCIENCE**

Volume 54 No.2
December 2020

2020 NMJS Editorial Board

Table of Contents

Editor's Note

The *New Mexico Journal of Science* (*Journal*) is the annual publication of the New Mexico Academy of Science (NMAS). Each volume of the *Journal*, which began publication in 1960, contains research papers and review articles deemed of interest to the scientists, educators, and citizens of New Mexico. Some volumes have addressed topics of historical, social, or economic interest while others have emphasized scientific areas in which New Mexico is particularly active.

Volume 54 Number 2 is a special edition that features winners of the 2020 New Mexico Junior Academy of Science paper competition for high school students. Additionally, this special edition presents other papers by the competition participants and contributors to recent volumes of the *Journal*. Inclusion in the special edition provided high school authors with an experience in the peer review process. In addition to providing peer review, members of the new Editorial Board worked with the authors to improve their papers to a high standard following the publication model of the Canadian Science Fair Journal.[1]

The *New Mexico Journal of Science* is available for free download from the NMAS website at www.nmas.org. This enables the NMAS to reach a wide readership. Prior to 2008, the Academy mailed paper volumes of the *Journal* only to its members. Those hard copies are available to the public upon request.

Anton Sumali, Ph.D.
Editor-in-Chief
New Mexico Journal of Science

[1]Ng, R.; Slivitzky, K.; Webster, R.; McNally, D. Extending the science fair project beyond the walls of the gymnasium with the Canadian Science Fair Journal. *Communications Biology*, 2 *(367)*, 2019.

Climate Change on Crocodilians: Modeling the Effects of Variations in Rainfall on Crocodilians and their Ecosystem

*Karin Ebey**

Los Alamos High School, Los Alamos, NM

ABSTRACT

Climate change is projected to cause significant changes to global precipitation patterns. To explore how crocodilians and their ecosystems are impacted by variations in rainfall, a model was created using a novel adaptation of the Lotka-Volterra equations. The model uses a time step of months and includes a crocodilian population, three plant species, and eight other animal species. Each year, populations are impacted by predator-prey interactions and reproduction. Rainfall only impacts the ecosystem through the plant populations. This model was validated by running it with Louisiana rainfall data from 1970-2018 and comparing the outputs to measured alligator nest count data from that time. The model populations followed similar patterns to the nest count data, showing that the model accurately describes how rainfall affects the ecosystem. Changes in the amount of rainfall cause the populations to increase or decrease in proportion to the change in rainfall. Changes in the timing of rainfall affect the seasonal variation of plant populations, which causes animal populations to increase or decrease depending on whether the plant populations are above or below average when they reproduce. Using the results of this model, a management program was designed with specific recommendations to protect crocodilians and their ecosystems from rainfall variations.

KEYWORDS: Crocodilians, Simulation, Rainfall

INTRODUCTION

Climate change is projected to have many effects on the earth including higher mean global temperatures, increased hurricane severity, and changes in global precipitation patterns (Walsh et al., 2014; USGCRP, 2017; National Aeronautics and Space Administration, 2019). Changes in global precipitation patterns are likely to have a significant impact on ecosystems because water is essential to life (USGCRP, 2014). The timing and amount of precipitation determine the amount of energy available for use in ecosystems through the growth of plants (Zeppel et al., 2014). In the future, precipitation is predicted to be more extreme with some regions receiving increased rainfall while others suffer from drought. Also, the timing of precipitation is projected to shift, for example, precipitation shifting from summer to winter (Walsh et al., 2014).

There are 25 species of crocodilians living in wetlands around the world (Grigg and Kirshner, 2015). Crocodilians are important natural resources because as apex predators, they are

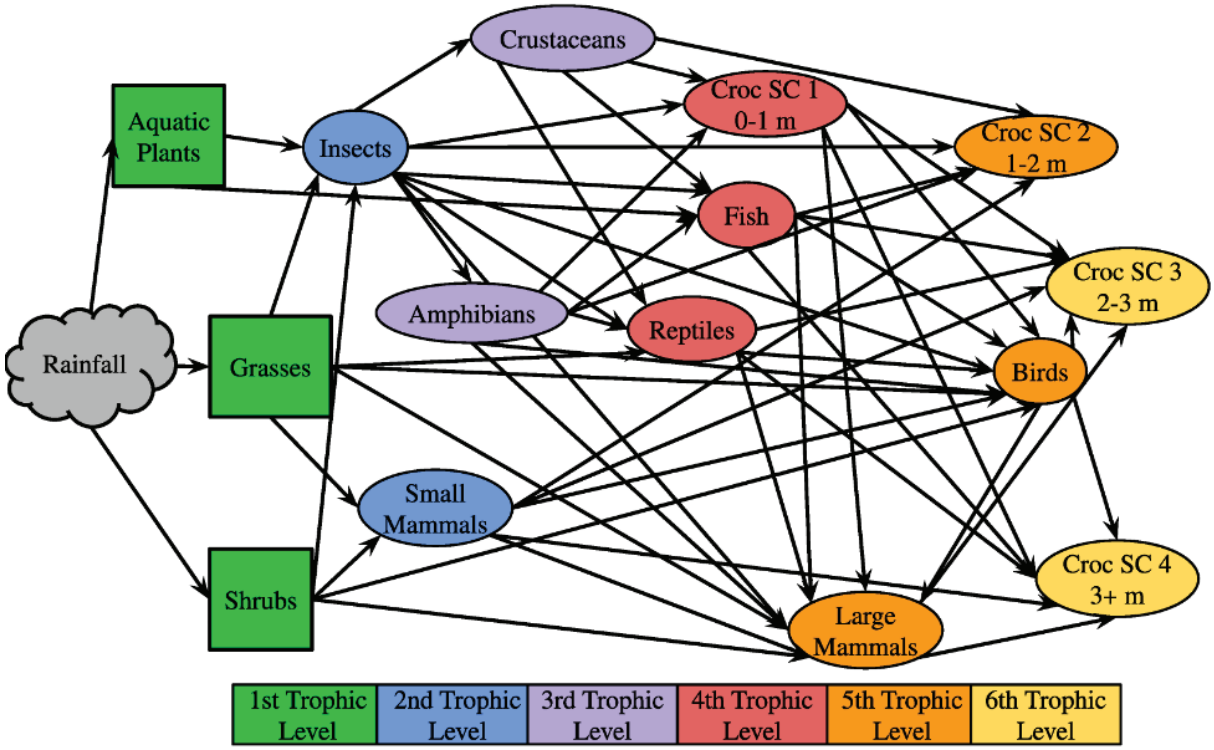

Figure 1. The food web modeled. Arrows show the flow of energy through the ecosystem pointing from prey species to their predator species.

essential for maintaining ecosystem health, and they serve as ecosystem engineers creating extensive burrows and nest mounds which provide other species habitat and access to water (Somaweera et al., 2020). Crocodilians are also important culturally and economically through tourism and the sale of their hides (Grigg and Kirshner, 2015; Somaweera et al., 2020). In the coming years, crocodilians and their ecosystems are likely to be impacted by climate change through changes in their habitat, prey availability, and their temperature dependent sex determination (Stevenson, 2019), although temperature dependent sex determination is unlikely to significantly affect crocodilians because they produce females at both high and low temperatures (Gonzalez et al., 2019). This project focuses on the effects of variations in rainfall on the populations of species in crocodilian's ecosystems. Knowledge of how crocodilians may respond to climate change is essential to prepare management programs to protect them. The purpose of this experiment was to better understand how crocodilians and their ecosystems are impacted by variations in rainfall patterns with the goal of developing a management program to keep their ecosystem stable. In this project, the effects of variations in the magnitude and timing of rainfall on the ecosystem were explored to better understand how changes in rainfall affect all the species through interspecific interactions in the crocodilian's ecosystem.

EXPERIMENTAL METHODS

For this experiment, a computer model of a crocodilian population in a representative general ecosystem in a generic location was created using an adaptation of the Lotka-Volterra equations. A general ecosystem is used to get a basic understanding of the effects of variations

in rainfall on crocodilians as a first step towards creating detailed models of each crocodilian species for accurate and specific management information. A model was used because it allows exploration of how variations in rainfall affect ecosystems in a controlled setting and without any risk to the species. Additionally, a model allows for the projection of the effects of more extreme rainfall patterns than have been observed to date (Gotelli, 2008).

Model

The model was created by writing a code using the Python 3.6.1. language. This model includes a crocodilian population, three plant types, and eight other general animal classes, for example, fish or birds, as shown in Figure 1 and Table 1. The classes included in the model are representative of typical species in aquatic ecosystems inhabited by crocodilians. In this work, these classes are referred to as species because each class is modeled as one population. In the food web in Figure 1, the species are arranged by trophic level, with arrows showing energy flow through the ecosystem (National Geographic, 2019). The food web is simplified using a single population for each representative class and simplified predator-prey interactions, to give a basic understanding of a generic crocodilian ecosystem. The crocodilian population is modeled with four size classes (SC). Crocodilians cannibalize their young, so hatchling crocodilians are a prey source for the adults (Delany et al., 2011). The other animal species are modeled as homogenous populations, which are assumed to not cannibalize themselves. Plants are modeled as biomass in kilograms of plant matter. In Table 1, each species individual mass, reproductive rate, hatch rate, and energy needs are shown. The animal species' energy needs were calculated based on the mass of the animals and whether they are ectothermic or endothermic (Nagy et al., 1999). The model uses discrete time, with time modeled as separate steps, to represent the seasonal impact of different processes on each species, with predator-prey interaction occurring each month, animals reproducing at different times of the year, and seasonal rainfall variations (Gotelli, 2008).

Model Summary

The Lotka-Volterra equations are the standard way to model predator-prey interactions (Gotelli, 2008). For this project, a novel adaptation of the Lotka-Volterra equations was developed based on Gotelli, 2008. Some limitations of the Lotka-Volterra model include that it describes only a two species system, that reproduction occurs each time step, that prey species make up a fixed proportion of the predator's diet, that the system's energy is constant, and that predator populations do not die out immediately without prey (Gotelli, 2008). The model created for this experiment is innovative by modeling a complex ecosystem with many species, having species reproduce only in specific months as they do in the wild, using a dynamic approach to vary predator diets to match prey abundances, including plants to make the system's energy dynamic, and modeling starvation deaths proportional to the amount of prey with predators dying out if there is no prey.

In the model, rainfall only affects the ecosystem through the plant populations. Every month the populations are affected by predator-prey interactions, which cause prey to die from being consumed and predators to die if their energy needs are not met. Plants reproduce every month and animals reproduce only in certain months as shown in Table 2. Once a year the crocodilian population ages with some members of each size class moving up to the next.

The equations used are described in the Appendix.

Species	Mass (*grams*)	Reproductive Rate (*young/ female*)	Hatch Rate *(percent of young that are viable)*	Mass Based Energy Needs (*grams/ year/ individual*) (calculated based on Nagy et al., 1999)
In: Insects (Snallshire and Swash, 2014)	1	300	5%	23
Sm: Small mammals (Lee, 2013)	340	8	55%	41040
Cr: Crustaceans (Dunover, 2016)	32	350	10%	285
Am: Amphibians (Mitchell, 2019)	45	2000	5%	385
Fs: Fish (Indiana Division of Fish and Wildlife, 2012)	340	6000	0.7%	2990
Re: Reptiles (Wilson, 2019)	230	10	50%	2090
Br: Birds (Cornell Lab, 2017)	680	8	60%	76320
Lm: Large mammals (National Park Service, 2016)	45000	3	83%	737640
Croc: Crocodilians (in four Size Classes [SC]) (Grigg and Kirshner, 2015)	SC1-500 SC2-10000 SC3-30000 SC4-75000	40	30%	SC1-3280| SC2-51840 SC3-138600 SC4-312840

Table 1. The animal species in the model. All are homogeneous populations except for the crocodilians. Abbreviations given in Column 1 are used in Table 2.

Rainfall Effects on Plants

Plants die if the amount of rainfall received varies from their water needs, either higher or lower (Good et al., 2017). Aquatic plants require 3 inches of rain each month; grasses, 4.3 inches; and shrubs, 4 inches (Davis and Fromme, 2016; University of California, 2019). Plants die at a higher rate when there is too little rain than too much (Good et al., 2017). Rainfall also affects plant growth, that is their reproduction defined as the addition of biomass to the population either through physical growth or production of seeds, which occurs every month. The plant growth rate varies by month (Orsenigo et al., 2014) as shown in Table 2. Plant growth is limited by a carrying capacity determined by the amount of rainfall in the previous season. Although other factors affect plant growth, in this simplified model their effects are assumed negligible to focus on the effects of variations in rainfall.

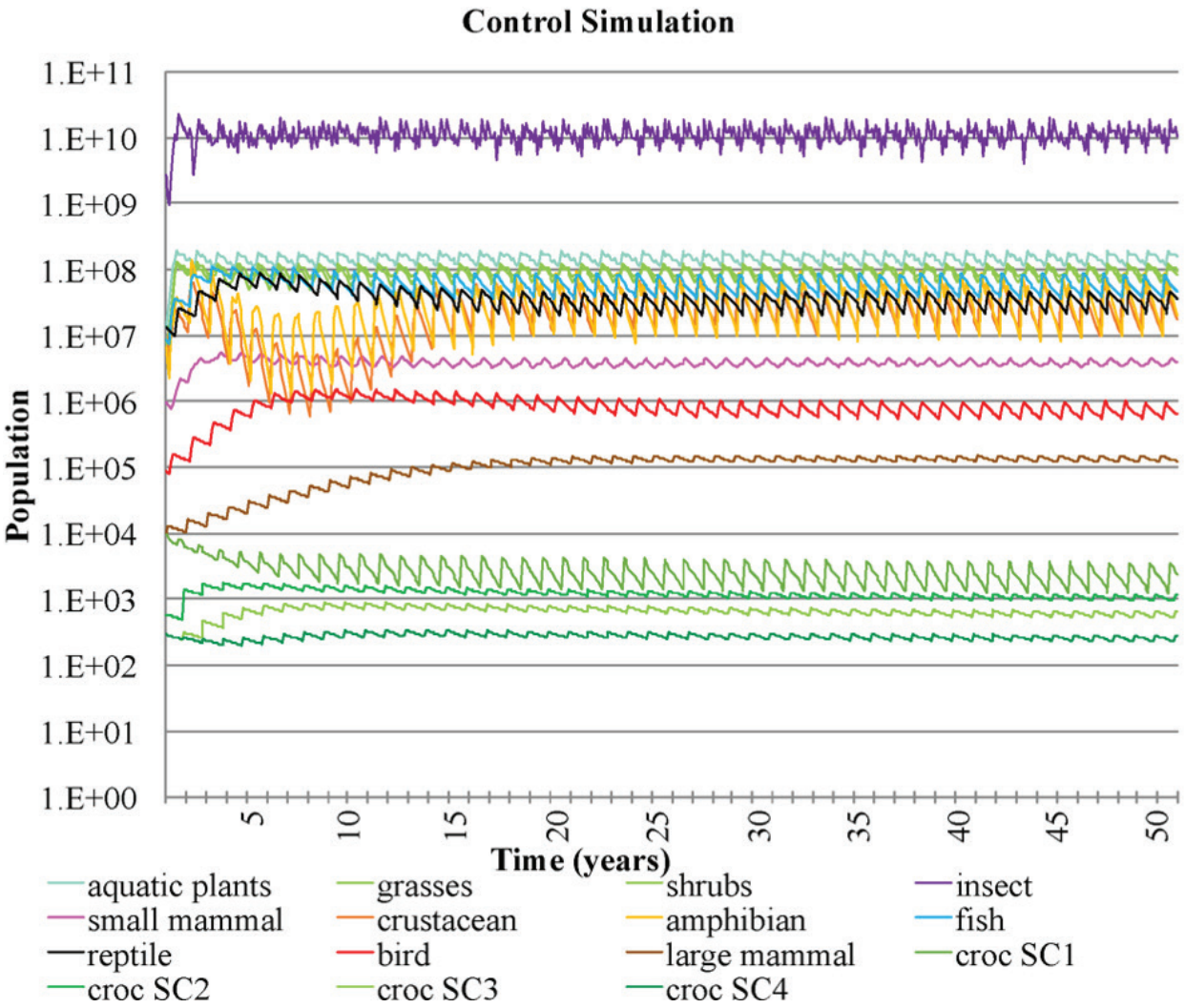

Figure 2. The control simulation, with normal rainfall values as shown in Table 2. Population is plotted as a function of time in years. The populations are plotted using a logarithmic scale to show all the populations in proportion to one another.

Predator Prey Interactions

Each month, predator and prey populations interact with one another as shown in Figure 1, resulting in consumption and starvation deaths. In this simplified model, it is assumed that all individual deaths can be accounted for by either starvation or consumption. From these interactions, prey dies from being consumed and predators die in proportion to the fraction of their energy requirements not met. Crocodilians do not have food preferences and consume species in proportion to their abundance (Grigg and Kirshner, 2015); this trait was assumed for all predators in this model. For predators that consume multiple species of prey, a dynamic approach was taken to divide their energy requirements among their prey species. The proportion of the predator's diet that a certain prey species fulfills varies from month to month based on their abundance relative to the other prey species.

Season	Winter			Spring			Summer			Fall		
Month	1	2	3	4	5	6	7	8	9	10	11	12
Normal Rainfall (Louisiana averages inches) (National Weather Service and National Oceanic and Atmospheric Administration)	5.23	3.46	3.66	3.33	5.20	6.85	5.63	4.86	5.26	4.90	4.43	4.68
Proportion of Yearly Rain	21.5%			26.75%			27.5%			24.25%		
Species Reproducing (Wilson, 2019; Indiana Division of Fish and Wildlife, 2012; Lee, 2013; Snallshire and Swash, 2014; Grigg and Kirshner, 2015; Dunover, 2016; National Park Service, 2016; Cornell Lab, 2017; Mitchell, 2019)	In	In Lm	In Sm Cr	In Sm Cr Am Fs Br	In Sm Cr Am Fs Br	In Sm Cr Am Fs	In Sm Am Re	In Sm Re Croc	In Sm	In	In	In
Plant Growth Rate (Orsenigo et al., 2014)	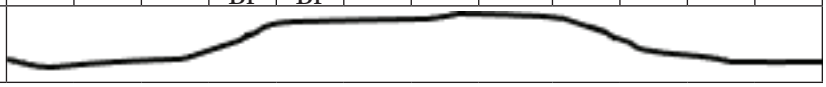											

Table 2. A year in the model. The normal rainfall is the monthly averages for Louisiana from 1970-2018 and is used for the control simulation. Animals reproduce in only certain months of the year as they do in the wild. Plants grow every month, but their base growth rate varies from season to season.

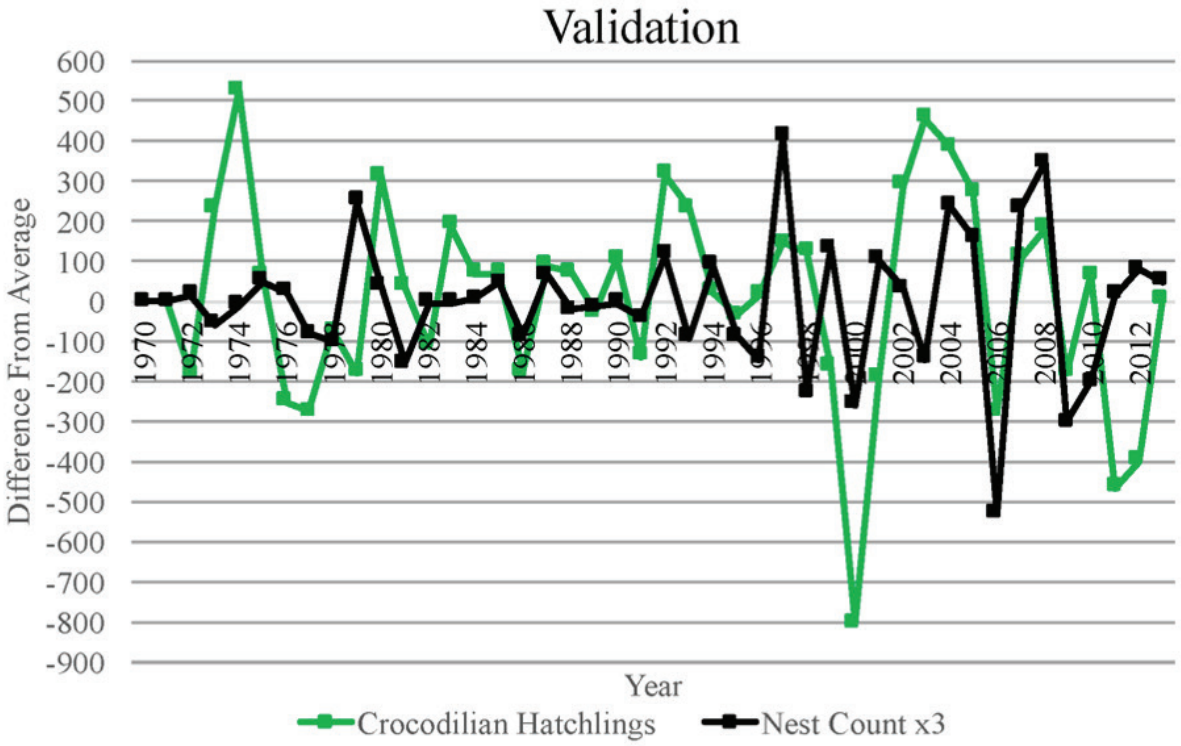

Figure 3. The detrended nest count data and crocodilian hatchling data from the model. The detrended nest count data is tripled to allow for easy comparison to the crocodilian hatchling data in the plot. The trends in the two data sets are compared for similarity, rather than exact magnitudes, as many factors affect the wild populations that are not included in the model. After 1985, the crocodilian hatchling population follows a similar pattern to the nest count data.

Animal Reproduction

Animal reproduction occurs in certain months for each species based on when they reproduce in the wild as shown in Table 2. In this simplified model, animal reproduction is limited by the species prey populations (National Geographic, 2019), and all other factors affecting reproduction like habitat quality are assumed negligible. Reproduction is limited by a carrying capacity, set by the species' prey populations. The number of possible young can exceed the carrying capacity, but the actual number of young never does.

Crocodilian Aging

Once a year the crocodilians age. A small portion of each size class moves up to the next one because individuals spend several years in each size class (Grigg and Kirshner, 2015). Changes in size classes are limited by the amount of prey in the system because growth requires energy.

Control Simulation

To establish a baseline, the simulation was first run with normal rainfall values as shown in Table 2. This control simulation was run for 50 years, as shown in Figure 2, where all the

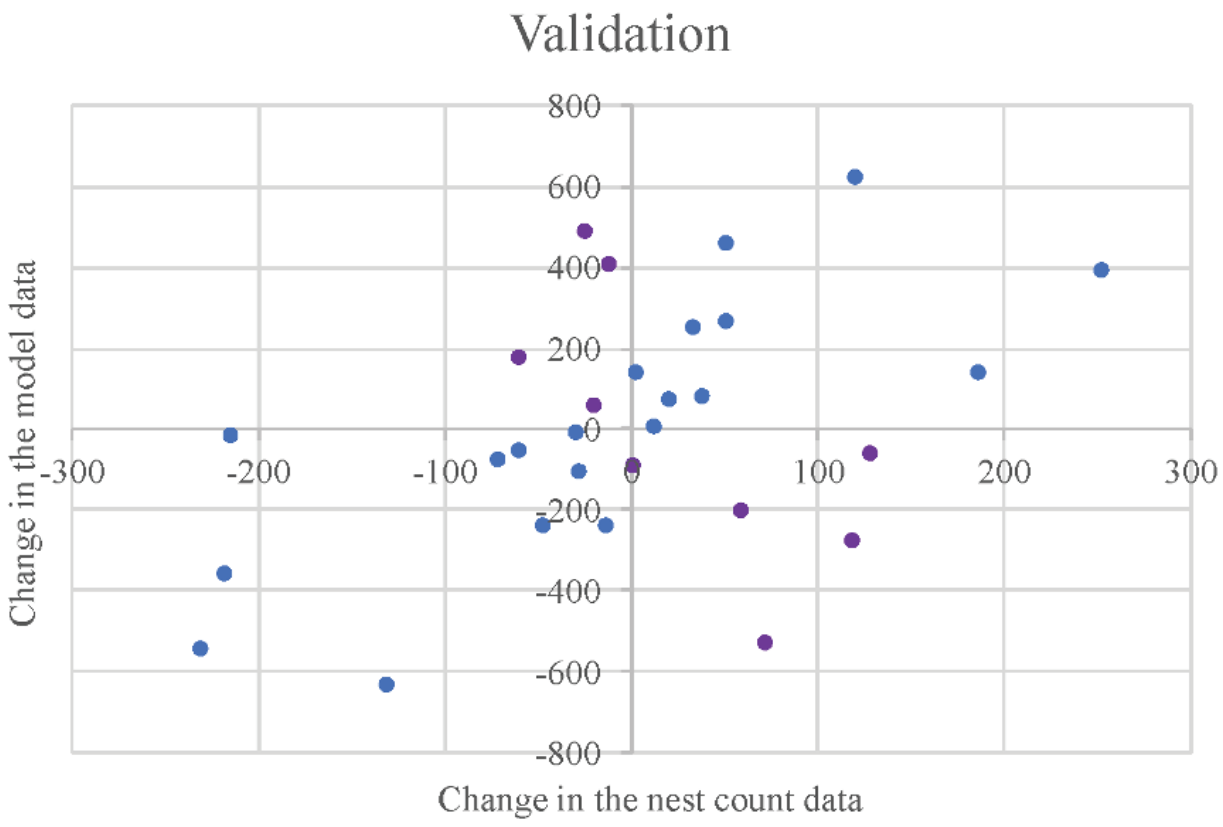

Figure 4. Scatter plot of the year to year change in the nest count data (x-axis) and the change in the model data (y-axis). Points in quadrants I and III are blue and represent years when the nest count and model data followed the same trend, and points in quadrants II and IV are purple and represent years when they did not follow the same trend. 20 of the 29 points are in quadrants I and III.

populations are plotted as a function of time. The populations settle in the first decade and are arranged based on the food chain, where prey have higher populations than their predators. Oscillations each year are due to reproduction.

Validation

A model must be validated with data from the real system (Gotelli, 2008). To validate this model, it was run using Louisiana rainfall data from 1970 to 2018 (National Centers for Environmental Information and National Oceanic and Atmospheric Administration, 2019). This simulation was initialized by running it for nine years with normal rainfall to allow the populations to settle and then with the Louisiana rainfall data. The model results were compared to Louisiana alligator nest count data from 1970 to 2018 (Louisiana Department of Wildlife and Fisheries, 2019). The nest count data approximates the alligator hatchling population, so the crocodilian size class 1 population in the model was used for comparisons. The raw nest count values (not shown) have an upward trend reflecting the alligator's endangered status in the 1970s and the significant conservation efforts since then (Louisiana Department of Wildlife and Fisheries, 2019). Nest count data is affected by the time of year, time of day, and habitat type surveyed (Chabreck, 1966).

Many factors affect wild alligator populations including human interactions, hurricanes, temperature, and habitat quality (Lance et al., 2010; Louisiana Department of Wildlife and Fisheries, 2019; Grigg and Kirshner, 2015). These factors were not accounted for in the model, so the model data cannot be directly compared to the nest count data. To remove the significant increase due to conservation from 1970 to 1990, nest count data was detrended by calculating a five-year running average and subtracting the average from the data, removing the overall increasing trend in the nest count data due to conservation to examine the year to year variation in the populations. This detrending does not remove the effects of other factors on the nest count data. The crocodilian size class 1 population data was also detrended by calculating the average population and subtracting that from the yearly average, so the model data could be compared to the nest count data as shown in Figure 3. The detrended data are centered around zero, as they represent the difference from the average. If the values are greater or less than zero, then the population is above or below average, respectively. The general pattern of the variations in the nest count data was compared to the variations in the crocodilian hatchling (size class 1) population because the nest count data was affected by factors not included in the model.

The crocodilian hatchling population in the simulation generally followed the pattern of the nest count data as shown in Figure 3, but the correlation is not perfect. For the first 15 years of the Louisiana rainfall data, the variations in the model population do not correlate significantly with the variations in nest count, likely because those were the first years of taking nest count data, so the counts may not be as accurate. From 1985 on, the model population variations correlate with the variations in the nest count data. When the nest count data is above or below average, the model population is also above or below average, well demonstrated in 1985–1987 and 2004–2009, where the model hatchling population variations are the same as the nest count variations.

To get a quantitative understanding of the correlation, for both data sets, the year to year difference in the detrended data was calculated and compared as shown in Figure 4, with

each point being the change in the nest count data (x-axis) and the change in the model data (y-axis) for a specific year. In Figure 4, only data from after 1985 was used since there was little correlation between the nest count and model data prior. A positive value means that the population increased compared to the previous year and a negative value means that it decreased. Points in quadrants I and III represent years when the nest count data and the model data both increased or decreased respectively, whereas points in quadrants II and IV represent years when the nest count data and the model population followed a different pattern. The majority of the points, 20 out of 29, fall in quadrants I and III as shown in Figure 4.

Differences are due to uncertainties in both the data and the model. The nest count data is the best population data available for crocodilians, despite its limitations (Chabreck, 1966). The model does not perfectly represent the ecosystem as it does not include many factors that affect the populations. For example, the model is more sensitive to changes in rainfall than the real system. In the validation simulation, the insect population in the model died out

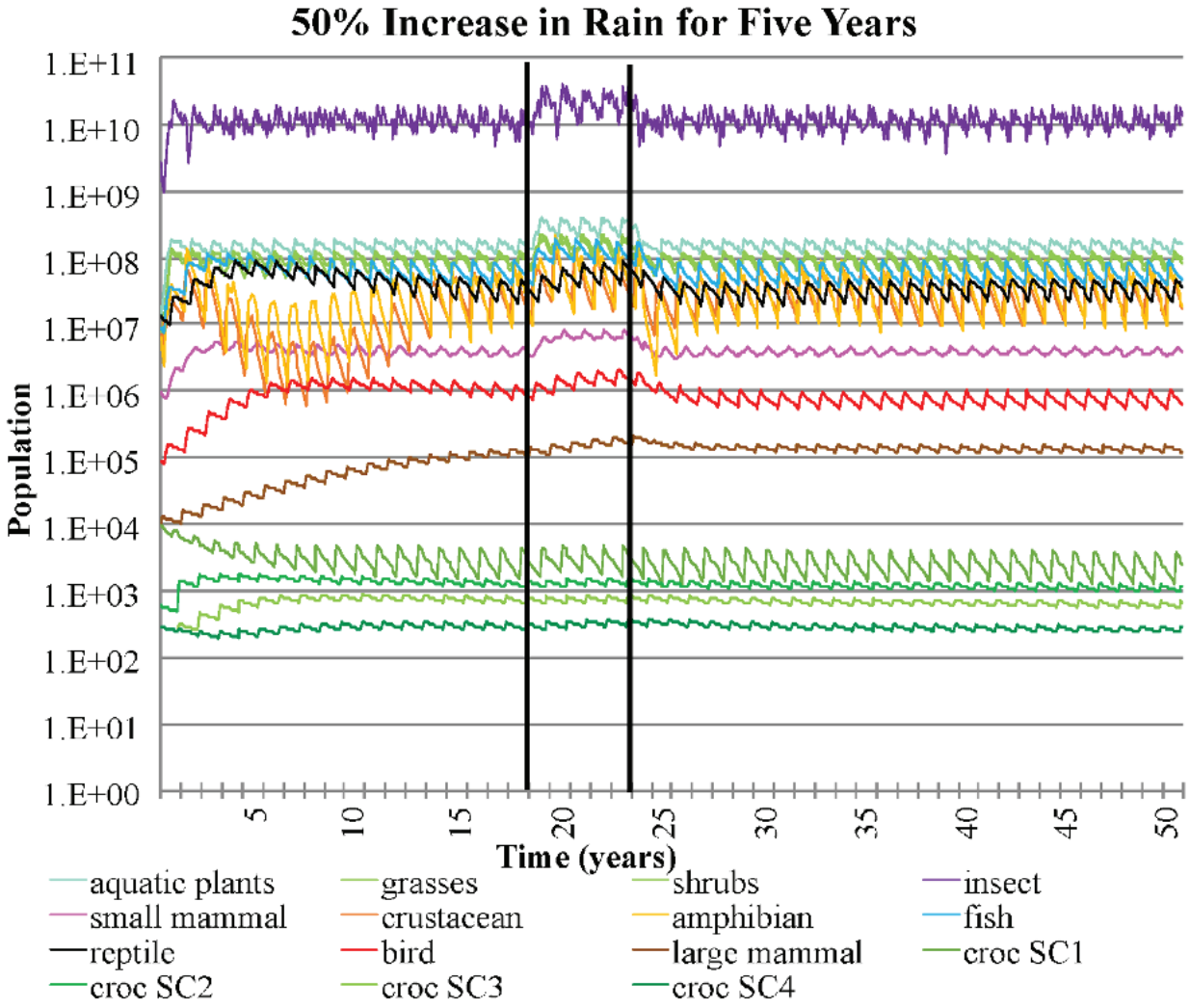

Figure 5. The populations with 19 years of normal rainfall, five years with a 50% increase in rainfall, and normal rainfall for the remainder of the simulation in the same format as Figure 2. In all plots, vertical lines indicate when the rain is changed. The populations increase in response to the rainfall change and return to normal quickly when the rain returns to normal.

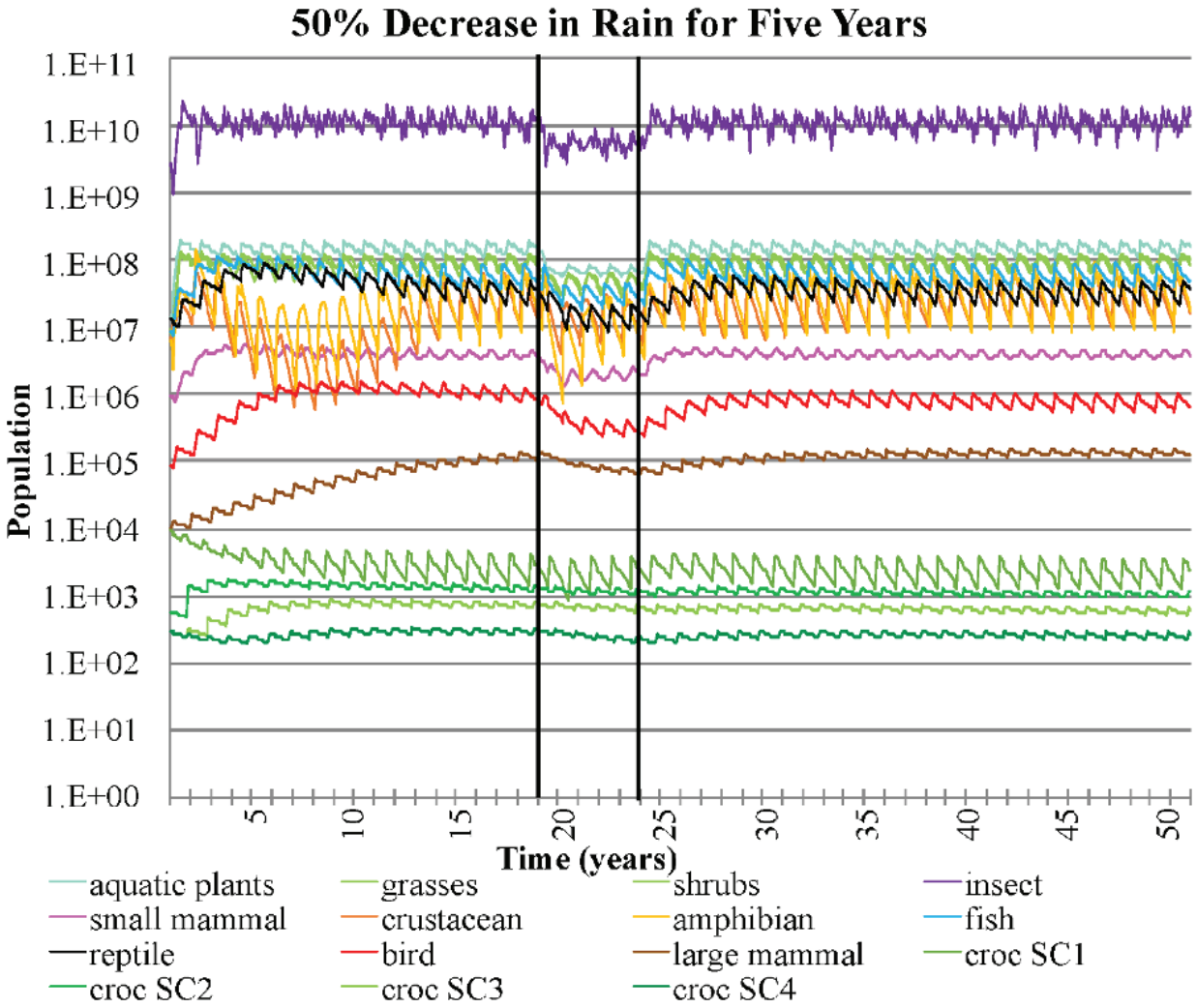

Figure 6. The populations with 19 years of normal rainfall, five years with a 50% decrease in rainfall, and normal rainfall for the remainder of the simulation in the same format as Figure 2. The populations drop in response to the rainfall change and return to normal quickly when the rain returns to normal.

in 2016. This occurred because there was an unusually large amount of rainfall after several months with little, causing the insect's predator populations to increase, while the insect population was low. Given the limitations with the nest count data and the limitations with the model, the correlation observed in response to specific rainfall conditions shows that the model describes how crocodilian populations respond to changes in rainfall. This model thus can be used to explore and predict how crocodilians and their ecosystems may respond to new rainfall patterns.

Variations in Rainfall

Once the model was validated it was then run with variations in rainfall. Over 50 simulations were run. First, the simulation was run with variations in the amount of rainfall, with normal rainfall for 19 years, then increased or decreased rainfall for 5, 10, 15 years, and finally normal rainfall for the rest of the simulation. Many magnitudes were tested ranging from a

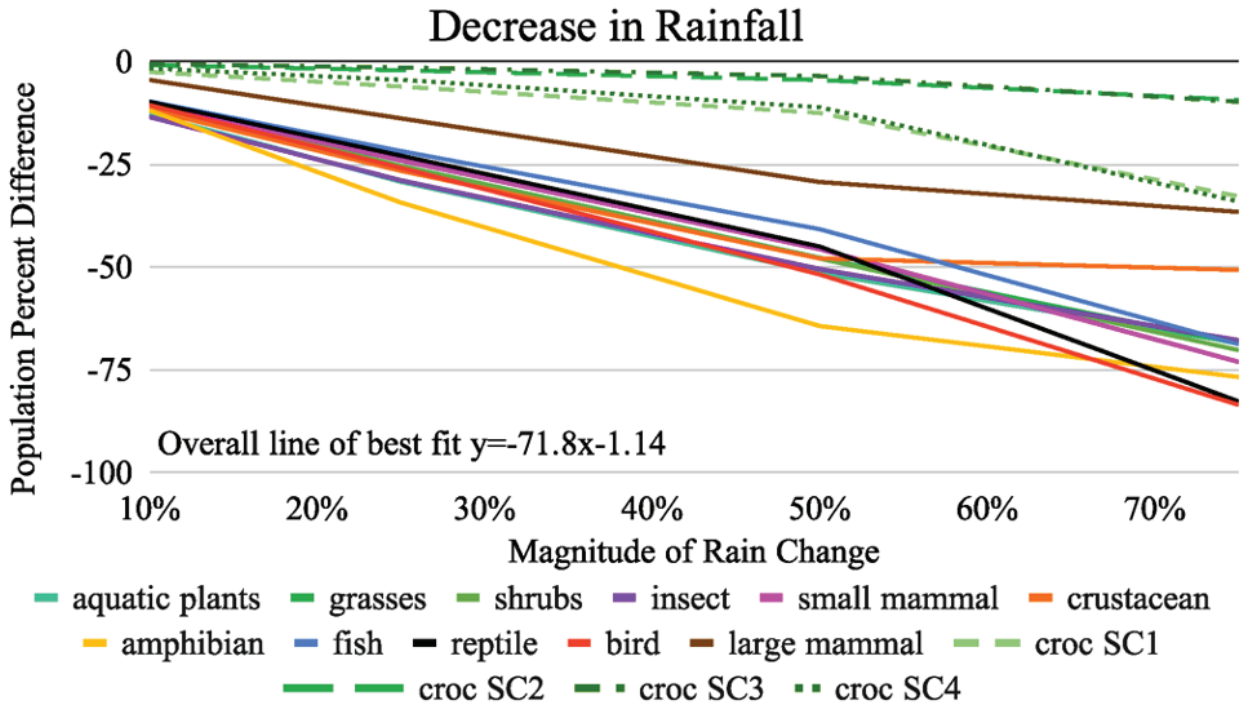

Figure 7. The percent difference in the populations as a function of the magnitude of the rain change when the amount of rainfall is decreased. Overall a linear trend is followed. The colors for the species are the same as in Figure 2.

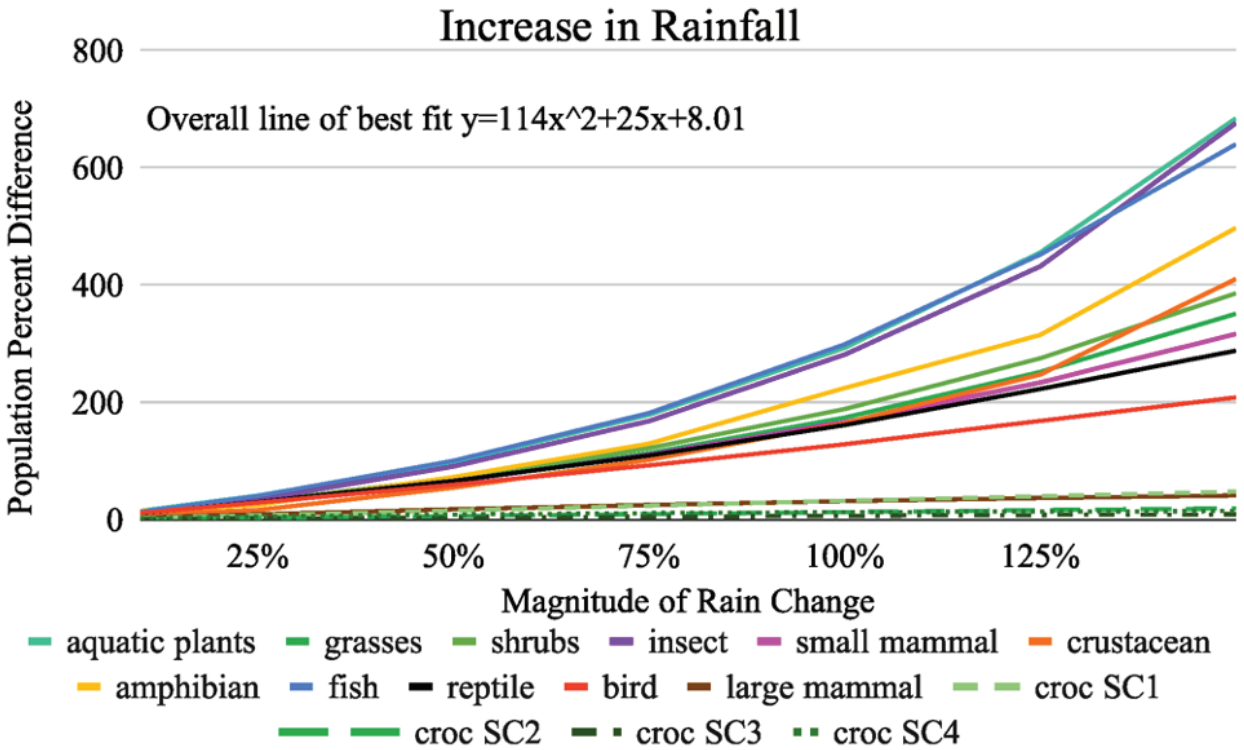

Figure 8. The percent difference in the populations as a function of the magnitude of the rain change when the amount of rainfall is increased. Overall there is a quadratic trend. For the crocodilians and large mammals, the trend is linear. The format is the same as in Figure 7.

100% decrease to a 150% increase in rainfall. Then, the simulation was run with variations in the timing of rainfall, with normal rainfall for 19 years, then a change in the timing of rainfall for 15 years, and finally normal rainfall for the rest of the simulation. With a change in rainfall timing, the system receives the same amount of rain each year, but with different amounts coming in each season. Many timing changes were tested including the same amount of rain each season (25% of the yearly rainfall each season, 25-25-25-25) and having a peak or a drop in the amount of rainfall each year (Peak: 40% of the rain in one season and 20% in each of the other three seasons, 40-20-20-20; Drop: 10% of the rain in one season and 30% in three seasons, 10-30-30-30). Finally, the simulation was run with a change in both the amount and timing of rainfall, with normal rainfall for 19 years, then a change in the amount and timing of rainfall for 15 years, and finally normal rainfall for the rest of the simulation.

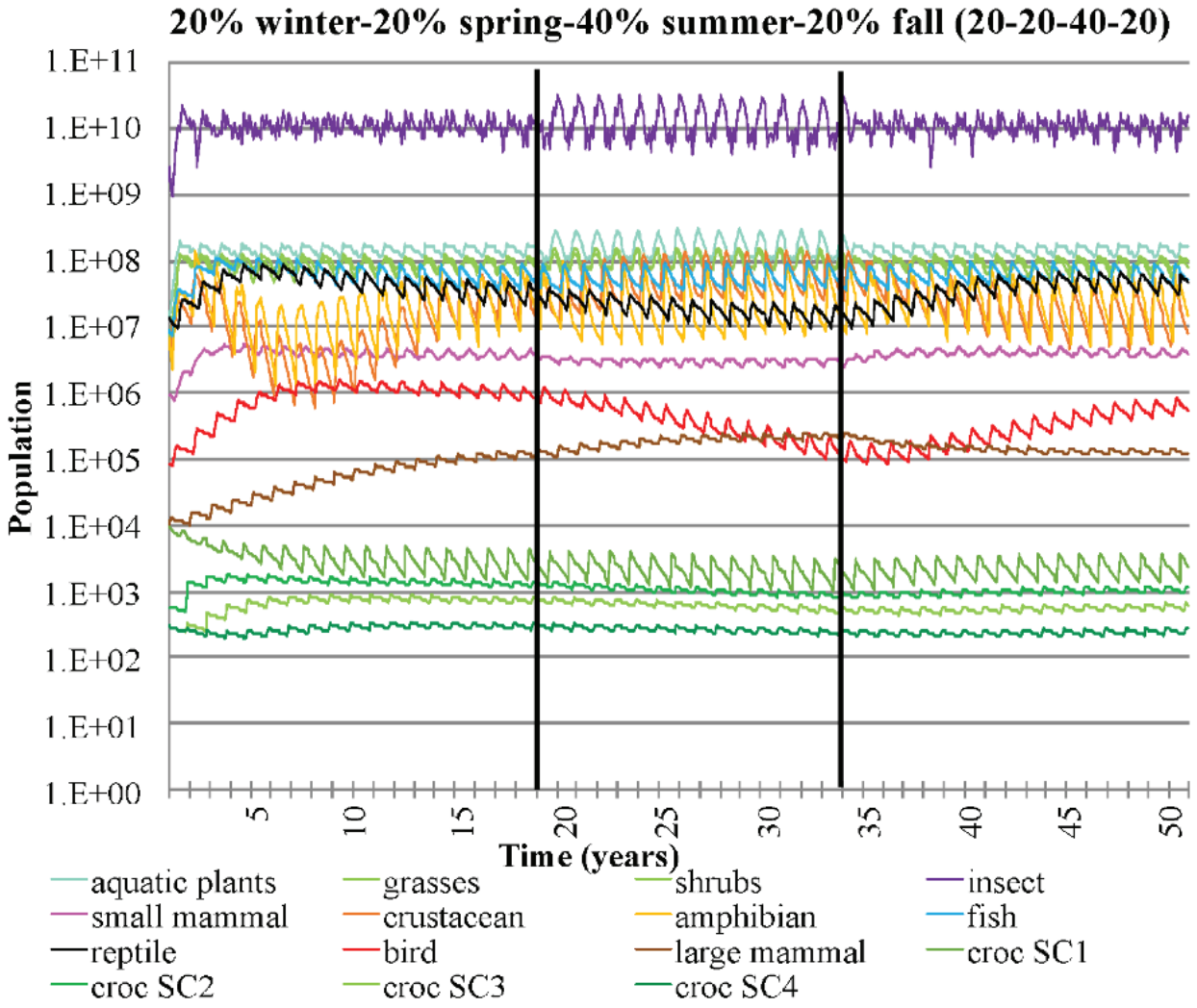

Figure 9. The populations with normal rain for 19 years, 40% of rainfall coming in summer and 20% in the other seasons for 15 years, and normal rainfall for the rest of the simulation in the same format as Figure 2. The populations had only slight changes as rainfall peaks in summer with normal rainfall patterns.

RESULTS AND DISCUSSION

Variations in the Amount of Rainfall

Simulations were run with variations in the amount of rainfall with 19 years of normal rainfall, 5 years with a change in the amount of rainfall between years 19 and 24, and normal rainfall for the remainder of the simulation as shown in Figure 5 with a 50% increase in rainfall and Figure 6 with a 50% decrease in rainfall. Figures 5 and 6 show the populations plotted as a function of time in years. In Figure 5, all the populations increase when the rainfall is increased, and in Figure 6, all the populations decrease when the rainfall is decreased. When the rainfall returns to normal, the populations increase or decrease back to their original levels.

The amount of rainfall determines the amount of energy in the ecosystem through the plant populations, so with increased rainfall there is more energy and with decreased rain-

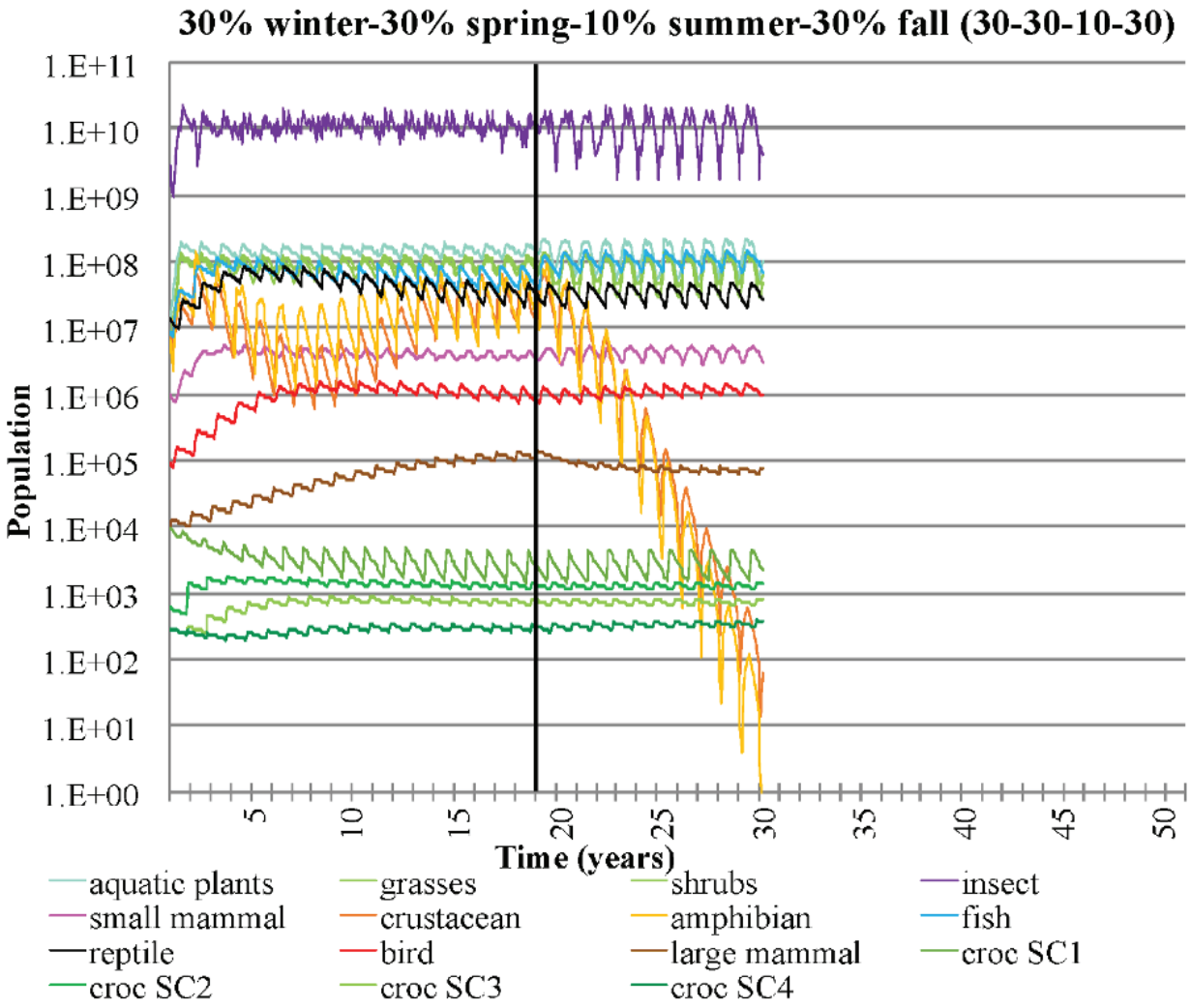

Figure 10. The populations with normal rain for 19 years, 10% of rainfall coming in summer and 30% in the other seasons for 15 years in the same format as Figure 2. The plant and insect populations were high for most of the year with a large quick drop. The amphibians and crustaceans died out, ending the simulation run, as the insect population was low when they reproduced.

fall less, and the populations vary directly with the amount of energy in the system. After the rainfall amount is changed, populations of species at the bottom of the food chain, like insects and amphibians, quickly plateau at their new base population level, which is higher or lower than normal depending on the rain change. Populations of species at the top of the food chain, like large mammals, do not plateau, rather they continue to increase or decrease until the rainfall returns to normal. This occurs because these populations take longer to be impacted by the rainfall as they are not directly dependent on the plant populations. There is a time lag between when prey species and their predators are affected by the change in rainfall. The duration of the rainfall change affects only how much populations at the top of the food chain are impacted because these populations continue to increase or decrease over the entire period of the rain change, while species lower down the food chain plateau and remain at the same level. Once the amount of rainfall returns to normal, the populations also return to normal. If the rainfall was decreased, the populations simply increase back to their original levels. If the rainfall was increased, the populations decrease back to their original level, but some populations, like the crustaceans and amphibians, drop further than their baseline before returning to normal. This occurs because their population exceeds a level that can be sustained by their prey populations, which have just decreased back to normal, causing them to miss out on reproduction.

The magnitude of the increase or decrease in rainfall determines the magnitude of change in the populations as shown in Figures 7 and 8. Figures 7 and 8 show the percent difference in the populations from normal rainfall as a function of the change in the amount of rainfall. With decreased rainfall, the magnitude of the change in the populations increases linearly with the magnitude of the rainfall change as shown in Figure 7, but with increased rainfall, it increases quadratically as shown in Figure 8. That is, an increased magnitude of change in the amount of rainfall has more effect on the populations when the rain is increased than decreased. This occurs because the plant carrying capacity is modeled as an exponential function, so there is a greater difference in the plant carrying capacity with increased rainfall than with decreased rainfall at the same magnitude compared to normal. Species at the top of the food chain, like crocodilians, are less impacted by variations in the amount of rainfall than species lower down the food chain, like amphibians and plants. When the amount of rainfall is increased, species at the top of the food chain show a linear relationship between the magnitude of the rain change and change in the populations as shown in Figure 8. Changes in the amount of rainfall can have significant effects on the ecosystem leading populations to die out with large changes in rainfall. Populations died out when there was a greater than 80% decrease in rainfall or a greater than 125% increase in rainfall when the rainfall returns to normal.

Variations in the Timing of Rainfall

Changes to the timing of rainfall affect the relative magnitudes of the populations and the seasonal variations in the plant populations: the plant populations increase in seasons when the carrying capacity is high and decrease when low. Some animal populations increase while others decrease, based on the seasonal variations of the plant population and when the species reproduce. Figure 9 shows the populations with a change in the timing of rainfall between years 19 and 34 where 40% of the rainfall comes in summer and 20% of the rainfall comes in each of the other seasons (20-20-40-20, last row of Table 3). With the rainfall peaking

in summer, the bird population decreases while the large mammal population increases, as the birds reproduce in spring and the large mammals reproduce in winter, which is closer to the peak in rainfall, and the other populations are relatively unchanged. Figure 10 shows the populations with a change in the timing of rainfall between years 19 and 34 where 10% of the rainfall comes in summer and 30% of the rainfall comes in each of the other seasons (30-30-10-30, second row of Table 3). With the rainfall being lowest in summer, the amphibian and crustacean populations drop significantly, while the other populations are less affected, with the large mammal population decreasing slightly, and the reptile population increasing slightly. In Figure 10, the amphibian and crustacean populations die out because their reproduction is reduced by drop in rainfall, coupled with all the species that reproduce in late spring and summer having normal reproductive rates. The effects of changes to the timing of

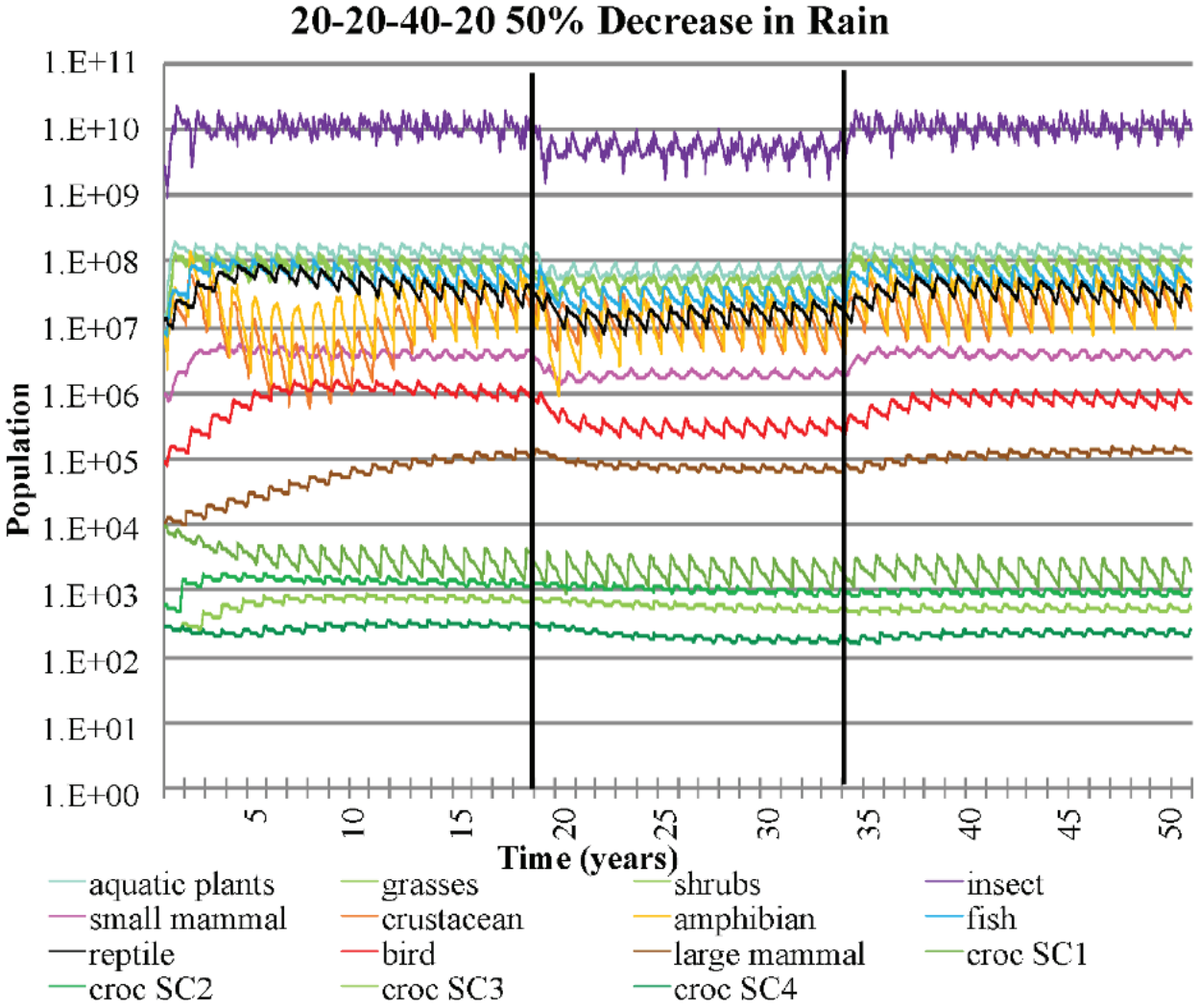

Figure 11. The populations with normal rain for 19 years, a 50% decrease in rainfall with 40% of rainfall coming in summer and 20% in the other three seasons for 15 years, and normal rainfall for the rest of the simulation in the same format as Figure 2. All the populations decrease with slight variations in their relative magnitude and then return to normal quickly once the rain is back to normal.

rainfall range from mild, as in Figure 9, with populations behaving rather normally, to severe, with populations dying out as in Figure 10. Populations die out when prey and predator populations get out of balance, due to a large difference in plant populations between seasons.

In Table 3, several simulations with changes to the timing of rainfall are summarized, where the first column tells the percent of the yearly rainfall that comes in winter, spring, summer, and fall, the second column describes the key rainfall pattern for the simulation, and the third column tells when and how the plant carrying capacity is affected. The plant carrying capacity is determined by the previous season's rainfall so there is a one-season time lag in the response to rainfall. For example, if there is little rain in winter, the plant carrying capacity will be low in the spring as shown in Table 3.

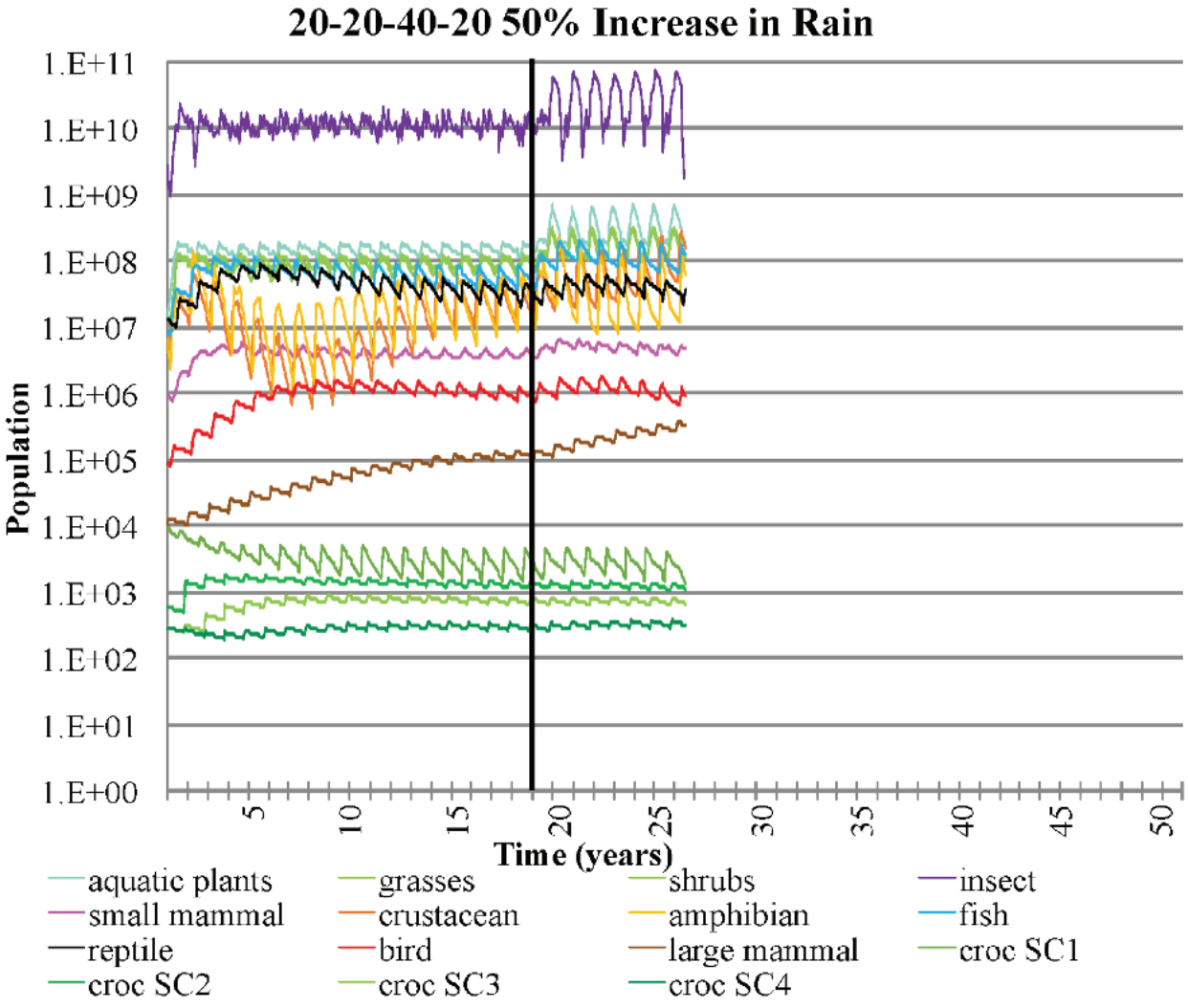

Figure 12. The populations with normal rain for 19 years, a 50% increase in rainfall with 40% of rainfall coming in summer and 20% in the other three seasons for 15 years in the same format as Figure 2, the insect population dies out.

Simulation	Rainfall	Plant Carrying Capacity	Population	Season Species Reproduces			
				Winter	Spring	Summer	Fall
10-30-30-30	Drops in Winter	Drops in Spring	Increases	Large mammals	Fish		
			Decreases		Birds, Amphibians, Crustaceans	Small mammals, Reptiles, Crocodilians	
30-30-10-30	Drops in Summer	Drops in Fall	Increases		Fish, Birds	Small mammals, Reptiles, Crocodilians	
			Decreases	Large mammals	Amphibians, Crustaceans		
40-20-20-20	Peaks in Winter	Peaks in Spring	Increases		Fish, Birds	Small mammals, Reptiles, Crocodilians	
			Decreases	Large mammals	Amphibians, Crustaceans		
20-20-40-20	Peaks in Summer	Peaks in Fall	Increases	Large mammals	Crustaceans		
			Decreases		Fish, Birds, Amphibians	Small mammals, Reptiles, Crocodilians	

Table 3. Simulations with a timing change. In general, animal populations increase when the plant population is elevated when they reproduce and decrease when the plant population is low when they reproduce. There are exceptions: for example, the amphibian population always decreases.

The plant populations increase overall when their carrying capacity is high during spring or summer when their base growth rate is higher, and decrease when their carrying capacity is high in fall or winter as their base growth rate is lower. Insects are the first animals impacted by variations in the timing of rainfall because they reproduce each month, and their population follows the plant population pattern. The other animal species are impacted later and these populations follow their normal seasonal patterns because they reproduce only at certain times of the year. These animal populations increase or decrease depending on whether the plant population is above or below average when they reproduce as shown in Table 3, where species are placed in the last four columns based on when they reproduce. These columns are divided into two rows, with species whose populations increase in the upper row and species whose populations decrease in the lower row.

Variations in the Amount and Timing of Rainfall

The ecosystem response to changes in both the amount and timing of rainfall is a hybrid of the individual responses as shown in Figures 11 and 12 with the timing of rainfall changed so 40% of the rainfall comes in summer and 20% of the rainfall comes in the other seasons with a 50% decrease (Figure 11) and a 50% increase (Figure 12) in rainfall amount during years 19

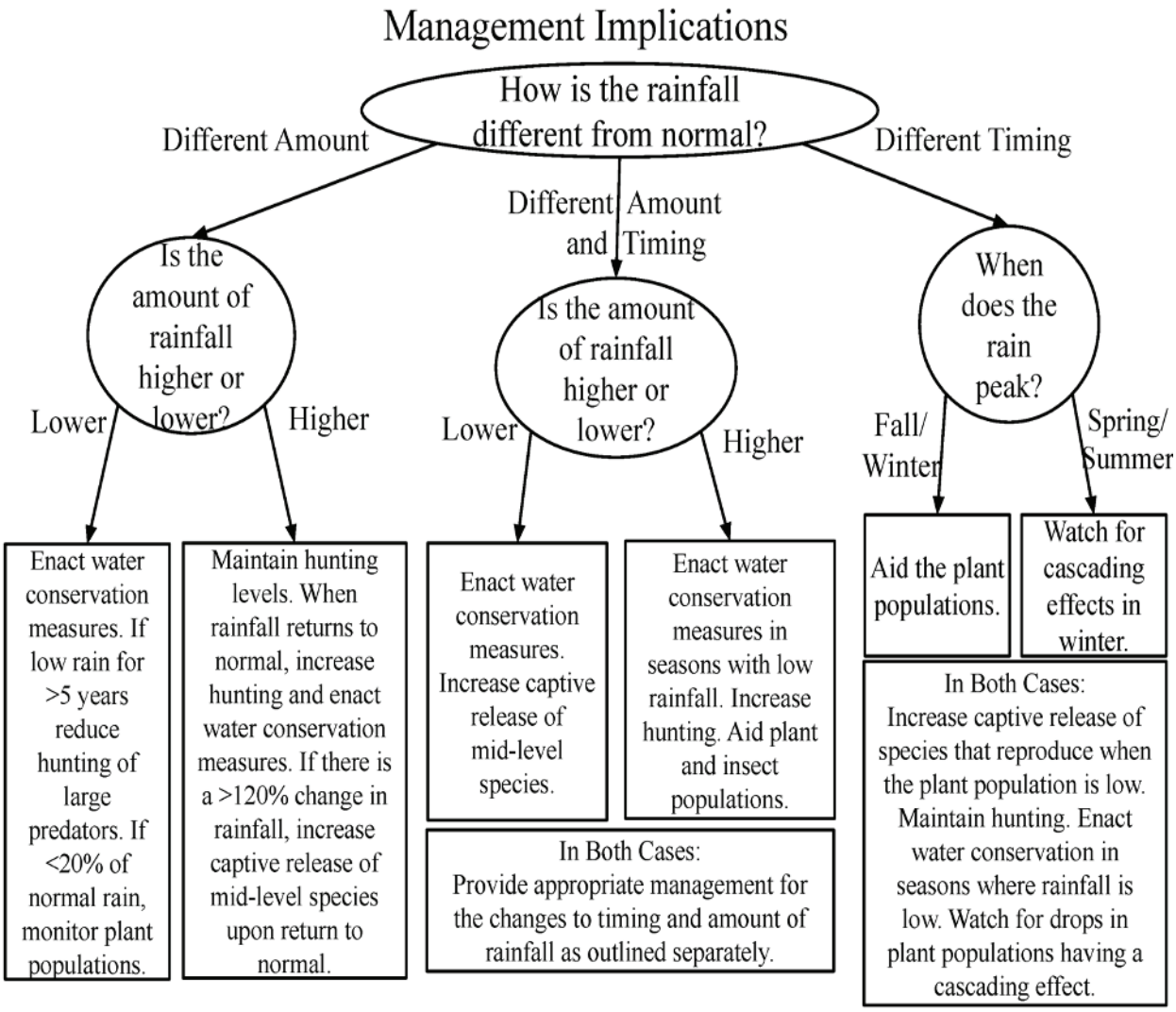

Figure 13. Management program for how humans can help protect crocodilians and their ecosystems from variations in rainfall.

to 29. In Figure 11, the populations decrease because the rainfall is decreased, but the effects of change in the timing of rainfall is reduced as the populations decrease a similar amount. This occurs because having decreased rainfall overall reduces the effects of changes in the timing of rainfall because the seasonal variation in the plant carrying capacity is reduced as shown by the small oscillations in the plant populations in Figure 11. In Figure 12, the populations increase because the rainfall increased, but the populations increase at different rates than without a change in the timing of rainfall. The insect population dies out because of the significant increase in all the populations. Increased rainfall overall amplifies the effects of changes in the timing of rainfall because the seasonal variation in the plant carrying capacity is increased as shown by the large oscillations in the plant populations in Figure 12. The timing of rainfall determines the seasonal variations in the plant populations and the relative magnitudes of the populations, while the amount of rainfall determines the magnitude of seasonal oscillations and the base population levels. Overall, changes in the timing of rainfall have a greater effect on the populations because the relative magnitudes of the populations

are changed, while with changes in the amount of rainfall, these are maintained. Compared to a normal amount of rainfall and this timing change, as shown in Figure 9, the populations have smaller oscillations with decreased rainfall as shown in Figure 11 and larger oscillations with increased rainfall as shown in Figure 12. Populations die out with increased rainfall and timing changes because the ecosystem is unstable due to the large seasonal variation in the plant populations.

CONCLUSIONS

Summary

The results of this simplified model show that variations in rainfall can have significant effects on crocodilians and their ecosystem. Changes in the amount of rainfall cause the populations to increase or decrease in direct relation to the rain change as shown in Figures 5, 6, 7, and 8. Changes in the timing of rainfall cause the populations to increase or decrease depending on whether the plant population is above or below average when a species reproduces, delayed one season from the rainfall pattern as shown in Figures 9 and 10 and Table 3. Changes in both the timing and amount of rainfall yield a hybrid response of those with changes in the amount and timing of rainfall separately as shown in Figures 11 and 12.

Plants are first impacted by rainfall changes because rainfall determines their carrying capacity. Next impacted are animals at the bottom of the food chain, like small mammals and amphibians because they rely directly on plants for food as shown in Figures 5, 6, 9, 10, 11, and 12. It takes time for species at the top of the food chain, like crocodilians, to be impacted because they consume many species of prey and with the predator's diet shifting based on the abundance of the prey populations, all prey populations must be quite different for these species' populations to change. This time lag is very important in the ecosystem response as it determines when species are impacted by changes in rainfall. A similar time lag between prey and predator populations has been observed in hare and lynx populations, where the lynx population follows its prey population, the hare, with a slight delay (Krebs et al., 2001). This model produces this common pattern in prey and predator populations, corroborating the results. The ecosystem is very sensitive to sudden large changes in rainfall because of this time lag. Species lower down the food chain, which are more directly impacted by the rain change, are affected before species higher up the food chain. This leads to an imbalance between predator and prey populations, which can be devastating especially when the amount of rainfall decreases.

Applications

Models, like this one, have the unique potential to explore many future climate scenarios that would otherwise be impossible with field studies. More models need to be developed and validated to prepare for climate change effects on ecosystems.

Extreme and chaotic variations in rainfall are probable in the near future (Walsh et al., 2014). Crocodilians and their ecosystems are apt to be adversely affected by climate change and its effects on rainfall patterns. Chaotic rainfall patterns will likely cause their ecosystems to become unstable because the ecosystem is sensitive to sudden changes in rainfall. Extreme

periods of drought would be harmful to crocodilians because as large predators they are greatly affected by extended periods of low rainfall.

The effects of climate change have the potential to be disastrous for crocodilians and their ecosystems. It is important to slow or prevent climate change before ecosystems are destroyed and biodiversity is lost. Additionally, it is important to prepare for the coming disruption that ecosystems face from climate change by developing and testing management programs to protect ecosystems from becoming unstable due to abnormal rainfall patterns. Proper management response will become increasingly important as rainfall patterns are projected to become more extreme and chaotic.

From the results of this experiment, management recommendations were developed (Figure 13) indicating how human interactions can help the ecosystem respond to variations in rainfall. In general, it is important to monitor rainfall patterns and keep track of how they compare to a region's norms. The management plan gives recommendations based on how the rainfall pattern varies from normal, using management actions such as hunting, water conservation, and captive release of farm raised individuals to aid the populations. For example, if the timing of rainfall is changed so that rainfall peaks in winter, the recommendations are to aid the plant populations with reduced grazing and logging to keep their populations from decreasing overall, increase farm release of birds, amphibians, crustaceans, fish, small mammals, reptiles, and crocodilians, species that reproduce when the plant populations are low, maintain hunting levels so predator populations do not get out of proportion with prey populations, and conserve water in spring and summer to reduce the seasonal variation in the plant populations. The practices outlined in these management recommendations have the potential to help keep the crocodilian ecosystem stable face of changing rainfall patterns. More research, though, is needed to create species specific management recommendations and to determine the efficacy of the recommendations presented here. Modeling techniques can help prepare management programs for future threats and may prove quite valuable in protecting crocodilians and all creatures from climate change because a management program can already in place allowing efforts to aid the populations to begin immediately after unusual rainfall patterns are observed.

Future Directions

The results of a model must be interpreted with regards to the assumptions of the model (Gotelli, 2008). This model represents a generalized crocodilian ecosystem including broad classes of prey with the goal of understanding generally how crocodilians are affected by variations in rainfall. Models for specific crocodilian species and ecosystems should be developed to more accurately represent a system and get more detailed management insights. A major assumption of this model is that rainfall only affects the ecosystem through the plant populations. In reality, rainfall also affects the quality and quantity of freshwater habitats and crocodilian nesting success (Eversole et al., 2013; Grigg and Kirshner, 2015). The effects of rainfall on aquatic habitat should be accounted for in the model. For example, if water levels were decreased, aquatic species would have a lower carrying capacity. This model also assumes that species do not adapt in response to changes in rainfall. In the future, this model should also include species adaptations; for example, plant species becoming more drought resis-

tant or animal species changing their timing of reproduction. These additions to the model would allow for a better understanding of all the effects of variations in rainfall and should be accounted for when designing management programs. Field studies and theoretical techniques should be combined to design and validate models. Data from the field such as how rainfall affects species, what factors most significantly affect species reproduction rates, and the ratio of populations between trophic levels, can improve the accuracy of models and highlight important variables to include. Additionally, accurate population data from all species in the ecosystem should be collected over many years and be used to further validate the model. Conservation is a pressing issue that should be addressed using all tools available by combining field work and modeling.

AUTHOR INFORMATION

Corresponding Author

*Karin Ebey, 47gharials@gmail.com

ACKNOWLEDGMENT

I thank Rosalyn Rael for mentoring me and assisting me with editing. I thank my mother for assisting me with editing. I thank my teacher Ms. Meyer for being my sponsor.

REFERENCES

Chabreck, R. Methods of Determining the Size and Composition of Alligator Populations in Louisiana. *Proc. Southeastern Game and Fish Comm. Conf.* **1966**, 20:105-112, https://www.rwrefuge.com/uploads/4/9/4/2/49423019/chabreck_1966-_size_and_composition_of_alligator_populations.pdf.

Cornell University. All About Birds: Great Blue Heron. 2017, www.allaboutbirds.org/guide/Great_Blue_Heron/overview#.

Davis, S. and Fromme, D. Scheduling Irrigation for Agronomic Crops Using Estimation Methods. LSU Ag Center, 2016, https://www.lsuagcenter.com/profiles/aiverson/articles/page1475509152276.

Delany, M.; Woodward, A.; Kiltie, R.; Moore, C. Mortality of Alligators Attributed to Cannibalism. *Herpetologica*. **2011**, 67(2), p. 174-185.

Dunover, L. Kentucky Critter Files: Kentucky Crayfish. University of Kentucky Entomology, 2016, www.uky.edu/Ag/CritterFiles/casefile/relatives/crayfish/crayfish.htm.

Eversole, C.; Henke, S.; Powell, R.; Janik, L. Effect of Drought on Clutch Size and Hatchling Production of American Alligators in Texas. *Herpetological Conservation and Biology*. **2013**, 8(3): 756-763.

Gonzalez, E.; Martinez-Lopez, M.; Morales-Garduza, M.; Garcia-Morales, R.; Charruau, P.; Gallardo-Cruz, J. The sex-determination pattern in crocodilians: A systematic review of three decades of research. *Journal of Animal Ecology*. **2019**.

Good, S.; Morre, G.; Miralles, D. A Mesic Maximum in Biological Water Use Demarcates Biome Sensitivity to Aridity Shifts. *Nature Ecology and Evolution.* **2017**. Vol 1:1883-1888.

Gotelli, N. *A Primer of Ecology;* Sinauer Associates: Sunderland, MA, 2008.

Grigg, G. and Kirshner, D. *Biology and Evolution of Crocodylians;* Cornell University Press: Ithaca, NY, 2015.

Indiana Division of Fish and Wildlife. Animal Information Series: Crappies (Pomoxis). 2012, www.in.gov/dnr/fishwild/files/fw-crappies.pdf.

Krebs, C.; Boonstra, R.; Boutin, S.; Sinclair, A.R.E. What Drives the 10-year Cycle of Snowshoe Hares? The ten-year cycle of snowshoe hares—one of the most striking features of the boreal forest—is a product of the interaction between predation and food supplies, as large-scale experiments in the yukon have demonstrated. *BioScience*. **2001**, 51(1): 25-35, https://doi.org/10.1641/0006-3568(2001)051[0025:WDTYCO]2.0.CO;2.

Lance, V.; Elsey, R.; Butterstein, G.; Trosclair, P.; Merchant, M. The Effects of Hurricane Rita and Subsequent Drought on Alligators in Southwest Louisiana. *Journal of Experimental Zoology.* **2010**, 313A:106-113.

Lee, E. Eastern Cottontail Rabbit. Pennsylvania State University, 2013, www.psu.edu/dept/nkbiology/naturetrail/speciespages/cottontail.htm.

Louisiana Department of Wildlife and Fisheries. Louisiana's Alligator Management Program 2018-2019 Annual Report. 2019, www.wlf.louisiana.gov/assets/Resources/Publications/Alligator/2018 -2019_Alligator_Annual_Report.pdf.

Mitchell, J. Barking Treefrog. *Amphibia Web,* University of California, 2019, amphibiaweb.org/species/808.

Nagy, K.; Girard I.; Brown, T. Energetics of Free Ranging Mammals, Reptiles, and Birds. *Annual Review of Nutrition*. **1999**.

National Aeronautics and Space Administration. Climate Change. *Precipitation Measurement Missions,* 2019, pmm.nasa.gov/science/climate-change.

National Centers for Environmental Information and National Oceanic and Atmospheric Administration. Climate Data Online. 2019, www.ncdc.noaa.gov/cdo-web/datasets#GSOM.

National Geographic. Food Web. *Resource Library Encyclopedia Entry*, 2019 www.nationalgeographic.org/encyclopedia/food-web/.

National Park Service. Black Bears. 2016, www.nps.gov/subjects/bears/black-bears.htm.

National Weather Service and National Oceanic and Atmospheric Administration. Climate Information: Lake Charles, Louisiana. www.weather.gov/lch/KLCH.

Orsenigo, S.; et al. Some like it hot and some like it cold, but not too much: plant responses to climate extremes. *Plant Ecology*. **2014**, 215(7).

Snallshire, D. and Swash, A. Life Cycle and Biology. British Dragonfly Society, 2014 british-dragonflies.org.uk/content/life-cycle-and-biology/.

Somaweera, R.; et al., The Ecological Importance of Crocodylians: Towards Evidence Based Justification for their Conservation. *Biological Reviews.* **2020**.

Stevenson, Colin. *Crocodiles of the World;* New Holland Publishers: London, U.K., 2019.

University of California. Landscape Water Conservation and Irrigation Management. University of California Center for Landscape and Urban Horticulture. Department of Agriculture and Natural Resources, 2019, ucanr.edu/sites/UrbanHort/Water_Use_of_Turfgrass_and_Landscape_Plant_Materials.

USGCRP. Groffman, P. M., P. Kareiva, S. Carter, N. B. Grimm, J. Lawler, M. Mack, V. Matzek, and H. Tallis. *Ch. 8: Ecosystems, Biodiversity, and Ecosystem Services. Climate Change Impacts in the United States: The Third National Climate Assessment*. J. M. Melillo, Terese (T.C.) Richmond, and G. W. Yohe, Eds., U.S. Global Change Research Program, 200-201, **2014**.

USGCRP. *Climate Science Special Report: Fourth National Climate Assessment, Volume I.* Chapter 1, "Our Globally Changing Climate". Wuebbles, D.J., D.W. Fahey, K.A. Hibbard, D.J. Dokken, B.C. Stewart, and T.K. Maycock (eds.). U.S. Global Change Research Program, **2017**, doi: 10.7930/J0J964J6. https://science2017.globalchange.gov.

Walsh, J.; Wuebbles, D.; et al. *Our Changing Climate.* "Precipitation Change." *National Climate Assessment,* **2014**, nca2014.globalchange.gov/report/our-changing-climate/precipitation-change.

Wilson, J. D. Glossy Crayfish Snake. Savannah River Ecology Laboratory, University of Georgia, 2019, srelherp.uga.edu/snakes/regrig.htm.

Zeppel, M.; Wilks, J.; Lewis, J. Impacts of extreme precipitation and Seasonal changes in precipitation on plants. *Biogeosciences*. **2014**, 11:3083-3093, doi.org/10.5194/bg-11-3083-2014.

APPENDIX-MODEL EQUATIONS

For the model created in this experiment, a novel adaptation of the Lotka-Volterra model, the base predator-prey interaction model, was used. Each month the populations are impacted by rainfall, predator-prey interaction, and reproduction. Energy enters the ecosystem only through plant growth which is dependent rainfall. Rainfall only affects the ecosystem through the plant populations. The equations used in the model are described here with the variables used defined in Table A-1.

Variable	Definition	Variable	Definition
P (Name)	Population of Name Plants-pl; Prey-vt; Predators-me	CO	Conversion Coefficient
D	Plant Death Rate	DF	Percent of Predator's Diet Prey Species Fulfills
RN	Rain Needed by Plant Species	M	Mass of Individual
RR	Rain Received	Q	Reproductive Rate
G	Plant Growth Rate	X	Percent of Population Reproducing
RA	Rainfall Average	CC	Prey Determined Carrying Capacity
CU	Consumption Rate	H	Hatch Rate
F	Feeding Limit	A	Aging Rate

Table A-1. Variables used in the model equations in order of use.

Rainfall Effects on Plants

Plants die if the rainfall varies from their water needs, whether there is too little or too much rain as shown in Equation 1 (Good et al., 2017). Plants die at a higher rate when there is too little rain than when there is too much rain. The amount of plant deaths is directly proportional to the difference between the amount of rain received and the amount of rain needed.

$$P(pl) = P(pl) - \left(D * P(pl) * \left(\frac{|RN-RR|}{RN}\right)\right) \quad (1)$$

Rainfall also affects plant growth, their reproduction, which occurs every month. Plant growth is modeled using the logistic growth equation, where exponential growth is limited by a carrying capacity (Gotelli, 2008). Plant growth is governed by a growth rate and a carrying capacity, both depend on the amount of rainfall as shown in Equation 2. The base growth rate varies seasonally as shown in Table 2 (Orsenigo et. al, 2014), but is also dependent on the current month's rainfall. There is a set minimum growth rate when there is no rainfall, but with rainfall the growth rate increases steadily until the rainfall is about 1.5 times the plants' water needs, where it levels off (Good et al., 2017). This was modeled using a variation of the exponential function, e^{-x}. The carrying capacity (the last term in Equation 2) limits the actual

amount of plant growth based on the previous season's rainfall. The carrying capacity has a set minimum of $10^{7.6}$ kilograms of plant matter when there is no rainfall. A rainfall average is calculated in each of the four seasons and is compared to the water needs of the plant species. This value is used to determine the next season's carrying capacity.

$$P(pl) = P(pl) + P(pl) * G * \left(1 - \left(e^{-2*\left(0.05+\frac{RR}{RN}\right)}\right)\right) * \left(1 - \frac{P(pl)}{10^{7.6+0.4*\frac{RA}{RN}}}\right) \quad (2)$$

Predator Prey Interactions

Each month, predator and prey populations interact with one another as shown in Figure 1, resulting in consumption and starvation deaths. In consumption, prey die from being consumed by predators as shown in Equation 3. In starvation, the predators die in proportion to the fraction of their energy requirements that are not met as shown in Equation 4, where all predators automatically die to represent the scenario if no prey is consumed with individuals added back to the population, do not die, for every unit of prey consumed. These processes are described with three parameters: consumption rate, conversion rate, and feeding limit; each interaction has a unique set of parameters (Gotelli, 2008). The consumption rate limits the amount of prey consumed based on the time required for the predator to capture the prey. The conversion coefficient defines the amount of prey that must be consumed by individual predators so they do not die of starvation. The feeding limit defines the maximum amount of prey the predators consume based on their energy needs.

$$P(vt) = P(vt) - \Sigma\left(\frac{P(vt)*P(me)*CU}{1+P(vt)*CU*F}\right) \quad (3)$$

$$P(me) = P(me) - P(me) + \Sigma\left(\frac{CO*P(vt)*P(me)*CU}{1+P(vt)*CU*F}\right) \quad (4)$$

The feeding limits were calculated each month by determining the amount of prey the predators need to consume based on their energy requirements as shown in Table 1. Many of the predators consume multiple species of prey, so their energy requirements are split among their prey species using a dynamic approach, assuming that predators do not have food preferences. The proportion of a predator's energy requirements that a certain prey species fulfills varies each month based on their relative abundance to the other prey species. The relative abundance of prey species is determined by comparing the total mass of a specific prey species to the total mass of all prey species for that predator as shown in Equation 5. The feeding limit for the specific predator and prey interaction is determined by multiplying the proportion of the energy requirements that the prey species fulfills with the total feeding limit.

$$DF = \frac{P(vt)*M}{\Sigma\, P(vt)*M} \quad (5)$$

Animal Reproduction

Animal reproduction occurs in certain months for each species as shown in Table 2. Animal reproduction is modeled using the logistic growth equation, where exponential growth is limited by the resources in the system as shown in Equation 6 (Gotelli, 2008). In Equation 6, the population is multiplied by one half because only the females reproduce. For species that reproduce over several months, like amphibians, the population used is from the first month of their reproductive season because hatchlings are not reproductively mature. The reproductive rate, shown in Table 1, is the number of young per adult female, without limitations on population growth. The population growth is then limited by a carrying capacity based on the prey populations as shown in Equation 7, where the prey populations are multiplied by the conversion rate to determine how many predators can be sustained, the proportion of the predator's diet that prey species fulfills, and 0.2 because reproduction requires more energy than survival. The hatch rate, shown in Table 1, determines how many of the young are successfully added to the population depending on a species parental care habits.

$$P = P + Q * P * 0.5 * X * \left(1 - \frac{P}{CC}\right) * H \tag{6}$$

$$CC = \Sigma(CO * P(vt) * DF * 0.2) \tag{7}$$

Crocodilian Aging

Once a year the crocodilians age where small portion of each size class moves up to the next one. Aging is limited by the amount of prey in the system, and because growth requires more energy than what is needed to survive, aging is limited further than reproduction as shown in Equation 8.

$$P(aged) = P * A * \left(1 - \left(\frac{P}{0.01 * CC}\right)\right) \tag{8}$$

Engineering a Desiccant-Driven ($CaCL_2$) Self-Contained Solar Distillation System to Collect Drinking Water from the Atmosphere

*Ryan S. Helmer**

Jefferson Montessori Academy, Carlsbad, NM

ABSTRACT

Fresh water accounts for 2.5% of the planet's water, and the UN's estimated 7.7 billion people on Earth are taxing that supply. With 3,100 cubic miles of freshwater vapor trapped in the atmosphere, a desiccant-driven solar distillation system may be a viable solution to a crisis in areas with limited water sources. An octahedron-shaped solar distillation system was designed and built using impact-resistant polycarbonate and stainless steel and tested in 45–100 ºF temperatures under diverse weather conditions. Calcium Chloride absorbed ambient water vapor then the still utilized solar energy to help regenerate the $CaCl_2$ by forcing it to release the water through solar distillation. The design eliminated the traditional trough system and was managed by one person. While productivity was dependent on climatic conditions, the still could produce 6.5 ounces with external temperatures above 85 ºF. External temperatures below 60 ºF produced measurable water of 2.5+ oz with full sun exposure. The predominant factor contributing to higher water collections was the amount of solar exposure on any given day. Insulation of the stainless steel base and black cloth substrates allowed for internal temperatures above 110 ºF on mid–60 ºF cold weather days.

KEYWORDS: Desiccant Water Production, Solar Distillation System, Water Distillation using Calcium Chloride, Drinking Water Solutions, Water Sourcing with Desiccants, Engineered Water Collection

INTRODUCTION

For millions of years, the amount of freshwater on our planet has remained much the same. The earth's hydrologic cycle has continuously moved that water through a cycle of evaporation and precipitation again and again. Yet as global populations rise, humans are finding themselves in a drinking water crisis that is becoming a race for survival. With freshwater accounting for only about 2.5% of the water on our planet, the 7.7 billion people on earth, as estimated by the U.N. World Population Prospect (2019), are taxing this water source.

While for much of the current population, this crisis is not a concern, for others, it is a devastating reality. The U.N.'s 2030 Agenda goal SDG6 that sets a goal of ensuring available and sustainable management of drinking water is not close to being on track (U.N., 2015). We need drinking water to survive. According to the Geneva Sphere Project (2004), in emergency situations, the human body needs 2.5 – 3 liters of drinking water a day depending on climate and individual physiology.

It is necessary to understand how global freshwater is used and how that use has changed. Freshwater withdrawals globally are estimated by the United Nations at 69% agriculture, 19% industry, and 12% municipal (Aquastat, 2014). At the same time, global diets are changing from starchy foods to more meat and dairy, and those foods require more water. The *Water Footprint Assessment Manual* (Hoekstra et al., 2011) details that producing 1 kg of rice requires 3,500 liters of water, while 1 kg of beef uses about 15,000 liters. Even a cup of coffee requires 140 liters overall to produce.

Beyond dietary shifts that are expected to continue, the climate changes we are experiencing are adding to the crisis. NASA's Gravity Recovery and Climate Experiment, GRACE, tracked the movement of freshwater around the globe from 2002 to 2016 (NASA, 2018). The data showed the wet climates are getting wetter and dry climates are losing groundwater creating global hotspots that are expanding.

Safely managed drinking water services are still only available to about 71% of the global population, with the average for rural areas being only 53%, according to UNICEF (2019). Uganda, and other highly rural under-developed countries, ranked as low as 7% coverage. While solutions have been proposed to resolve the inequalities of poor drinking water access in rural, arid climates, one answer may rest in finding ways for individuals to be responsible for their supply.

In coastal regions, water collection is being attempted through fog harvesting, but it is regionally limited. Solar stills for brine and brackish water distillation are certainly an option. These types of stills have been used for hundreds of years, dating back to the 16th century in the Middle East. In 1872, a Swedish engineer, C. Wilson, designed and built the first solar distillation plant in Chile at a saltpeter mine. Using the mine's effluents, fresh drinking water was distilled to supply drinking water to the mining community (Kalogirou, 2009). This type of highly concentrated brine solution distillation indicates that water can be pulled from solutions under the right conditions.

Problem

Can this process be taken one step further and applied to arid climates where water sources are not available? The answer is yes. In areas of groundwater scarcity, there is still atmospheric water vapor that can be accessed. The problem is how to access it. The volume of water in our atmosphere is about 3,100 cubic miles, or enough to cover the ground with approximately 2.5 in. of water if it all rained down at once (Gleick, 1996). That water just needs to be collected.

In 2017, MIT started developing a high surface area material called metal-organic frameworks (MOFs) that can extract potable water from desert air. According to one of the developers, O. Yaghi, the cost of the process has yet to be determined (Chandler, 2017). Similar to this laboratory-created compound, there are other readily producible hygroscopic materials. Desiccants like $CaCl_2$ provide a natural way to absorb water vapor.

Previous student experimentation on this project has concluded that $CaCl_2$ is among one of the most effective non-toxic, food-grade desiccants for use in solar still freshwater production. Prior year's experimentation also showed that by increasing surface area of a specific

volume of $CaCl_2$ solution increased the amount of water vapor absorbed, resulting in higher distillation yields. William and colleagues at the University of Egypt have shown successful results using $CaCl_2$; however, the tests for this study were selected, non-continuous test days, so consistent success was not recorded (William et al., 2015).

While solar distillation of brine or brackish water may help solve the drinking water solutions to people with access to those sources, this is not a viable solution for a large percentage of the global population. In June 2019, the World Health Organization estimated 785 million people lacked fundamental drinking water sources (WHO, 2019). This service is defined as a 30-minute round trip to collect water. When there is no fresh groundwater source available—even one that is contaminated source—there is still a need to find a simple method of supplying drinking water. With over 3,100 cubic miles of freshwater trapped in vapor in our atmosphere (Gleick, 1996), it may be possible to tap into that source. Redesigning a solar distillation container that will provide safe drinking water using a readily available desiccant, such as $CaCl_2$, is a solution that needs to be explored.

Criteria

The design criteria were developed over the last two years of desiccant type and surface area studies and was based off of previous problems and goals. The criteria determined for creating a successful prototype were defined in the following:

- The solution should provide a distillation system that requires minimal daily maintenance.
- Water collection should be a simple 2-step method of water collection: 1) absorption of water vapor by the calcium chloride and, 2) release of the water through solar distillation.
- Distillation system should be able to be operated by one person.
- The still should rely on solar energy, with no requirements for electricity, so that the availability to low-income communities is possible.
- Materials used to build the prototype should resist damage from different weather conditions, including rain, wind, and extreme heat.
- Materials used in construction should be affordable and readily available.
- The $CaCl_2$ desiccant must be contained inside the still but separate from collected, distilled water to avoid contamination.
- The surfaces in contact with distilled water must not be toxic to humans or cause distilled water to be contaminated.
- The design should reach consistent daily collection measurement levels with the understanding that weather is still a constraint.

Constraints

While experimenting with Calcium Chloride absorption and regeneration using solar energy, several constraints had become apparent. While taking in the design criteria stated above, constraints considered in the design and build included:

- Weather change—temperature, humidity, wind—is the most critical constraint as it will directly affect water condensation and collection.
- The collected distilled water must pass drinking water testing, including pH, alkalinity, and hardness.
- Accessibility and affordability of materials needed needs to be considered as the prototype has the potential to be needed globally.
- $CaCl_2$ is corrosive to metals, so while it will be housed inside the solar still, it requires safe container considerations.

MATERIALS AND METHODS

Desiccant Selection

Distillation is a simple process that can be used to purify water. It uses a heat source to evaporate water and separate that water from dissolved matter. In solar distillation, the energy used is heat from the sun. The engineering of a solar distillation unit that utilizes a powerful desiccant, however, requires a firm understanding of not only $CaCl_2$ but the materials that will house the chemical.

Calcium Chloride is hygroscopic and able to attract and hold water molecules from the surrounding environment. $CaCl_2$ is a deliquescent substance, meaning when it is exposed to air, it rapidly absorbs the surrounding water vapor and tends to become a liquid. It can absorb several times its weight in ideal conditions and will eventually dissolve its crystal lattice in water. For example, at 85 °F and 22% relative humidity—a mild, arid summer climate—solid $CaCl_2$ will absorb enough water vapor to liquefy. During a period of 70% humidity and 77 °F temperatures, 1 lb of $CaCl_2$ can absorb 2.5 lb of water vapor. These numbers are based on studies completed by multiple chemical companies that manufacture $CaCl_2$ (Occidental Chemical).

Surface tension was an important factor in choosing this desiccant. Surface tension acts as a barrier or wall on a liquid's surface. When Calcium Chloride has absorbed enough water vapor to liquify, its surface tension decreases as temperature increases. Water molecule movement in and out of the solution is related to viscosity. Once solid $CaCl_2$ liquifies with water, it is a solution, and that solution has a thickness and strength to hold itself together (viscosity) on a molecular level (Occidental Chemical).

However, as temperatures increase, $CaCl_2$ solution viscosity decreases and allows more molecular movement. So, as the molecules in the solution become agitated from a temperature increase, it should be easier to pull water from the solution. Regeneration of the desiccant can be done in temperatures as low as 116.6 °F (Bouzenada et al., 2013). Its non-toxic

and food-safe properties make $CaCl_2$ a useful component. Caution, however, must be noted with $CaCl_2$ as it is highly corrosive to metals.

Still Design

There have been decades of study regarding solar distillation designs. The most common still design is a single basin with a sloping glass condensation panel, as illustrated in Figure 1. The single basin is coated in dark material for absorption of heat and holds brine or brackish water at the same time. The single condensation panel, however, prevents full exposure of the sun unless the still is moved repeatedly to follow the sun as it travels across the sky.

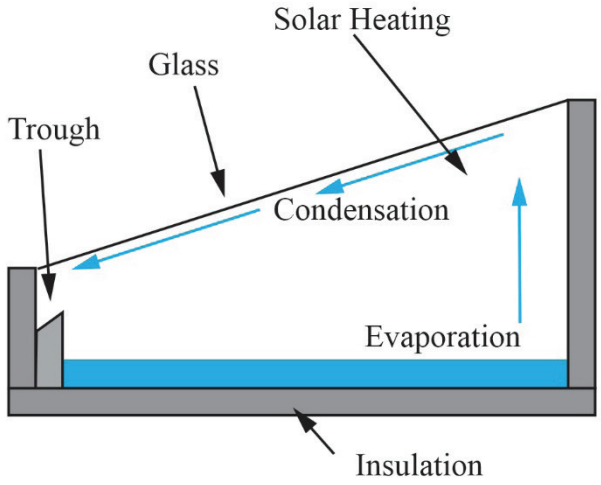

Figure 1. Diagram of a single basin solar still with sloping glass condensation panel.

Double basin, spherical, hemispherical, tubular, pyramid, and concentrator coupled single basin solar stills have been studied by engineers for productivity. In a 2012 article published in the International Scholarly Research Notices (Arunkumar et al., 2012), engineers concluded that concentrators coupled with stills offering higher condensation areas were more productive. The angle of the condensation panels is also an important consideration of the design. An Egyptian study of condensation panel angles—tested from 30° to 50°—published at the 2016 7th International Renewable Energy Congress showed promising increases of up to 40% in distillate accumulation at lower panel angles (Kabeel et al., 2016). The experimental study was completed in Tanta City, Egypt, a similar latitude as this project's testing location.

It was determined that the design of the distillation system would utilize a combination of successful still features—materials, shape, angles—that would provide the best measurable water collection. Successful still elements included large condensation surface areas, materials that withstood the elements, and shapes that increased solar heating. As a result, in order to increase the condensation surfaces, a square-based pyramid was built for the still top, with the four pyramid side panels of the top of the still angled within the successful 30° to 50° panel angles of other researched studies.

Condensation panel materials in solar stills have long been a topic of debate. While everything from plastic bags to hard plastics to glass has been used, the need for a material that is nearly impervious to weather conditions is essential. Polycarbonate, often called Lexan, has about 200x the impact resistance of glass and is 30x stronger than acrylic. Acrylic is 17x more impact resistant than glass. Both plastics are 50% lighter than glass. Polycarbonate offers greater insulation capabilities than glass and still allows 89% light transmission. Acrylic, on the other hand, offers 92% light transmission (Hydrosight GmbH). Both polycarbonate and acrylic are more chip-resistant than glass, but polycarbonate is nearly indestructible and is

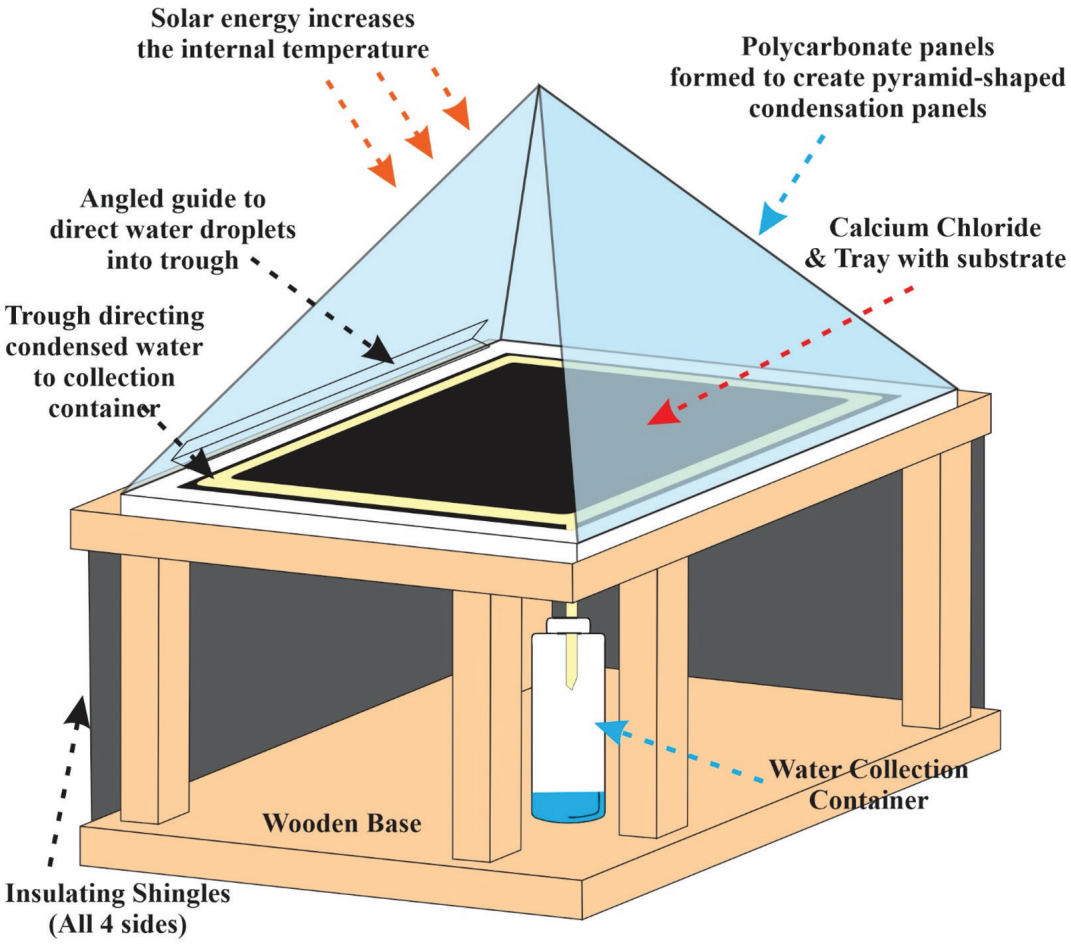

Figure 2. Diagram of Prototype 1 using a flat basin and angled troughs for water collection from the polycarbonate condensation panels.

used in thick panels as bulletproof protection. The strength of polycarbonate comes with a price or 2-3 times that of acrylic. The deciding advantage that polycarbonate has over acrylic is polycarbonate's continuous working temperature is 240 °F, which is much better that acrylic's 130 °F (A & C Plastics Inc.).

Attempts were made to minimize the need to use metal materials in this solar distillation system for two reasons: $CaCl_2$ corrosion and galvanic corrosion. Corrosion in traditional solar stills is a common issue due to the high sodium content of brackish and saltwater. $CaCl_2$ is an inorganic salt compound, and also highly corrosive to metals. Galvanic corrosion is the result of an electrochemical reaction that can occur when one anode and one cathode metals are used in conjunction with an electrolyte such as water. As the electrolyte passes from one metal to another, the anode can lose electrons to the cathode, causing the anode metal to disintegrate or corrode (Avenston LLC). That corrosion can create acidic water, rendering a still's collection non-drinkable.

Figure 2 represents the initial prototype design. The footprint of the still measured about 35 sq. inches. The base of the solar still was designed using plastics to eliminate corrosive issues while it housed the $CaCl_2$. The trough system was a traditional water collection plan, except it was also limited to plastics. To record internal temperatures without opening the condensa-

tion top, a digital temperature probe was permanently hung midway between the peak of the pyramid top and the $CaCl_2$. Appendix A provides photos of the build.

Once the prototype was built, it was placed into daily operation. Anhydrous $CaCl_2$ was loaded into the basin and given five days of exposure to the air to bring it to a solution using only water vapor. A single testing period began at 8:00 p.m. each day with a 12-hour evening exposure phase followed by a 12-hour daily distillation phase. The flat base sides of the condensation panels were oriented to the cardinal directions so that direct exposure would begin as the sun rose. Every attempt was made to maintain continuous testing.

Daily procedures for a single test period involved the following steps:

1. 8:00 p.m. – Open the condensation top to allow for atmospheric exposure of the $CaCl_2$.
2. 8:00 a.m. – Replace the condensation top and check seal with base.
3. 12:00 p.m. – Check and record internal temperature with digital probe.
4. 3:30 p.m. – Check and record internal temperature with digital probe.
5. 7:30 p.m. – Measure distilled water in collection bottle prior to opening still for $CaCl_2$ exposure.
6. Record all measurements: water collected, daily external temperature highs, evening humidity average, and weather breakdown of cloudy, partly cloudy, or sunny as well as any observations regarding operation, design problems, ideas.

The success of the prototype was based on long-term testing periods. Once the still was operating uninterrupted for a period of five days, samples were used for water testing. While the system performed well initially, failures with the trough materials occurred once internal temperatures reached 170 °F. With the failure of the initial prototype, it was determined that material choices in the design needed to be revisited.

Prototype 2, shown in Figure 3, was built with several new changes incorporated into the distillation unit. With the failure of the trough in the original prototype, it was determined that a more streamline pyramid still should be built to eliminate the trough. To execute a trough-less still, there had to be a single, uninterrupted flow direction from the condensation panels into the collection bottle. The most apparent design was a diamond or octahedron shape using the original square pyramid shape top and an inverted pyramid-shaped top.

Food grade stainless steel was selected as the still's base material instead of galvanized steel that is used in construction. Galvanizing is the process of hot-dipping a metal in zinc to prevent corrosion. Industrial uses are varied, and while galvanized pipes are still considered safe to transport water, there is some concern with low pH waters because they are corrosive due to their acidity (APEC Water Systems). Distilled water from solar stills can test at pH levels on the lower spectrum at 5.5 to 6.0 pH. The combination of the still's internal heat and the water's acidity can potentially release higher than allowable zinc levels into the collection water, making galvanized steel an inferior choice to stainless steel.

The condensation panel configuration changed in three ways. The panel angles were created to match the latitude of the location, approximately 32°. This angle also took full

advantage of the most solar exposure to the panels during the summer months. This angle matched the latitude of the testing location and meant the panels would receive equal solar exposure when the sun was at its highest daily location during that season. The lateral edges of the panels were reinforced with metal brackets prior to sealing the edges with silicone. Finally, an aluminum right angle edge was added to the inside base edges after being coated in a non-toxic silicone sealant. This edge provided a directional flow of the water away from the base edge and onto the inverted stainless-steel base as well as providing a lip to seal in the

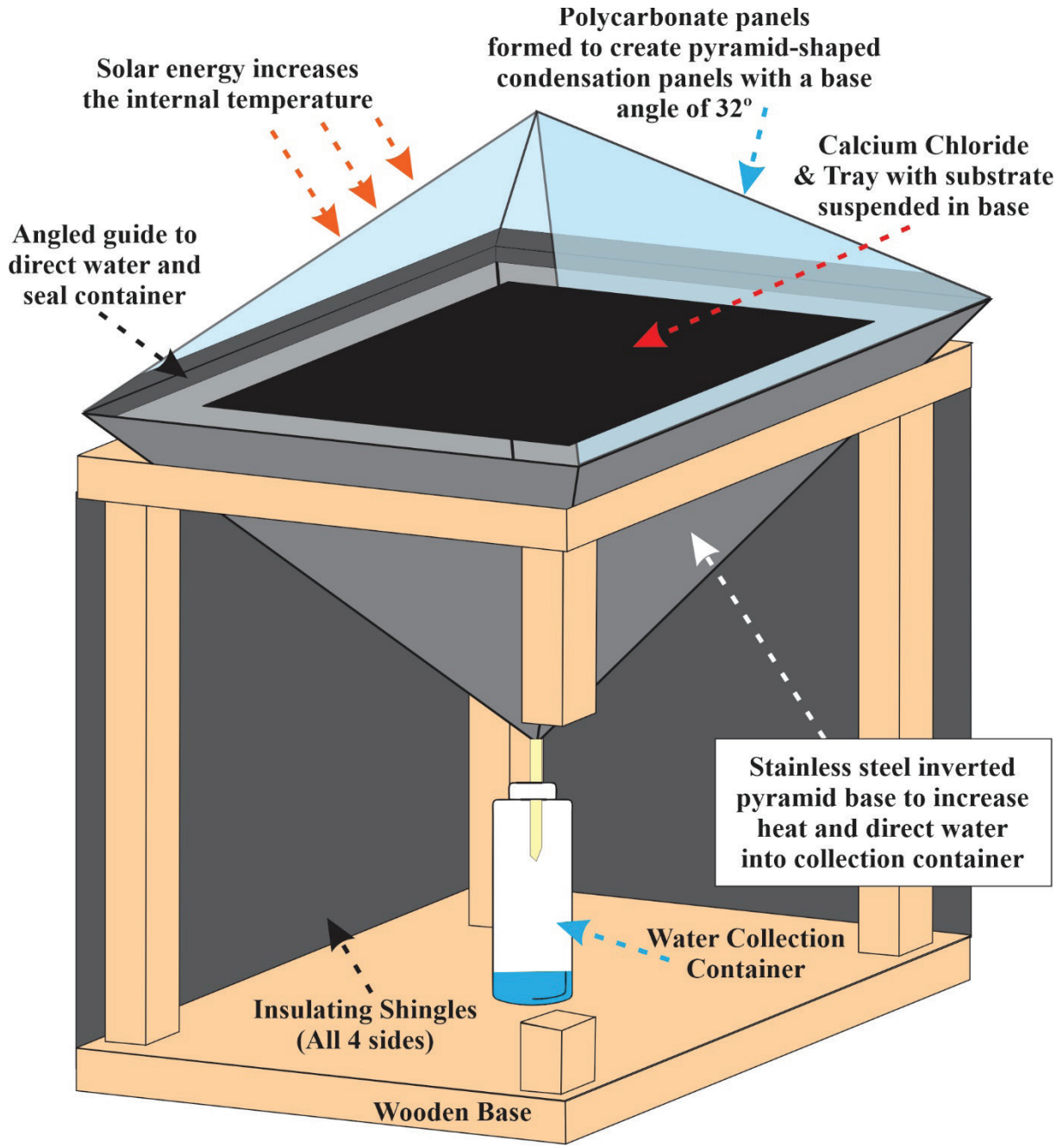

Figure 3. Diagram of Prototype 2 using polycarbonate panels for the condensation top and a stainless steel inverted base to eliminate troughs for collection and provide solar concentration for increased internal heat.

internal air during the condensation period. A thin line of waterproof/weatherproof stripping was added along the edge of the still base to prevent the two metals from contact and help maintain a closed environment in the still.

With the introduction of two metals into the design—the aluminum edge on the condensation panel and a stainless-steel base—the Calcium Chloride containment had to be redesigned. The solution was to create a suspended tray that allowed the distilled water to flow freely to the bottom of the still for collection. After several trial trays, the final 22" square tray was built from hard plastic and polycarbonate to prevent issues with $CaCl_2$ or galvanic corrosion. Additionally, the $CaCl_2$ was moved to a set of smaller food-grade containers with a similar total surface area to facilitate moving the desiccant should the still require repairs.

With the addition of asphalt panels to the base structure and R32 insulation between the still base and asphalt panels, the water collection area was protected from the elements, and the internal heat was better maintained in cooler weather. Black felt substrate in the $CaCl_2$ trays also held in heat. Appendix B provides photos of the build.

RESULTS

Prototype 2 was in operation for 79 days of testing with the closed distillation process occurring from 8:00 am to 8:00 pm. The data from the testing days was divided into three categories: SUNNY being clear skies with no clouds, PARTLY CLOUDY being clouds either half of a given day or sporadically throughout the day, and CLOUDY being total cloud cover during distillation. This division allowed for detailed understanding of the effects of internal and external temperatures, humidity, and solar radiation exposure during distillation periods. Appendix C is a full list of the raw data collected. Prototype 1 data was not included in the results or discussion.

It should be noted that when temperatures dropped below 65 ˚F at night during the water absorption period, the $CaCl_2$ began to crystalize. This required the $CaCl_2$ trays to be brought inside away from the low temperatures in order to remain in solution form and continue absorbing water molecules.

Water collection measurements consistently peaked during days with the most solar exposure except for two consecutive days—test days 10 and 11—of zero water collected. These two days immediate followed repairs. During these two days it was discovered that a series of small openings in the prototype's seals allowed temperature equalization and prevented condensation. These two days were eliminated in order not to skew averaging data, and this brought the number of test days used in the summary results down to 77 : 44 SUNNY, 21 PARTLY CLOUDY, and 12 CLOUDY test periods.

The total amount of water collected during the entire test phase was 3913 mL on SUNNY days, 534 mL on PARTLY CLOUDY days, and 378 mL on CLOUDY days. On SUNNY days this averaged to 88.9 mL—over 3 times the average of 25.4 mL collected on PARTLY CLOUDY days and 2.5 times the averaged 31.5 mL on CLOUDY days.

External daily high temperatures of 70 °F and warmer accounted for the greatest amounts

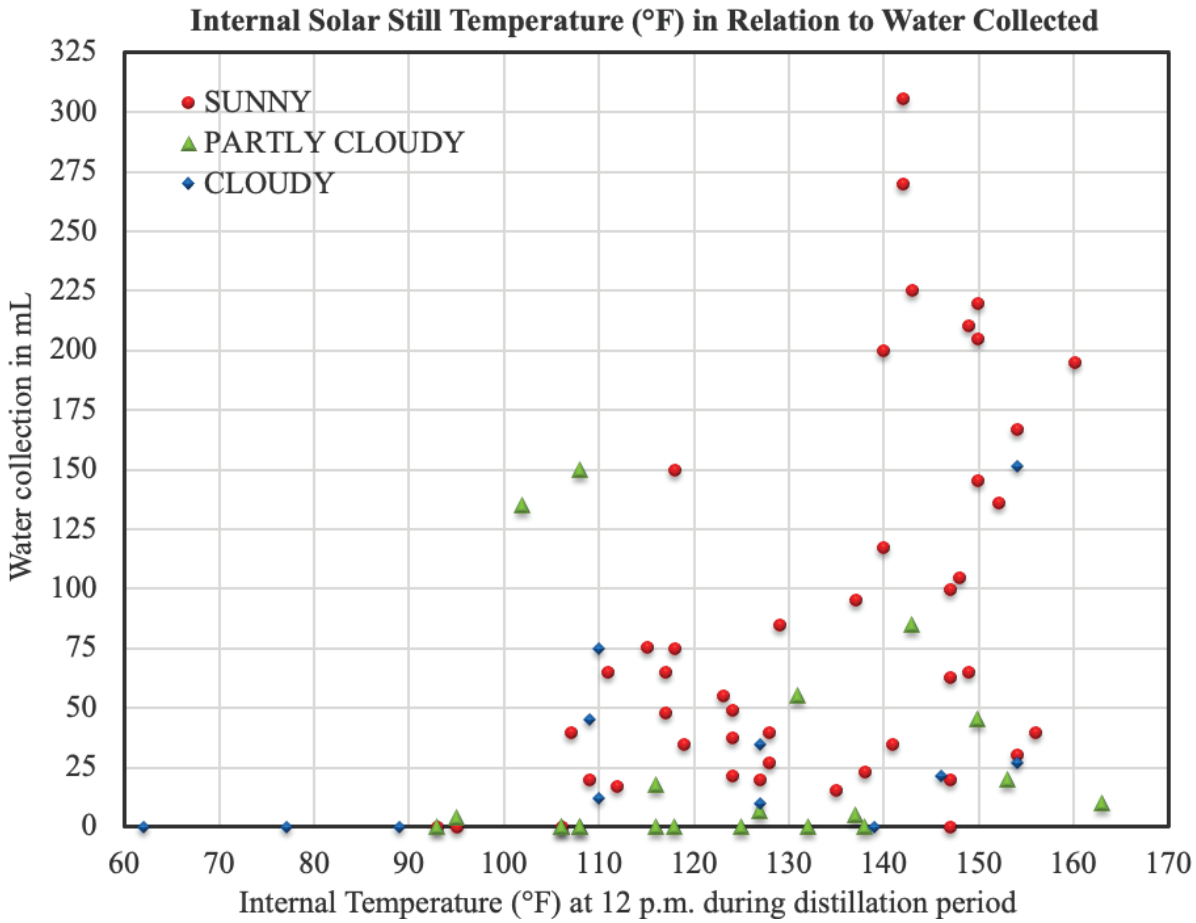

Figure 4. A comparison of daily internal still temperatures taken at noon in relation to the total water collected for that day. The graph further details the results by categorizing solar exposure.

of water collected with averages increasing to 105.5 mL during SUNNY days, 40.5 mL during PARTLY CLOUDY days, and 45.8 mL during CLOUDY days.

Internal temperatures of the solar still ranging 140 °F to 150 °F were the most productive SUNNY water collection days with an average daily amount of 142.9 mL. A comparison of PARTLY CLOUDY and CLOUDY days cannot be made as the data is not as consistent.

In addition to testing the distillation design, a 16-part drinking water test was performed on the distilled water collected in Prototype 2. The testing strips used were FDA-approved ON4HOME water test strips that included hardness, pH, Fluoride, Chlorine, Nitrate, Nitrite, and total alkalinity, as well as low range heavy metals. This test was also performed on bottled distilled water, tap water, and Aquafina bottled drinking water for comparison. The noticeable difference among the tests was the alkalinity of the tap water in comparison to the distilled, Aquafina, and Prototype 2 water which registered within normal ranges.

A second, more detailed, pH test was conducted using Med Lab Diagnostics test strips. The results showed the tap water tested at about 7.5 pH while the other samples, including the Prototype 2 distilled water, ranged from 5.5–6.0 pH. These tests were performed on multiple samples over the course of the experimental phase.

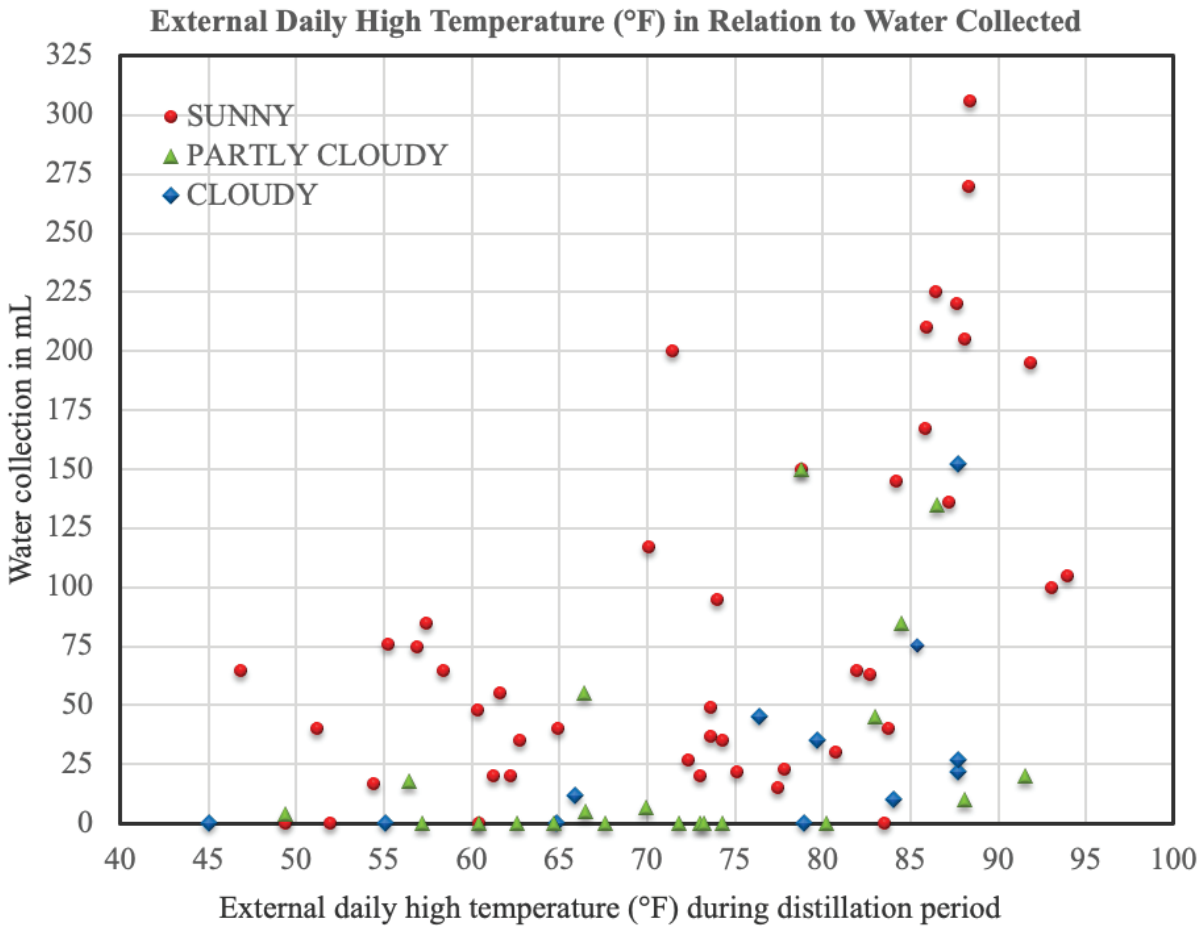

Figure 5. A comparison of daily external temperature highs in relation to the total water collected for that day. The graph further details the results by categorizing solar exposure.

Chloride is an essential electrolyte for the human body but it can also cause corrosion. Due to prototype galvanic corrosion problems that had to be solved, it was decided that a separate test would be conducted to verify that the solar distilled water collected was not picking up chloride ions. WaterWorks™ chloride test strips were used and provided a range from 0–500 ppm. Results consistently showed the samples were below the EPA secondary drinking water standard of 250 ppm.

CONCLUSIONS

The advantages of the final prototype still design were quickly apparent. The stainless steel base helped regulate the still's internal temperature because it held heat better than the plastic base and the exposed sections visible through the condensation panels doubled as a concentrator of the solar energy, directing it toward the $CaCl_2$ trays. This increase of solar energy, or heat, helped with the regeneration of the desiccant and increasing condensation. While the prototype $CaCl_2$ solar still was unable to produce the desired two liters of distilled water, there was a lot of data gathered for future designs and testing.

During testing periods with full solar exposure, sunny days, the external daily highs could

range from 70°–90 °F without dropping the internal temperature below 140 °F. At 46.8 °F and full solar exposure, the still maintained an internal temperature of 111 °F and produced 65 mL. This was not expected, but it does indicate that the still can possibly operate in a variety of regions.

Cloud coverage of any kind interfered with the distillation process, although if the cloudy cover burned off in the morning hours, production was only slightly decreased. Heavy periods of high humidity also increased the amount of water vapor absorbed and provided unusually high collection measurements the next day. This does not mean to suggest the $CaCl_2$ was compromised with rainwater. During rainy periods, a waterproof tarp was secured well over 12in from the desiccant surface to allow for water vapor absorption but not rainwater.

Since the experimental phase of this prototype was long enough to see seasonal changes and a drop in the sun's position, it was noticed that the condensation on the panel directly exposed to the sun at noon decreased as the sun's position moved lower in the sky. Whether this decreased condensation on the direct sun-facing panel can be corrected by adjusting the position of the still has yet to be tested.

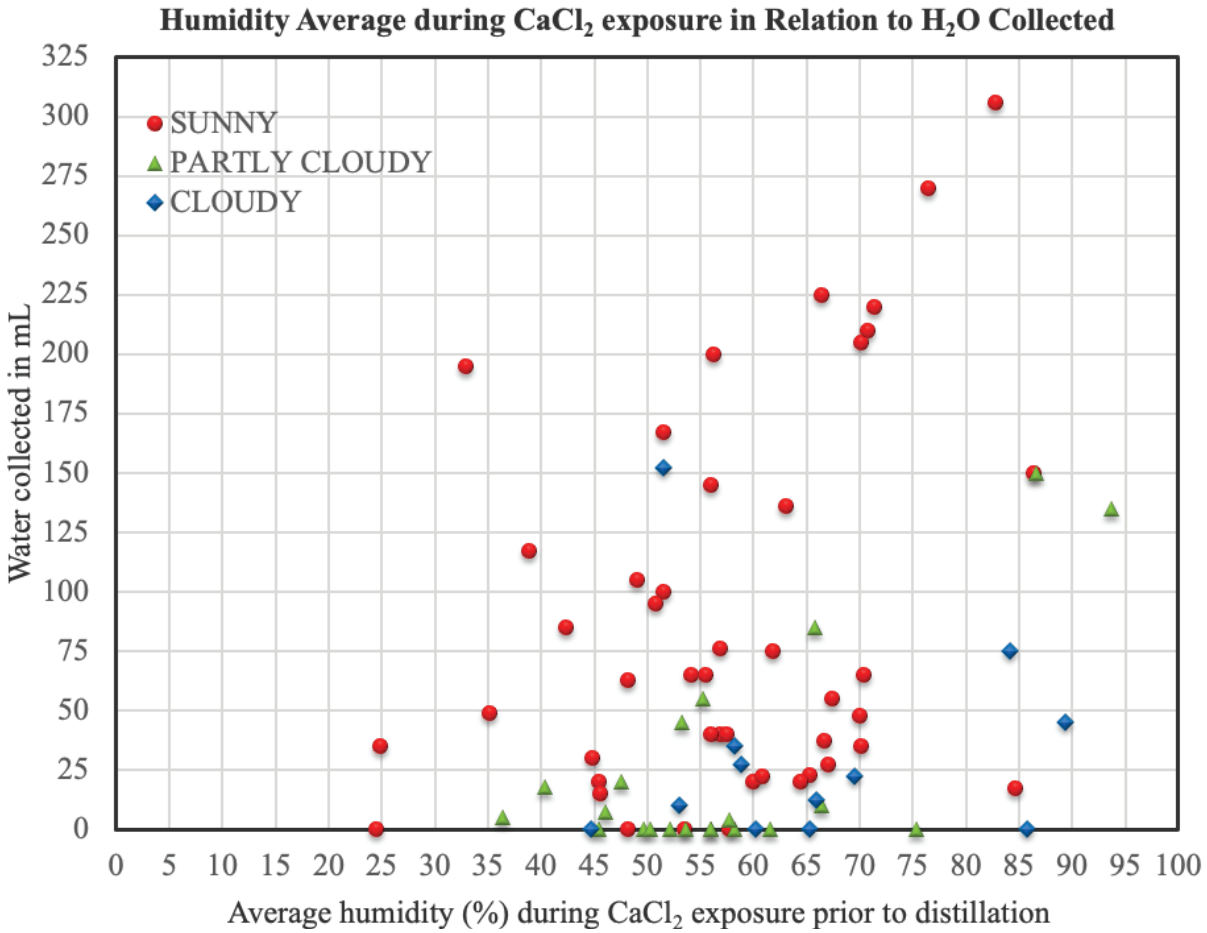

Figure 6. A comparison of average humidity readings during the night of CaCl2 air exposure prior to the condensation period (8 am to 8 pm) in relation to the total water collected for that day. The graph further details the results by categorizing solar exposure.

It also needs to be noted that as the $CaCl_2$ began to crystallize once temperatures during the absorption period dropped below about 60 °F yet was able to deliquesce to a solution within the first hour of solar exposure. The distillation process, however, was not as effective during the colder periods. Moving the desiccant to a warmer location—and allowing it to absorb water vapor—eliminated some of the problems but options need to be studied more.

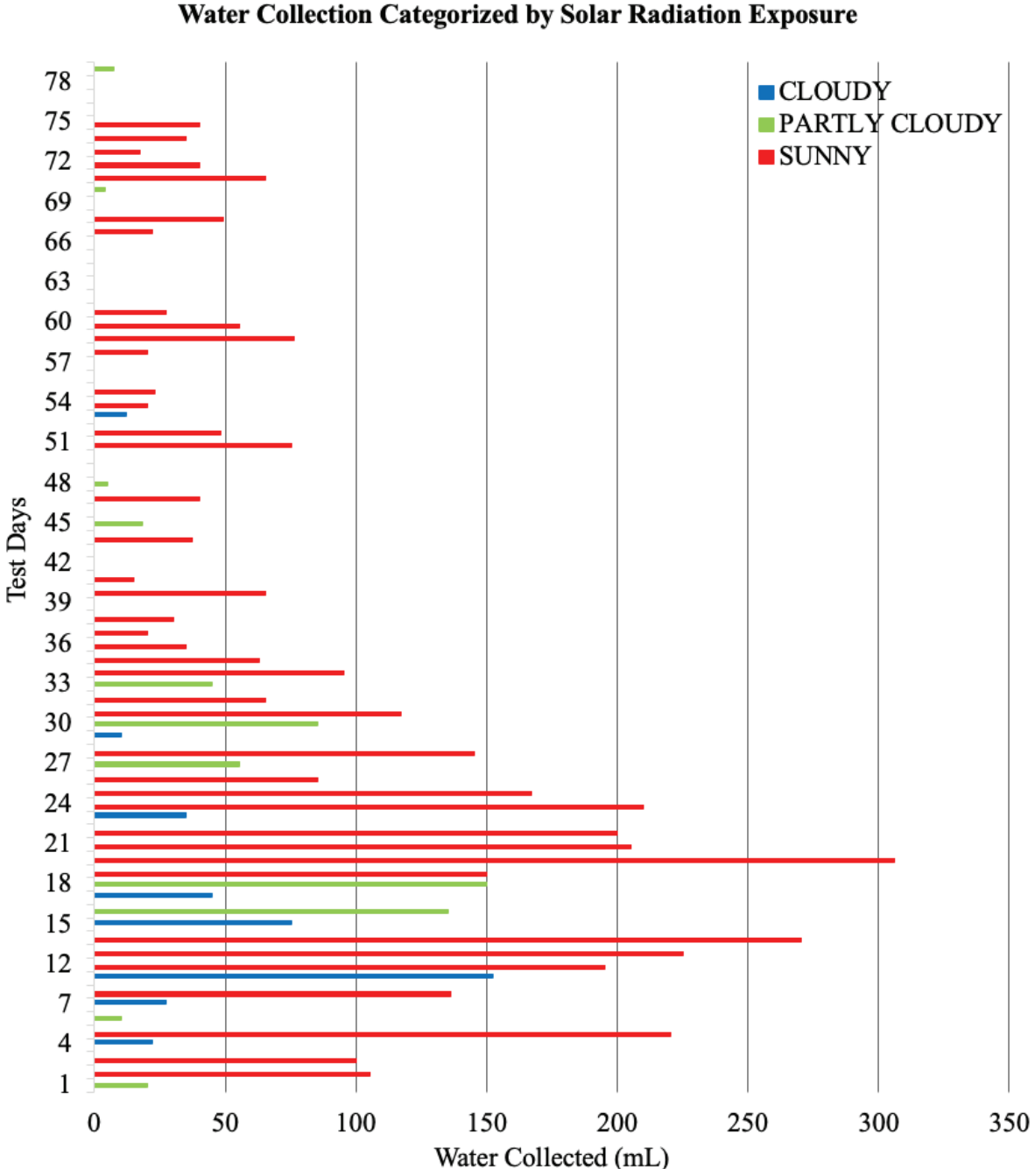

Figure 7. A chart showing daily water collection in relation to the solar exposure to show trending. This chart represents the total daily collection of distilled water as divided into the three solar exposure categories. As the daily temperatures cool, the amount of water collected decreases. It should be noted, however, that as the daily high temperatures began to drop and remain in the 50 °F to 65 °F range, the solar still remained active with full solar exposure during the distillation period. The water measurements values are also available in Appendix C.

Further Work

The ability of the condensation panels to allow solar heat energy to pass through to the inner still system is critical as without the internal heat the $CaCl_2$ will not begin the regeneration process and give up the water molecules. The polycarbonate was selected because of its durability and its insulation capabilities; however, an unexpected property of the material was discovered during the testing phase.

While cleaning the outside of the polycarbonate panels during one of the condensation test periods, it was observed that wiping a hand across the surface of the panel caused the condensed water droplets to gather together, creating larger droplets. This effect could be repeated nearly every time it was attempted. A working hypothesis may be that the polycarbonate was allowing a static charge to be conducted through the panel surface. Dry human skin, when it comes in contact with other solids, has a high tendency to give up electrons and become positive in charge (Kurtus, 2018). Water molecules are polarized molecules that arrange randomly in a liquid state, but the positive charge from the skin caused the molecules to orient the negative oxygen toward the positive charge and begin to clump. The implication of this discovery means that if a positive charge can be regularly maintained over the outer surface, the condensation inside the still will increase as the water molecules pull together. Additionally, slight vibrations on the panels increase the movement of the larger droplets downward in the still for collection, allowing more surface area for coalescing water molecules to condense on the panels. These features merit more study.

AUTHOR INFORMATION

Corresponding Author

*Ryan S. Helmer, ryanhelmer03@gmail.com

ACKNOWLEDGMENT

This project is the culmination of 3 years of experimenting and building in an effort to find a solution to drinking water using an unconventional method like $CaCl_2$, and it could not have been possible without the support of so many people. Deanna Weston-Helmer was a source of financial support for materials, acted as a project assistant to record data in an emergency, aided with the building of the prototypes when it required two people, has provided the vector graphic software and assisted with finalizing the drawings and charts, and provided structuring advice, editing, and proofreading of this paper. Kerrie Thatcher, my sponsor and science teacher, has assisted in checking my progress, helped keep me on track, and has been so incredibly encouraging for the last three years.

ABBREVIATIONS

$CaCl_2$, Calcium Chloride; F, Fahrenheit; GRACE, Gravity Recovery and Climate Experiment; NASA, National Aeronautics and Space Administration; SDG, Sustainable Development Goal; UN, United Nations; H_2O, Water; WHO, World Health Organization.

REFERENCES

Acrylic Sheets vs. Polycarbonate Sheets. A & C Plastic Inc. https://www.acplasticsinc.com/informationcenter/r/acrylic-vs-polycarbonate

Acrylic Vs. Polycarbonate. Hydrosight GmbH, Germany. https://www.hydrosight.com/acrylic-vs-polycarbonate-a-quantitative-and-qualitative-comparison

APEC Water Systems. Are There Any Potential Health Risks Associated with Corrosion Byproducts from Water Transported Through Galvanized Drinking Water Pipes? City of Industry, California. https://www.freedrinkingwater.com/water_health/health2/corrosion-byproducts2-galvanized-drinking-pipes-health-risks-page2.htm

AQUASTAT - FAO's Global Water Information System on Water and Agriculture. http://www.fao.org/aquastat/en/

Arunkumar, T.; Vinothkumar, K.; Ahsan, A.; Jayaprakash, R.; Kumar, S. Experimental study on various solar still designs. ISRN *Renew Energy* 2012;569381:1–10.

Bouzenada, S.; Salmon, T.; Fraikin, L.; Kaabi, A.; Léonard, A. Experimental investigation on mass transfer for regeneration of liquid desiccant. *Renewable Energy and Power Quality Journal*, March 2013, No.11.

Calcium Chloride: A Guide to Physical Properties. Occidental Chemical Corporation. https://www.oxy.com/OurBusinesses/Chemicals/Products/Documents/CalciumChloride/173-01791.pdf

Chandler, D. Water, water everywhere… even in the air. *MIT News* (online:). April 14, 2017. http://news.mit.edu/2017/MOF-device-harvests-fresh-water-from-air-0414

Fact Sheet: Drinking Water. World Health Organization, June 14, 2019. https://www.who.int/news-room/fact-sheets/detail/drinking-water

Galvanic Corrosion Considerations for PV Arrays. Kyiv, Ukraine. Avenston LLC. March 23, 2016. https://avenston.com/en/articles/corrosion-pv/

Gleick, P. H. Water resources. In *Encyclopedia of Climate and Weather*, ed. by S. H. Schneider, Oxford University Press, New York 1996; vol. 2, pp. 817-823.

Hoekstra, A. Y.; Chapagain, A. K.; Aldaya, M. M.; Mekonnen, M. M. The Water Footprint Assessment Manual: Setting the Global Standard. 2011 Earthscan.

Humanitarian Charter and Minimum Standards in Disaster Response. The Sphere Project. 2004. Geneva, Switzerland. http://www.sphereproject.org

Kabeel, A.E.; Abdelgaied, M.; Almulla, N. Performance of pyramid-shaped solar still with different glass cover angles: Experimental study. *7th International Renewable Energy Conference* (IREC), 2016.

Kalogirou, S. A. 2009, *Solar Energy Engineering: Processes and Systems.* Academic Press (Elsevier Inc.). Pg. 30.

Kurtus, R. Materials that Cause Static Electricity. School for Champions LLC. January 2018. https://www.school-for-champions.com/science/static_materials.htm#.XkHDZ1VKios

NASA satellites reveal major shifts in global freshwater. May 16, 2018. https://climate.nasa.gov/news/2734/nasa-satellites-reveal-major-shifts-in-global-freshwater/

Transforming our world: the 2030 Agenda for Sustainable Development. *United Nations – General Assembly*. September 25, 2015. New York.

UNICEF. 2019. Progress on household drinking water, sanitation and hygiene 2000-2017. Special focus on inequalities. New York: United Nations Children's Fund (UNICEF) and World Health Organization (WHO)

World Population Prospect 2019. United Nations. https://population.un.org/wpp/Graphs/Probabilistic/POP/TOT/900

William, G.E.; Mohamed, M.H.; Fatouh, M. Desiccant system for water production from humid air using solar energy. Energy, Volume 90, Part 2, October 2015, pp 1707-1720.

APPENDIX A
IMAGES OF PROTOTYPE #1

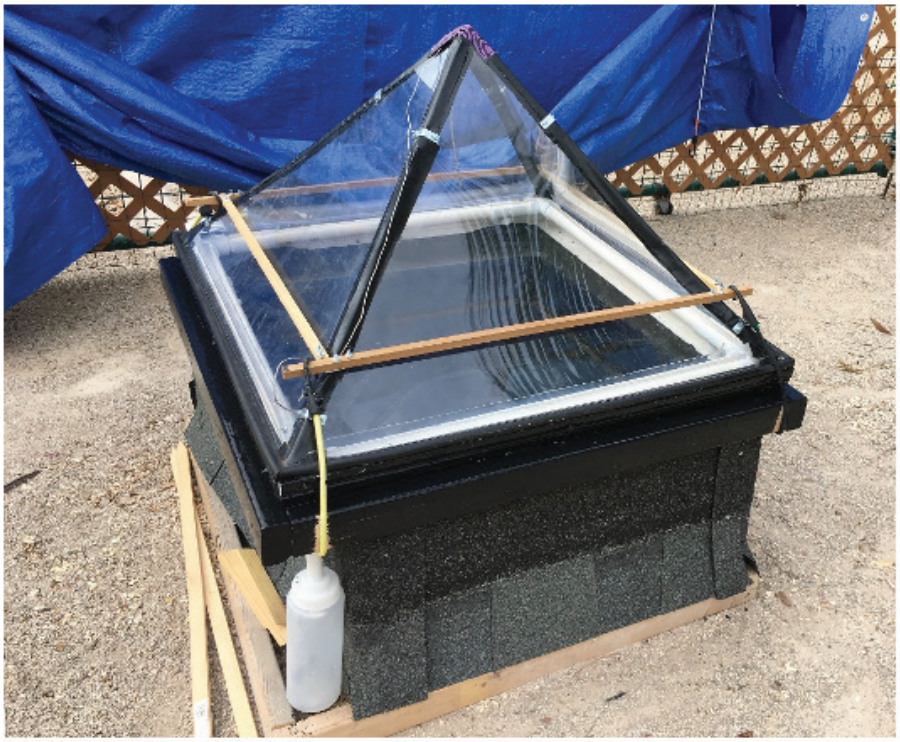

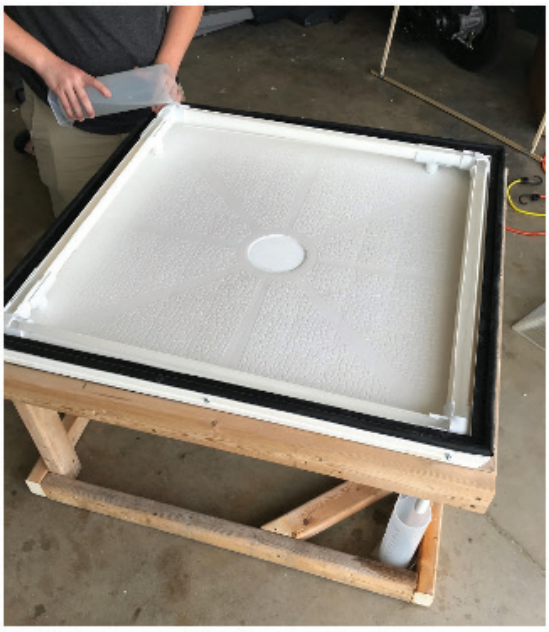

TOP: Final version of Prototype #1 in testing phase. BOTTOM LEFT: Testing of the plastic trough system during construction. BOTTOM RIGHT: Condensation on the polycarbonate panels during the daily solar exposure.

APPENDIX B
IMAGES OF PROTOTYPE #2

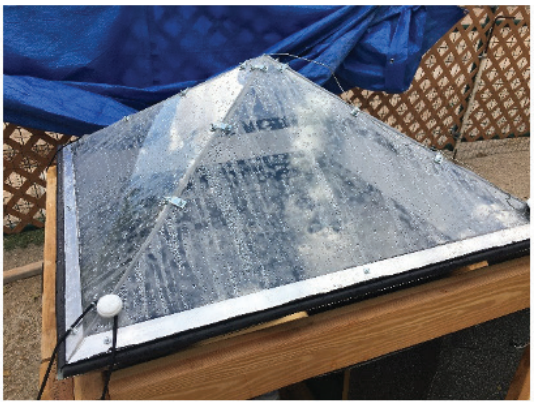

TOP LEFT: Final version of Prototype #2 in testing phase. TOP RIGHT: Image of prototype prior to addition of insulation and asphalt shingles around base. BOTTOM LEFT: Condensation on the polycarbonate panels during the daily solar exposure. BOTTOM RIGHT: Collection bottle of distilled water prior to measuring volume.

APPENDIX C

Solar Exposure VS. Water Collected (water measurements in mL)

PROTOTYPE #2

Test Day	Sunny	Partly Cloudy	Cloudy	Daily high temp °F	12pm Internal temp °F	Notes
1		20		91.5	153	
2	105			93.9	148	
3	100			93	147	
4			22	87.7	146	
5	220			87.6	150	
6		10		88.1	163	
7			27	87.7	154	
8	136			87.2	152	
9			152	87.7	154	
10	0			91.9	154	*seal leaks
11	0			96.3	159	*seal leaks
12	195			91.8	160	
13	225			86.4	143	
14	270			88.3	142	
15			75	85.4	110	
16		135		86.5	102	
17			45	76.4	109	
18		150		78.8	108	
19	150			78.8	118	
20	306			88.4	142	
21	205			88.1	150	
22	200			71.4	140	
23			35	79.7	127	
24	210			85.9	149	
25	167			85.8	154	
26	85			57.4	129	
27		55		66.4	131	
28	145			84.2	150	
29			10	84	127	
30		85		84.5	143	
31	117			70.1	140	
32	65			81.9	149	
33		45		83	150	
34	95			74	137	
35	63			82.7	147	
36	35			74.3	141	
37	20			73.2	147	
38	30			80.7	154	
39			0	45	62	*Colder during mid-condensation than start
40	65			58.4	117	
41	15			77.4	135	
42	0			83.5	147	* lack of measurement

43		0		60.4	116	
44	37			73.6	124	
45		18		56.4	116	
46		0		73	132	*$CaCl_2$ removed from outside
47	40			83.7	156	evening due to crystallization
48		5		66.5	137	
49			0	64.8	89	
50			0	78.9	139	
51	75			56.9	118	
52	48			60.3	117	
53			12	65.9	110	
54	20			62.2	127	
55	23			77.8	138	
56		0		80.2	118	
57		0		74.3	138	
58	20			61.2	109	
59	76			55.2	115	
60	55			61.6	123	
61	27			72.3	128	
62			0	55.1	77	*$CaCl_2$ started to crystallize
63		0		71.8	125	
64		0		57.2	108	
65		0		64.7	106	
66		0		73.2	108	
67	22			75.1	124	
68	49			73.6	124	
69	0			51.9	93	*NOTE temp/no water/sunny
70		4		49.4	95	*Possible dew measurement
71	65			46.8	111	
72	40			51.2	107	
73	17			54.4	112	
74	35			62.7	119	
75	40			64.9	128	
76		0		62.6	106	
77	0			60.4	106	
78		0		67.6	93	
79		7		69.9	125	

Mission-Critical Communications Planning Over Contested RF Spectrum with Deep Reinforcement Learning Aided Artificial Intelligence

*Milidu N. Jayaweera**

La Cueva High School, Albuquerque, NM

ABSTRACT

Mission-critical communications (MCC) refer to those that support operations involving high risk to human life and property. As radio frequency (RF) spectrum becomes highly contested, ensuring mission-success with MCC requires intelligent planning policies. This project develops a novel game-theoretic model for MCC and a Deep Q-Network (DQN) implemented Deep Reinforcement Learning (DRL) based Mission-Critical Communications Protocol (MCCP) to learn to complete a mission within given resource-constraints against an adversary. An example critical mission is defined as two radios exchanging messages within a given time-constraint over a two-way communication link in the presence of a jammer. Mission-planning requires radios to learn when and how to switch directions vs. channels in response to the behavior of the adversarial jammer as well as wireless channel anomalies. Through extensive-form sequential-game modeling, the problem was shown to be too complex to solve analytically and beyond traditional reinforcement-learning due to uncountable state-space. Results on an actual wireless network showed that the DQN-implemented DRL could achieve mission-success with as high as 0.9 probability. A new DRL algorithm called Deep Policy Hill Climbing was developed that outperformed the original DQN-DRL algorithm. Beyond MCC, this framework can be applied to a wide-variety of planning under uncertainty problems that arise, for instance, in disease control, refugee crises, disaster relief and resource-allocation in management.

KEYWORDS: Deep Policy Hill Climbing, Deep Q-Networks, Deep Reinforcement Learning, Game Theory, Mission-critical Communications, Mission-critical Communications Protocols, Nash Equilibrium, Sequential Games, Subgame Perfect Equilibrium

INTRODUCTION

From Isaac Asimov's *Bicentennial Man* to the *Terminator* franchise, developing *Artificial Intelligence* (AI) capable of learning to make decisions by itself has long been a human fascination. Formal scientific and engineering approaches to developing AI are commonly known as *machine learning* (ML). A seldom considered novel application of machine learning and AI is in *mission planning*.

Many modern military, humanitarian, and scientific missions critically depend on *over-the-air* (OTA) wireless communications between agents/nodes. A failure in the communications network can be catastrophic, costly, and even life-threatening. Figure 1 shows an example in

which a rocket launch is managed remotely by two locations. Such distributed control of critical missions is becoming increasingly desirable to reduce the chances of human error and to defeat deliberate sabotage by rogue actors.

This gives rise to the importance of mission-critical communications (MCC) planning since mission-success now crucially depends on the communications system. *Mission-critical communications* refers to reliable communications between nodes that will lead to mission-success in operations involving high risk to human life and property, especially when there are deliberate and adversarial *jamming signals* (1). Most existing work on MCC focuses on the reliability of communications infrastructure (2). As RF spectrum becomes highly contested, however, ensuring success of missions involving distributed agents as in Figure 1 requires such infrastructure to be supported by *mission-critical communications protocols* (MCCP) that implement intelligent planning policies. Both design of *mission-critical communications planning* techniques and their implementation as MCCPs are problems that have not yet received sufficient attention despite their growing importance.

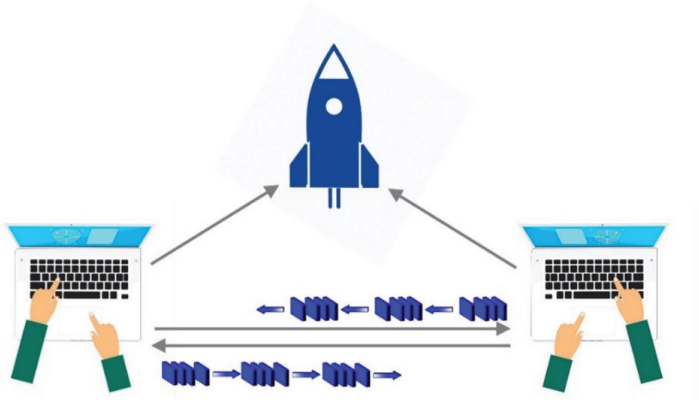

Figure 1. Mission-Critical Communications Planning for Distributed Control of a Rocket Launch.

Mission-critical communications planning is one example from the general problem of *planning-under-uncertainty* (3) encountered in different fields ranging from how to assign resources in a manufacturing plant to how to respond to an adversary in a war-like conflict. Mathematically, a broad class of planning problems can be modeled as a *Markov Decision Process* (MDP) (4). In an MDP, an agent takes *action* a_t in an environment characterized by a *state* s_t and receives a *reward* r_t. Agent's goal of mission-success can be modeled as maximizing an accumulated discounted-reward. Agent's actions effect the environment so that the next state is not only a function of the current state but also of the agent's selected action. Thus, the next state of the environment s_{t+1} is determined according to the transition probabilities $P(s_{t+1} \mid s_t, a_t)$ where $P(s_{t+1} \mid s_t, a_t)$ is the probability of state s_{t+1} given action a_t was executed in current state s_t.

If all state transition probabilities and rewards were known exactly, the so-called *Bellman optimality equations* characterize the optimal planning policy which can be solved using *Dynamic Programming* (4). When these are unknown, *reinforcement learning* (RL) is a popular machine learning paradigm for obtaining optimal planning policies (5).

The MCC planning, however, is more difficult than classic MDPs for three reasons: First, there are adversaries that attempt to hinder the mission by deliberately jamming signals. This turns the problem into a *stochastic game* (6). Second, state transition probabilities are not only unknown but also can be time-varying due to the nature of the wireless links (7). Third, the state of a *mission-critical communications game* may take values on an uncountable set rendering the traditional RL techniques not applicable.

The project objective is to develop a new approach to solve the MCC planning problem by leveraging the recent advances in *Deep Reinforcement Learning* (DRL). The project defines the MCC problem to be OTA sharing of mission-critical information residing at two distributed agents within a given time constraint. The MCC planning problem is to select at each decision epoch who should transmit information packets and on which channel, as shown in Figure 2.

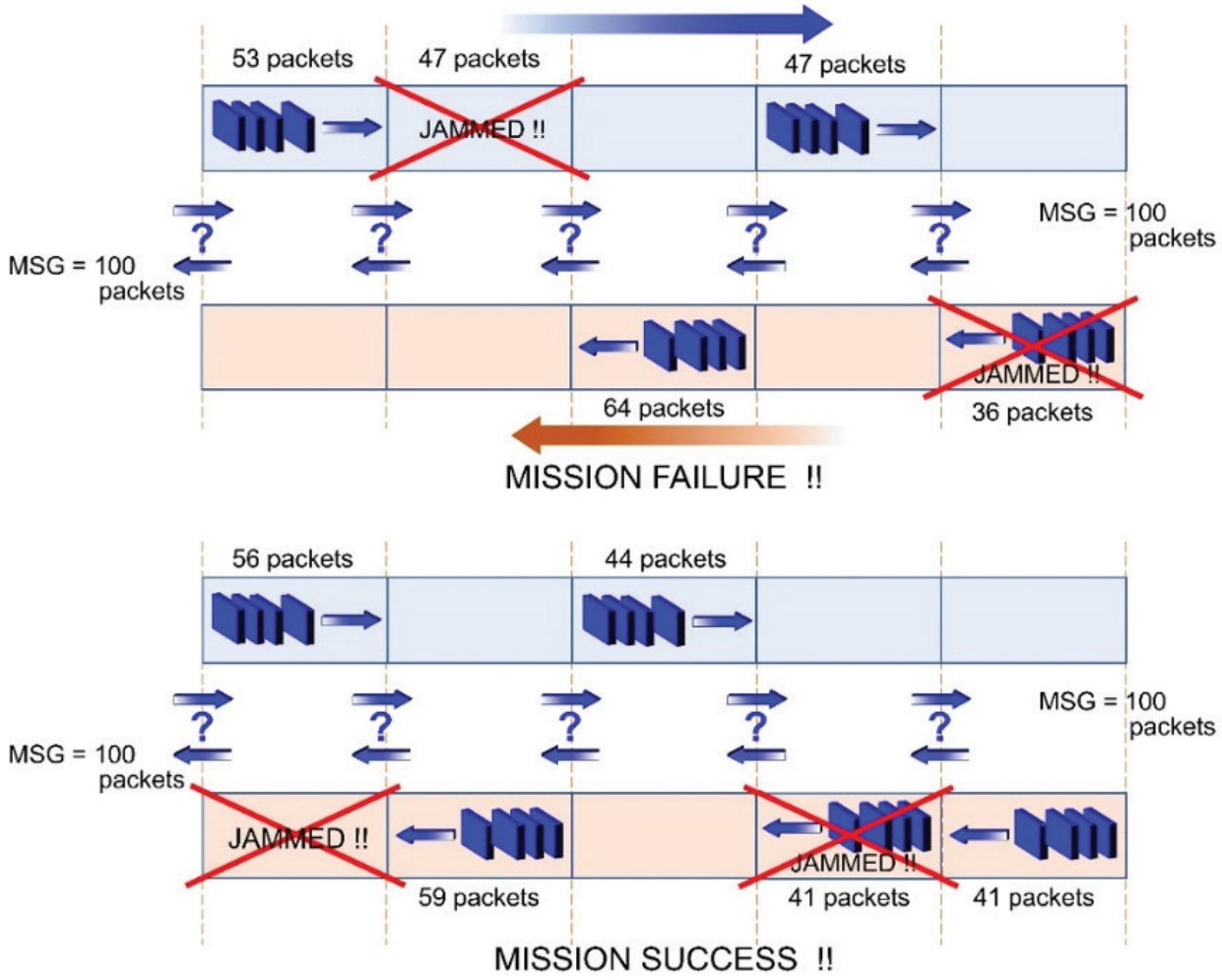

Figure 2. Dependence of Mission-Success and Failure on a Mission-Critical Communications System.

We develop a general game-theoretic model of this MCC planning problem that lends itself for the application of DRL. Then, we design and implement a *Deep Q-Network* (DQN) based DRL algorithm to learn effective planning policies that lead to mission-success with

high probability. The project also proposes a new DQN-based DRL algorithm, termed *Deep Policy Hill Climbing (DPHC)* which is shown to beat the original DQN-DRL algorithm when applied to the MCC planning problem (8). These algorithms are used to develop a MCCP for a two-node network made of Universal Software Radio Peripheral (USRP) Software-defined Radios (SDRs). Finally, the MCCP is implemented on this real wireless network and the effectiveness of the DQN-based DRL MCC planning is shown for exchanging OTA mission-critical information in the presence of a jammer and wireless channel anomalies.

THEORETICAL BASIS

First, we develop a mathematical model for the MCC planning problem using game-theory. Consider two nodes, A and B, that need to exchange their private, unique messages with each other within a given time constraint of N decision-epochs for a mission to be successful. The messages of nodes A and B are made of N_A and N_B and packets, respectively. There are M/2 frequency channels in each direction. At each decision-epoch, nodes make a decision on who should transmit using which channel. Since channels are unidirectional, the choice of channel also implies which node will transmit. This is a finite-horizon sequential decision problem in which N decisions are to be made so that N_A and N_B packets can be exchanged in the two directions. To develop a formal approach to solving this mission planning problem, we use game theory.

The MCC planning problem is an extensive-form game made of N sequential actions. Since two nodes are on one side against either the nature or a jammer, or both, the two nodes are represented by a single "Radio" player. The other player is the nature or the jammer. Figure 3

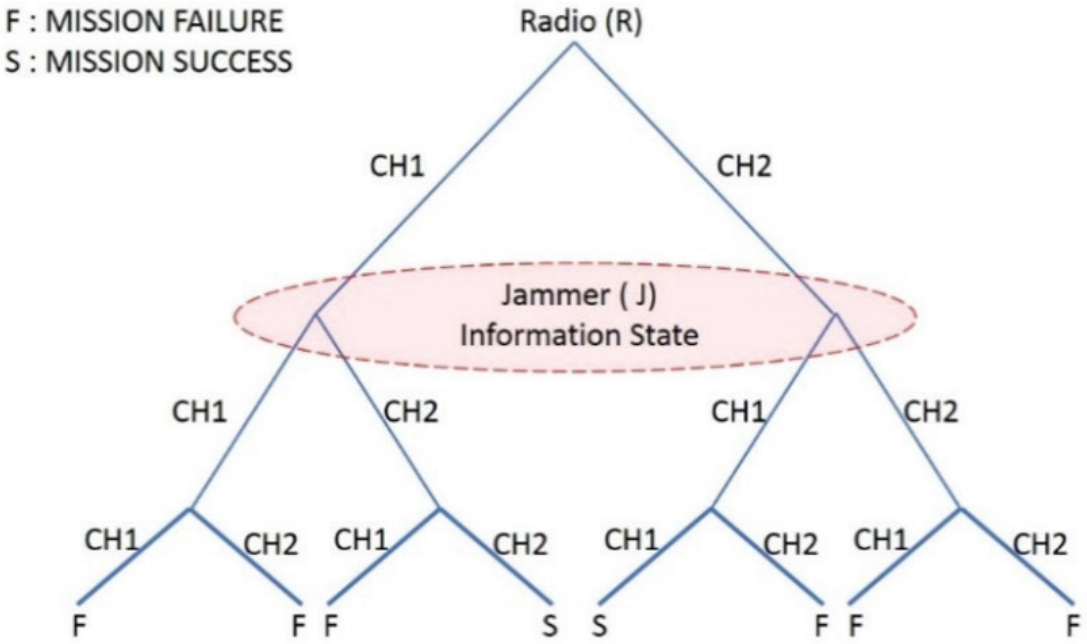

Figure 3. Extensive-form Game Representation of the Mission-Critical Communications Planning Problem with Two Decision Epochs.

shows the extensive-form game representation of a mission consisting $N = 2$ epochs with each link having one frequency channel (CH 1 from A to B and CH 2 from B to A).

The game played at each decision epoch can be characterized by a *state* that represents the progress of nodes towards completing the mission. Hence, this is a *stochastic*, or a *Markov*, game. At each epoch of the game/mission, a channel is selected with the goal of ensuring exchange of messages of each other before the N decision epochs are over. Since what matters is the mission success or failure at the end of the N periods, we define the reward for selecting action a when in state s at time t as

$$r_t(s,a) = \begin{cases} 1 & if\ L_A^t = 0\ \&L_B^t = 0 \\ -1 & if\ (L_A^t \neq 0\ or\ L_B^t \neq 0)\ \&\ T_R^t = 0 \\ 0 & otherwise \end{cases} \quad (1)$$

Where $L_A{}^t$, $L_B{}^t$ and $T_R{}^t$ denote the remaining packets at node A, remaining packets at node B and the remaining time before the mission runs out of time respectively.

A suitable formulation is to seek a channel selection policy over the mission-duration (MD) in order to maximize the following *discounted-reward*:

$$R = \sum_{t=1}^{N} \gamma^t r_t \quad (2)$$

Where $0 \leq \gamma \leq 1$ is a discount-factor. The most well-known solution concept for games is the Nash Equilibrium (NE). However, in extensive-form games the NE proves inadequate since some NE action sequences may not look credible when players are half-way through the mission, although they might have looked credible at the outset. Hence, when solving extensive-form games, the most common goal instead is to find a so-called *subgame perfect equilibrium (SPE)* which is an NE of the game with the additional requirement that any restriction of the strategy is a NE for the corresponding restriction of the game for all sub-games of the game (6).

In the MCC planning game, the number of policies to consider can be very large and even uncountable. For example, observe from Figure 3 that the number of action paths increases exponentially with mission-duration N and the channels on each link, making analytically solving for the desired equilibria in real-time impractical. For example, finding a solution along the game-theoretic criterion of sub-game perfect equilibrium can be computationally prohibitive. Adding an adversary (i.e., a jammer) further increases the game's complexity.

As a practical solution that can be applicable to a wide range of situations, this project proposes to train a suitable *artificial neural network* (ANN) through DRL to learn an optimal MCC plan. Such neural networks are called the DQN's (8).

EXPERIMENTAL METHODS

Deep Q-Network DRL Solution for Mission-Critical Communications Planning Problem: Since the radio's decisions must be a function of the amount of message packets remaining at each node ($L_A{}^t$ and $L_B{}^t$) as well as the remaining time from the mission-duration ($T_R{}^t$), we define the state s_t of the game at time t as the following 4-tuple:

$$s_t = (L_A^t, L_B^t, a_{t-1}, T_R^t)^T \tag{3}$$

Where a_{t-1} denotes the channel selected at the previous decision-epoch. An experience-tuple is defined as $x = (s, a, r, s')$ if executing action $a_t = a$ when in state st = s results in system transitioning to the new state $s_{t+1} = s'$ while observing a reward $r_t = r$.

Shallow RL uses a *Q-table* to learn a discretized version of the optimal *state-action value function,* denoted as $Q(s_t,a)$, from which an optimal policy can be obtained (5). If the input state s_t takes a continuum of values, as in the MCC planning problem, using a Q-table to learn the state-action value function is not possible since there is an infinite number of states. Therefore, this project constructed an ANN to learn the state-action value function. The idea is to train the ANN sufficiently so that when the game state $s_t = (L_A{}^t, L_B{}^t, a_{t-1}, T_R{}^t)^T$ is input to the ANN, it can output the corresponding $Q(s_t,a)$ estimates from which an optimal policy can be obtained.

The DQN Algorithm, developed by the Google DeepMind in 2015, is a clever extension of the classic *Q-Learning algorithm* to handle very large (or even uncountable) state-action spaces (8). It uses a *Deep Neural Network* (DNN) as a function estimator to approximate the state-action value function $Q(s_t,a)$ and succeeds in learning the *optimal state-action value function* $Q^*(s, a)$ thanks to two innovative concepts: *experience-replay* and the *target network* (8). The experience replay avoids the temporal correlations of experiences used for training which can lead to non-convergence of ANN weights. The use of a so-called target Q-network removes the problem of having to learn a moving target. Figure 4 shows the DQN-DRL algorithm for MCC planning developed in this project. We denote this as the DQN Algorithm #1.

At each decision-epoch, the DQN Algorithm #1 either picks the action with the highest estimated $Q(s,a)$ value according to the DQN output, or randomly with an appropriate *exploration rate* ϵ. After executing the chosen action, nodes observe a reward r depending on whether the nodes succeeded in completing the mission or not and the resulting next state s'. The *experience tuple* $x=(s, a, r, s')$ is added to *the experience replay memory* and then a random *minibatch* of L experience tuples is drawn from the replay memory. These L experience tuples are used to update the weights of the DQN assuming that the desired output is the one that is predicted by the target Q-network. As is the case with all ANNs, DQN Algorithm #1 uses a variation of the so-called *back propagation algorithm* to update the weights (9).

Mission-Critical Communications Planning in a Real Wireless Network made of Software-defined Radios: The DQN-based DRL of MCC planning was fully-implemented as a protocol on an MCC network formed of real wireless transceiver hardware. We used two USRP SDRs as two radio nodes (A and B). Each node has a unique message to convey to the other node for

the mission to be a success. Two communication links were then defined going in opposite directions: A → B and B →A. Two channels each assigned to each link: Channels 1 and 2 for sending messages from A to B and Channels 3 and 4 for sending those from B to A.

Initialize $DQN\ Q(.)$ weights, set target $DQN\ Q_T = Q$

For mission episode $m = 1: M$

$\epsilon_n \leftarrow \epsilon_n - \frac{(\epsilon_0 - \epsilon_f)}{n}$

If mod (episode, T) == 0

Set $Q_T(.) = Q(.)$

For $n = 1: N$ mission duration

1. When In state $S^t = [\ L_A^t, L_B^t, a^{t-1}, T_R^t\ ]$, select action a such that :

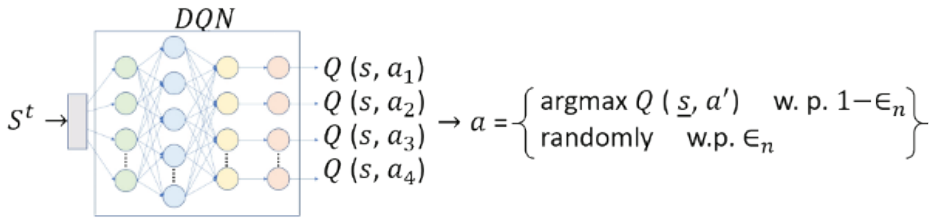

2. Execute action a, and observe next state $s^{t+1} = s'$ and reward $r^t = r$.

3. Add the experience tuple $e = (s, a, r, s')$ to the experience replay memory.

4. Select a random minibatch of experience $\mathcal{E}$ of size L from experience replay memory.

4a. For each $\underline{e_l} = (s_l\ , a_l, s_l', a_l) \in \mathcal{E}$

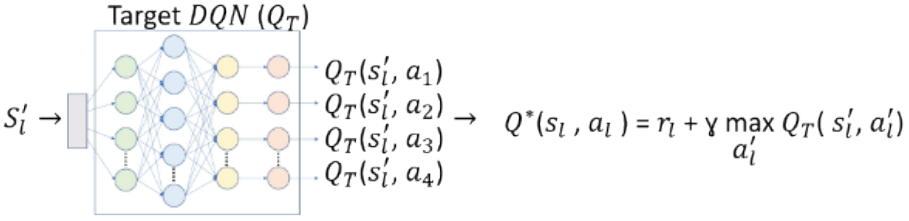

4b.

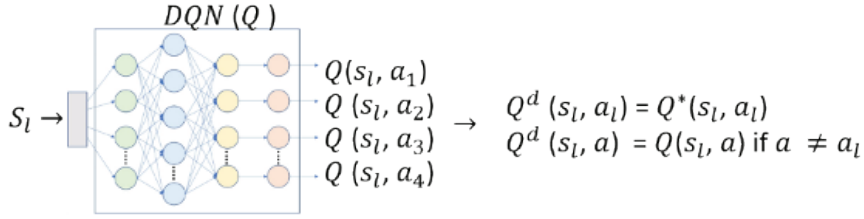

4c. $err(a) = Q_d(s_l, a\ ) - Q\ (s_l, a\ )$ for $\forall a$.

4d. Update DQN weights to minimize err vector.

end.

end.

Figure 4. DQN Algorithm #1: Deep Q-Network Deep Reinforcement Learning (DQN-DRL) Algorithm.

The total time available to complete the mission, called the mission-duration, is N decision epochs. Within each decision epoch of duration T_d, a node can transmit a random number of packets. In terms of decision epoch index k, for $k = 1,\ldots,N$, the state s_k of the game at decision epoch k is $s_k = (L_A^k, L_B^k, a_{k-1}, T_R^k)^T$.

The implementation of DQN-based MCC planning on USRPs required the development of an MCCP protocol for two USRPs to establish and maintain a wireless link. This MCCP was implemented in LabVIEW and integrated in to the USRP hardware over an Ethernet port. Each USRP was connected to its own computer terminal running LabVIEW software. For networking simplicity, we implemented the DQN-DRL only at the node A USRP and made Node B execute actions learned at node A and provided to it over a wireless feedback channel by A.

For this scheme to work, the USRP A which maintains the DQN needs to be able to determine if and when a node's receiving channel is jammed so that it can decide whether to transmit or receive and which channel to switch to. To construct the state s_k at epoch k, it must also know how much message is remaining on B's side (L_B^k), as well as its own (L_A^k).

Obviously, Node A always knows the value of L_B^k. It can also determine if its own reception is jammed by observing how many packets it receives within a decision epoch and comparing that with a threshold. For Node A to learn the value of L_A^k, Node B must send Node A acknowledgments for packets it receives. For this also we used the same feedback channel: In each decision epoch, node B feedback the number of packets received from node A so far when it successfully decodes a packet. We assume that the feedback channel operates on a completely separate frequency from the four communications channels used for actual message packets and is sufficiently secure so that the action decisions and acknowledgment messages cannot be jammed.

Figure 5 shows the timing flow-graph of the designed MCCP that was implemented on a wireless network made of two USRP SDRs. In the example in Figure 5, the action sequence selected by the DQN agent is channels 1, 3, 4, and 2.

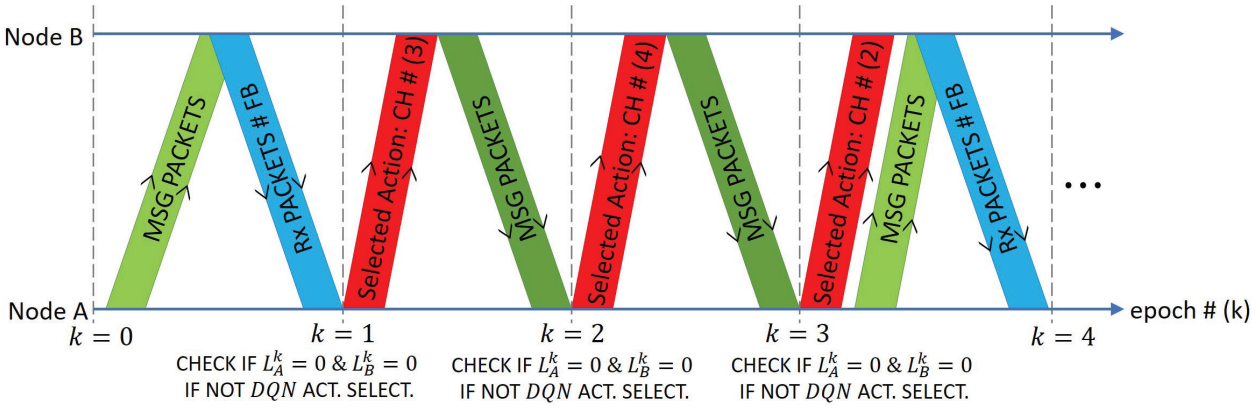

Figure 5. Designed and Implemented DQN Planning-based Mission-Critical Communications Protocol.

Statistical Modeling of Over-the-Air Mission-Critical Communications for Offline Training of Deep Q-Network: Directly constructing a DQN in LabVIEW and training on USRP hardware in real-time is a time-consuming task since an actual communications mission may last 10 to 20 minutes. Hence, a DQN was first designed, trained, and tested offline by simulating the entire system made of radios and jammers in MATLAB and then fine-tuned by updating weights during real-time MCC. For this approach to be successful, the MATLAB simulation needs to be as close to the real communications system as possible.

The critical quantity that needs to agree with the actual wireless network is the number of packets successfully communicated OTA during each decision epoch on links from nodes A to B and B to A, denoted respectively by random variables X_A and X_B. We model X_A and X_B as *normal random variables* (10).

A normal random variable is fully characterized by its mean and the variance (10). If $X_{A,i}$ and $X_{B,i}$, for $i = 1, \ldots, n$, denote a collection of measurements of X_A and X_B, the means and the variances of packet throughput per decision epoch on each direction can be estimated as follows:

$$\mu_A = \frac{1}{n}\sum_{i=0}^{n} X_{A,i} \quad \text{and} \quad \mu_B = \frac{1}{n}\sum_{i=0}^{n} X_{B,i} \tag{4}$$

$$\sigma_A^2 = \frac{1}{n}\sum_{i=0}^{n}\left(X_{A,i} - \mu_A\right)^2 \quad \text{and} \quad \sigma_B^2 = \frac{1}{n}\sum_{i=0}^{n}\left(X_{B,i} - \mu_B\right)^2$$

where μ_A and μ_B are the means of X_A and X_B, respectively and σ_A^2 and σ_B^2 are the variances of X_A and X_B, respectively. Then during each decision epoch of a simulated mission, we draw X_A according to the following normal pdf (similarly, for X_B) (10):

$$p_{X_A}(x) = \frac{1}{\sqrt{2\pi}\sigma_A} e^{-\frac{1}{2\sigma_A}(x-\mu_A)^2} \tag{5}$$

Adversarial Jammer Design and Implementation: The jammer is a separate radio capable of transmitting on any channel in either link. The developed sequential jammer jams channels one at a time in a pre-defined order. It jams a channel for a certain duration and changes to the next channel. The initial channel of this jammer is drawn uniformly randomly. Hence, even with a pre-defined sweeping pattern, this jammer can pose a significant challenge to an MCC link due to the randomness observed in the jamming sequence in different mission trials. This was implemented as a protocol on LabVIEW and integrated on to a third USRP SDR.

A Brand-New DQN-DRL Algorithm: Deep Policy-hill Climbing (DPHC) Algorithm: A drawback of the *Q-Learning algorithm* (11) used in the DQN Algorithm #1 is that it can only learn *pure strategies*. A pure strategy assigns 100% probability to a single action. However, a mixed strategy assigns probabilities to several different actions. This ensures the possibility of learning an NE since mixed strategy NE are guaranteed to be present while pure strategy NE may not always exist (6). Moreover, traditional Q-Learning can suffer from possible slow convergence in multi-agent games (12). The so-called Policy Hill Climbing (PHC) algorithm is a formal approach to learn mixed strategies in multi-agent games (13).

For the first time, this project developed a Deep PHC algorithm that accelerates the policy learning through a variable learning rate. In Figure 6 we show the newly developed *Deep Policy-hill Climbing* (DPHC) DRL algorithm for MCC planning that we have denoted as the DQN Algorithm #2. As can be seen from Figure 6, the DPHC algorithm operates similar to the DQN

Initialize $DQN\ Q(.)$ weights, set target $DQN\ Q_T = Q$

For mission episode m= 1 : M

$\epsilon_n \leftarrow \epsilon_n - \frac{(\epsilon_0 - \epsilon_f)}{n}$

If mod (episode, T) = = 0

Set $Q_T(.) = Q(.)$

For $n = 1: N$ mission duration

1.When in state $S^t = [L_A^t, L_B^t, a^{t-1}, L_R^t]$, select action a such that :

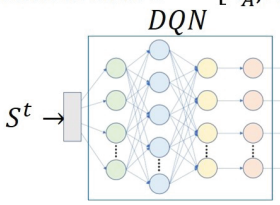

$$\rightarrow a = \begin{cases} \text{Argmax } Q(s, a') & \text{w.p. } 1-\epsilon_n \\ \text{randomly} & \text{w.p. } \epsilon_n \end{cases}$$

2. Execute action a, and observe next state $s^{t+1} = s'$and reward $r^t = r$.

3. And the experience tuple $e = (s, a, r, s')$ to the experience replay memory.

4. Select a random minibatch of experience $\mathcal{E}$ of the size L from the experience replay memory.

4a. For each $e_l = (s_l, a_l, s_l', a_l) \in \mathcal{E}$

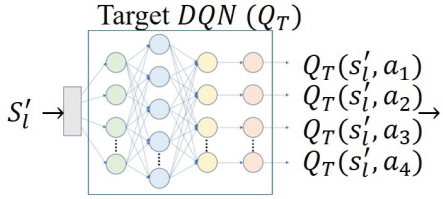

$$\rightarrow Q^*(s_l, a_l) = r_l + \gamma \max_{a_l'} Q_T(s_l', a_l')$$

4b.

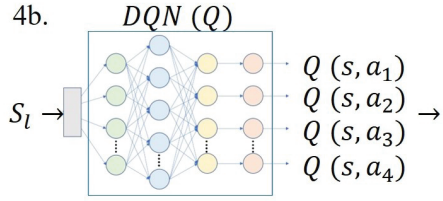

If, $a_l = \arg\max_{a'} Q(s_l, a')$

$Q^d(s_l, a_l) = Q^*(s_l, a_l) + \delta$

$Q^d(s_l, a) = Q(s_l, a_l) - \frac{\delta}{(M-1)}$ if $a \neq a_l$

Otherwise

$Q^d(s_l, a_l) = Q^*(s_l, a_l)$

$Q^d(s_l, a) = Q(s_l, a_l)$ if $a \neq a_l$

4c. $err(a) = Q_d(s_l, a) - Q(s_l, a)$ for $\forall a$.

4d. Update DQN weights to minimize eff vector.

end.

end.

Figure 6. DQN Algorithm #2: Deep Policy-hill Climbing (DPHC) Deep Reinforcement Learning Algorithm.

but for a key difference in updating the weights in step (4d): we reinforce those action choices that are the best for that state according to the current DQN by amplifying the desired $Q(s,a)$ for those actions while de-emphasizing those for the remaining actions.

RESULTS

Since the primary objective of mission-planning is achieving mission-success, our main performance metric is the *mission-success probability* (MSP) defined as:

$$mission\ success\ probability\ (MSP) = \frac{\#\ of\ missions\ completed\ successfully}{total\ \#\ of\ missions} \tag{6}$$

To show that the DQN is an effective approach for solving the MCC planning problem, performance of the DQN was evaluated in five cases.

In the first case based entirely off MATLAB simulations, we simulated a general MCC planning problem in which the message at each node is made of five packets and during each decision epoch a single packet can be transmitted. We used an ANN made of three hidden layers with 24 neurons each. Both input and output layers are made of four neurons each corresponding to the length of the state vector and the number of channels. We denote this as the 4x24x24x24x4 net.

Figure 7 shows the MSP during and after training for mission-durations *N=10, 12* or *14* epochs in the presence of a sequential jammer. Since initial channel of this jammer is drawn uniformly randomly, even with a pre-defined sweeping pattern, it poses a significant challenge to the mission-success. Figure 7 not only shows the effectiveness of DQN in learning good planning policies, but also shows how difficult the learning problem is as the mission-duration tightens.

Figure 8 shows the effectiveness of the MCC planning with a DQN-DRL (after training over 10K missions) when compared to random decisions. Clearly, DQN-DRL results in MCC planning policies that are significantly better performing than those with random decisions. We quantify this by defining the *Percentage Mission-Success Improvement* (PMSI) relative to the random planning as below:

$$Percentage\ Mission\ Success\ Improvement\ (MSI) = \frac{MSP_{DQN} - MSP_{RP}}{MSP_{RP}} \times 100\% \tag{7}$$

where MSP_{DQN} and MSP_{RP} refer, respectively, to MSP with DQN based DRL and with random planning.

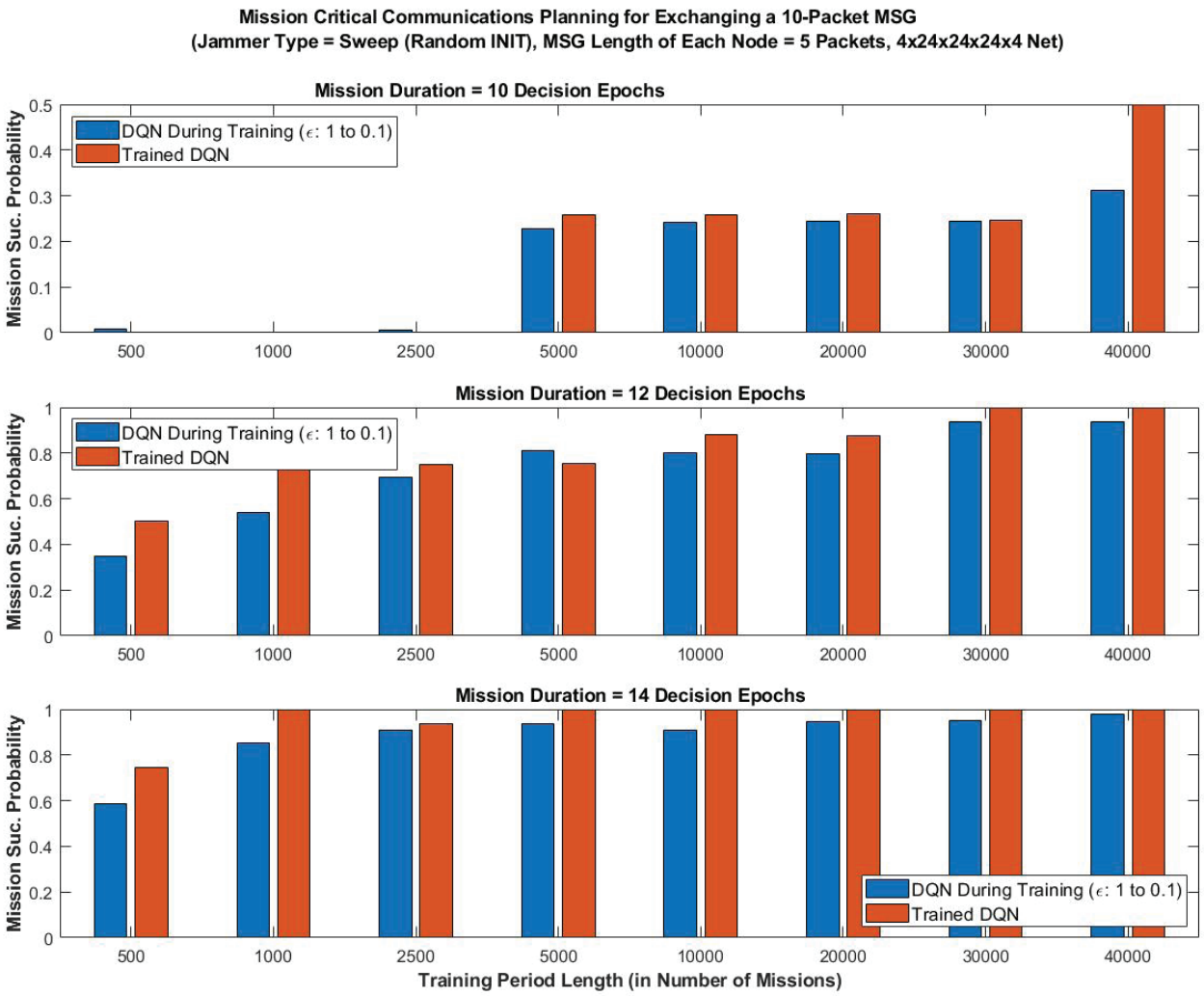

Figure 7. Mission-Success Probability of DQN-based Mission-Critical Communications Planning during and after Training in the Presence of a Sequential Jammer. (TOP) Planning Over 10 Decision Epochs, (MIDDLE) Planning Over 12 Decision Epochs, (BOTTOM) Planning Over 14 Decision Epochs.

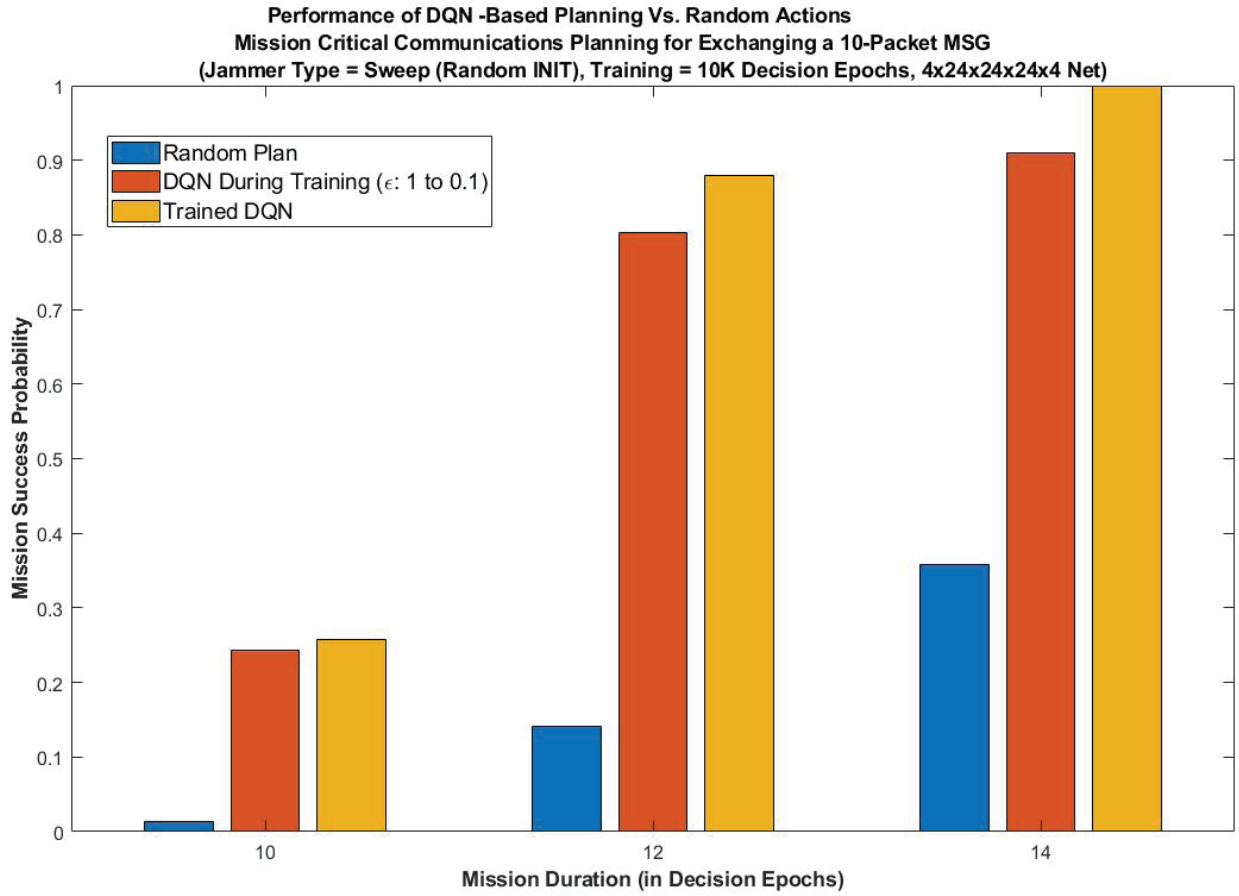

Figure 8. Performance Improvement of DQN-based Mission-Critical Communications Planning during and after Training Compared to Random Planning Lengths in the Presence of a Sequential Jammer (Different Mission-Durations).

Table 1 shows the computed PMSI improvements after training corresponding to the results shown in Figure 8. The improvements are more pronounced for shorter mission-durations since there is more room for improvement due to the smaller MSPs.

Mission-Duration (decision epochs)	Percentage Mission-Success Improvement (PMSI)
10	1739%
12	520%
14	179%

Table 1. Percentage Mission-Success Improvement with DQN-DRL Planning Relative to Random-decision Planning.

Next, we offline trained a DQN suitable for the hardware-implemented MCC system built with USRPs controlled by LabVIEW. The four channel frequencies were 2.04 GHz, 2.08 GHz, 2.12 GHz and 2.16 GHz. Both nodes used QPSK modulation at 50K symbols/second. The feedback channel operated at frequency 2.38GHz using the same modulation. We assigned each node a message made of 100 packets. Each packet contained a critical information that was packed in to 5888 bits. Before transmission 1380 guard bits and 1104 synchronization bits were added so that each transmit packet was about 8372 total bits.

To pre-train a DQN in offline simulations, we estimated the means and variances of random variables X_A and X_B corresponding to the number of successful packet transmissions from node A to B and B to A, respectively. For this, we collected the number of packets transferred on each link during a decision epoch as shown in Table 2.

Link	Ep. 1	Ep. 2	Ep. 3	Ep. 4	Ep. 5	Ep. 6	Ep. 7	Ep. 8	Ep. 9	Ep. 10
A to B ($X_{A,i}$)	72	71	67	78	81	87	90	82	89	75
B to A ($X_{B,i}$)	84	87	70	89	84	79	72	77	80	86

Table 2. Number of Successful Packet Transmissions During a Decision Epoch.

From these measurements we computed the means and the variances of packet throughput per decision epoch on each direction as follows:

$$\mu_A = \frac{1}{n}\sum_{i=0}^{n} X_{A,i} = 79.200 \quad \text{and} \quad \mu_B = \frac{1}{n}\sum_{i=0}^{n} X_{B,i} = 80.800$$
$$\sigma_A^2 = \frac{1}{n}\sum_{i=0}^{n}\left(X_{A,i} - \mu_A\right)^2 = 63.505 \quad \text{and} \quad \sigma_B^2 = \frac{1}{n}\sum_{i=0}^{n}\left(X_{B,i} - \mu_B\right)^2 = 60.628 \tag{8}$$

Figure 9 shows the MSP with the above model for the packet transmission distribution on each link for mission-durations of $N = 4, 6$ and 8 decision epochs.

Figure 10 shows the MSP of the DQN-DRL mission-critical communications planning compared to random planning while Table 3 shows the PMSI corresponding to the results shown in Figure 10.

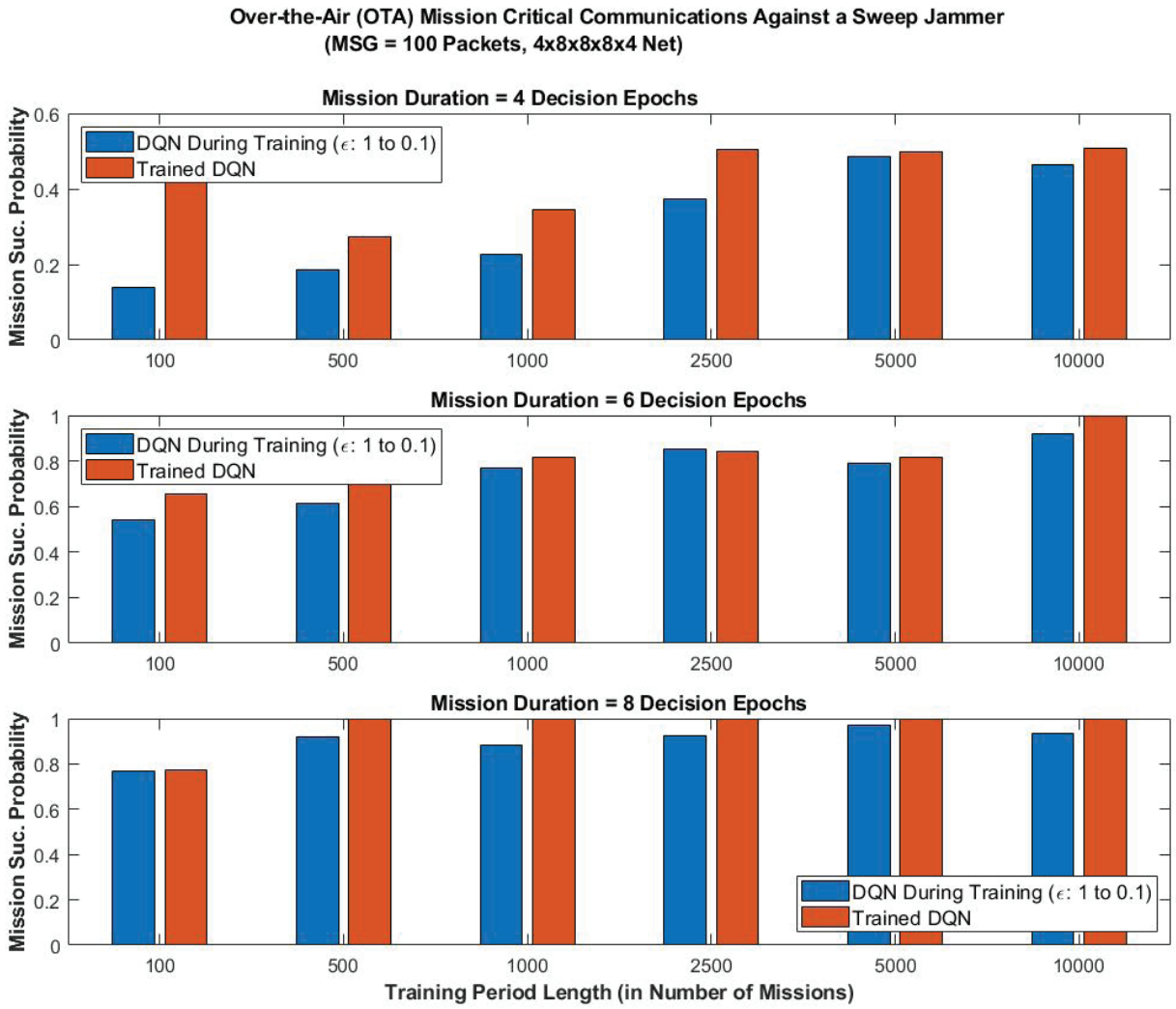

Figure 9. Mission-Success Probability of DQN-based Mission-Critical Communications Planning in a Wireless Network during and after Training in the Presence of a Sequential Jammer. (TOP) Planning Over 4 Decision Epochs, (MIDDLE) Planning Over 6 Decision Epochs, (BOTTOM) Planning Over 8 Decision Epochs.

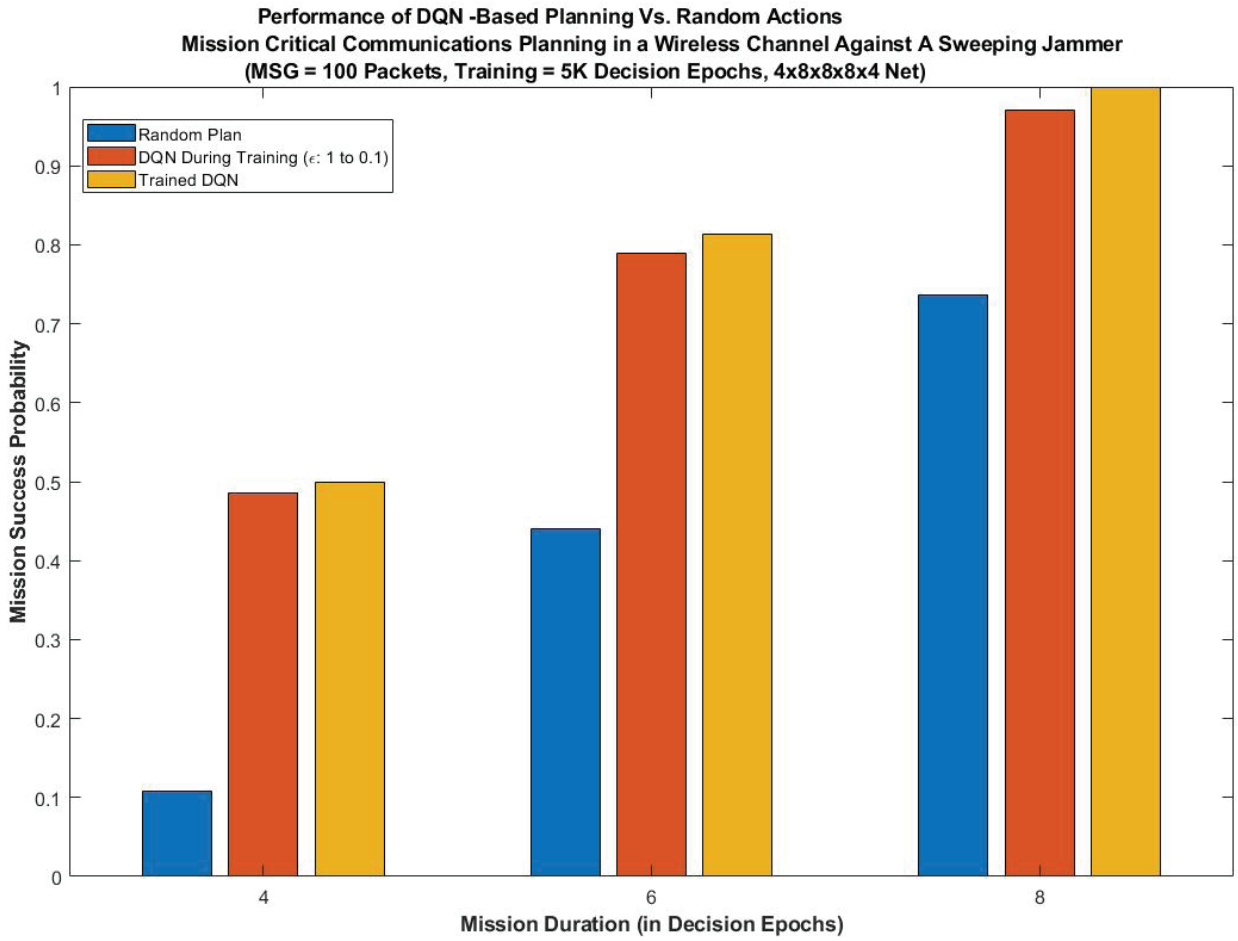

Figure 10. Performance Improvement of DQN-based Mission-Critical Communications Planning in a Wireless Network during and after Training Compared to Random Planning Lengths in the Presence of a Sequential Jammer (Different Planning Lengths).

Table 3 shows that the trained DQN-based MCC planning achieves significantly better mission-success improvements over random planning policies. Again, with tighter mission-durations, the improvements are more pronounced since MSPs are relatively low.

Mission-Duration (decision epochs)	Percentage Mission-Success Improvement (PMSI)
4	359%
6	85%
8	36%

Table 3. Percentage Mission-Success Improvement with DQN-DRL Planning Relative to Random-decision Planning in a Wireless Network Simulated with Estimated Throughput Parameters.

The third set of experiments evaluated the DQN-based MCC planning performance with OTA mission-critical information exchanges in an actual wireless network made of USRP SDRs. The DQN made of the 4x8x8x8x4 net trained for a mission-duration of *N=6* epochs over a *20K* training period was integrated into the node A's LabVIEW program to implement the MCCP protocol. The actual OTA MCC testing of the two-node link in the presence of

a sequential jammer was performed at the Communications Lab at the University of New Mexico. Jammer was designed to sequentially jam channels starting from a random channel with a channel change every 3 epochs.

Figure 11 shows the remaining packets at node A (Left Y-axis) and node B (right Y-axis) at each decision epoch as the mission evolves. Each decision epoch was about 150 seconds so that the duration of a single mission made of six decision epochs was about 15 minutes. Figure 11 summarizes results obtained over 10 mission trials. As can be observed from Figure 11, only 1 out of the 10 missions ended in failure showing the power of DQN-based DRL to learn effective mission planning policies in dynamic channels with wireless propagation anomalies and adversarial jammers.

We denote by random variable T the number of decision epochs for completing the mission when the mission was successfully completed. Table 4 shows observed values of T for the above 10 mission trials.

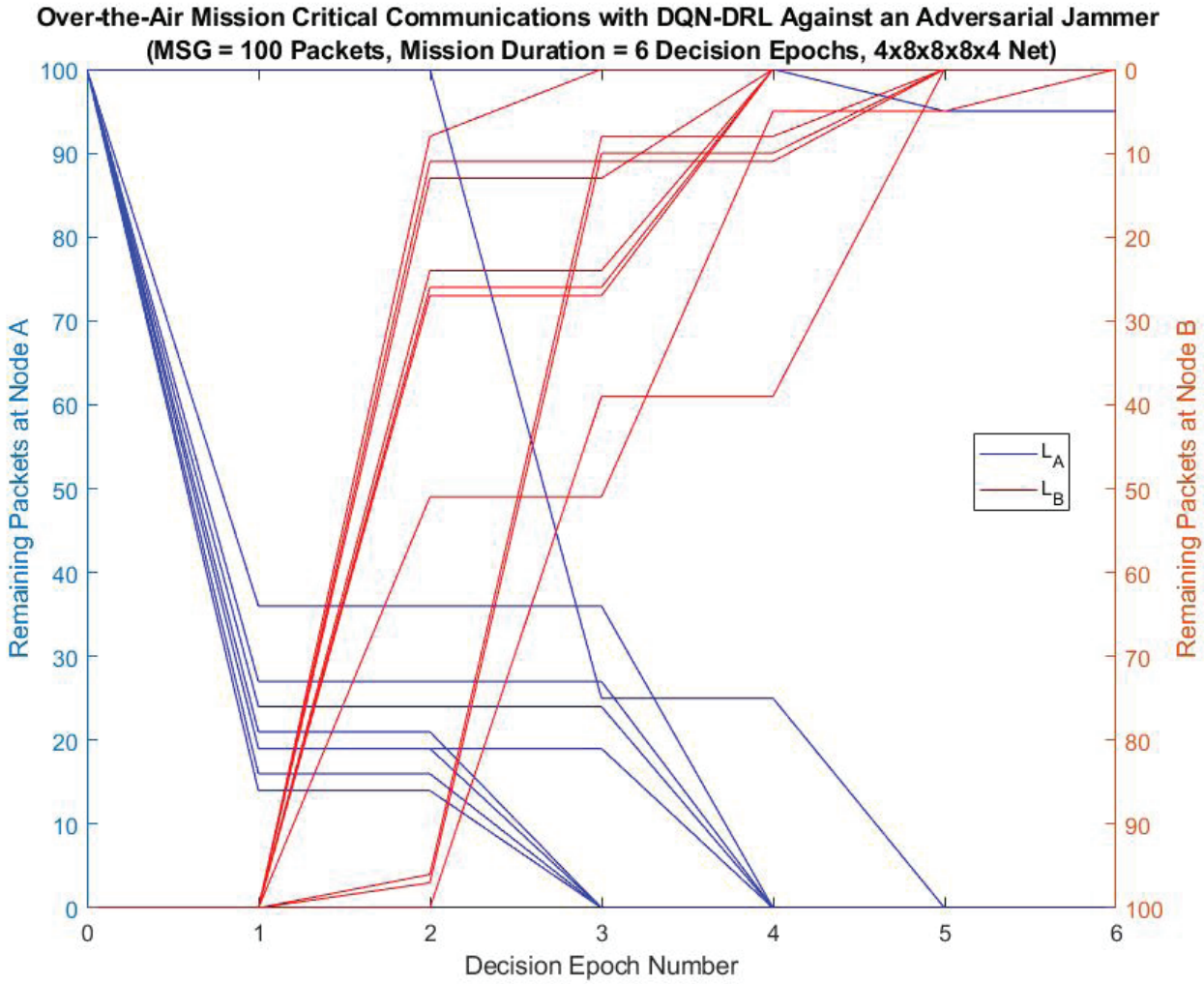

Figure 11. Critical Message Exchange Performance of DQN-based Mission-Critical Communications Planning in an Actual Wireless Network in the Presence of a Sequential Jammer.

Mission #	1	2	3	4	5	6	7	8	9	10
Epochs for mission completion (T)	4	6	5	N/A	4	5	4	4	5	5

Table 4. Number of Decision Epochs to Complete Each Successful Over-the-Air Mission.

From this data we compute the average duration for mission completion, denoted by the symbol T with a line over it, when the mission is completed:

$$\bar{T} = \frac{1}{K}\sum_{i=1,T_i\leq N}^{n} T_i = 4.67 \text{ decision epochs} \quad (9)$$

Where $K \leq N$ is the number of missions that was completed successfully. The spread of T around this average can be characterized by its standard deviation computed as:

$$standard\ deviation\ of\ T = \sqrt{\frac{1}{K}\sum_{i=0,T_i\leq N}^{n}\left(T_{,i} - \bar{T}\right)^2} = 0.7071 \quad (10)$$

Fourth case was to evaluate the performance of MCC planning in wireless networks with DQN-based DRL for larger critical message lengths of 250 and 500 packets. Tables 5 and 6 summarize the performance averaged over 10 trials for different mission-durations.

MD = 8 decision epochs			MD = 10 decision epochs			MD = 12 decision epochs		
MSP_{DQN}	MSP_{RP}	PMSI	MSP_{DQN}	MSP_{RP}	PMSI	MSP_{DQN}	MSP_{RP}	PMSI
0.51875	0.06698	674%	0.83853	0.27745	202%	0.88875	0.52955	68%

Table 5. Averaged Performance of MCC Planning with DQN-DRL in Simulated Wireless Networks with Estimated Realistic Throughput Parameters. Message Size = 250 Packets.

MD = 16 decision epochs			MD = 18 decision epochs			MD = 20 decision epochs		
MSP_{DQN}	MSP_{RP}	PMSI	MSP_{DQN}	MSP_{RP}	PMSI	MSP_{DQN}	MSP_{RP}	PMSI
0.52749	0.06768	679%	0.64726	0.19251	236%	0.83078	0.36954	125%

Table 6. Averaged Performance of MCC Planning with DQN-DRL in Simulated Wireless Networks with Estimated Realistic Throughput Parameters. Message Size = 500 Packets.

Tables 5 and 6 affirm the effectiveness of DQN-based MCC planning in ensuring mission-success with drastically higher likelihoods compared to what is achievable with random planning.

Finally, we evaluated the performance of our new DPHC algorithm compared to the Google DeepMind's original DQN algorithm. Figure 12 shows the MSP achieved under DQN and DPHC algorithms during training and testing.

According to Figure 12, the DQN outperforms DPHC during training, while during testing, DPHC-DRL outperforms the DQN. The reason is that during training, we force our DPHC to select actions according to a mixed policy whereas original DQN is allowed to follow the pure strategy suggested by the DQN. This makes the DPHC to select inferior actions that lead to mission-failure. However, these failures allow it to learn a more robust decision policy. During testing, on the other hand, both DQN and DPHC are allowed to select actions according to the greedy pure strategy derived from the predicted Q(s,a). Now, the DPHC's more robust policy is capable of planning MCC more successfully while original DQN displays somewhat erratic performance. With 10K training, the new DPHC achieves a PMSI of 29% relative to the original DQN.

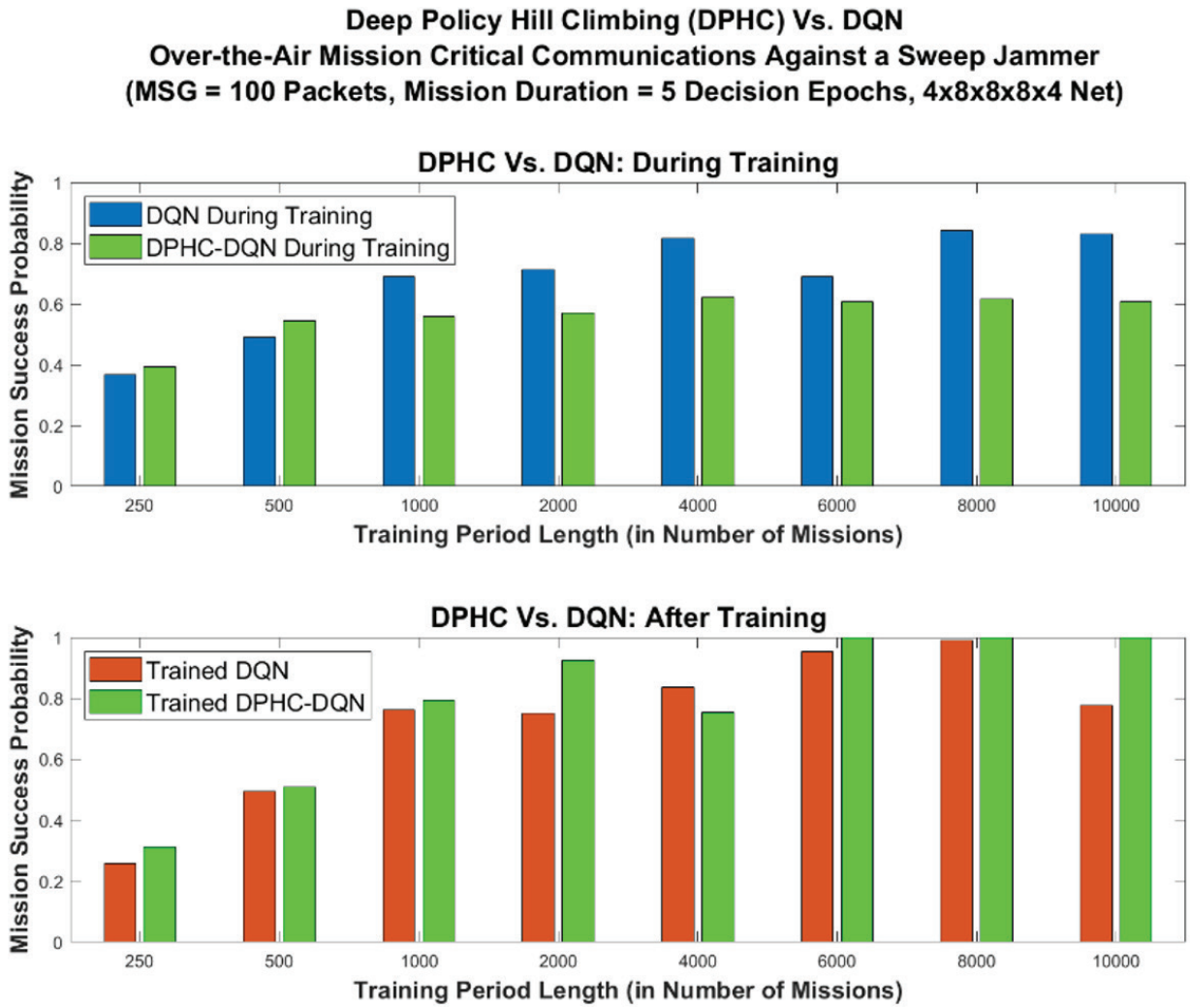

Figure 12. Comparison of Mission-Success Probability of DQN-based and the Newly Designed DPHC-based Mission-Critical Communications Planning (Over 6 Decision Epochs) in the Presence of a Sequential Jammer. (TOP) during Training. (BOTTOM) after Training.

DISCUSSION

The first experiment case established the potential of the proposed approach in a simplified setting without the added complications of wireless channel anomalies, node synchronizations, computational/processing delays, and USRP hardware imperfections. Results in Figures 7 and 8 verified that indeed MCC planning with DQN-based DRL can lead to significant performance improvements compared to random policies. For example, for mission-durations of 14 epochs, the DQN's MSP of 0.9998 is a 179% improvement over the random planning. This case also served to offer guidelines on how to select the overall structure of the ANN as well as parameter values such as learning rate and training period length.

The second case used a faithful simulation of wireless networks with estimated throughput parameters to train a DQN that has a good chance of performing well once integrated into the actual hardware. The key to the success of this approach was good statistical modeling and

estimation of the key parameters that affect the MCC planning. The 90% MSP achieved in the third case, once a DQN trained with this model was integrated in to the real USRP hardware based wireless network, proved that our statistical modeling and estimation approach of the associated parameters are indeed reasonable.

As seen in Figure 10, the DQN does considerably better in all tested mission-durations compared to random planning. Tables 5 and 6 showed that these conclusions hold even with larger critical information messages of 250 and 500 packets. In all cases, the reported performance metrics were evaluated by averaging over 10 trials to reduce the effects of statistical variations.

Finally, we compared the performance of the MCCP based on the developed DPHC Algorithm to that based on the original DQN algorithm. As Figure 12 illustrates, our DPHC proved on-par or better than the DQN after the training.

Looking ahead towards future work, since the DQN must learn to complete a mission as quickly as possible, a new reward system can be designed to assign higher rewards whenever a mission is completed with a smaller number of decision epochs, while a fixed negative reward is assigned for those failed missions as before. For example, if the nodes managed to finish 2Td time intervals before the mission duration, a total of +2 would be added to the episode reward rather than the meager +1. This incentivizes the DQN to complete a mission faster. Another future work is to analyze the effectiveness of the developed DQN-based DRL policies against other types of jammers such as Markov and smart jammers.

CONCLUSIONS

The contributions of this project are two-fold: First, the project developed a novel mathematical model for mission-critical operations and showed through MATLAB simulations that a DQN can learn how to solve the associated planning problem. Second, it explored an example scenario of exchanging OTA messages in a real wireless network formed of USRP SDRs within a time constraint. In addition, a new DPHC algorithm was developed that outperformed the Google DeepMind's DQN algorithm significantly. Hence, the project not only serves as an important contribution to the field of MCC planning but also shows the relevance of the developed DQN-based DRL approach to a wide range of planning under uncertainty problems. These include disease control, food/crop management, refugee crises, troop distribution, and stock optimization to name a few.

Ultimately, this project demonstrates that DQN-based DRL can be an effective solution for mission planning problems. Since currently most mission-critical operations are being carried out manually making them prone to human error that can lead to disastrous outcomes, this project serves to make the case for adapting AI techniques to remove or reduce the risk of human errors in high stake missions.

AUTHOR INFORMATION

Corresponding Author

*Milidu Jayaweera, milidutkd@gmail.com

ACKNOWLEDGMENT

I would like to thank Dr. Sudharman Jayaweera for getting me access to the UNM Communications Laboratory and Dr. Mohamed A. Aref for aiding in laboratory experiments. Special thanks to my science teacher Mrs. Lena Eddings for her time filling out the numerous forms to ensure my participation in the contests of my choosing.

ABBREVIATIONS

AI, Artificial Intelligence; ANN, Artificial Neural Network; DNN, Deep Neural Network; DPHC, Deep Policy Hill Climbing; DQN, Deep Q-Network; DRL, Deep Reinforcement Learning; MCC, Mission-critical Communications; MCCP, Mission-critical Communications Protocol; MD, mission-duration; MDP. Markov Decision Process; ML, Machine Learning; MSP, Mission-success Probability; NE, Nash Equilibrium; OTA, over-the-air; PMSI, Percentage Mission-success Improvement; RL, Reinforcement Learning; SDR, Software-defined Radio; SPE, Subgame Perfect Equilibrium; USRP, Universal Software Radio Peripheral.

REFERENCES

1. Grover, K.; Lim, A.; Yang, Q. Jamming and Anti-jamming Techniques in Wireless Networks: A Survey. *International Journal of Ad Hoc and Ubiquitous Computing.* **2014**, 17(4), 197-215.

2. Understanding the Difference Between Mission-Critical and Business-Critical Communications; https://usatcorp.com/understanding-the-difference-between-mission-critical-and-business-critical-communications/

3. Blythe, J. An overview of planning under uncertainty. *AI Magazine*. **1999**. 20(2), 37-54.

4. Puterman, M. L. *Markov decision processes: Discrete stochastic dynamic programming*. John Wiley & Sons: Hoboken, NJ, 2010.

5. Sutton, R. S.; Barto, A. G. *Reinforcement learning: an introduction*. The MIT Press: Cambridge, MA, 2012.

6. Leyton-Brown, K.; Shoham, Y. *Essentials of Game Theory*. Morgan & Claypool Publishers, 2008.

7. Rappaport, T. S . *Wireless Communications: Principles and Practices*. Prentice-Hall, 2002.

8. Mnih V.; et al. Human-level control through deep reinforcement learning. *Nature*. **2015**, 518(7540).

9. Duda, R. O.; Hart, P. E.; Stork, D. G. *Pattern classification*. Wiley-Interscience, 2000.

10. Leon-Garcia, A. *Probability, Statistics, and Random Processes for Electrical Engineering*. Pearson Prentice Hall: Upper Saddle River, NJ, 2008.

11. Watkins, C.; Dayan, P. Q-learning. *Machine Learning*. **1992**, 8(3), 279-292.

12. Schwartz, H. M. *Multi-agent Machine Learning*. Wiley: New Jersey, USA. 2014.

13. Bowling, M.; Veloso, M. Multiagent learning using a variable learning rate. *Artificial Intelligence***. 2002**, 136(2), 215-250.

Comparison of Different RNA-Binding Proteins in *Manduca sexta* Larva Memory Formation

Nathaniel E. Jobe [a)]*

Mallory N. Decker [b)]

William P. Burris [a)]

Veronica Evans [b)]

[a)] San Juan College High School, Farmington, NM

[b)] San Juan College, Farmington, NM

ABSTRACT

Multiple factors have been shown to affect how memories are formed and retained. In some studies, individual RNA-binding proteins that are found more commonly in the nervous system have been linked to the formation of short-term memory. Some of these RNA-binding proteins, Cytoplasmic Polyadenylation Element Binding protein (CPEB) and Pumilio, had been independently shown to affect memory formation. To see how these proteins affect memory formation, the protein concentrations are reduced by injecting double-stranded RNA molecules specific to the proteins into the larvae of *Manduca sexta.* The purpose of this study is to investigate how knockdowns of these proteins affect *M. sexta* memory formation and what happens when both proteins have a knockdown. The results of this study showed that when the larvae receive the knockdowns, the hornworm's memory improved when compared to the control group. There were multiple problems throughout the study, it needs to be repeated to demonstrate significance. One such problem being the non-statistically significant sample size of the experiment.

KEYWORDS: Cytoplasmic Polyadenylation Element Binding Protein, CPEB, Pumilio, Memory, RNA-binding, Small Interfering RNA, siRNA, Protein Knockdown

INTRODUCTION

This project is to determine the effect of knockdown Pumilio in *M. sexta* larva memory formation. Previous studies have examined the effects of a knockdown of another protein called cytoplasmic polyadenylation element binding protein 2 (CPEB2) on *M. sexta* larva memory formation. CPEB works by binding to a specific region of messenger RNA (mRNA) known as cytoplasmic polyadenylation element (CPE) on the 3' untranslated region[1]. When CPEB binds to the CPE it is responsible for both translational repression and translational activation by polyadenylation.

The Pumilio protein functions in a similar way as CPEB because it binds to a certain sequence on mRNA called the Pumilio Response Element (PRE)[2]. Like CPEB, Pumilio serves multiple functions within organisms and one of those functions is to help regulate memory formation and other neural processes[9]. There are multiple studies done that show that when

mice have a Pumilio knockdown or other problems related to proper Pumilio formation, the mice display problems making or retaining memories[7,8,10].

This research was done at San Juan College. The mentor, Dr. Evans, oversaw and managed the data collection in an ongoing investigation on the connection between CPEB2 and short-term memory in *M. sexta* larva and observed that by performing a knockdown for CPEB2 in *M. sexta* larva retain less memories than those that have not had a knockdown. Since both CPEB and Pumilio serve similar functions in memory formation, this study will investigate the relation between Pumilio in *M. sexta* larva and memory formation as well as comparing it to CPEB's relationship with memory formation. Finally, the study will investigate the effect of a knockdown of both RNA-Binding proteins. The expected result of the experiment is that the group of larvae that had a knockdown of both proteins would remember less than those that had only one protein knockdown or those that had no knockdowns. This project was funded by a grant through the Institutional Development Award (IDeA) from the National Institute of General Medical Sciences of the National Institutes of Health under grant number P20GM103451.

MATERIALS AND METHODS

siRNA Creation

Basic Local Alignment Search Tool (BLAST) Search. To conduct a BLAST search to determine if *M. sexta* had Pumilio protein, the researcher first searched the NCBI's protein database for Pumilio in an insect species closely related to *M. sexta*. For this blast search, the FASTA sequence from *Drosophila melanogaster* was used. This protein FASTA sequence was then used for the Insect Base BLAST search using blastp for *M. sexta*. This search pulled up five results for a Pumilio protein in *M. sexta*. From here the five FASTA sequences, with both protein and RNA sequences, were saved for other uses.

Clustal Omega Multiple Sequence Alignment System. Clustal Omega was used to determine sections of the five sequences found from the blast search had areas of high similarity. Firstly, Clustal Omega was used to find similarities in the protein FASTA sequence. All five protein sequences were put into the Clustal Omega program and all settings were left at their defaults. The program was run and produced a document with all the protein sequences aligned as seen in Figure 1.

The sequences where the proteins were identical were shown by asterisks. Since the protein Clustal Omega showed a large section of identical sequences, a DNA Clustal Omega was run. This also showed a long DNA sequence where all five were the same as seen in Figure 2.

siRNA Ordering. Using a section found from the DNA Clustal Omega, a sequence from roughly in the middle of the identical area was found. This sequence was 30 nucleotides long and was used as the basis of the siRNA that was made for this project. The sequence included cytosines, guanines, and thymine. This sequence is CGTGTCGCCCGGCGGCGTGCTGGCGCCGCG and is seen in Figure 2.

Figure 1. The Clustal Omega results for the amino acid sequences found from the BLAST search. This is an area that is identical between the six sequences found.

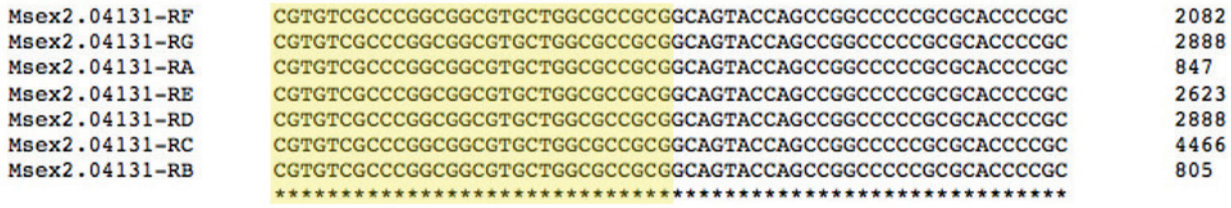

Figure 2. This Clustal Omega alignment is for the DNA sequence. The highlighted section shows the sequence used to create the siRNA.

Larva Maintenance

Larva Housing. The larvae were received shortly after hatching and were left in the food container they came in for four days in order to let them grow a little more. After four days, the larvae were moved into individual feeding tubes, that were also premade. Before they were moved into their new tubes, they were cleaned in a 1% bleach solution for a few seconds and rinsed in sterile water in hopes to alleviate a mold problem that was developing in the tube. The second shipment of the larva was received and was also left in the shipping container for four days. This set of larvae did not receive a bleach cleaning before being transferred to the individual feeding tubes. The second set of larvae also had a mold problem. Once the larvae were back in the tubes, they were put under a light to keep a constant temperature.

Larva Cleaning. About once a week, the tubes with any visible amount of mold were cleaned by sterilized a scoop with 95% ethanol between each use and the excrement and mold were removed. Once the mold was removed, the larvae were placed back into the tubes.

Larva Injection and Training

siRNA Injection Preparation. For the Pumilio knockdown group, the researcher added 20µl of the Pumilio siRNA (1µg/µl) to 990µl PBS (1X). For the Pumilio and CPEB knockdown group, the researcher added 20µl of the Pumilio siRNA (1µg/µl) and 20µl of the CPEB siRNA (1µg/µl) to 980µl PBS (1X). The main reason for the solution with both types of siRNA having an overall higher concentration of the siRNA's is that there was concern that using a half concentration of each individual siRNA wouldn't allow the individual siRNA to work as effectively.

Training Gel Setup. The gel was made with 7 g agarose powder and 35 ml of 2mM LiCl. This was combined and ddH_2O in order to reach 350 ml total. The LiCl was added to allow the electricity to pass through the gel. This was then poured into the bottom of the gel setup, with care to make sure the wires could be connected to the electricity. This can be seen in Figure 3.

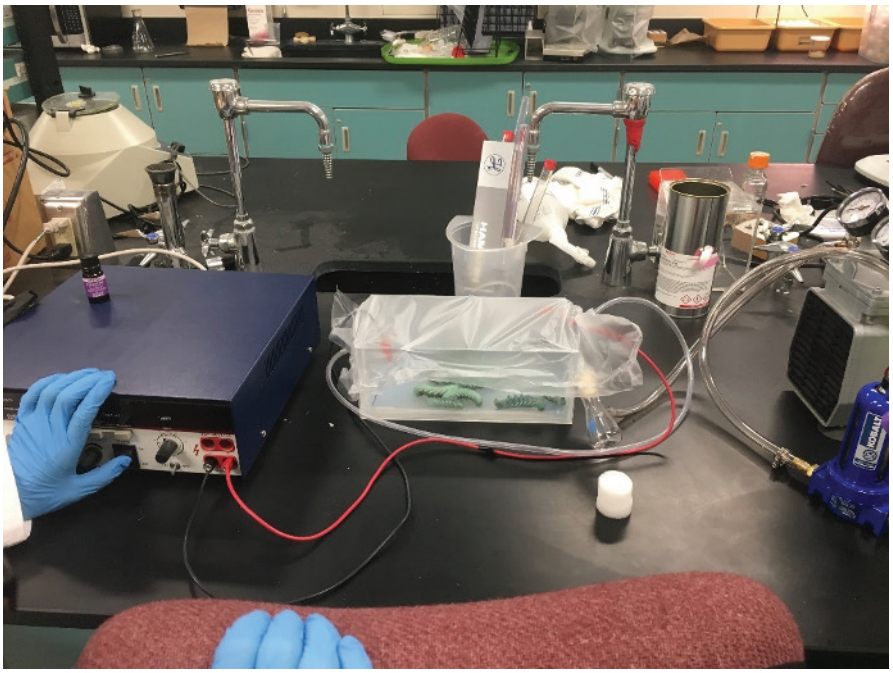

Figure 3. This photo shows the larvae in the gel box right before they would receive the shock.

Larva Injection. The larvae were removed from the feeding tubes and set in a container filled with ice, separated by different types of injections. Three hundred microliters of the siRNA mix for the group (Pumilio, CPEB, and Both) were pulled up into the syringes. Once the larvae have been on ice for at least five minutes to slow their metabolism, remove them from the ice and swab the area behind the third abdominal prolegs with ethanol to sterilize the area. The needle was put in at less than a 45º angle in the area that was swabbed and 25 µl of the corresponding siRNA was injected.

Larva Training. Lavender essential oil is placed in an Erlenmeyer flask that is connected to the gel box and air compressor. One group is placed on the gel and the gel box is covered in plastic wrap as seen in Figure 4.

Figure 4. A close-up view of the larvae inside the gel box.

Once larvae are in the box, turn the air compressor on for ten seconds. Immediately after the air compressor is turned off, turn the electricity on for ten seconds at 90 V. Remove that group of larvae and repeat for the rest of the larvae. Once all groups are done, wait thirty minutes and repeat. This was done a total of six times over a period of two hours thirty minutes. Once all training is done, place larvae in the corresponding food tube and wait until the next day.

Olfactometer Test. Place the same lavender oil in the Erlenmeyer flask attached to the Olfactometer Y-Tube. Setup the Y-Tube for the test as seen in Figure 5. Check airflow at the olfactometer's lowest setting, so that the lavender smell is making its way through the setup. Place the larva at the intersection of the tube and cover the end with mesh. Cover the setup with tin foil to make a dark environment. Turn on the air compressor for five minutes and record the larva's position. Once the data was recorded, the larvae were placed in labeled bags and frozen before disposal.

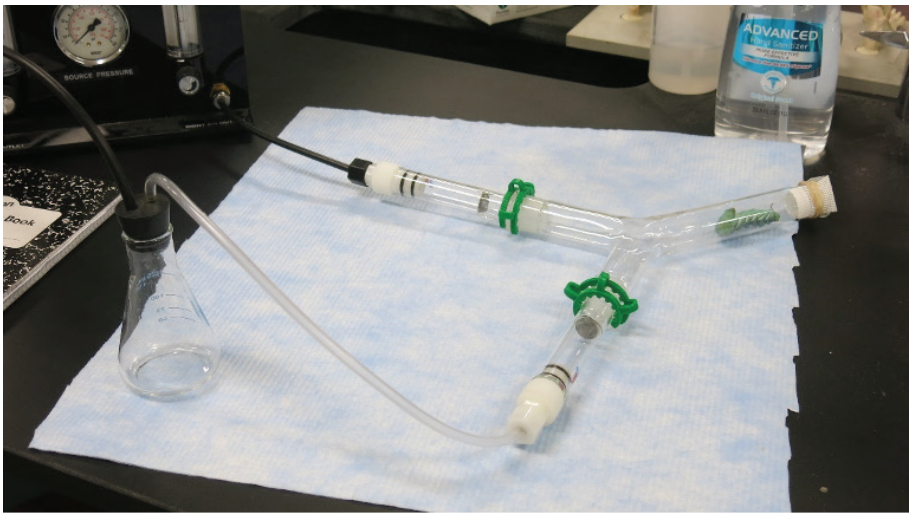

Figure 5. This is a photo of the y-tube setup before the foil was placed on top, showing the larva location.

RESULTS

The results indicate that the control group remembered less about the training test than both the Pumilio Knockdown group and the Pumilio/CPEB Knockdown group (Shown in Table 3 and 4 and Graph 1 and 2). For the purpose of this research, the "turned left" and the "no motion" observations indicate that the larva did not remember the training, while the other two observations show they remember the training. Additionally, the combination of both Pumilio and CPEB knockdowns did not seem to effect memory any more than just the Pumilio knockdown. The CPEB knockdown group showed that the hornworms remember more than the control group. Of all the groups, the control group had less larvae that remembered the training than any of the other groups that had the proteins knocked down.

Control				
Larva	Turned Left (Towards Smell)	Turned Right (Away from Smell)	Turned Around	No Motion
1				X
2			X	
3				X
4				X
5	X			
6		X		
7				X
8				X
9	X			
10			X	
Total	2	1	2	5

Table 1. Results from the control trial.

Pumilio Knockdown				
Larva	Turned Left (Towards Smell)	Turned Right (Away from Smell)	Turned Around	No Motion
1			X	
2	X			
3			X	
4		X		
5	X			
6			X	
7	X			
8			X	
9	X			
10			X	
Total	4	1	5	0

Table 2. Results from the Pumilio knockdown trial.

CPEB Knockdown				
Larva	Turned Left (Towards Smell)	Turned Right (Away from Smell)	Turned Around	No Motion
1		X		
2			X	
3			X	
4				X
5	X			
6		X		
7		X		
Total	1	3	2	1

Table 3. Results from the CPEB Knockdown trial.

Pumilio and CPEB Knockdown				
Larva	Turned Left (Towards Smell)	Turned Right (Away from Smell)	Turned Around	No Motion
1			X	X
2			X	
3	X			X
4		X		X
5	X			
6	X			
7			X	X

8			X	X
9			X	
10	X			
Total	4	1	5	5

Table 4. Results from the Pumilio and CPEB knockdown trial.

CONCLUSIONS

This study asked if disrupting the function of the RNA-binding proteins CPEB and Pumilio using RNA interference would have an effect on memory retention in *M. sexta* larvae. There were multiple novel outcomes of this work. One thing shown through this study is that *M. sexta* does have homologs of Pumilio proteins within the organism. Then, the results of the y-tube tests indicate that the larva that experienced the siRNA interference of the RNA binding proteins remembered more than the control group that had no siRNA interference. Also, the data indicates that the larvae with the CPEB siRNA injection remembered more when compared to the Pumilio and Pumilio/CPEB knockdown groups. Based on these results, the presented hypothesis should be rejected because the larvae with both protein knockdowns demonstrated greater avoidance of the negative stimulus than the control group. However, previous work in this lab has demonstrated that a higher percentage of untreated *M. sexta* larvae avoid the odor associated with the negative stimulus than shown in these experiments, suggesting that a larger sample size and more experiments may be needed. However, these results still suggest that CPEB and Pumilio do play some role in memory retention.

Due to the surprising results, different potential confounding factors have been identified that suggest that the results of this study should be interpreted with caution. One, the sample sizes for all four groups had different numbers of larvae. Two, there was difficulty matching the developmental stage of the larvae for the experiment. The Pumilio and the CPEB/Pumilio groups larvae at the beginning of the 5th instar while the control and the CPEB larvae were closer to the end of the 5th instar. Three, the larvae ordered for this experiment had a persistent problem with mold, which may have affected their behavior. In these experiments, lavender essential oil was used as the odor associated with the negative stimulus instead of the ethyl acetate that had been used previously in other studies and in this lab. This change in procedure was decided on due to ethyl acetate's negative health effects on humans. This study was also unable to verify that a knockdown affect from the siRNA injections. The experiment needed to be verified by looking for reduced RNA expression using RT-PCR or reduced protein expression by Western Blotting. For the next phase of this project, the sample sizes would need to be increased as well as keeping them consistent. Also, ways to test memory other than an olfactometer would be investigated

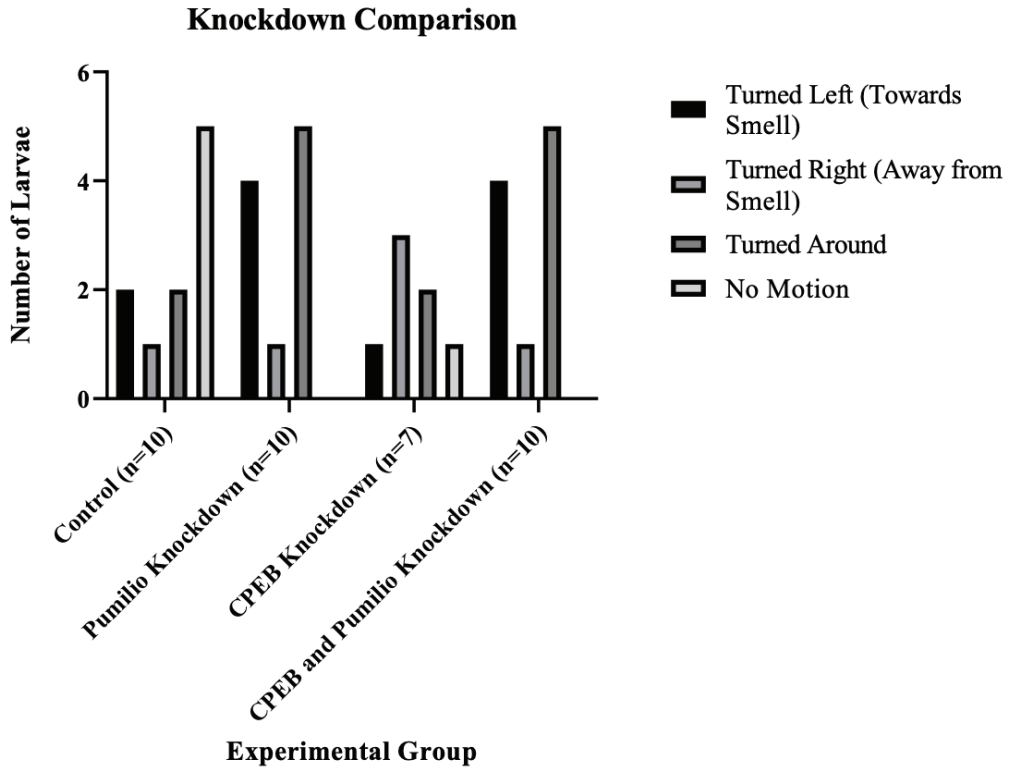

Graph 1. A comparison between all four groups, showing the four categories shown in the tables.

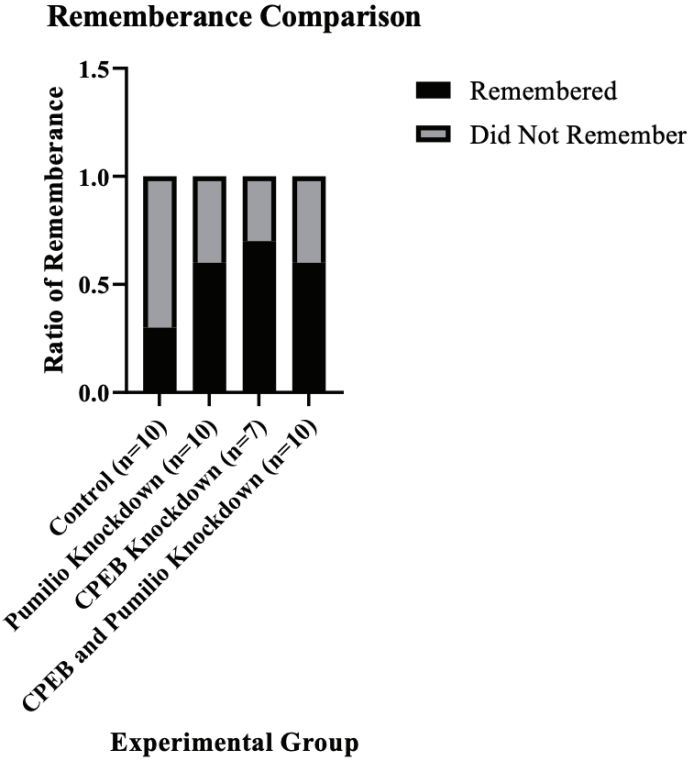

Graph 2. A comparison between the four groups separated by whether the data indicated the larvae remembered or if they did not remember, as defined in the results section.

AUTHOR INFORMATION

Corresponding Author

*Nathaniel Jobe, tater-tot03@hotmail.com

Funding Sources

The research reported in this publication was supported by an Institutional Development Award (IDeA) from the National Institute of General Medical Sciences of the National Institutes of Health under grant number P20GM103451.

ACKNOWLEDGMENT

The research reported in this publication was supported by an Institutional Development Award (IDeA) from the National Institute of General Medical Sciences of the National Institutes of Health under grant number P20GM103451. Also, the researcher would like to thank William Burris, Mallory Decker, and Veronica Evans, Ph.D.

ABBREVIATIONS

BLAST, Basic Local Alignment Search Tool; CPE, cytoplasmic polyadenylation element; CPEB, cytoplasmic polyadenylation element binding protein; ddH2O, double-distilled water; DNA, deoxyribonucleic acid; IDeA, Institutional Development Award: LiCl, Lithium Chloride; mRNA, messenger ribonucleic acid; NCBI, National Center for Biotechnology Information; PBS, Phosphate-buffered Saline; PRE, Pumilio Response Element; RNA, ribonucleic acid; RT-PCR, reverse transcription polymerase chain reaction; siRNA, small interfering ribonucleic acid.

REFERENCES

Charlesworth, A.; Meijer, H. A.; Moor, C. H.. Specificity factors in cytoplasmic polyadenylation. *Wiley Interdisciplinary Reviews: RNA* **2013,** *4*(4), 437-461. doi:10.1002/wrna.1171

Chen, G.; Li, W., Zhang; Q., Regulski; M., Sinha, N.; Barditch, J.; . . . Dubnau, J. Identification of synaptic targets of Drosophila Pumilio. *PLoS Computational Biology,Preprint* (2008) **2005**. doi:10.1371/journal.pcbi.0040040.eor

Dong, H.; Zhu, M.; Meng, L.; Ding, Y.; Yang, D.; Zhang, S.; . . . Xu, E. Y. *Pumilio2*regulates synaptic plasticity via translational repression of synaptic receptors in mice. *Oncotarget* ***2018,*** *9*(63). doi:10.18632/oncotarget.24345

Dong, S.; Wang, Y.; Cassidy-Amstutz, C.; Lu, G.; Bigler, R.; Jezyk, M. R.; . . . Wang, Z. Specific and Modular Binding Code for Cytosine Recognition in Pumilio/FBF (PUF)RNA-binding Domains. *The Journal of Biological Chemistry* **2011***, 286*(30), 26732-26742. doi:10.1074/jbc.M111.244889

Dubnau, J.; Chiang, A.; Grady, L.; Barditch, J.; Gossweiler, S.; Mcneil, J.; . . . Tully, T. The staufen/pumilio Pathway Is Involved in Drosophila Long-Term Memory. *Current Biology* **2003,** *13*(4), 286-296. doi:10.1016/s0960-9822(03)00064-2

Gennarino, V. A.; Palmer, E. E.; Mcdonell, L. M.; Wang, L.; Adamski, C. J.; Koire, A.; . . . Zoghbi, H. Y. A Mild PUM1 Mutation Is Associated with Adult-Onset Ataxia, whereas Haploinsufficiency Causes Developmental Delay and Seizures. *Cell* **2018,** *172*(5). doi:10.1016/j.cell.2018.02.006

Gennarino, V.; Singh, R.; White, J.; De Maio, A.; Han, K.; Kim, J.; . . . Zoghbi, H. . Pumilio1 Haploinsufficiency Leads to SCA1-like Neurodegeneration by Increasing Wild-Type Ataxin1 Levels. *Cell* **2015***, 160*(6), 1087-1098. doi:10.1016/j.cell.2015.02.012

Lu, G.; Hall, T. Alternate Modes of Cognate RNA Recognition by Human PUMILIO Proteins. *Structure* **2011***,19*(3), 361-367. doi:10.1016/j.str.2010.12.019

Siemen, H.; Colas, D.; Heller, H. C.; Brüstle, O.; Pera, R. A. . Pumilio-2 Function in the Mouse Nervous System. *PLoS ONE* **2011***,6*(10). doi:10.1371/journal.pone.0025932

Vessey, J. P.; Schoderboeck, L.; Gingl, E.; Luzi, E.; Riefler, J.; Leva, F. D.; . . . Macchi, P. Mammalian Pumilio 2 regulates dendrite morphogenesis and synaptic function. *Proceedings of the National Academy of Sciences* **2010***,107*(7), 3222-3227. doi:10.1073/pnas.0907128107

Utilizing *C. elegans* to Study Effects of Natural and Pharmaceutical Anti-Obesity Medications

*Louie Martinez**

Grants High School, Grants, NM

ABSTRACT

The purpose is to understand mechanisms associated with obesity and utilize natural or pharmaceutical anti-obesity medications on growth of nematodes. The hypothesis is anti-obesity medication, phentermine, would have the most significant effect on nematode population growth. The null hypothesis is there will be no significant difference between groups (blank, control, phentermine, bupropion, green tea, Mormon tea) tested. Five experiments were conducted examining population growth. Experiment one included 12 cultures, six each, non-genetically modified (WN2002) and genetically modified (RB1716) nematodes. Nematodes in experiment one were grown in (1:5) concentration. Experiment two-to-five, wildtype strain only and six cultures each, to pinpoint effects in model organism. Experiment two-to-three and four-to-five were grown in (1:10) and (1:12) concentrations respectively. Statistical analysis of variance (ANOVA) was conducted with [F (5, 30); $p < 0.05$] degrees of freedom and [F-critical= 2.53], [F (6, 42); $p < 0.05$] and [F-critical= 2.44]. Results: experiment 1 (WN2002) (F= 0.37), experiment 1 (RB1716) (F= 0.85), experiment two (F= 1.27), experiment three (F= 1.89), experiment four (F= 6.08), and experiment five (F= 4.00). T-tests were conducted to validate (ANOVA). Nematodes grown in (1:5) concentration show small population sizes and no observable significant effects. Nematodes grown in (1:10) concentration show small population sizes and no significant effects, but show effects comparing phentermine and green tea to blank (E3). Nematodes grown in (1:12) concentration show larger population sizes and significant effects.

KEYWORDS: *C. elegans*, Anti-obesity, HFCS, Population Growth

INTRODUCTION

Today, the growing concern surrounding obesity and complex weight-loss programs in the United States has led to an increased use of anti-obesity medications. Various Food and Drug Administration (FDA)-approved anti-obesity medications have been extensively clinically tested. This research project focuses on the effectiveness of various anti-obesity drugs on the excess lipid accumulation in genetically modified and non-genetically modified wild-type nematodes. Many different types of anti-obesity drugs are available through prescription, non-prescription, and commercial use which gives a wide range of supplements available to consumers, whether it be monitored under a licensed physician or self-supplemented. Nematode *Caenorhabditis elegans* (*C. elegans*) are utilized as invertebrate substitutes to more complex model organisms, such as mice, because of the availability, drastic price difference, and ethical responsibilities.

The increase in obesity rates in the United States may be associated with the excess sugar and caloric intake. Studies have been completed showing the adverse effects that various sugars, specifically high-fructose corn syrup (HFCS), can create when supplied in large, assessable quantities. HFCS is a complex polysaccharide with various forms and concentrations. The composition of HFCS is a combination of the monosaccharides ($C_6H_{12}O_6$), glucose and fructose, in varying concentrations for increased sweetness with lessened production and cost. The health effects associated with HFCS prompted concern to understand mechanisms of metabolic activity, excess lipid accumulation (obesity), and the utilization of natural and pharmaceutical anti-obesity medications. HFCS will be supplied as an independent variable additive per xenic culture to promote population growth and lipid accumulation.

C. elegans have a wide range of capability, due in part to the diversity, simplicity, and quantifiable analyses possibilities. *C. elegans* are non-parasitic, microscopic roundworms which have adapted to survive in all, or nearly all, biomes and environments on earth. Maintenance is efficient using personal protective equipment and safe laboratory techniques. *C. elegans* feed on *Escherichia coli* (*E. coli*) as their main food source, which facilitates the use of sterile laboratory techniques for inoculation and growth.

In order to fully analyze *C. elegans* in experimentation composed of population statistics, the understanding of the microscopic roundworm, as a single unit, must be achieved. Nematodes are characterized in the phylum Nematoda. The basic composition of the complex model organism, for research purposes, are as follows, (959) somatic cells with (300) being neurons controlling sensory activity (Edgley and Riddle, 2018). *C. elegans*' anatomical composition allows for research to be conducted to analyze anti-obesity medications with neuronal activity, "brain chemistry", as well as metabolic processes. The complex digestive tract is capable of metabolizing complex molecules, considering origin. In general, the wild-type *C. elegans* (N2) have an approximate lifespan of twenty-one days with novel generation approximately every three days (Zheng and Greenway, 2005). *C. elegans* are composed of two different strains when grown in populations, hermaphrodite and male. Hermaphrodites are more common, because of self-reproduction quality. *C. elegans* was the first multicellular organism to have its genome entirely sequenced, where "65%" of genes in the model organism have been shown to closely express human disease of medical and research interest (Zheng and Greenway, 2005, p. 186). Since the model organism *C. elegans* has the anatomical and genetic capabilities of expressing human obesity with accuracy, this experimentation will be conducted with wild-type (N2 and WN2002) strains and genetically modified (RB1716) strains.

The mechanisms and usages of the four treatments utilized in this research are as follows. Phentermine is an appetite suppressant that works metabolically and neurochemically in humans (Kim et al., 2006). A study utilizing phentermine as a medical weight loss supplement in Korean patients reported significant success in weight and waist circumference reduction with minimal reported side effects (Kim et al., 2006). Bupropion is an amino-ketone antidepressant normally used in conjunction with naltrexone for weight loss in brand name Contrave (Sherman et al., 2016). Bupropion, a weak dopamine and norepinephrine reuptake inhibitor, enhances [Pro-opiomelanocortin] (POMC) cell production and release of alpha-MSH and beta-endorphin in vitro", essentially working through neurochemical pathways

(Sherman et al., 2016). Green tea, a natural supplement believed to promote weight loss, will be utilized. Green tea has been shown to contain caffeine and flavonoid antioxidants speeding up the metabolic process (Kandola, 2018). Also, with the compounds present in green tea, the function has been shown to act through "inhibition of catechol O-methyl-transferase, and inhibition of phosphodiesterase" (Westerterp-Plantenga, 2010). Mormon tea, a natural supplement believed to promote weight loss, will be utilized. Mormon tea may provide aid for weight loss due to it containing tannins and alkaloids that may help increase metabolism (Staughton and Hegde, 2020).

The use of clinically tested and natural anti-obesity medications will be studied and quantified in several ways. Cultures grown on traditional agarose plates will be the main focus of the experimentation allowing the examination of population growth and statistical analysis. Other ways to facilitate research will include analysis on individual effects of anti-obesity medication on lipid accumulation of nematodes within an overall population. This can be accomplished through transfer of worms, (via platinum worm picker) onto individual agarose/microscopic slides fixed with chemicals that react to histochemical staining.

Analysis of effectiveness of the various anti-obesity medications/supplements may be accomplished through population counts and histochemical staining, quantifiable measures available in laboratory. Since raw data does not depict accurate population growth analysis, statistical analysis of variance (ANOVA) and statistical T-tests of the various experimentations will be conducted in order to pinpoint differences and effectiveness.

The purpose of this research is to understand various anti-obesity drugs and their effects on nematodes capable, similar to human processes, of weight gain. HFCS will be a controlled additive to all cultures to promote excess caloric intake. The variables will be the various anti-obesity medications and their ability to either reverse or heighten the effects of excess lipid accumulation.

The main goal of this research experiment is to understand if natural or pharmaceutical anti-obesity medications are a viable resource to combat obesity. This study can assist clinical researchers and medical professionals because of the similarities of the model organism, *C. elegans*, to humans and may give insight to potential treatment plans for patients. A study conducted with *C. elegans* can give valuable information for furthering a scientific suggestion and facilitate the use of more complex vertebrate organisms. The results may provide valuable insight to the overall effectiveness of anti-obesity medication and the potential beneficial and non-beneficial side effects accompanied by each remedial medication. The goal is to utilize the results gathered from this experimentation with nematodes and possibly create, or help support, correlations of model organism results to valuable human practicalities.

EXPERIMENTAL METHODS

Making Anti-Obesity Medication and Natural Anti-Obesity Remedy Solutions

All solutions were created following these procedures: Researcher equipped with personal protection equipment (PPE) for safety and sterility and solutions stored in sterilized centrifuge tubes.

Phentermine solution: Begin with a 15 mg capsule of phentermine, supplied from Parkhurst Pharmacy, and combine with 15 mL distilled water, weight of phentermine recorded with weigh boat and electronic scale, and solution held in a sterilized 15mL centrifuge tube. Aqueous solution is semi-soluble in distilled water so agitation with vortex mixer is crucial to solubility when pouring and creating experimental cultures.

Bupropion hydrochloride solution: Begin with a 10 mg immediate release (IR) tablet, supplied by Parkhurst Pharmacy, and combine with 10 mL distilled water, weight of the bupropion hydrochloride recorded with a weigh boat and electronic scale, and solution held in a sterilized 15 mL centrifuge tube. Aqueous solution is soluble in distilled water. Agitation with vortex mixer is completed for increased solubility for pouring and creating experimental cultures.

Green tea solution: Begin by weighing out one green-tea bag (2 g), measure 100 mL distilled water with a graduated cylinder and add water to 150 mL beaker, boil water in 30 second intervals; 2 minutes total, microwave covered with watch glass then remove from microwave with heat resistant glove, steep tea stirring with glass stirring rod, every 1–2 minutes for an overall time of 15 minutes, strain with #1 filter paper fitted in funnel placed on a funnel holding rack. Finally, place and store green tea in 50 mL centrifuge tube and let cool completely.

Mormon Tea solution: Begin by weighing out 2 g of Mormon tea, cut Mormon tea into smaller, homogenous pieces to be weighed and brewed, measure 100 mL distilled water with a graduated cylinder and add water to 150 mL beaker, boil water in 30 second intervals; 2 minutes total, microwave covered with watch glass then remove from microwave with heat resistant glove, steep tea stirring, with glass stirring rod, every 1–2 minutes for an overall time of 15 minutes, strain with #1 filter paper fitted in funnel placed on a funnel holding rack. Finally, place and store Mormon tea in 50 mL centrifuge tube and let cool completely.

Cultures made for Experiment One as follows: Two different strains, gathered from the Caenorhabditis Genetics Center utilized, strain WN2002 a wild-type strain and strain RB1716 a genetically modified strain. Six different cultures made and analyzed for each strain including: blank culture, control culture, phentermine culture, bupropion culture, green tea culture, and Mormon tea culture. Each culture in experiment one received ~15 mL nutrient growth medium, 2 mL of HFCS, and 1 mL of variable. The base use of one milliliter of variable solution was rationalized through dilution in preparation of solution and xenic culture. The concentration proved to be troubling, and without a specific constant classified weight of *C. elegans* as a single unit, alongside guidance from lab coordinator dilution decreases proved to be most reliable and probable for lab equipment available. Each culture received: *E. coli* arranged in a clockwise pattern (5 blots) as the main food source for the model organisms, 1 cm cube cut and transferred from master culture, from Caenorhabditis Genetic Center, to the culture. Nematodes were held in an incubator at 27–30 °C.

Cultures made for Experiment Two and Three with appropriate variable concentration adjustments as follows: One strain, gathered from Ward's Science, strain Wild Type (N2). Twelve different cultures made and analyzed for each strain including (six cultures for each experiment): blank culture, control culture, phentermine culture, bupropion culture, green tea culture, and Mormon tea culture. Each culture, in experiment two and three, received ~15 mL nutrient growth medium, 1 mL of HFCS, and 0.5 mL of variable. Each culture received:

E. coli arranged in a clockwise pattern (5 blots) as the main food source for the model organisms, 1 cm cube cut and transferred from master culture, from Ward's Science. Nematodes were held in an incubator at 27–30 °C.

Cultures made for Experiment Four and Five with appropriate variable concentration adjustments as follows: One strain, gathered from Ward's Science, strain Wild Type (N2). Twelve different cultures made and analyzed for each strain including (six cultures for each experiment): blank culture, control culture, phentermine culture, bupropion culture, green tea culture, and Mormon tea culture. Each culture, in experiment two and three, received ~15 mL nutrient growth medium, 1 mL of HFCS, and 0.25 mL of variable. Each culture received: *E. coli* arranged in a clockwise pattern (5 blots) as the main food source for the model organisms, 1 cm cube cut and transferred from master culture, from Ward's Science. Nematodes were held in an incubator at 27–30 °C.

Counting *C. elegans* for qualitative and quantitative analysis: After initial transfer, a start count is recorded utilizing dissecting microscope. After 24 hours, cultures are re-assessed to determine if an additional 1 cm cube from master culture should be re-transferred to ensure presence and growth of nematodes. Every 24 hours, depending on availability and access of lab on weekends, worm count of every culture is recorded. If population count exceeds ~150 nematodes culture split into four quadrants and count multiplied by four. For experiments one through three, 5 total days were recorded, and total "Day Count" for analysis is 6 days including start count. Yields of population size and days for experimentation is low, so adjustments are made to cultures to combat issue.

Statistical analysis for experimentation: Statistical Analysis of Variance (ANOVA) used to compare the means between different groups in an experiment completed by computing sum of squares between groups, sum of squares within groups, and total sum of squares to calculate an F-statistic and F-Critical Value. Statistical T-Tests completed by computing T-Tests used to compare individual culture with the population patterns observed in blank culture and control culture.

RESULTS

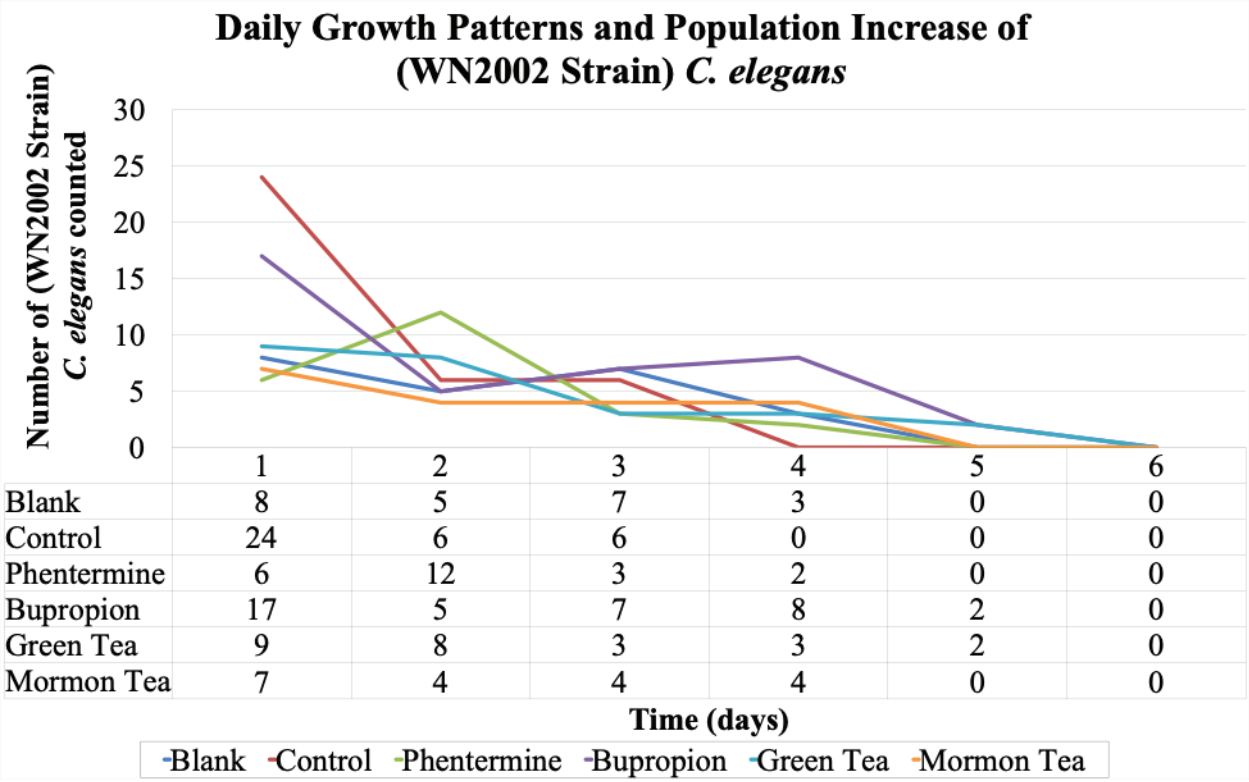

	1	2	3	4	5	6
Blank	8	5	7	3	0	0
Control	24	6	6	0	0	0
Phentermine	6	12	3	2	0	0
Bupropion	17	5	7	8	2	0
Green Tea	9	8	3	3	2	0
Mormon Tea	7	4	4	4	0	0

Figure 1.1. Daily Growth Patterns and Population Increase for Experiment 1 (CGC-WN2002).

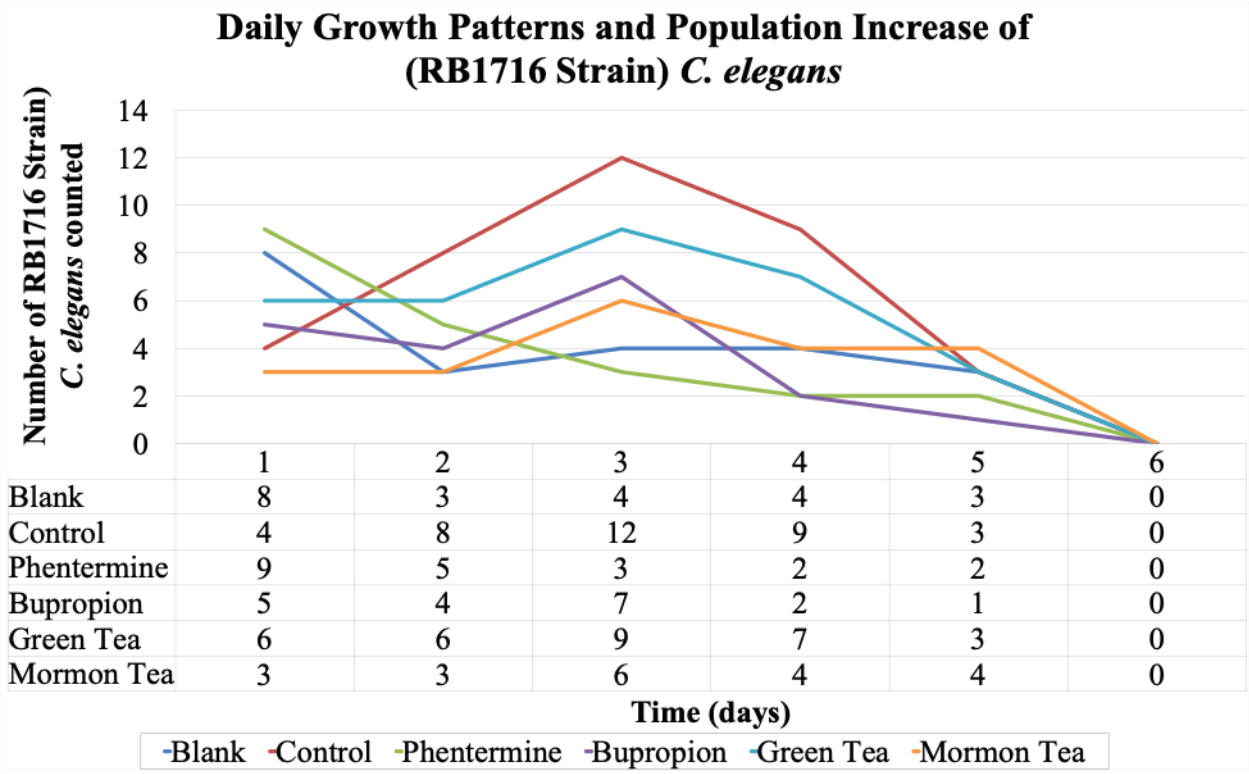

	1	2	3	4	5	6
Blank	8	3	4	4	3	0
Control	4	8	12	9	3	0
Phentermine	9	5	3	2	2	0
Bupropion	5	4	7	2	1	0
Green Tea	6	6	9	7	3	0
Mormon Tea	3	3	6	4	4	0

Figure 1.2. Daily Growth Patterns and Population Increase for Experiment 1 (CGC-RB1716).

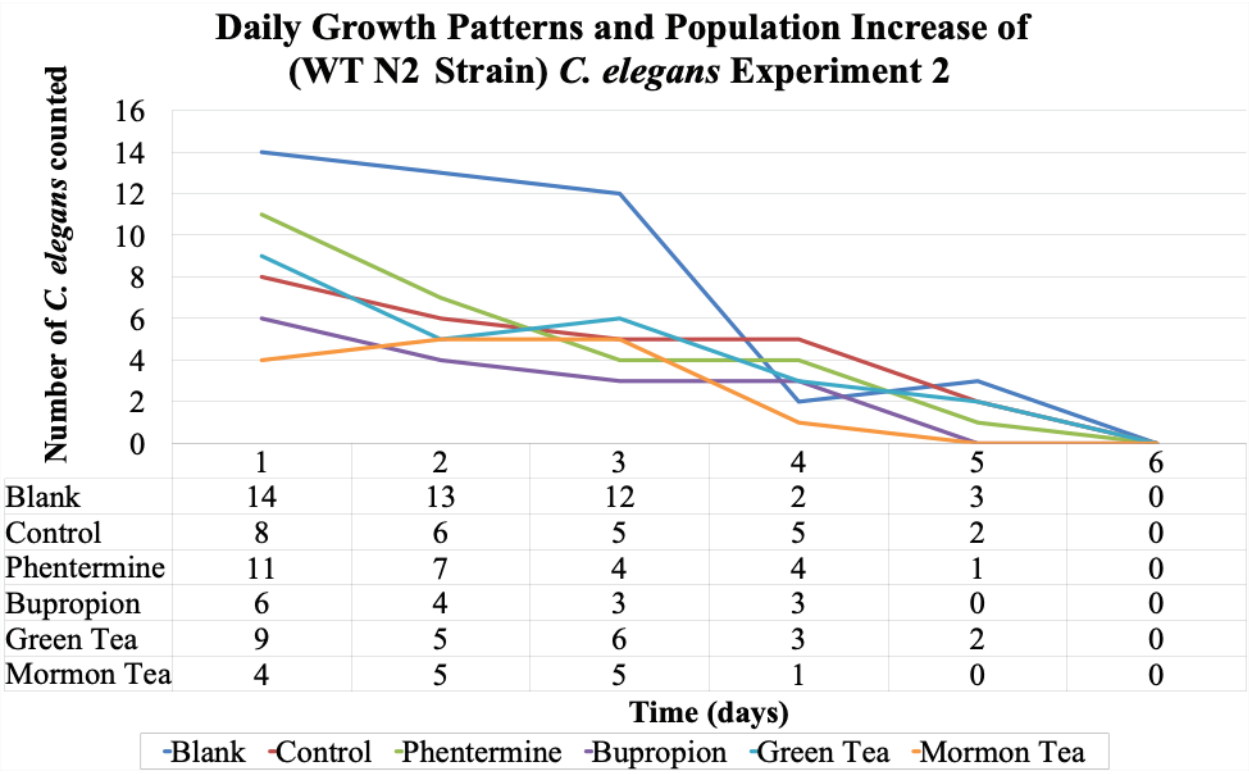

	1	2	3	4	5	6
Blank	14	13	12	2	3	0
Control	8	6	5	5	2	0
Phentermine	11	7	4	4	1	0
Bupropion	6	4	3	3	0	0
Green Tea	9	5	6	3	2	0
Mormon Tea	4	5	5	1	0	0

Figure 2. Daily Growth Patterns and Population Increase for Experiment 2 (Wild Type N2).

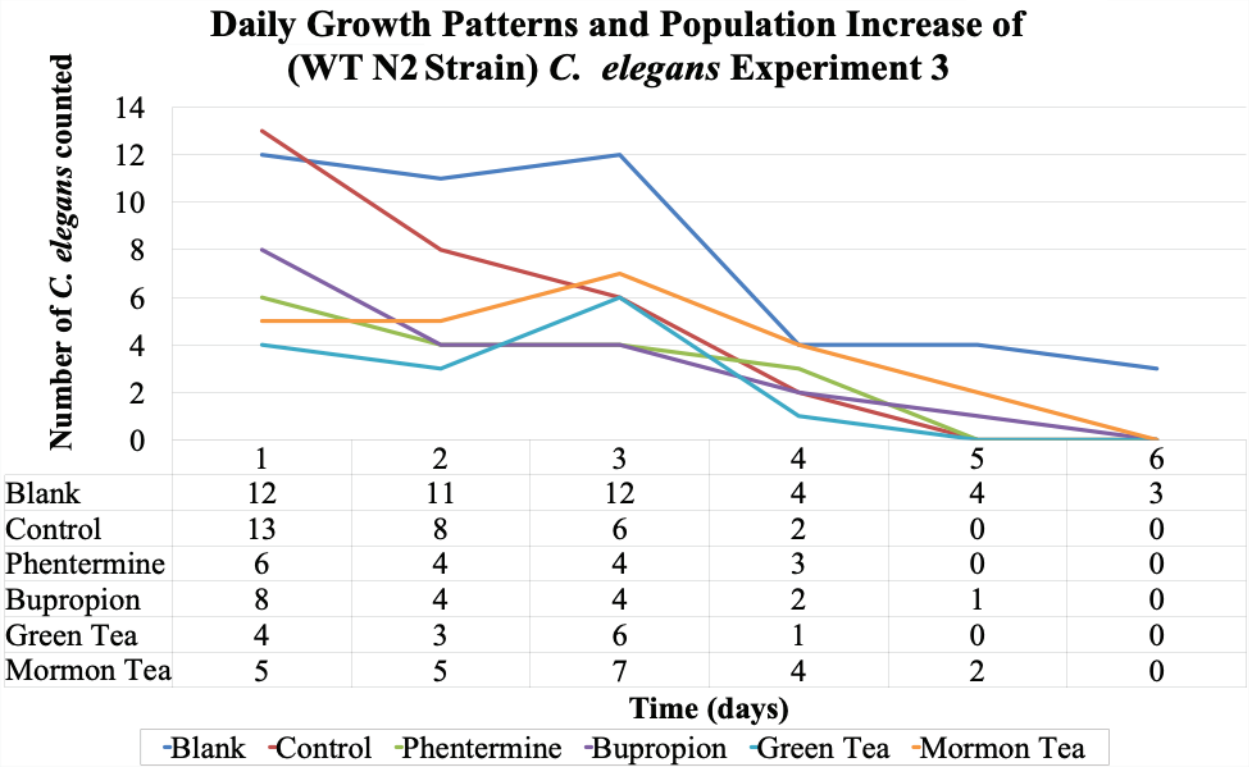

	1	2	3	4	5	6
Blank	12	11	12	4	4	3
Control	13	8	6	2	0	0
Phentermine	6	4	4	3	0	0
Bupropion	8	4	4	2	1	0
Green Tea	4	3	6	1	0	0
Mormon Tea	5	5	7	4	2	0

Figure 3. Daily Growth Patterns and Population Increase for Experiment 3 (Wild Type N2).

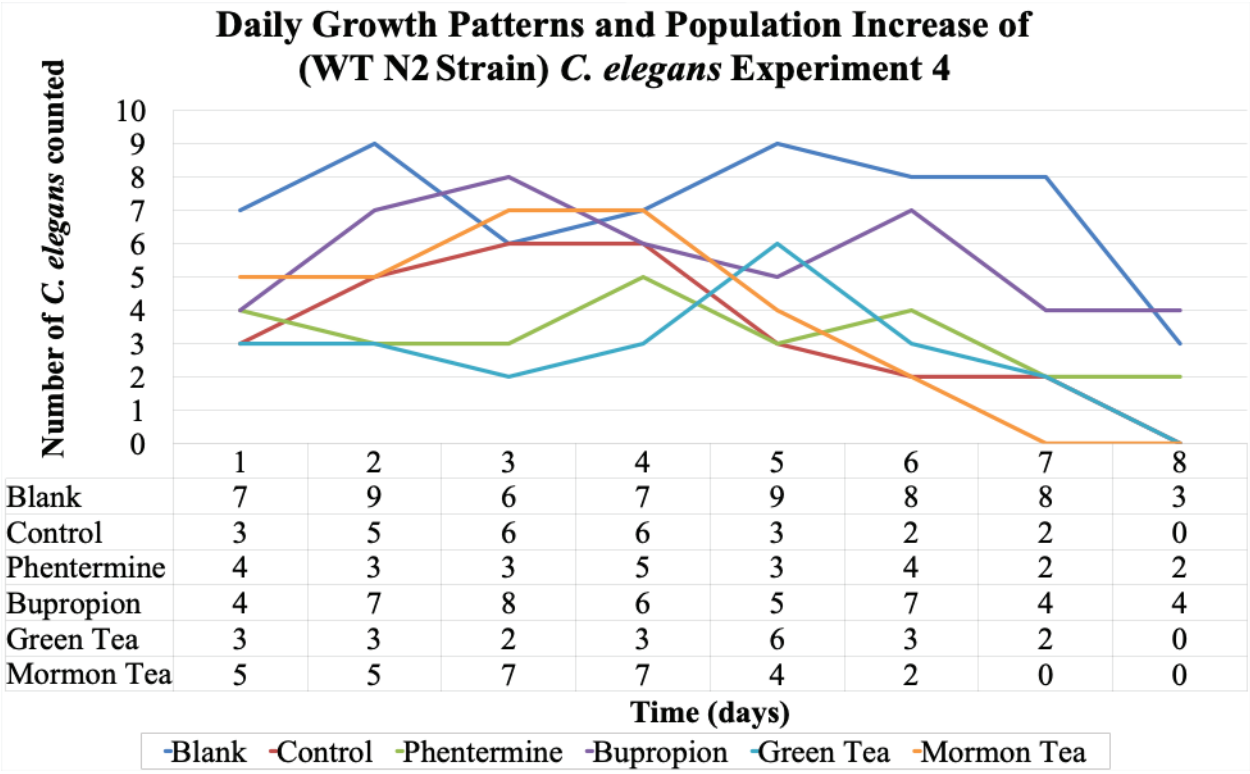

	1	2	3	4	5	6	7	8
Blank	7	9	6	7	9	8	8	3
Control	3	5	6	6	3	2	2	0
Phentermine	4	3	3	5	3	4	2	2
Bupropion	4	7	8	6	5	7	4	4
Green Tea	3	3	2	3	6	3	2	0
Mormon Tea	5	5	7	7	4	2	0	0

Figure 4. Daily Growth Patterns and Population Increase for Experiment 4 (Wild Type N2).

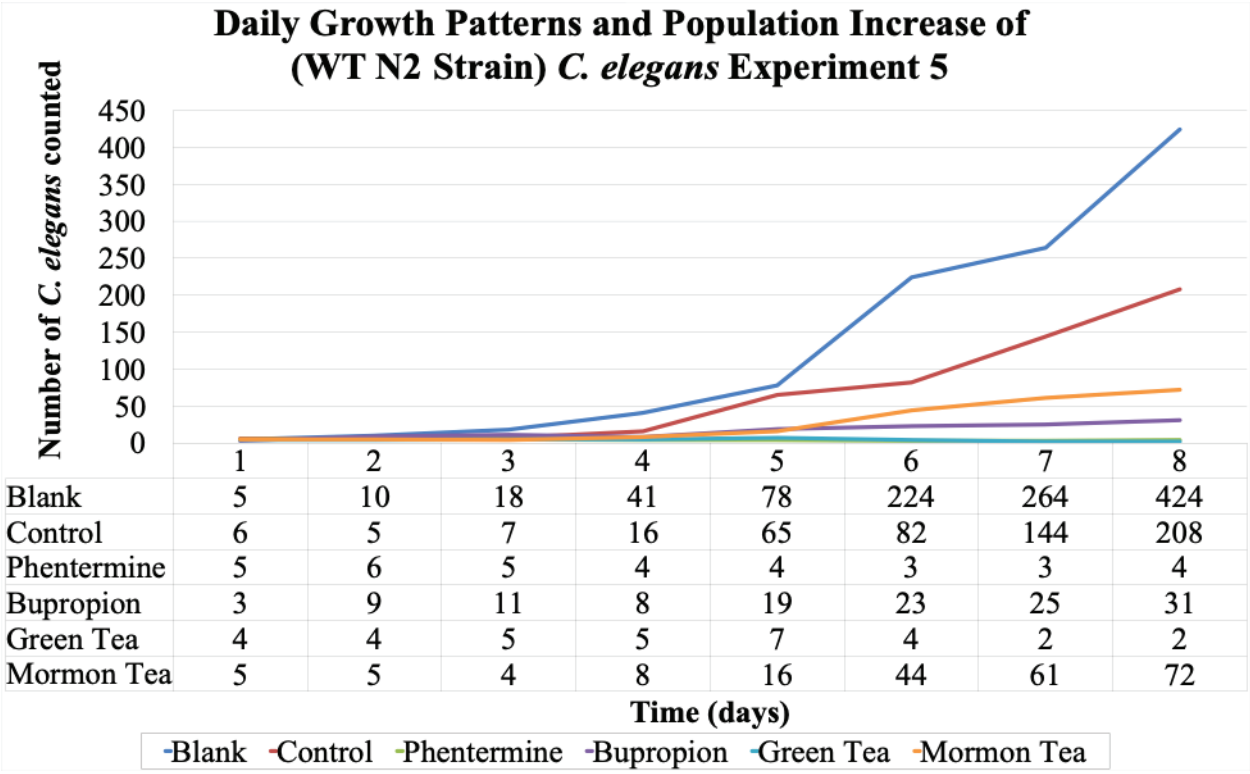

	1	2	3	4	5	6	7	8
Blank	5	10	18	41	78	224	264	424
Control	6	5	7	16	65	82	144	208
Phentermine	5	6	5	4	4	3	3	4
Bupropion	3	9	11	8	19	23	25	31
Green Tea	4	4	5	5	7	4	2	2
Mormon Tea	5	5	4	8	16	44	61	72

Figure 5. Daily Growth Patterns and Population Increase for Experiment 5 (Wild Type N2).

DISCUSSION

Experiment one tested genetically modified nematodes and non-genetically modified nematodes and the effects that natural and pharmaceutical medications had to combat effects associated with HFCS, and potentially, obesity. *C. elegans* were acquired through the Caenorhabditis Genetics Center, supplying a wild-type strain, WN2002, and a modified strain, RB1716, which expresses [gene nhr-49] which has been shown to promote lipid accumulation, making strain RB1716 desirable for experimentation. The overall population yield in experiment one, for both sets of cultures, was limited with short lifespans. The population size was observed and recorded over approximately six days, resulting in data that could be analyzed using mathematical and statistical analysis. Since interpreting population curve graphs poses a challenge to concrete answers about differences between groups, two statistical tests were conducted to understand results. The first conducted test was the statistical analysis of variance (ANOVA) to test differences of variances between groups. The (ANOVA) conducted was with raw data and single factor. First, for strain WN2002, the sum of squares within groups, sum of squares between groups, and total sum of squares was calculated along with degrees of freedom [F (5,30)] to find and interpret the F-value. The F-value is found by dividing the sum of squares between groups by their degrees of freedom, dividing the sum of squares within groups by their degrees of freedom, resulting in two numeric values. The formula will result in, F= [(sum of squares between groups/degrees of freedom) / (sum of squares within groups/degrees of freedom)]. Experiment one results from WN2002 strain was (F= 0.37) with (Critical value; 2.53) showing that there was no significant difference between the groups tested. Experiment one results from RB1716 strain was (F= 0.85) with (Critical value; 2.53) showing that there was no significant difference between the groups tested.

Statistical t-tests compare the variances between two different groups by computing mean, standard deviation, and variance to calculate a t-test value. The t-tests conducted were "two-sample assuming unequal variances" and "P (T≤t) two-tail". Control/blank for experiment one WN2002 strain the t-test value was (p = 0.61), control/phentermine t-test value was (p = 0.62), control/bupropion t-test value was (p = 0.91), control/green tea t-test value was (p = 0.67), and control/Mormon tea t-test value was (p = 0.50).

Control/blank for experiment one RB1716 strain the t-test value was (p = 0.30), control/phentermine t-test value was (p = 0.29), control/bupropion t-test value was (p = 0.22), control/green tea t-test value was (p = 0.72), and control/Mormon tea t-test value was (p = 0.22). Since all the computed values did not satisfy the t-test, (P < 0.05), to show that variation was statistically (95% accurate), determine acceptance or rejection of null hypothesis.

After experiment one yielded small population sizes, experiment two setup was slightly altered. Nematodes wild type (N2) from Ward's Science were utilized being crucial of cost, and concentrations of variables were altered. Experiment two results show (F = 1.27) with (Critical value; 2.53) showing that there was no significant difference between the groups tested. The F-value was slightly higher in experiment two, indicating that there is a higher chance that there may be significant data between either the variables and the control or the variables and the blank. The t-tests conducted were "two-sample assuming unequal variances" and "P(T≤t) two-tail". Control/blank for experiment two the t-test value was (p = 0.32), control/phentermine t-test value was (p = 0.94), control/bupropion t-test value was (p = 0.30),

control/green tea t-test value was (p= 0.93), and control/Mormon tea t-test value was (p = 0.26). These t-test results show that there is no significant statistical difference, individually, between the experimental groups tested.

Experiment three was structured exactly as experiment two to test if the data acquired was able to be replicated. Nematodes wild type (N2) was used, and concentrations of variables were kept the same. Experiment three results show (F = 1.89) with (Critical value; 2.53) showing that there was no significant difference between the groups tested. The F-value was slightly higher in experiment three but was similar to the F-value computed in experiment two. The t-tests conducted were "two-sample assuming unequal variances" and "P(T≤t) two-tail". Control/blank for experiment three the t-test value was (p = 0.33), control/phentermine t-test value was (p = 0.42), control/bupropion t-test value was (p = 0.78), control/green tea t-test value was (p = 0.32), and control/Mormon tea t-test value was (p = 0.68). These t-test results show that there is no significant statistical difference, individually, between the experimental groups tested. There was though, in experiment three statistical adverse effects when the phentermine and green tea were compared the blank.

After experiment two and three yielded small population sizes, experiment four and five experimental setups were slightly altered. Concentrations of variables were altered. Experiment four results show (F = 6.08) with (Critical value; 2.44) indicating that there was a significant difference between the groups tested. The F-value was slightly higher in experiment two, indicating that there is a higher chance that there may be significant data between either the variables and the control or the variables and the blank. The t-tests conducted were "two-sample assuming unequal variances" and "P(T≤t) two-tail". Control/blank for experiment four the t-test value was (p = 0.003), control/phentermine t-test value was (p = 0.88), control/bupropion t-test value was (p = 0.03), control/green tea t-test value was (p = 0.53), and control/Mormon tea t-test value was (p = 0.77). These t-test results show that there is significant statistical difference between some of the experimental groups tested.

Experiment five results show (F = 4.00) with (Critical value; 2.44) showing that there was a significant difference between the groups tested. The F-value was slightly higher in experiment two, indicating that there is a higher chance that there may be significant data between either the variables and the control or the variables and the blank. The t-tests conducted were "two-sample assuming unequal variances" and "P(T≤t) two-tail". Control/blank for experiment two the t-test value was (p = 0.30), control/phentermine t-test value was (p = 0.05), control/bupropion t-test value was (p = 0.10), control/green tea t-test value was (p = 0.05), and control/Mormon tea t-test value was (p = 0.20). These t-test results show that there is no significant statistical difference between the experimental groups tested.

CONCLUSIONS

Experiment one dealt with two different strains of nematodes and the concentration, (1:5) variable to agar concentration, seemed out of proportion and did not allow proper population growth. Experiment one yielded low daily population counts and an overall six-day experiment. The main focus of experiment one was utilizing the WN2002 strain as a control for the RB1716 strain which showed possible correlation to lipid accumulation and obesity.

The cultures were also designed to avoid discrepancies caused by experimental setup. In both strains, there was a control culture with only HFCS and no anti-obesity medication as well as a blank with only nutrient growth medium. The experimental designed ensured that any adverse effects or non-adverse effects that would have occurred in the experimental variable cultures were due only to that added supplement.

The results from experiment one for statistical analysis of variance (ANOVA) and statistical t-tests shows that overall, there was no adverse effects between the groups at a (1:5) concentration. This may be due to the over-concentration and nematodes inability to sustain a population size adequate enough to analyze holistically. Since this was a concern, the experimental setup was altered in order to test and find out if the concentration of variable to agar was the cause of the low population numbers.

Experiment two and three were conducted with the wild type strain (N2), in order to examine the natural and anti-obesity medications with nematodes, remaining cost-conscious because of the costs associated with purchasing and shipping genetically modified nematodes. Experiment two and three also received a lower concentration of variable to agar, (1:10). This was an attempt to ensure that the variables were not becoming too toxic for the model organism to reproduce and sustain a large population size. Experiment two and three also yielded smaller population sizes and lasted for an overall six-day experiment. The cultures also all seemed to acquire minimal white fungus after approximately three days of growth. The fungus was common on all cultures surrounding, mostly, the 1 cm transferred block from the acquired master culture.

The results from experiment two and three were expected to be very similar, because of their exact experimental setup and treatment. The results from both statistical analysis of variances (ANOVA) and t-tests comparing variables to the control showed no significant statistical effects between the variables and the control culture at a (1:10) concentration. The t-test in experiment three comparing the blank/phentermine and blank/green tea showed ($p < 0.05$) showing that there was some statistical significance between these added supplemental variables and population growth. As of now, the effects seem to be adverse, but the natural and pharmaceutical medications may be providing the anti-obesity traits that would limit lipid accumulation in the nematodes. Further analysis and larger population sizes required for confirmation.

The results from experiment four and five were expected to be very similar, because of their exact experimental setup and treatment. The experiments yielded much higher population counts and overall, eight-day experiments. The results from both statistical analysis of variances (ANOVA) showed significant statistical effects between the variables and the control culture at a (1:12) concentration. The t-tests in experiment four comparing the control/blank and control/bupropion showed ($p < 0.05$) showing that there was some statistical significance between these added supplemental variables and population growth. In experiment five the results from both statistical analysis of variances (ANOVA) showed significant statistical effects between the variables and the control culture at a (1:12) concentration.

Due to lab non-availability post formal COVID-19 closings and restrictions, histochemical staining and individual analysis of composition of nematodes was unattainable. With further analysis or future research, assessing glucose, complex polysaccharide, and lipid concentra-

tion per single nematode using distinct histochemical stain could potentially grant more thorough insight on effectiveness of anti-obesity medications and quantifiable lipid accumulation data.

AUTHOR INFORMATION

Corresponding Author

*Louie Martinez, louie.r.martinez@gmail.com

Funding Sources

Mr. Alexander (Teacher/Sponsor) handled the funding for materials. Caenorhabditis Genetics Center's contribution of genetically and non-genetically modified nematodes was utilized for the experimentation.

ACKNOWLEDGMENTS

Research for this project would not have been possible without many contributing companies and individuals.

I would like to thank the Caenorhabditis Genetics Center (CGC) for providing two separate strains of nematode *Caenorhabditis elegans*. The CGC made research on genetically modified nematodes, strain RB1716, and non-genetically modified nematodes, strain WN2002 possible. I would like to thank Parkhurst Pharmacy for providing the pharmaceutical anti-obesity medications utilized in this research project.

I would like to thank Dr. Valdivia for providing the proper documentation required for experimentation with the pharmaceutical anti-obesity medication. I would like to thank Mr. Alexander for guiding me throughout the entire science-fair process, willing to stay for long hours in the laboratory, providing equipment in the laboratory and purchasing any supplies needed. I would like to thank Mr. Alexander for being my teacher, my mentor, and an inspiration to many.

I would also like to thank my family and friends who have been supportive throughout this process. I appreciate everyone who is willing to support my research and continually strive to academically enrich students living in rural communities.

ABBREVIATIONS

FDA, Food and Drug Administration; *C. elegans*, *Caenorhabditis elegans*; *E. coli*, *Escherichia coli*; HFCS, high-fructose corn syrup; CGC, Caenorhabditis Genetics Center; WN2002, Caenorhabditis Genetics Center wild-type nematode strain; RB1716, Caenorhabditis Genetics Center genetically modified nematode strain; Wild-Type N2, Ward's Science wild-type nematode strain.

REFERENCES

Center for Drug Evaluation and Research. Bupropion hydrochloride Information, 2016. https://www.fda.gov/drugs/postmarket-drug-safety-information-patients-and-providers/bupropion-hydrochloride-marketed-wellbutrin-zyban-and-generics-information

Edgley, Mark; Riddle, Lab. What is C. elegans? *College of Biological Sciences*. (**2018, November 28**). https://cbs.umn.edu/cgc/what-c-elegans

Gadde, K. M.; Parker, C. B.; Maner, L. G.; Wagner, H. R.; 2nd, Logue, E. J.; Drezner, M. K.; Krishnan, K. R. Bupropion for weight loss: an investigation of efficacy and tolerability in overweight and obese women. *Obesity Research*. **2001**, 9(9), pp. 544–551. DOI: 10.1038/oby.2001.71

Johnson, R.; Kuby, P. *Elementary Statistics*. Australia: Brooks / Cole. 2007, pp. 592-599, 658-675.

Jurgens, T.; Whelan, A. M. Can green tea preparations help with weight loss? *Canadian Pharmacists Journal*. **2014**, 147(3), pp. 159–160. DOI: 10.1177/1715163514528668

Kandola, A. Green tea for weight loss: Does it work?, January 8, 2018. https://www.medicalnewstoday.com/articles/320540#weight-loss

Kao, L. S.; Green, C. E. Analysis of variance: is there a difference in means and what does it mean? *The Journal of Surgical Research*. **2008**, 144(1), pp. 158–170. DOI: 10.1016/j.jss.2007.02.053

Kim H. Y. Analysis of variance (ANOVA) comparing means of more than two groups. *Restorative Dentistry & Endodontics*. **2014**, 39(1), pp. 74–77. DOI: 10.5395/rde.2014.39.1.74

Kim, K. K.; Cho, H. J.; Kang, H. C.; Youn, B. B.; Lee, K. R. Effects on weight reduction and safety of short-term phentermine administration in Korean obese people. *Yonsei Medical Journal*. **2006**, 47(5), pp. 614–625. DOI: 10.3349/ymj.2006.47.5.614

Kim T. K. T test as a parametric statistic. *Korean Journal of Anesthesiology*. **2015**, 68(6), pp. 540–546. DOI: 10.4097/kjae.2015.68.6.540

Kim T. K. Understanding one-way ANOVA using conceptual figures. *Korean Journal of Anesthesiology*. **2017**, 70(1), pp. 22–26. DOI: 10.4097/kjae.2017.70.1.22

nhr-49 (gene) - WormBase: Nematode Information Resource. https://wormbase.org/species/c_elegans/gene/WBGene00003639#0-9f7-10

Phentermine-FDA, June 2013. https://www.accessdata.fda.gov/drugsatfda_docs/label/2013/202088s005lbl.pdf

Phentermine: MedlinePlus Drug Information, 2017. https://medlineplus.gov/druginfo/meds/a682187.html

Prescription Medications to Treat Overweight and Obesity, July 1, 2016. https://www.niddk.nih.gov/health-information/weight-management/prescription-medications-treat-overweight-obesity.

Sherman, M. M.; Ungureanu, S.; Rey, J. A. Naltrexone/Bupropion ER (Contrave): Newly Approved Treatment Option for Chronic Weight Management in Obese Adults. *P&T: A Peer-Reviewed Journal for Formulary Management*. **2016**, 41(3), pp. 164–172.

Staughton, J.; Hedge, R. 7 Proven Benefits of Mormon Tea, July 10, 2020. https://www.organicfacts.net/health-benefits/herbs-and-spices/mormon-tea.html

Table of critical values for the F distribution (for use with ANOVA), 2005. http://users.sussex.aC.uk/~grahamh/RM1web/F-ratio table 2005.pdf

The New Generation of Weight-Loss Drugs: Which Is Best?, 2015. https://www.psychologytoday.com/us/blog/the-antidepressant-diet/201502/the-new-generation-weight-loss-drugs-which-is-best.

Wadhwa RR, Marappa-Ganeshan R. T Test. *StatPearls. Treasure Island (FL): StatPearls Publishing*. (**2020 April 16**). https://www.ncbi.nlm.nih.gov/books/NBK553048/

WELLBUTRIN (bupropion hydrochloride) tablets-FDA, May 2017. https://www.accessdata.fda.gov/drugsatfda_docs/label/2017/018644s052lbl.pdf

Westerterp-Plantenga M. S. Green tea catechins, caffeine and body-weight regulation. *Physiology & Behavior*. **2010**, 100(1), pp. 42–46. DOI: 10.1016/j.physbeh.2010.02.005

Zheng, J.; Greenway, F. L. Caenorhabditis elegans as a model for obesity research. *International Journal of Obesity*. **2005**, 2012, 36(2), pp. 186–194. DOI: 10.1038/ijo.2011.93

The Effects of Fermented and Cultured Supplements on Dog's Gut Microbiome

*Gianna Nilvo**

School of Dreams Academy, Los Lunas, NM

ABSTRACT

The dog's microbiome has emerged as the crucial moderator in the interactions between food and the body. This study was conducted to examine the canine gut microbiome, testing the effects of probiotic supplements (fermented sauerkraut and cultured and unpasteurized Kefir) on overall gut microbiome composition. The hypothesis is that adding fermented sauerkraut and unpasteurized and cultured kefir supplements would shape the gut microbiota reflecting significant change in the alpha diversity (including *Firmicutes*:*Bacteroidetes* ratio), richness (Shannon Index), and evenness specifically while looking at the relative abundance of each dog. This study engaged seven dogs eating the same raw, dehydrated diet with protein over a 6-week period with the addition of fermented and cultured food supplements. All dogs' gut microbiomes were analyzed using 16s rRNA gene sequencing through Animal Biome test kits to gather the alpha taxonomic composition of each dog at the beginning (baseline) and 6-weeks of adding fermented and cultured supplements. The results suggest that the driving force in microbiota composition when looking at alpha levels of relative abundance, evenness, diversity, and richness in dogs is specific to the individual, with dogs presenting various representations of main phylum and major genus. The statistical significance suggests that evenness and *Firmicutes*:*Bateroidetes* ratio were significant (P< 0.001) when compared between mean control value of dogs not treated with probiotic supplements versus the seven dogs treated for 6-weeks with probiotic supplements. Data also suggests that when dogs live in the same household, they tend to have similar taxonomic gut microbiome communities. Today, society is seeing a rise in microbiome-associated disorders in dogs (animals in general) and even in humans, and understanding differing effects on the gut microbiome will shape how we treat chronic issues not just for our canines, but pets and even humans.

KEYWORDS: Gut Microbiome, Diversity, Evenness, Richness, Probiotics

INTRODUCTION

Dogs have a unique collection of hundreds of different types of single-celled microorganisms (bacteria and other microbes) that inhabit the gastrointestinal tract (GI) of cats and dogs in the digestive tract (Simpson et al., 2002). The gut microbiome is directly connected to the brain via the Vagus nerve and 80% of the immune system is controlled by the gut microbiome (Barko, 2018). The microbiome affects almost every aspect of a dog's health to include weight, allergies, digestive issues, and even mental health. When gut bacteria are out of balance in a dog, disorders such as inflammatory bowel disease (IBD), allergies, diabetes, and digestive issues can result.

This study was conducted to answer if adding fermented sauerkraut and cultured and unpasteurized Kefir (items easily found in grocery stores) have an effect on a dog's gut microbiome when added to their daily meal intake? The hypothesis if adding fermented sauerkraut and unpasteurized and cultured kefir supplements would shape the gut microbiota reflecting significant change in the alpha diversity, richness, and evenness specifically while looking at the relative abundance of each dog.

Biodiversity describes the variety and variability of all living organisms within a given ecological area. Biodiversity can be used to refer to the number of species, their genetic diversity, or habitat variety. There are two main components that contribute to biodiversity—species richness and species evenness. Species richness describes the number of different species present in an area (more species = greater richness). Species evenness describes the relative abundance of the different species in an area (similar abundance = more evenness).

Role of the canine physiological gut microbiome

The interaction between gut microbiota, its host, and other somatic cells regulates many functions, such as digestion, host metabolism, vitamins synthesis (vitamin K and complex B), biotransformation of bile acids, xenobiotics metabolism, correct maturation of gastrointestinal cells, and defense against pathogenic bacteria (Steiner and Ruaux, 2008). Therefore, the microbiota can be defined as a metabolically active "organ" (Mondo et al., 2019), a living ecosystem in itself. Serotonin, a neurotransmitter, is mostly produced in the intestine, which has led to the development of the gut-brain axis concept (O'Mahony, 2015). A healthy and stable microbiome can simultaneously act as pro-and anti-inflammatory, keeping a balance to prevent excessive inflammation while still being able to promptly respond to infections (Tizard, 2018).

The microbial communities along the tract vary to reflect the microenvironment and physiological functions of each intestinal segment. Commensal bacteria (bacteria found in the intestine and other anatomical locations of the intestine) have a fundamental role on the induction, shaping, and function of the host immune system, which in turn is important in the development of the physiological gut structure and the identification of pathogens from commensal bacteria (Mondo et al., 2019). Commensal bacteria act on the host's immune system to induce protective responses that prevent colonization and invasion by pathogens; these bacteria can directly inhibit the growth of respiratory pathogens by producing antimicrobial products/signals and competing for nutrients and adhesion sites (Kahn et al., 2019). Furthermore, commensal bacteria have a fundamental role on the induction, shaping, and function of the host immune system, which in turn is important in the development of the physiological gut structure and the identification of pathogens from commensal bacteria (Mondo, 2019). Along the GI tract, bacterial sequences typically belong to one of five phyla: *Firmicutes*, *Fusobacteria*, *Bacteroidetes*, *Proteobacteria*, and *Actinobacteria* (Pilla et al., 2020).

Dysbiosis is an imbalance in bacterial composition, and bacterial metabolic activities and bacterial distribution inside the gut change (Pilla, 2019). Dysbiosis is defined when the reduction of bacterial diversity, loss of beneficial bacteria, and overgrowth of pathogens (Pilla, 2019) occurs. A state of dysbiosis is found in a wide range of diseases, such as inflammatory bowel disease (IBD), obesity, allergy, and diabetes, but it is unclear if it is a cause or a consequence (Pilla, 2019). Several studies about these diseases have indicated the presence of a

microbial alteration, but no consistent pattern of microbiota changes has yet been observed (Pilla, 2019).

Many of the bacteria in a dog's microbiome is inherited from its mother after birth and other bacteria from the environments and other animals (including humans) that a dog is exposed to in early years (Barko, 2018). These bacteria influence a dog for the rest of its life. Barko (2018) states that although the foundational bacteria taxon of gut communities is established in a dog's early years, the gut microbiome changes over time with age, diet, and animal's lifestyle. If a dog is prescribed antibiotics or other medication, the gut microbiome could shift quickly and can take at least a year or more to bring balance back after the dog is taken off the medications.

Canine gut microbiome studies

Besides the diet, probiotics, prebiotics, and antibiotics administration affect, and change microbiota composition, but their efficiency is not clear. The use of pre-and probiotics is broadly spread in human medicine to preserve or restore a healthy condition (Sanders et al., 2018). The employment of these devices is new in veterinary medicine and pet treatment.

Prebiotics are more recent and, in accordance to their first definition given in 2015, they are "a non-digestible compound that, through its metabolization by microorganisms in the gut, modulates composition and/or activity of the gut microbiota, thus conferring a beneficial physiological effect on the host" (Bindels et al., 2015). Nowadays, several research studies reported benefits from the addition of prebiotics in pets' diets.

Despite the variations of taxa along the GI tract, samples from specific regions of the tract are difficult to obtain, and therefore most clinical studies focus on the fecal microbiota. Canine fecal samples reliably present most of the relevant taxa, unlike humans, in which most significant taxa are closely associated with the mucosa (Vázquez-Baeza et al., 2016). Recently, the development of new molecular technologies, such as next-generation sequencing (NGS), has allowed understanding the complexity and diversity of gut-microbial communities (Kim et al., 2017). Molecular-phylogenetic analysis of the bacterial 16S rRNA gene has created a more detailed inventory of bacteria groups present in the bowel. (Mondo et al., 2019) To date, there are limited comprehensive reviews or scientific work of the intestinal microbiome specifically regarding the importance of the intestinal microbiome in dogs and cats.

There are some studies about the use of probiotics in the domestic canine diet. Zentek et al, (2003) found that in dogs, an intake of 1.5% inulin could reduce fecal pH and increase *Bifidobacteria* population. Using 16S rRNA sequencing, it has been shown that dogs fed with a relatively small amount of dietary fiber change the structure of gut microbiota, increasing the density of *Firmicutes* and decreasing that of *Fusobacteria* (Middlebos et al, 2010). Another study underlined how a dietary supplementation of fructo-oligosaccharides (FOS) induces beneficial effects, such as the growth of *Bifidobacteria*, and it improves the digestibility of several minerals in the entire GI tract in the dog (Pinna et al, 2018).

Another study, chicory root (a source of inulin), improved fecal scores, increased *Bifidobacterium*, and decreased *C. perfringens* in the feces of healthy dogs (Zentek et al, 2003). A meta-analysis (several different studies on the same topic to review trends) of 15 stud-

ies including 65 different treatment conditions showed that fecal shorty chain fatty acids (SFCA) concentrations increase linearly with prebiotic doses (Patra, 2011). Furthermore, it also revealed that fecal *Bifodobacteria* and *Lactobacillus* increase with prebiotic doses and no changes for pathogenic *C. perfringens* or *E. coli*. The prebiotics were not related to the composition of the dog's diet, suggesting that prebiotic therapies can provide benefits independent of the diet (Patra, 2011).

Probiotic supplementation studies have shown benefits in small animals in several clinical trials. A small clinical trial with a probiotic strain of *Saccharomyces boulardii* improved clinical signs in dogs with IBD and protein losing enteropathy (Mustafa et al., 2016). In dogs with food-responsive diarrhea treated with lyophilized *Lactobacillus* for 21 days along with diet change, there were increased *Lactobacilli* and decreased *Enterobacteria* in the feces accompanied by improved clinical signs (Sauter, 2006). In another study of 36 dogs with acute gastroenteritis, a probiotic combination improved clinical signs compared to a placebo (Herstad et al., 2010). In a shelter-based study, this probiotic, administered with metronidazole, improved fecal scores compared to dogs treated with metronidazole alone (Fenimore, et al., 2017).

While variations in composition are observed between different studies, it is important however to note that regardless of the methods used, key bacterial species are consistently present in fecal samples of healthy dogs indicating the presence of a core fecal bacterial community. The fecal microbiome of healthy dogs is co-dominated by three phyla: *Fusobacterium*, *Bacteroidetes*, and *Firmicutes* (Middelbos et al., 2010) When reviewing the literature, a wide variation in percentages of specific bacterial taxa can be seen. It is important to remember that the methods for sequencing and data analysis are in constant evolution, and much of those variations can be attributed to different sequencing and data analysis methods.

By understanding the relationship between a dog's microbiome and digestibility of the food consumed, we can gain insights into the manipulation of diet on the gut microbiome and treating the problem of the gut microbiome versus prescribing medication because of digestive issues, diabetes, skin allergies, and other diseases in veterinarian medicine.

METHODS

Materials

Seven dogs (Table 1 in Appendix A) were selected by Volhard Dog Nutrition based on an already consistent, fresh dehydrated Volhard diet which uses raw protein as the common baseline for feeding and their regional living location. Either the Volhard AM Porridge/PM Crumble or NDF2 raw diet was distributed to each dog directly from the raw dog food nutrition company. Cultured with probiotic Wildbrine sauerkraut and Answers raw goat milk was used for the whole food supplement feeding each day, with each owner given locations to purchase the same items to administer to their dogs each day. Two complete Animal Biome test kits were used per dog ($75 per kit) for non-invasive fecal samples collections and were funded by Volhard Dog Nutrition.

Controls and variables of study

The experimental controls were the amount and type of Volhard raw diet used, amounts of fermented and cultured sauerkraut (1 Tbsp/10 pounds), and unpasteurized and cultured Answers raw goat milk (1 Tbsp/10 pounds). Independent variables identified were fermented and cultured sauerkraut and the unpasteurized and cultured raw goat milk. Variables dependent to this research were the age of dog, breed of dog, medications before and during the study, type of water dog ingests, health of dog prior and during research, activity level of each dog, whether the dog was spayed or neutered, length of time outdoors, and process of dog's birth.

Supplemental dog feeding protocol for study

Each dog owner was asked to follow the following supplemental feeding protocol (with no changes to the diet) each day during the 6-week testing period set by a certified nutritionist at Volhard Dog Nutrition: (1) In the morning, add one tablespoon for every ten pounds the dog weighs of fermented and cultured Wildbrine sauerkraut to their morning NDF2 or AM Porridge feeding and (2) In the evening, add one tablespoon for every ten pounds the dog weighs of unpasteurized and cultured Answers raw goat milk to NDF2 or PM Crumble feeding. Each meal also contained adding any type of meat protein.

Procedure

The research was conducted over a 6-week period (collection times set by Volhard Dog Nutrition) gathering information from a beginning baseline of dogs not on fermented and cultured supplements to a 6-week period of adding fermented and cultured supplements to daily diet. Volhard Nutritional Dog Food Company assisted in recruiting their own canine clients to participate in the study, utilizing dogs who were on Volhard's raw food diet for more than two years. I used a digital survey that was completed by each owner to collect background demographic data on each dog participating in the study; and a participant form was given to each owner outlining whole food supplemental feeding protocols for each meal, timeline of fecal collections for the study, and research summary plan that outlined the research being conducted. Animal Biome collection kits were ordered and shipped to each owner by Volhard Dog Nutrition. Owners used the Animal Biome testing kit and directions to collect a non-invasive pea-sized fecal sample from their dog before adding the whole food supplements to their dog's daily diet. The fecal samples were registered online with Animal Biome and shipped for testing. Each dog owner was asked to follow a supplemental whole food feeding protocol each day during the 6-week testing period after baseline fecal collection. After 6-weeks of daily whole food supplements, the Animal Biome kit was used to collect another pea-sized fecal sample and shipped for testing. Animal Biome extracts the DNA from all the bacteria in the sample (16s rRNA gene sequencing) then amplifies a small region from each cell (like a bacteria barcode) and sequences thousands of them to then provides raw data on taxon, phylum, family, and class of bacteria found in each fecal sample. Pre-probiotic and post-probiotic results from Animal Biome were provided to each dog owner and then given to me for analysis.

Alpha diversity analysis assesses the diversity within a sample. In alpha diversity, we used two different metrics: observed species to assess richness and Shannon index to assess

evenness and diversity. The Shannon Wiener Index is a measure of diversity that combines species richness (the number of species in a given area) and their relative abundances. In the Shannon diversity index (H), p is the proportion (n_i//N) of individuals of one particular species found (n) divided by the total number of individuals found (N) and then multiplied by the natural logarithm of this proportion (ln p_i). The resulting product is summed (∑) across species (s) and multiplied by -1.

$$H = -\sum_{i=1}^{S} \frac{n_i}{N} \log_2 \left(\frac{n_i}{N} \right) \quad (1)$$

Shannon's equitability (J') or evenness can be calculated by dividing Shannon's diversity index (H') by the total number of species in the or the richness (H'_{max}). Equitability assumes a value between 0 and 1 with 1 being complete evenness and zero signifying no evenness.

$$J' = \frac{H'}{H'_{max}} \quad (2)$$

Statistical significance was assessed with 999 permutations using the two-sample t-test.

RESULTS

To assess variability and composition of dog gut microbiota, a cross-sectional study was performed with 7 dogs from 6 breeds and 14 fecal sample collections. A total of 5 phyla and 24 genera were taxonomically classified (Figure 1; Table 2 in Appendix B) from the 14 fecal samples collected at initial (baseline) and then 6-weeks after fermented and cultured supplemental feeding protocol was added for individual canines.

The relative abundance differed in each individual canine, not only at the phylum level but also at the deeper taxonomic levels such as genus (Figure 1; Table 2 in Appendix B). The most abundant genus detected was *Fusobacterium* with percentages ranging from 16.5–42.2% after 6-weeks with fermented and cultured supplements in all canines. Other abundant trends of increasing taxonomic genus levels (Figure 1; Table 2 in Appendix B): *Bacteroides* increased after 6–weeks in all seven individuals; *Collinsella* and *Sutterella* increased after 6-weeks in six of seven dogs; and *Peptoclostridium* increased or was present after 6-weeks in three dogs. On the other hand, *Lachnospiraceae* were present in all dogs at 2.6% or less for both fecal sample collections. *Blautia* percentages decreased in five of seven dogs after 6-weeks. However, some dogs presented individual-specific genus percentages after 6-weeks: *Escherichia* with 1.6% for Dog H-02; *Dialister* at less than 1.8% for Dog H-02 and Dog L-07; *Anaerobiospirillum* with 3.4% for Dog R-05; *Catenibacterium* at 1-3.5% for Dogs H-02 and R-05; *Tyzzerella* at 1.1% after 6-weeks for Dog G-01; and *Faecalitalea* at 1.1% for Dog R-05. Depending on the individuals, genus representing more than 5% (Table 2 in Appendix B) was describing from 75.4 to 98.1% of total microbiota composition.

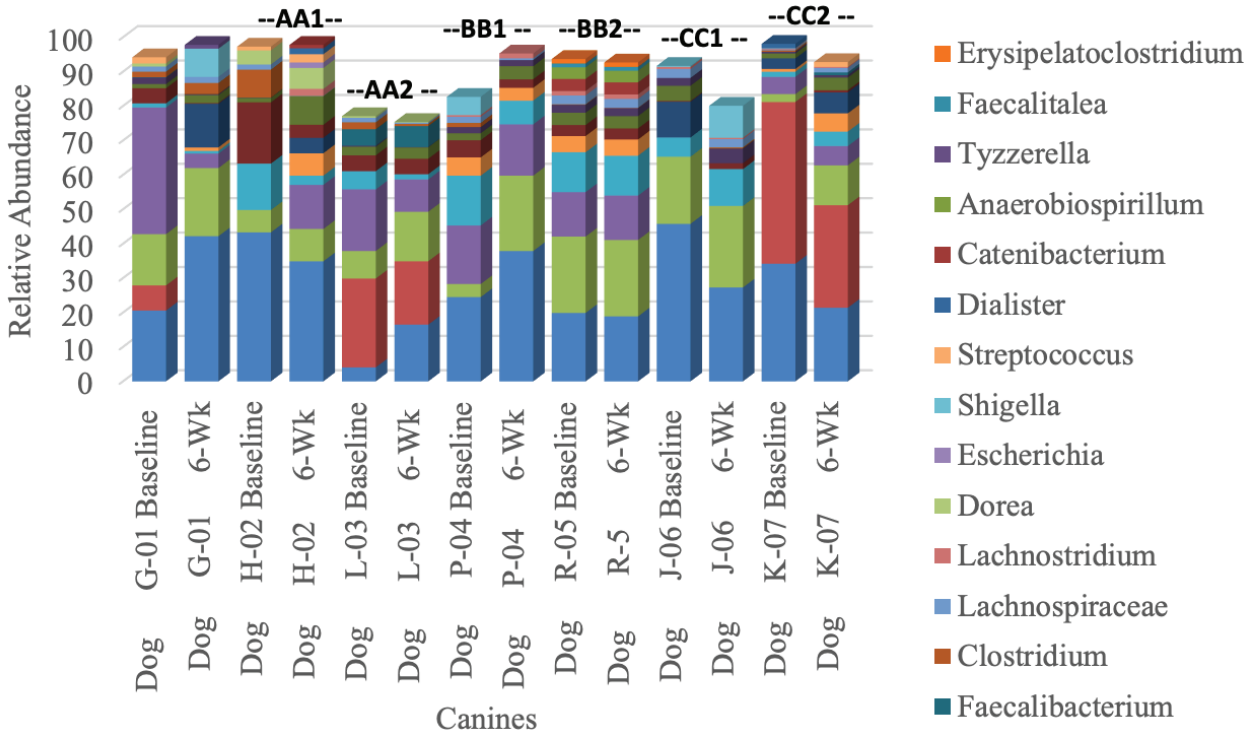

Figure 1. Bar Plot Representing Fecal Microbiome Composition at Phylum Level of Canines at Baseline and 6-Week (Treated with Fermented and Cultured Supplements). Raw data collected from each dog owner provided by Animal Biome. AA, BB, and CC show dogs that live in the same home.

The abundances of the main phyla differed for each fecal sample and individual (Figure 2; Table 3). The main phyla found in all seven dogs were: *Proteobacteri*a (1.2–9.9%), *Firmicutes* (10–45.8%), *Fusobacteria* (4.1–45.8%), *Bacteroidetes* (3.8–52.4%), and *Actinobacteria* (0–17.8%). Furthermore, none of the dogs had a predominant phylum (>50% of the total abundance) over the others. After 6-weeks on cultured and fermented supplements, four of seven dogs increased in *Fusobacteria*, and three of seven dogs increased in *Firmicutes* and *Bacteroidetes*. Dog K-7 showed little to no percentages of *Proteobacteria* or *Actinobacteria* at baseline or after 6-weeks for its taxonomic composition. Dogs living in the same household showed similar percentages in phyla, however, Dogs labeled as AA1 and AA2 (Figure 2; Table 3) showed differences in Proteobacteria and Fusobacteria percentages both at baseline and 6-week collections.

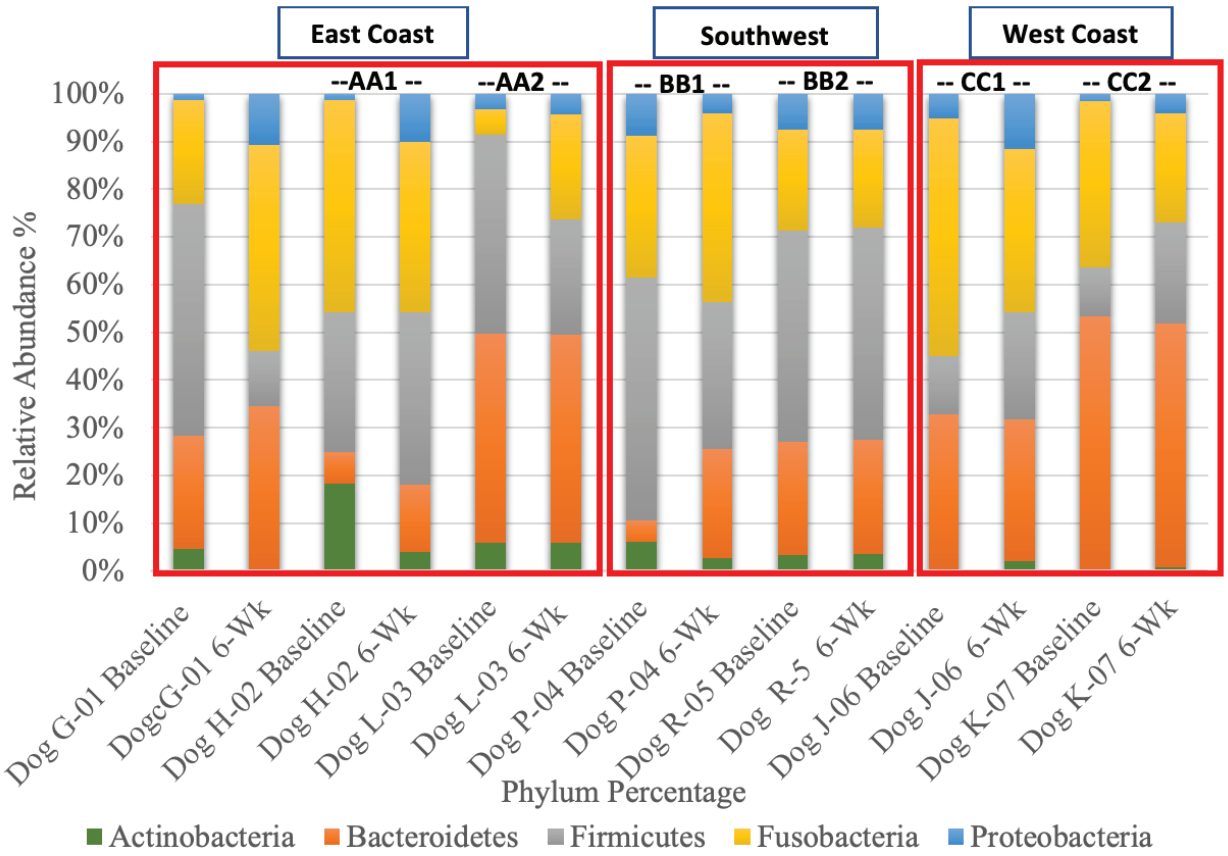

Figure 2. Alpha Diversity Percentage of Relative Abundance of Phylum Composition of Baseline and 6-Week Values of Canines. Data was collapsed for each individual dog by grouping Phylum. AA, BB, and CC show dogs that live in the same household.

Phylum	Dog G-01 Baseline	DogcG-01 6-Wk	Dog H-02 Baseline	Dog H-02 6-Wk	Dog L-03 Baseline	Dog L-03 6-Wk	Dog P-04 Baseline	Dog P-04 6-Wk	Dog R-05 Baseline	Dog R-5 6-Wk	Dog J-06 Baseline	Dog J-06 6-Wk	Dog K-07 Baseline	Dog K-07 6-Wk
Actinobacteria	4.4	0.2	17.8	3.8	4.6	4.5	5	2.5	3.2	3.2	0.2	1.7	0	0.6
Bacteroidetes	22.2	33.6	6.5	13.9	33.8	32.8	3.8	21.9	22.2	22.2	29.9	23.7	52.4	47.5
Firmicutes	45.8	11.3	28.4	35.3	32.1	18.3	42.1	29.2	41.4	41.4	11.1	18.1	10	19.6
Fusobacteria	20.6	42.2	43.3	34.9	4.1	16.5	24.5	37.9	19.9	18.9	45.8	27.3	34.2	21.4
Proteobacteria	1.2	10.5	1.3	9.9	2.5	3.3	7.3	3.8	7	7	4.7	9.3	1.5	3.7

Table 3. Alpha Diversity Percentage of Relative Abundance of Phylum Composition of Baseline and 6-week Values of Canines. Data was collapsed for each individual dog by grouping Phylum.

The alpha diversity, evenness, and richness differed for each individual dog. Alpha diversity is the mean species diversity in sites or habitats at a local scale. Figure 3 shows three of seven dogs diversity increased, and three of seven dogs diversity decreased. It is worthy to note that the dogs living in the same household (BB1, BB2, CC1, CC3) alpha diversity showed similar values after the second fecal collection and analysis was completed. The mean control of 2.2 for diversity are dogs (>1,000 sample size of dogs in Animal Biome data system) not on fermented or cultured supplements and used to compare the seven dogs in the study. When the diversity of the dogs in the study for the second fecal sample collected was averaged, this mean was 2.09.

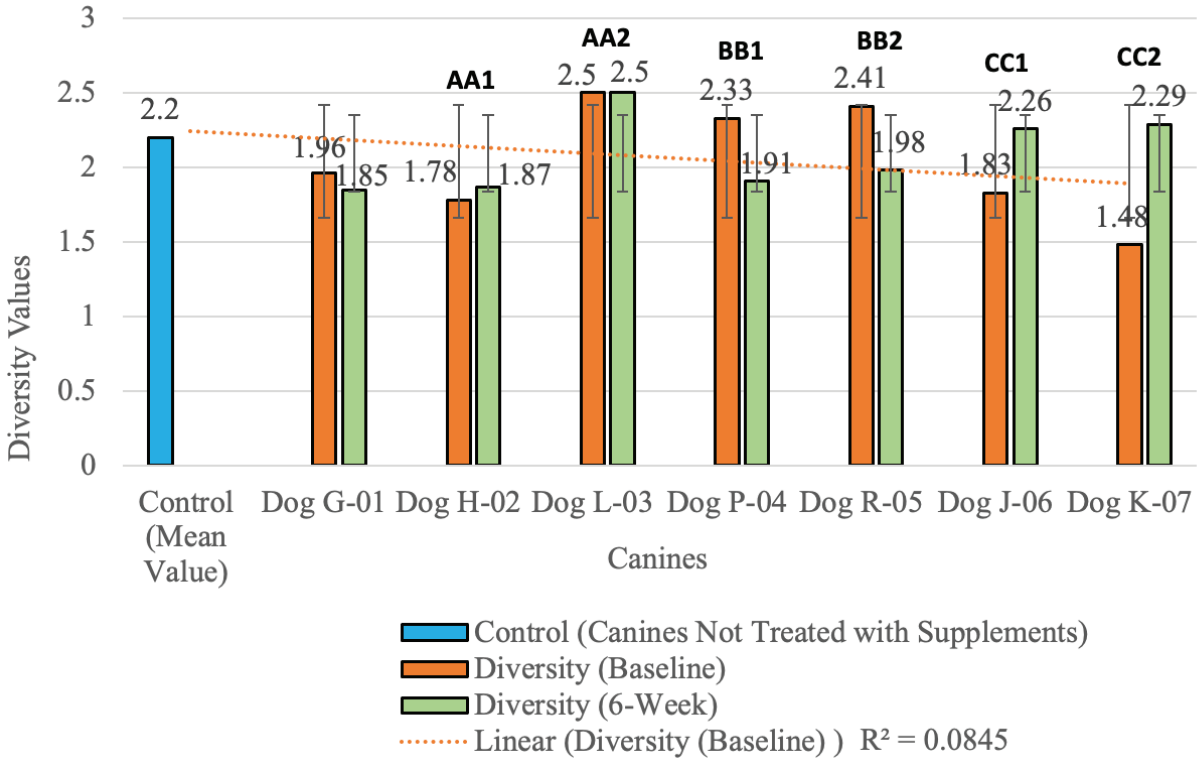

Figure 3. Alpha Diversity at Genus Level of Canines at Baseline (No Cultured and Fermented Supplements) Versus 6-Week (Treated with Fermented and Cultured Supplements). R squared is the goodness of fit based off the average mean of dogs not on cultured and fermented supplements. AA, BB, and CC show dogs in the same household.

Alpha richness is the number of species found in the sample collected. Figure 4 shows five of the seven dogs' richness in species increased when the second fecal sample was analyzed. The dogs living in the same household (BB1, BB2, CC1, CC3) alpha richness showed similar values after the second fecal collection and analysis was completed, in contrast, dogs AA1 and AA2 live in the same household and both decreased in richness. The mean control of 38 for richness are dogs (>1,000 sample size of dogs in Animal Biome data system) not on fermented or cultured supplements and used to compare the seven dogs in the study. When the diversity of the dogs in the study for the second fecal sample collected was averaged, this mean was 32.

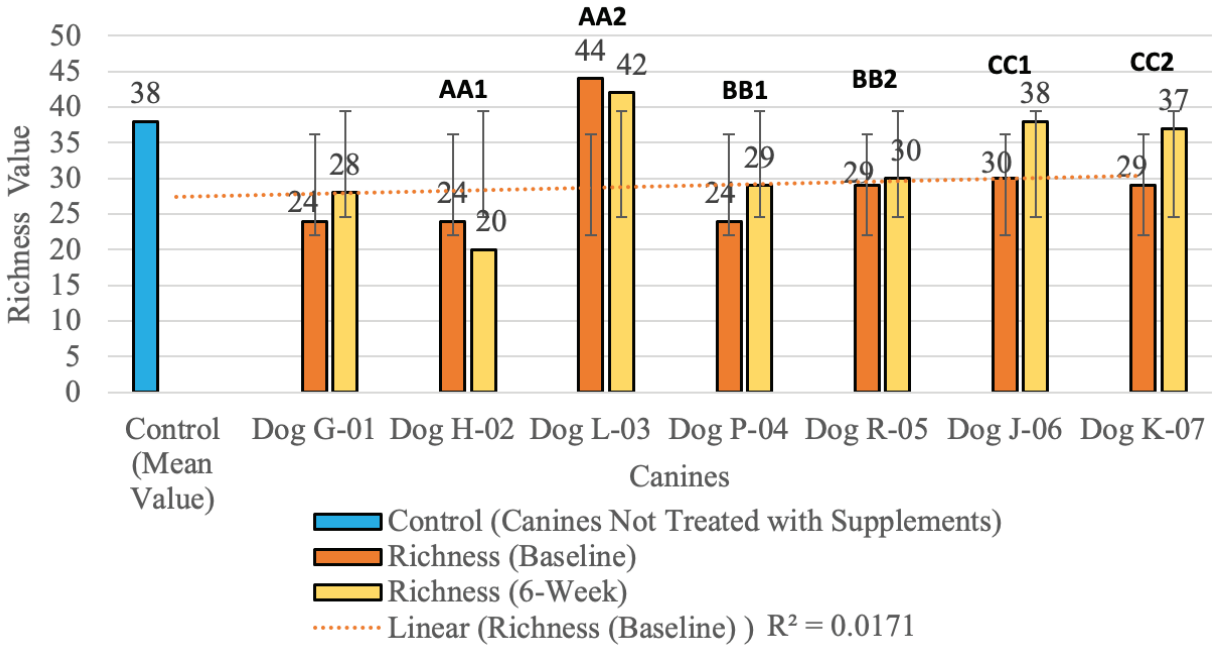

Figure 4. Alpha richness at Genus Level of Canines at Baseline (No Cultured and Fermented Supplements) Versus 6-week (Treated with Fermented and Cultured Supplements). R squared is the goodness of fit based off the average mean of dogs not on cultured and fermented supplements. AA, BB, and CC show dogs in the same household.

Alpha evenness refers to how close in numbers each species in an environment is. This was mathematically defined using the Shannon Wiener Index, a measure of biodiversity which quantifies how equal the community is numerically. Figure 5 shows three of the seven dogs' evenness increased by 0.07. However, three of seven dogs also decreased by 0.07 in evenness. The dogs living in the same household (AA1, AA2, BB1, BB2, CC1, CC3) evenness also showed similar values after the second fecal collection and analysis was completed. The mean control of 0.6 for evenness are dogs (>1,000 sample size of dogs in Animal Biome data system) not on fermented or cultured supplements and used to compare the seven dogs in the study. When the diversity of the dogs in the study for the second fecal sample collected was averaged, this mean was 0.61.

The ratio of *Firmicutes* to *Bacteroidetes* (F:B) was also calculated (Figure 6). F:B was calculated by dividing the abundance of *Firmicutes* and *Bacteroidetes* for each individual dog. Four of the 7 dogs F:B ratio decreased from baseline (not on supplements) to 6-weeks (on supplements). Dog P-04 had a significantly high F:B ratio at 15.15 and decreased to 1.52 after 6-weeks. The mean control of 7.9 for evenness are dogs (>1,000 sample size of dogs in Animal Biome data system) not on fermented or cultured supplements and used to compare the seven dogs in the study. When the diversity of the dogs in the study for the second fecal sample collected was averaged, this mean was 1.05.

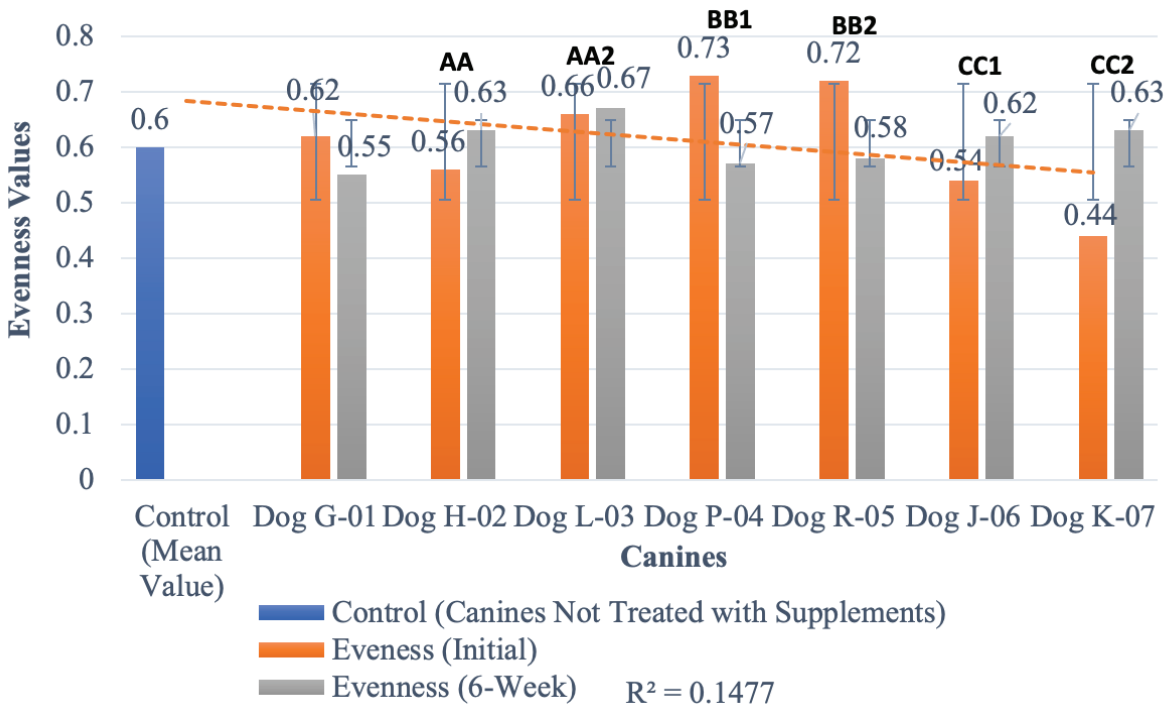

Figure 5. Alpha Evenness at Genus Level of Canines at Baseline Versus 6-week (Treated with Fermented and Cultured Supplements). R squared is the goodness of fit based off the average mean of dogs not on cultured and fermented supplements. AA, BB, and CC show dogs in the same household.

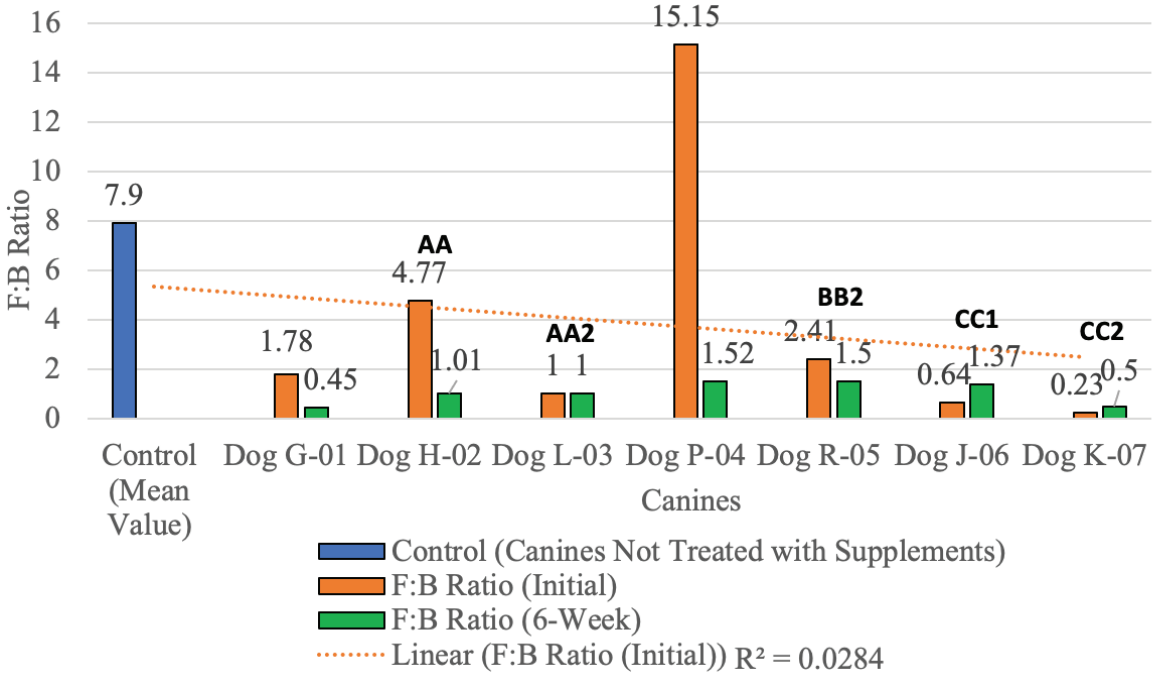

Figure 6. Alpha Firmicutes to Bacteroidetes (F:B) Ratio of Canines at Baseline Versus 6-week (Treated with Fermented and Cultured Supplements). AA, BB, and CC show dogs in the same household.

DISCUSSION

Overall, the results suggest that the driving force in microbiota composition when looking at alpha levels of relative abundance, evenness, diversity, and richness in dogs is the individual when looking at the phyla and genus structures of each dog. Studies on humans have also reported that interindividual variation is high and defines a "personal microbiome" (Human Microbiome Project Consortium, 2012). The fecal microbiome of healthy dogs is co-dominated by three phyla: *Fusobacterium, Bacteroidetes, and Firmicutes* (Middelbos, 2010; Hand, 2013) In this study, these three phyla were also seen to be more abundant in percentages.

When reviewing the literature, a wide variation in percentages of specific bacterial taxa can be seen. Within this core bacterial community, several major genera belong to the phylum *Firmicutes*. The genus consistently found in each dog were: *Megamonas*, *Blautia*, *Ruminococcus*, *Clostridium*, and *Lachnospiraceae*. *Megamonas* was more prevalent in abundance in this phylum. The phylum *Fusobacteria* was also abundant amongst all dogs by genus *Fusobacterium*. *Fusobacterium* abundance is increased in dogs with access to the outdoors (Song, 2013), and higher levels of *Fusobacterium* are also seen in other carnivore species (Bermingham, 2017). *Bacteroidetes* was also another abundant phylum in all dogs, with genus *Bacteroides* being abundant in all dogs' fecal samples collected. Wildbrines sauerkraut contained *Bifidobacterium bifidum*, *Bifidobacterium lactis*, *Bifidobacterium longum*, *Lactobacillus acidophilus*, *Lactobacillus casei*, *L. rhamnosus*, *Lactobacillus reuteri*, *Lactobacillus salivarius*, *L. salivarius*, and *Streptococcus thermophilus*; and the Answers kefir contained *Lactococcus lactis* and *Leuconostoc mesenteroides*. These fermented and cultured foods added to daily diet could be contributors to increased percentages in the phylum *Firmicutes* and *Actinobacteria* specifically. *Fusobacteria* had a more consistent increase in abundance over time in four of the seven dogs and may be an effect of the addition of the fermented and cultured supplements. The combined *Prevotella* and *Bacteroides* abundances seem to be inversely related to phylum *Fusobacteria* abundance, which might indicate that they occupy the same niche (Vázquez-Baeza, 2016). *Proteobacteria* and *Actinobacteria* phyla are typically colonizers of the small intestine and in physiological conditions will present in smaller numbers in fecal samples, and their increase is associated with many diseases (Pilla, 2019).

The alpha diversity, evenness, and richness were calculated using two-sample T-test calculations (Table 4) and did not show any significant changes when fermented and cultured foods were added for 6-weeks to the dogs' already established daily meal intake. However, dogs living in the same household (BB1, BB2, CC1, CC2) had similar diversity and richness values (both increased) after 6-weeks and in turn, dogs (AA1 and AA2) in the same household decreased and had similar values for diversity only. All dogs living in the same household also showed similar values for evenness after a 6-week fecal collection. Table 5 shows that there was significance in evenness ($P < 0.001$) when looking at 6-week fecal collections with fermented and cultured foods to the mean control value (>1000 sample size of dogs in Animal Biome data system) of dogs not on any cultured or fermented foods.

Bacteroidetes phylum protects against obesity and diseases due to not digesting fat well. Whereas, *Firmicutes* are a common phylum found in the gut and aids in the digestion of fat (required for energy) and linked to obesity and inflammation. The percentage of *Bacteroidetes* increased in three of the seven dogs and the *Firmicutes* decreased in six of the seven

dogs. When calculated, four of the seven dogs' overall *Firmicutes* to *Bacteroidetes* (F:B) ratio decreased after 6-weeks. A two-sample T-test (Table 5) was performed against both baselines and against a mean control (>1000 sample size of dogs in Animal Biome data system) of dogs not on cultured or fermented foods. F:B ratios showed no real statistical significance except when mean control value to 6-weeks F:B values were compared (P,0.001). Research shows *Firmicutes* abundance along with probiotics to help crowd out certain bacteria, could possibly treat obesity and weight gain (Abenavoli, 2019).

	Significance (< 0.01)	P Value	Number of Samples (N)	Degrees of Freedom (N - 1)	Mean of Baseline with No Supplements (M1)	Mean with 6-Week Supplements (M2)	Difference	Standard Error of Difference	Standard Deviation (SD)	t Ratio
Diversity	No	0.76471	7	6	2.04	2.09	-0.05	0.03	0.38	-0.3
Richness	No	0.476527	7	6	29.14	32	-2.86	15.12	6.82	-0.7
Evenness	No	0.947536	7	6	0.61	0.61	0	0	0.08	0.07
F:B Ratio	No	0.233258	7	6	3.71	0.98	2.74	4.71	2.17	1.26

Table 4. Two-sided T-Test with 99% Confidence Intervals with N=7 Alpha Level Comparing Canines Baseline Data with No Cultured and Fermented Supplements Versus Canine Data Collected After 6-weeks Adding Fermented and Cultured Supplements To Daily Meals.

	Significance (< 0.01)	P Value	Number of Samples (N)	Degrees of Freedom (N - 1)	Mean of Control Value of Canines Not on Supplements (M1)	Mean with 6-Week Supplements (M2)	Difference	Standard Error of Difference	Standard Deviation (SD)	t Ratio
Diversity	No	0.345597	7	6	2.00	2.09	-0.09	0.01	0.1	-1
Richness	No	0.054783	7	6	38	32	6	7.95	2.82	2.13
Evenness	Yes	< .00001	7	6	0.6	0.61	-0.55	0	0	-35
F:B Ratio	Yes	< .00001	7	6	8	0.98	6.95	0.03	0.17	41.3

Table 5. Two-Sided T-Test with 99% Confidence Intervals with N=7 Alpha Diversity Level Comparing Canine Baseline Data (with No Cultured and Fermented Supplements) Versus Canine Data Collected After 6-weeks (with Fermented and Cultured Supplements To Daily Meals)

In addition, individual variations in the microbiome profile exist and should be taken into account especially since this is a small sample group of seven dogs. This study is also limited to alpha diversity (variation within an individual microbiome) whereas beta diversity, the microbial variation between individuals, using PCoA and other statistical analysis could have been examined for this study. In addition, this was a 6-week study. Ideally, fecal collections at the beginning (baseline), 1 month, 2 months, 6 months, and 1 year would be more ideal to see the variations of the gut microbiome over time.

CONCLUSION

The gut microbiota is essential for the health of all mammals because it participates in the host's vital physiological processes and development. Alterations of the intestinal microbial populations are associated with a variety of gastrointestinal and systemic illnesses. Therefore, understanding the gut microbiota could be useful in the diagnosis of illness and disease and change the types of therapy procedures used.

Future research studies should clarify the mechanisms that regulate the interactions between the microbiota and the host. More studies have to be done about the use of probiotics, prebiotics, and FMT in the restoration of a state of eubiosis. While recent advances in DNA sequencing and computational technology have revolutionized the field of microbiomics, many questions remain unanswered, including how long the gut microbiome takes to recover from disease, drugs, or other environmental factors by better understanding the mechanisms of action and duration of efficacy of different treatments on the gut microbiome (Arnold et al, 2016). The identification of alpha and beta bacterial taxa with bacteria-derived compounds (plants, fermented and cultured whole foods) should be investigated further to look at explaining the mechanisms underlying interactions between the microbiome and host, describing the process of microbiome maturation during host development and its impact on early-life and adult health outcomes, clarifying its role in the pathogenesis of diseased states, land assessing the viability of diagnostic tests and therapies designed to assess and treat conditions associated with underlying health issues (Kho, 2018).

Continued research beyond this will be to statistically analyze this data with beta diversity using PCoA, adding additional dogs to the study, adding additional fecal collections over the course of a year, and compare the beta diversity to gender, living location, activity level, gender, age, and weight of dogs. Do dry or wet foods to that of a raw diet with protein on fermented and cultured foods have a significant difference in relative abundance?

Today, society is seeing a rise in microbiome-associated disorders in dogs (animals in general) and even in humans, and understanding differing effects on the gut microbiome will shape how we treat chronic issues not just for our canines, but pets and even humans.

AUTHOR INFORMATION

Corresponding Author

*Gianna Nilvo, giannanilv01@gmail.com

Funding Sources

Funding of Animal Biome fecal test kits, Volhard raw dog food diet for canines in the study, selection of canines in the study, and setting feeding protocol for this research study were provided by Volhard Dog Nutrition located in Marlton, New Jersey by Jen Carter, Certified Nutritionist and Vice President of Marketing and Sales. Gianna Nilvo declares no conflict of interest in this research study.

ACKNOWLEDGEMENTS

I would like to thank my Science Fair Chair and a National Science Advocate for the Society for Science at School of Dreams Academy. Mrs. Nilvo, for her mentorship in assisting me with my research paper and abstract, competition paperwork, finding assistance on teaching me statistical analysis, and oral presentation prep. Jennifer Carter, Vice-President of Volhard Dog Nutrition Company and animal nutritionist who reached out to me with expressed interest in collaborating with them on completing statistical analysis study of dogs on their raw dog food. She spent hours assisting me with a financial donation for the cost of the Animal Biome test kits for each dog, time and support in my study, selecting canines for the study, and lots of knowledge from her expertise in the pet food industry. I would also like to express my sincere gratitude to the New Mexico Journal of Science who conducted a peer review of my research paper providing feedback to improve my research writing and allowing me to publish my research study.

REFERENCES

Abenavoli, L.; Scarpellini, E.; Colica, C. et al. Gut Microbiota and Obesity: A Role for Probiotics. *Nutrients*. **2019**,11(11):2690, doi:10.3390/nu11112690.

Arnold JW, Roach J, Azcarate-Peril MA. Emerging Technologies for Gut Microbiome Research. *Trends Microbiol*. **2016**, 24(11):887-901. doi:10.1016/j.tim.2016.06.008

Barko, P.C., McMichael, M.A., Swanson, K.S., and Williams, D.A. 2018. The gastrointestinal microbiome: a review. *Journal of Veterinary Internal Medicine*. **2018**, 32(1):9-25, doi:10.1111/jvim.14875.

Bermingham EN, Maclean P, Thomas DG, Cave NJ, Young W. Key bacterial families (Clostridiaceae, Erysipelotrichaceae and Bacteroidaceae) are related to the digestion of protein and energy in dogs. *PeerJ*. **2017**, 5:e3019. Published 2017 Mar 2. doi:10.7717/peerj.3019.

Bindels LB, Delzenne NM, Cani PD, Walter J. Towards a more comprehensive concept for prebiotics. *Nat Rev Gastroenterol Hepatol*. **2015**, 2(5):303-310, doi:10.1038/nrgastro.2015.47.

Fenimore A, Martin L, Lappin MR. Evaluation of Metronidazole With and Without Enterococcus Faecium SF68 in Shelter Dogs With Diarrhea. Top Companion Anim Med. 2017 Sep;32(3):100-103. doi: 10.1053/j.tcam.2017.11.001.

Hand D, Wallis C, Colyer A, Penn CW. Pyrosequencing the canine faecal microbiota: breadth and depth of biodiversity. *PLoS One*. **2013**, 8(1):e53115. doi:10.1371/journal.pone.0053115.

Herstad HK, Nesheim BB, L'Abée-Lund T, Larsen S, Skancke E. Effects of a probiotic intervention in acute canine gastroenteritis--a controlled clinical trial. J Small Anim Pract. **2010** Jan;51(1):34-8. doi: 10.1111/j.1748-5827.2009.00853.x. PMID: 20137007.

Human Microbiome Project Consortium. Structure, function and diversity of the healthy human microbiome. *Nature*. **2012**, 486(7402):207-214, doi:10.1038/nature11234.

Khan, R., Petersen, F. C., & Shekhar, S. Commensal Bacteria: An Emerging Player in Defense Against Respiratory Pathogens. *Frontiers in immunology*. **2019**,*10*, 1203, doi.org/10.3389/fimmu.2019.01203.

Kho ZY, Lal SK. The Human Gut Microbiome - A Potential Controller of Wellness and Disease. *Front Microbiol*. **2018**, 9:1835. Published 2018 Aug 14. doi:10.3389/fmicb.2018.01835.

Kim, J., An, JU., Kim, W. et al. Differences in the gut microbiota of dogs (*Canis lupus familiaris*) fed a natural diet or a commercial feed revealed by the Illumina MiSeq platform. *Gut* Pathog. **2017**, 9, 68, doi.org/10.1186/s13099-017-0218-5.

Middelbos IS, Vester Boler BM, Qu A, White BA, Swanson KS, Fahey GC Jr. Phylogenetic characterization of fecal microbial communities of dogs fed diets with or without supplemental dietary fiber using 454 pyrosequencing. *PLoS One*. **2010**, 5(3):e9768, doi:10.1371/journal.pone.0009768

Mondo E, Marliani G, Accorsi PA, Cocchi M, Di Leone A. Role of gut microbiota in dog and cat's health and diseases. *Open Vet J*. **2019**, 9(3):253-258, doi:10.4314/ovj.v9i3.10.

Mustafa A, Wajid B, Guard M, Minamoto Y, Lidbury J, Steiner J, Serpedin E, Suchodolski J. A Dysbiosis Index to Assess Microbial Changes in fecal samples of dogs with chronic enteropathy. Journal of Veterinary Internal Medicine 2016;17.

O'Mahony SM, Clarke G, Borre YE, Dinan TG, Cryan JF. Serotonin, tryptophan metabolism and the brain-gut-microbiome axis. *Behav Brain Res*. **2015**, 277:32-48. doi:10.1016/j.bbr.2014.07.027.

Patra (2011) Patra AK. Responses of feeding prebiotics on nutrient digestibility, faecal microbiota composition and short-chain fatty acid concentrations in dogs: a meta-analysis. *Animal*. 2011;5:1743–1750. doi: 10.1017/S1751731111000887.

Pilla R, Guard BC, Steiner JM, et al. Administration of a Synbiotic Containing *Enterococcus faecium* Does Not Significantly Alter Fecal Microbiota Richness or Diversity in Dogs With and Without Food-Responsive Chronic Enteropathy. *Front Vet Sci*. 2019;6:277. Published **2019** Aug 30. doi:10.3389/fvets.2019.00277

Pilla R, Suchodolski JS. The Role of the Canine Gut Microbiome and Metabolome in Health and Gastrointestinal Disease. *Front Vet Sci*. **2020**;6:498. Published 2020 Jan 14. doi:10.3389/fvets.2019.00498

Pinna C, Vecchiato CG, Bolduan C, et al. Influence of dietary protein and fructooligosaccharides on fecal fermentative end-products, fecal bacterial populations and apparent total tract digestibility in dogs. *BMC Vet Res*. **2018**, 14(1):106, doi:10.1186/s12917-018-1436-x.

Sanders M.E, Merenstein D, Merrifield C.A, Hutkins R. Probiotics for human use. Nutr. Bull. **2018**, 43(3):212–225, doi.org/10.1111/nbu.12334.

Sauter SN, Benyacoub J, Allenspach K, Gaschen F, Ontsouka E, Reuteler G, Cavadini C, Knorr R, Blum JW. Effects of probiotic bacteria in dogs with food responsive diarrhoea treated with an elimination diet. J Anim Physiol Anim Nutr (Berl). **2006** Aug;90(7-8):269-77. doi: 10.1111/j.1439-0396.2005.00595.x.

Simpson J.M, Martineau B, Jones W.E, Ballam J.M, Mackie R.I. Characterization of fecal bacterial populations in canines: effects of age, breed and dietary fiber. *Microbiol. Ecol*. **2002**;44:186–197.

Song SJ, Lauber C, Costello EK, et al. Cohabiting family members share microbiota with one another and with their dogs. *Elife*. **2013**, 2:e00458, doi:10.7554/eLife.00458

Steiner J.M, Ruaux C.G. Small Animal Gastroenterology; Schlütersche Press: Hanover, Germany: 2008.

Tizard IR, Jones SW. The Microbiota Regulates Immunity and Immunologic Diseases in Dogs and Cats. *Vet Clin North Am Small Anim Pract*. **2018**, 48(2):307-322, doi:10.1016/j.cvsm.2017.10.008.

Vázquez-Baeza Y, Hyde ER, Suchodolski JS, Knight R. Dog and human inflammatory bowel disease rely on overlapping yet distinct dysbiosis networks. *Nat Microbiol*. **2016**, 1:16177, doi:10.1038/nmicrobiol.2016.177.

Zentek, J., Marquart, B., Pietrzak, T. et al. Dietary effects on bifodobacteria and clostridium perfringens on the canine intestinal tract. *Animal Physiology and Animal Nutrition*. **2003**, 87: 397-407, doi.org/10.1046/j.0931-2439.2003.00451.x.

APPENDIX A

Dog	Age (Years)	Gender	Breed	Weight (lb)	Volhard Diet (Type)	Living Location	Activity Level (Hours/Day)	Medication
G-01	4	Female	Beagle	21	AM/PM	Culpeper, VA	6 to 8	Thyroxine
H-02	10	Female	Yorkshire Terrier	7.9	AM/PM	Louisa, VA	8	
L-03	3	Female	Hound	32	AM/PM	Louisa, VA	8	
P-04	8	Male	Daschund Pug	13	NDF2	Albuquerque, NM	< 1	
R-05	5	Male	Corgi Chihuahua	10	NDF2	Albuquerque, NM	< 1	
J-06	<1	Male	Great Dane	135	NDF2	La Mirada, CA	2 to 4	Trazadone Gabapentin CBD
K-07	2	Male	Great Dane	148	NDF2	La Mirada, CA	2 to 4	

Table 1. Demographics of the Seven Canine Participants in the Study.

Phylum	Genus	Dog G-01 Baseline	Dog G-01 6-Wk	Dog H-02 Baseline	Dog H-02 6-Wk	Dog L-03 Baseline	Dog L-03 6-Wk	Dog P-04 Baseline	Dog P-04 6-Wk	Dog R-05 Baseline	Dog R-5 6-Wk	Dog J-06 Baseline	Dog J-06 6-Wk	Dog K-07 Baseline	Dog K-07 6-Wk
Actinobacteria	Collinsella	4.4	0.2	17.8	3.8	4.6	4.5	5	2.5	3.2	3.2	0.2	1.7	0	0.6
Bacteroidetes	Prevotella	7.3				25.8	18.4							47	29.8
Bacteroidetes	Bacteroides	14.9	19.8	6.5	9.4	8	14.4	3.8	21.9	22.2	22.2	20	23.7	2.3	11.6
Bacteroidetes	Alloprevotella		12.7		4.5							10	0	3.1	6.1
Bacteroidetes	Tyzzerella		1.1												
Firmicutes	Megamonas	36.8	4.2		12.8	17.9	9.4	17	14.9	12.9	12.9			5	5.6
Firmicutes	Blautia	1.2	0.8	13.5	2.7	5.3	1.5	14.5	6.9	11.6	11.6	5.6	10.7	1.5	4.2
Firmicutes	Peptoclostridium		1		6.5			5.3	3.7	4.7	4.7			0.8	5.3
Firmicutes	Ruminococcus	1.9	0.3	0.1		0.3	0.1	1.8	1.8	2.3	2.3	2.3	4.3	0.5	0.7
Firmicutes	Faecalibacterium	0.1				4.8	6.1								0.8
Firmicutes	Clostridium	1.6	3.2	8.1		2	0.6	1.2		0.1	0.1		0.3	0.4	0
Firmicutes	Lachnospiraceae	1.5	1.8	1.5	0.1	1.3	0.4	1.8	0.5	2.6	2.6	2.6	2.4	0.3	1.3
Firmicutes	Lachnostridium				2			0.5	1.4	1.3	1.3	0.6	0.4	0.2	0.3
Firmicutes	Dorea	0.9		4.1	6.1	0.5	0.2								
Firmicutes	Streptococcus	1.8		1.1	2.4										1.4
Firmicutes	Dialister				1.7									1.3	
Firmicutes	Catenibacterium				1					3.5	3.5				
Firmicutes	Faecalitalea									1.1	1.1				
Firmicutes	Erysipelatoclostridium									1.3	1.3				
Fusobacteria	Fusobacterium	20.6	42.2	43.3	34.9	4.1	16.5	24.5	37.9	19.9	18.9	46	27.3	34.2	21.4
Proteobacteria	Sutterella	1.2	2.3	1.3	8.3	2.5	3.3	2	3.8	3.6	3.6	4.4	0	1.4	3.7
Proteobacteria	Escherichia				1.6										
Proteobacteria	Shigella		8.2					5.3				0.3	9.3	0.1	
Proteobacteria	Anaerobiospirillum									3.4	3.4				
% of Microbiota Explained by Taxa >5%		94.2	97.8	97.3	97.8	77.1	75.4	82.7	95.3	93.7	92.7	91.7	80.1	98.1	92.8

Table 2. Genus and Phylum Percentages of Baseline and 6-Week Data of Canines in Study Versus Control Value of Canines Not on Fermented and Cultured Supplements.

FDA-Approved Drugs that can Prevent Cytokinesis of the *Caulobacter crescentus* Bacteria

*Ksenia Sevostianov**

Las Cruces High School, Las Cruces, NM

ABSTRACT

The overuse of antibiotics in recent years has resulted in a development of antibiotic-resistant bacteria. There are two potential solutions to overcome this problem. New drugs can be developed, but this takes considerable time and money. Old drugs can also be remade and reused, and bacteria may have a harder time becoming resistant. The energy of interaction between protein FtsZ (found in *Caulobacter crescentus* bacteria) and 7,409 Food and Drug Administration (FDA) approved drugs was calculated using a Python code, where negative values represented high energy of interaction and positive values, low energy of interaction. The drugs that had the highest energy of interaction are recommended for further experimentation.

KEYWORDS: Antimicrobial resistance, Superbugs, Antibiotics, *Caulobacter crescentus*, FtsZ Protein, Energy of Interaction

INTRODUCTION

Since the post-antibiotic era, "superbugs" have become a rising threat to treating diseases and infections. Superbugs is a term used to describe strains of bacteria or fungi that are resistant to most antibiotics used today. Resistant bacteria that cause pneumonia, skin infections, etc. are just some of the dangers we now face (Dugassa and Shukuri, 2017). Antibiotic resistance is a natural process of evolution that happens over time when bacteria slowly adapt or mutate to ensure their survival against drugs that are meant to kill them. Kapoor et al. (2017) reviewed the resistance mechanisms.

Developing new drugs and replacing existing antibiotics is not a good solution, because new drugs require lengthy clinical trials and toxicity tests, and approval is a complex procedure—the FDA only approved 1-3 new medications per year in the last 50 years (Figure 1). Also, it may not take very long for bacteria to become resistant to these new drugs, and the range of medications we can still use will get smaller and smaller.

An important characteristic of an antimicrobial drug is selective toxicity; it discerns the microbial target from host cells and only kills or prevents growth in the microbes while causing little to no harm to the host. Most of the drugs going through clinical trials are antibacterial because bacteria provide a better target variety for selective toxicity, compared to fungi or viruses. Each category of antibacterial drugs has a unique way to affect the microbes (Kirmusaoglu et al., 2019). Antibiotics can slow down or stop the growth of bacteria by targeting the cell wall or membrane. They also target protein and nucleic acid synthesis. Protein synthesis is performed by ribosomes which are nucleoprotein (nucleic acid bonded to

protein) complexes that are made up of a small and large subunit. Antibiotics can also work as antimetabolites by blocking the folate metabolism (therefore DNA synthesis) in a pathway that involves para-aminobenzoic acid (PABA) and two acids that help make folic acid: dihydrofolic acid (DHF) and tetrahydrofolic acid (THF). Antibiotics can block DNA gyrase, which

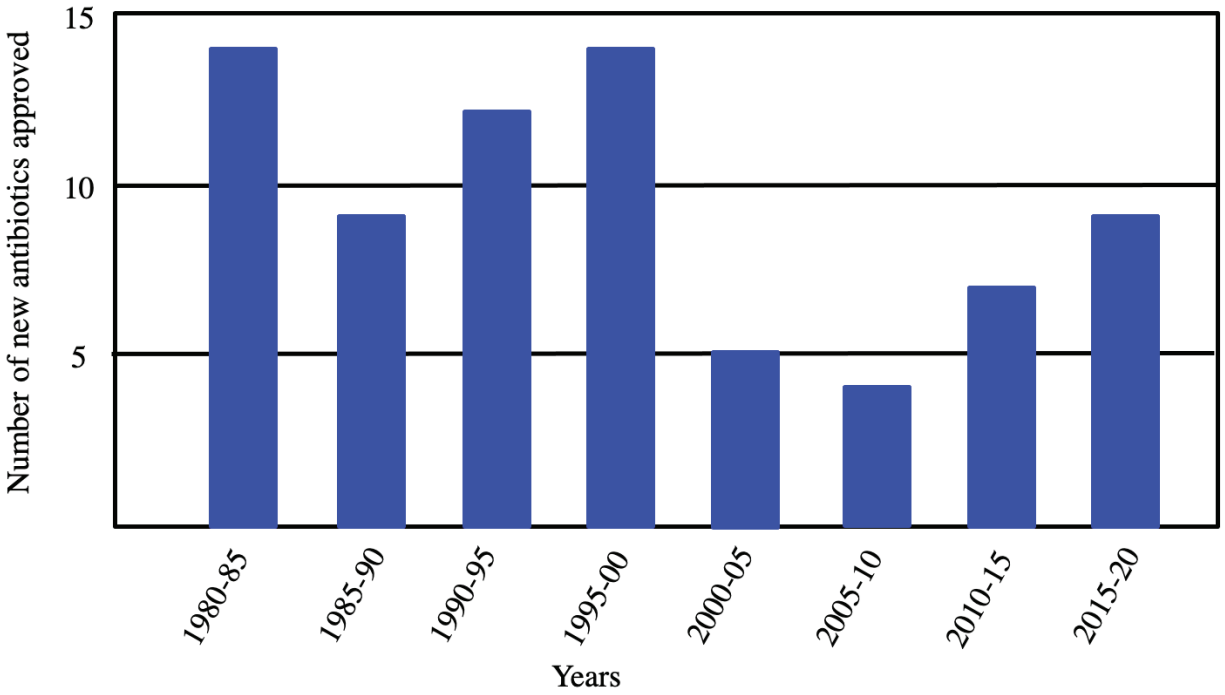

Figure 1. Number of new antibiotics approved by FDA (using data from the Wall Street Journal).

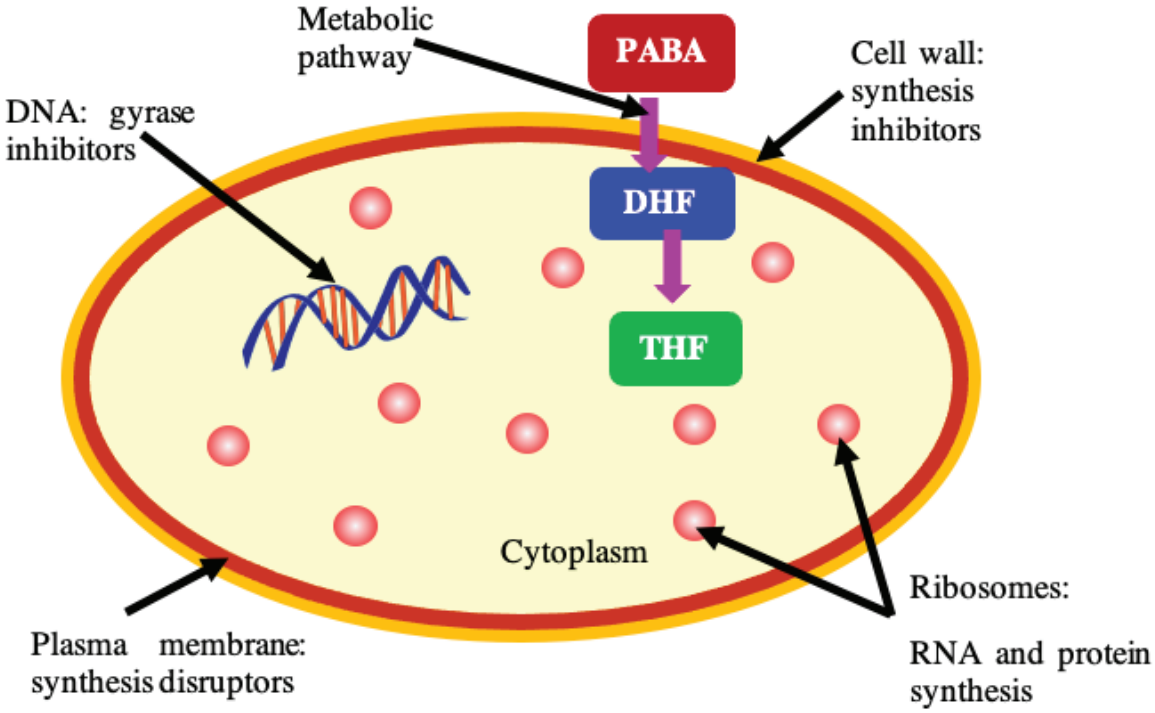

Figure 2. Mechanisms of work of antibacterial drugs.

is an enzyme that modifies the molecular arrangement of DNA, playing a role in replication and transcription. Figure 2 illustrates these mechanisms.

Antimicrobial resistance (AMR) occurs when a strain of bacteria resists antibiotics that usually prevent or slow their growth, which allows them to resist drugs. Since the 1990s, bacteria have been growing more harmful because of resistance genes (resistomes), which allow them to become resistant to various antibiotics. Today, many bacterial pathogens are resistant to antibiotics because they get or create antimicrobial-resistant genes, found mainly on plasmids and chromosomes. There are various methods like conjugation, transformation, and transduction when vulnerable strains can get resistance genes with transposons that support different resistance genes to combine with host chromosomes or plasmids. There are currently four basic mechanisms of bacterial drug resistance (Kapoor et al., 2017): target alteration, change to membrane permeability, efflux pump, and antibiotic degradation via enzymes (Figure 3).

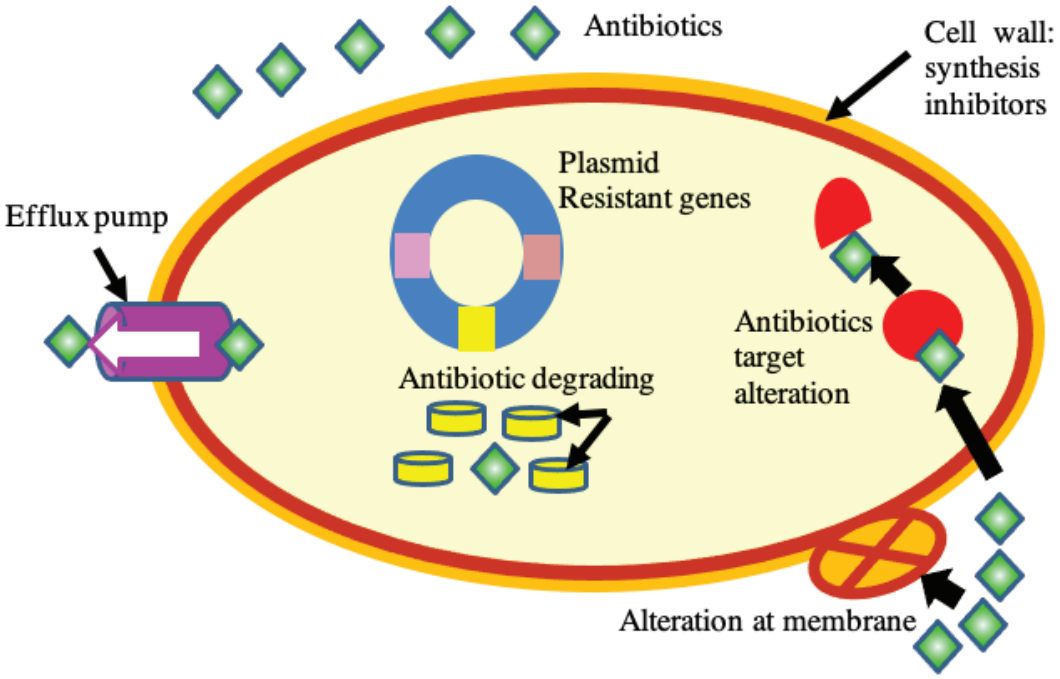

Figure 3. Four mechanisms of drug resistance: target alteration, change to membrane permeability, efflux pump, and antibiotic degradation via enzymes.

As superbugs become a bigger threat, the problem of treatment and developing new drugs is arising. New drugs that can effectively fight bacterial infections and diseases are needed. Developing drugs that can kill the bacteria is not the best approach. Instead, we need to slow down or even stop bacterial growth, while discontinuing the use of antibiotics, because they have little to no effect on the bacteria anymore.

This paper proposes an alternative approach that is based on the observation of the role of the protein FtsZ (Figure 4) during cytokinesis of the bacteria *C. crescentus* (de Boer et al., 1992). This protein moves to the middle of the cell during division and assists in cytokinesis. For this project, the ability of various inhibitors to block the active site of FtsZ was investigated. If the active site is blocked, the protein cannot participate in the bacterial division.

The principal work here is to calculate the energy of interaction between FtsZ and several inhibitors. The inhibitors were 7409 FDA-approved drugs that are not used as antibiotics- the bacteria could have resistance against it. Information about these drugs is taken from Kyoto Encyclopedia of Genes and Genomes (KEGG) Database (LigandBox) (Kawabata et al., 2013) because this database has the widest range of publicly available information about the drugs. It is convenient to use *C. crescentus* as a model bacterium because it is easy to track its cell division: each stage of the division is unique and contrasting. Using this kind of approach for various other bacteria could be a key for finding or developing drugs that bacteria aren't resistant to and will take a long time to develop resistance.

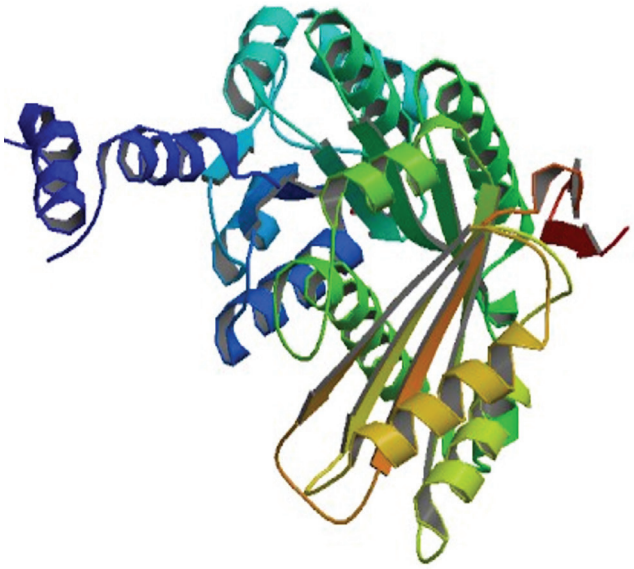

Figure 4. Crystalline structure of filamenting temperature-sensitive mutant Z (FtsZ) protein (PDB code: 1W59; image generated by PyMOL).

MATERIALS AND METHODS

To calculate the energy of interaction, data from FDA-approved drugs provided by KEGG, which is a collection of databases dealing with genomes, biological pathways, diseases, drugs, and chemical substances, was used. The KEGG DRUG database contains information about the active ingredients of approved drugs in Japan, the USA, and Europe. Part of this database is used in LigandBox (Kawabata et al., 2013), a 'ready-to-dock' database of small chemical compounds for virtual drug screening on computer docking studies. The database is downloadable in the form of a MOL2 file and, in December 2019, contained 7,409 records. The records were transformed to a PDBQT file using PubChem, an open-access database of chemical molecules and their activities against biological assays. The system is maintained by the National Center for Biotechnology Information which is part of the United States National Institute of Health (NIH). PubChem contains substance descriptions and small molecules with fewer than 1000 atoms and 1000 bonds. The database is growing continually. The energy of interaction between 7,409 ligands available in Ligand Box and FtsZ protein was calculated using the AutoDock Vina program which is a suite of automated docking tools designed to predict how small molecules, such as substrates or drug candidates, bind to a receptor of a known 3D structure. It is an open-access program developed by the Molecular Graphics Lab at The Scripps Research Institute, La Jolla, CA. Each molecule available in the Lig and Box was placed at the active site of the FtsZ protein in the Autodock Vina code. After the energy of interaction was calculated, the result was recorded in the output file. Finally, all the records in the output file were ranked by energy value. For this procedure, a Python utility program was written.

Python Code

The algorithm of the Python utility code is given in Figure 5.

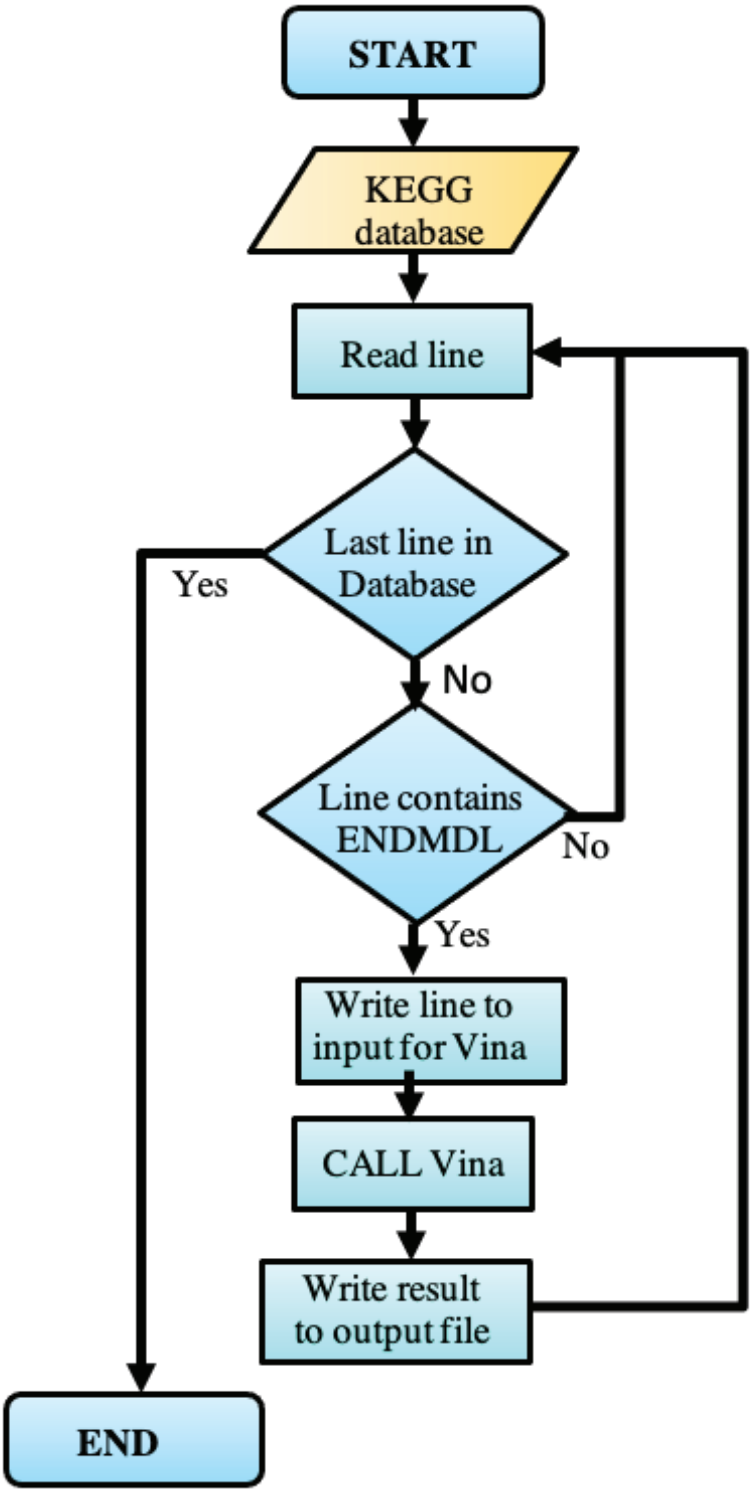

Figure 5. Each line in the KEGG database was analyzed. If the line contained ENDML, that line became the input for the AutoDock Vina program. This program was then called, and the result was written for the output file.

Docking the Inhibitors

The energy of interaction between FtsZ and the inhibitors was calculated with Autodock Vina. Negative energy corresponds to the attraction between the inhibitor and protein. Autodock Vina considers Coulombic forces between the atoms as well as Van der Waals's forces. The input data includes pdb files with the crystalline structure of the FtsZ protein taken from the PubChem database, the configuration file with the approximate coordinates of the active site, and the size of the optimization box that binds the space for the search of the optimal position of the ligand, and the pdb file with the molecule of the ligand read from the KEGG database. The resulting energy change due to the presence of the inhibitor is given as the function of the ligand orientation angles. Those with maximal absolute value were used. Autodock Vina gives the calculated changes in free energy in kcal/mol-1 (Table 1).

Table 1 shows results of the calculations for the twenty drugs which showed the highest energy of the bound state for the FtsZ–ligand complexes. (-11 kcal mol^{-1} or higher). For reader convenience, the KEGG number of each drug (taken from the database), the chemical formula, international ID, and the name used in the pharmaceutical industry are provided.

KEGG number	Energy (kcal/mol^{-1})	Chemical formula	International ID	Name
00006725-01	-12.1	C35H34N6O3F	D08981	Quarfloxin
00004026-01	-12	C35H30N4O4	D05029	Midostaurin
00005945-01	-11.6	C20H10N3O3F5Cl2	D07964	Fluazuron
00006874-01	-11.6	C22H24N6O2	D09610	Emicerfont
00004241-01	-11.4	C21H16N2	D05359	Paranyline hydrochloride
00007306-01	-11.3	C26H17N3O3F9Cl	D10361	Afoxolaner
00007374-01	-11.3	C33H39N7O4F2	D10465	Golvatinib tartrate
00006706-01	-11.3	C28H22N7OF3	D08953	Nilotinib
00007202-01	-11.2	C24H17N2O5F2	D10134	Lumacaftor
00007108-01	-11.2	C30H40N4O4F	D09981	Ulimorelin
00003390-01	-11.2	C25H21N4O4	D03978	Eltrombopag olamine
00006583-01	-11.1	C20H15N4O3F3	D08654	Trovafloxacin
00004025-01	-11.1	C18H13N3FCl	D05028	Midazolam maleate
00001979-01	-11.1	C20H15N4O3F3	D02123	Trovafloxacin mesylate
00000511-01	-11.1	C18H13N3FCl	D00550	Midazolam
00002557-01	-11.1	C30H22N4O4	D02773	Adozelesin
00000653-01	-11.1	C18H13N3FCl	D00696	Midazolam hydrochloride
00007109-01	-11	C30H40N4O4F	D09982	Ulimorelin hydrochloride
00004251-01	-11	C25H23N4O4Cl	D05378	Pazinaclone
00002865-01	-11	C41H50N6O2	D03249	Bisoctrizole

Table 1. The results of the calculations for the twenty drugs that showed the highest energy of the bound state for the FtsZ–ligand complexes. (-11 kcal mol^{-1} or higher).

RESULTS

The docking results show that the FtsZ molecule forms very stable complexes with the drug molecules listed in Table 1. This means that the drug molecules can only be in the free stage if all of the FtsZ molecules are already occupied. FtsZ binds to ligands unless it finds other molecules that might form more stable complexes, i.e. a molecule that has a higher energy of interaction with FtsZ (attraction is represented by a negative sign, while repulsion is positive). This means that these drugs can block FtsZ which assists in the cytokinesis of *C. crescentus* (Figure 6) and, therefore, can be used as potential antibiotics against this bacteria.

To verify this hypothesis, a follow-up experimental study is required. It will be necessary to break apart and examine the DNA of the *C. crescentus* bacteria that contains the protein FtsZ, insert the drug into the DNA, and examine its effects on the division of the bacteria. This experiment was not done because the COVID-19 pandemic prevented the author from working in the lab. Using this kind of approach for various other bacteria could be the key to finding or developing drugs that bacteria aren't resistant to and will take a long time to develop resistance against.

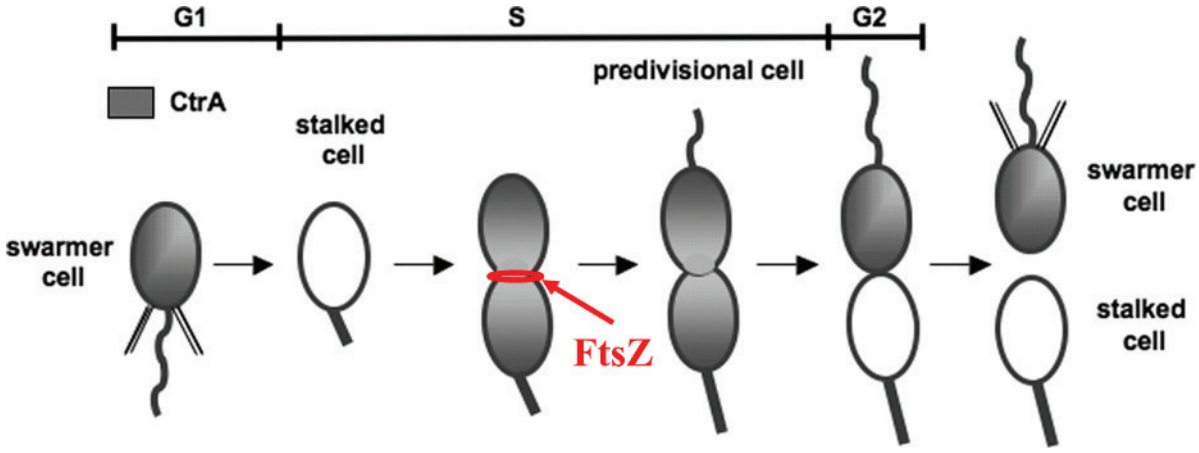

Figure 6. A schematic diagram of the *C. crescentus* cell cycle. (England et al., 2010).

CONCLUSIONS

The paper identified FDA-approved drugs that form stable complexes with FtsZ, a protein that assists in the cytokinesis of the bacteria *C. crescentus*. While this bacterium is mostly used, for example, as an important model organism for studying the regulation of the cell cycle, the proposed approach can be applied to other bacteria as well and could be a key for finding or developing drugs that bacteria aren't resistant to.

AUTHOR INFORMATION

Corresponding Author

*Ksenia Sevostianov, kseniasev303@gmail.com

ACKNOWLEDGMENTS

I would like to thank Drs. M. Talipov and P. Mera (NMSU) for their guidance in this research and for their careful instruction.

REFERENCES

Dugassa, J.; Shukuri, N.; Review on Antibiotic Resistance and Its Mechanism on Development. *Journal of Health, Medicine, and Nursing* **2017**, 1 (3), 1-17.

de Boer, P.; Crossley, R.; Rothfield, L.; The essential bacterial cell- division protein FtsZ is a GTPase. *Letters to Nature* 1992, 359, 254-256.

England, J.C.; Perchuk, B.S.; Laub, M.T.; Gober, J.W. Global Regulation of Gene Expression and Cell Differentiation in *Caulobacter crescentus* in Response to Nutrient Availability. *Journal of Bacteriology* **2010,** 192 (3), 819-833.

Kanehisa Laboratories, 1995-2021. *KEGG: Kyoto Encyclopedia of Genes and Genomes.* <https://www.genome.jp/kegg/>

Kapoor, G.; Saigal, S.; Elongavan, A.; Action and resistance mechanisms of antibiotics: A guide for clinicians. *Journal of Anesthesiology Clinical Pharmacology* **2017**, 33 (3), 300-305.

Kawabata, T.; Sugihara, Y.; Fukunishi, Y.; Nakamura, H. LigandBox : a database for 3D structures of chemical compounds. **2013** <http://www.mypresto5.com/ligandbox/cgi-bin/index.cgi>

Kirmusaoglu, S.; Gareayaghi, N.; Kocazeybek, B. Introductory Chapter: The Action Mechanisms of Antibiotics and Antibiotic Resistance. *Antimicrobials, Antibiotic Resistance, Antibiofilm Strategies and Activity Methods* **2019**, DOI: < http://dx.doi.org/10.5772/intechopen.85211 >

National Library of Medicine, National Center for Biotechnology Information. *PubChem.* <https://pubchem.ncbi.nlm.nih.gov/ >

Roland, D. Antibiotic Makers Struggle, Hurting War on Superbugs. Wall Street Journal 2020, < https://www.wsj.com/articles/antibiotic-makers-find-rewards-for-tackling-superbugs-are-scarce-11578259557 >

College Cost-Benefit Analysis Using Linear Regression Analysis, Pandas, and Seaborn

*Mario Sumali**

La Cueva High School, Albuquerque, NM

ABSTRACT

College is so expensive that student loans make up the second-biggest consumer debt in the nation. Some of the most expensive colleges produce alumni with low earnings. To slow down the growth of the problem, in 2015 the US Department of Education made available to the public the College Scorecard database which lists the costs and average alumni salaries, along with many other variables, of thousands of colleges. This paper features the Python data science tool Pandas and visualization tool Seaborn to reveal correlations among several important variables related to tuition and earnings. For a start, simple sorting of tuition shows that the few most expensive colleges do not produce alumni with the highest earnings. This paper then shows that the highest-earners-producing colleges achieve this to a large extent because those colleges give a large proportion of their degrees in graduate or professional degrees (MD, JD, Ph.D., MS, etc). That conclusion is enabled by a method presented here, based on linear regression analysis, to estimate Bachelor alumni's earnings from the Integrated Postsecondary Education Data System (IPEDS-reported) combined-Bachelor-and-Graduate alumni earnings. Furthermore, with or without adjustment for graduate earnings, highest-earners-producing colleges give a large proportion of their degrees principally in just a few fields of study: 1. Health professions (Bachelor's level, not including MD or Masters); 2. Engineering, including Computer Science; 3. Business. A few colleges produce high-earners in Social Sciences and Maritime Transportation (which were lumped into Engineering). The discovery of those highest income-producing fields from the College Scorecard is largely consistent with another study by Georgetown University which shows that STEM majors give significantly higher earnings than other majors. The study reports average earnings of college majors, which is important for students applying to colleges and may well determine the future of the students.

Major is a finer categorization of profession than fields of study. However, the Georgetown study does not attempt to correlate tuition of colleges to the alumni's earnings. Further analysis of the College Scorecard shows some correlation between the two. Colleges that tend to produce alumni with high earnings also tend to charge high tuition. Furthermore, public colleges tend to charge significantly less tuition than private colleges. However, colleges with high tuition do not necessarily produce alumni with high earnings. Thus, in terms of earnings, the major is far more important than the price tag or the name of the college. Nevertheless, for value comparison, the names of the top 32 colleges in terms of their average Bachelor's earnings (from College Scorecard adjusted for graduate degrees) and their tuition are given here, along with highest-earners-producing colleges in Health Professions and Engineering. College Scorecard reports the size of student debts at each college. The analysis shows that debt does not correlate with alumni earnings.

KEYWORDS: Choosing Colleges, Graduate Salaries, Graduate Boost Factor, University Tuition, Paying for College, College Debt

INTRODUCTION

A college education is very important for obtaining a well-paying job. On average, a Bachelor's degree results in roughly $1 million in higher lifetime earnings compared to a high school degree (Carnevale et al., 2015). However, college is so expensive that student loans are the number two consumer debt in the nation—$1.6 trillion in 2020, which is second only to home mortgages (Friedman, 2020). For comparison, far more consumers owe credit card debt than owe college debt, but credit card debt totals just above $1 trillion for the whole nation. The average student loan debt is $32,731, and 8.1 million Americans 50 years or older still owe around $25,000 in student loan debt. (Friedman, 2020). Why do students incur so much debt? The simple answer is that college is expensive. A college that we shall call "College 1647" charged $51,665 per year in tuition and fees in 2015. In addition to being expensive, that college does not produce alumni with high earnings. Six years after enrollment, the average graduate of College 1647 earns only $21,093/yr. With that little earning, the alumni cannot pay down their college loan debt quickly. Several colleges that charge less than $1,000/yr tuition have alumni with higher earnings than College 1647 alumni. Table 1 shows the wide range of average earnings of alumni of just a few colleges. Colleges that charge more in tuition do not necessarily produce high-earning alumni. Thus, today's applicants to colleges must be very careful in choosing which college to attend. The old idea of a "dream college" needs serious adjustment (Seeger, 2018).

College Name	Tuition, $/yr	Earning, $/yr
"College 1647"	51,665	21,093
"College 3874"	42,962	41,900
"College 1533"	37,489	18,500
Carnegie Mellon University	36,119	69,800
Worcester Polytechnic Institute	32,881	67,500
Bucknell University	31,788	57,700
Harvard University	43,938	70,300

Table 1. The high costs of colleges do not necessarily result in high earning.

DATA AND METHODS

The author wrote a Python code to read and process College Scorecard data and to present actionable results with lists and graphs for visualization. As a result of the US Department of Education's College Scorecard project, the Integrated Postsecondary Education Data System (*College Scorecard Data*, 2020) website reports hundreds of variables for each of over six thousand colleges in the US. The author downloaded all available databases from that website, dating back to 1996. The latest database, from 2016-2017, is too new to have data for earnings at 10 years after enrollment. Thus, the author uses the database from 2014-2015, the latest year for which the database contains earnings at 10 years after enrollment.

The Python code used the following libraries: **Pandas** is a module for data science. It implements numerous common statistics formulas. Additionally, **Scipy.stats** contains lower-level statistics functions, a few of which is used in the code. **Numpy** is necessary for nearly all significantly mathematical analyses. **Matplotlib** enables the creation of graphs for visualization. Additionally, **Seaborn** is a high-level library of common visualization routines, which runs on Matplotlib under the hood.

The variables used are listed in Appendix A. Most of the variable names follow the standard definitions given by the IPEDS database; they are written in ALL_CAPS. In contrast, the variables created by the author in the Python code are not in ALL_CAPS. Algebraic formulas derived and implemented by the author will be explained in the next section, which describes the research and coding in a logical sequence of data processing steps or conclusions. A few key lines in the code can be found in Appendix B as well, and some will be referred to in the discussions below.

Among over 7,700 colleges in the IPEDS database, the author is interested in applying to colleges that offer Bachelor's degrees. (In the database, HIGHDEG = 'Bachelor'.) This excludes two-year community colleges but includes all four-year undergraduate colleges and colleges that grant graduate (e.g., MS, Ph.D.) or professional (e.g., MD, JD) degrees *in addition* to Bachelor's degrees. There are almost 2,000 predominantly undergraduate colleges in the US. Most of them also give graduate degrees. In this analysis the author assumes that the most important variable for each college is the median earning of its alumni at six years after they enrolled, representing the early career stage after graduating with a bachelor's degree. In the IPEDS database, this variable is called MD_EARN_WNE_P6. Many colleges eliminated or suppressed the reporting of this earning, showing it as 'PrivacySuppressed'. The author excluded those colleges from the analysis. A few colleges are exclusively graduate/professional schools in practice (Medical, Law, Business) even though they reported their 'predominant degrees' (PREDDEG) as "Bachelor's". Among 1684 colleges that are listed to give bachelor's degrees, only 1636 list the number of undergraduate students. The rest show no undergraduate population and are listed in Appendix C. Those colleges are actually graduate/professional schools and are therefore excluded from the analysis. The cleaned list from the database (just over 1600 colleges) is placed in the Pandas dataframe **df_clean.** The author uses a Pandas command

```
df_clean = df_clean[df_clean['UGDS'].notnull()]
```
(1)

A few other similar steps are taken to exclude colleges that do not grant bachelor's degrees.

ALUMNI EARNING IS A FUNCTION OF GRADUATE STUDENT POPULATION

The most important variable in this analysis is the median earning at six years after graduation (MD_EARN_WNE_P6). Appendix D shows that this variable is distributed almost in a normal Gaussian fashion. A few colleges are on the low-end 'secondary' normal distribution. Those are mostly religious seminaries and colleges in US Territories outside the states. More interesting is the tail at the high-end of earnings, which are colleges that produce very high earners who are outside the main, approximate normal distribution.

Colleges that are exclusively graduate or professional schools, e.g. Medical or Law schools, produce alumni with high earnings. Excluding those colleges, Table 2 lists the top few highest-earners-producing colleges. Numbers in turquoise denote the undergraduate population that is smaller than the graduate population. Examination of Table. 2 and a few dozen more colleges on the top of the list reveals that most of these top highest-earners-producing colleges award more graduate degrees than Bachelors. Fourteen out of the 25 highest-earners-producing colleges do. We also observe that Thunderbird School of Global Management produced alumni with earnings at six years after enrollment (MD_EARN_WNE_P6) of $87,400/yr, which would rank it as the 4th highest-earners-producing "Bachelor's" college in the US. However, that college had 797 graduate or professional students and one undergraduate student. Therefore, we excluded that college from Table 2 although it passed the graduate-and-professional-schools filter in code line (1) above.

From the observations made with Table 2, we statistically hypothesize that the highest-earners-producing colleges have high graduate student proportions in their populations. To examine this hypothesis, we perform a linear regression analysis of earning as a function of graduate student proportion. Figure 1 shows alumni earnings at six years after enrollment

College Name	Earning, $/yr	Undergrads	Grads
St. Louis College of Pharmacy	120400	693	668
Albany Coll of Pharm&Health Sci	112100	1076	483
Samuel Merritt University	100100	523	979
Massachusetts Inst of Technology	82200	4476	6807
Oregon Health & Sci University	80000	847	2014

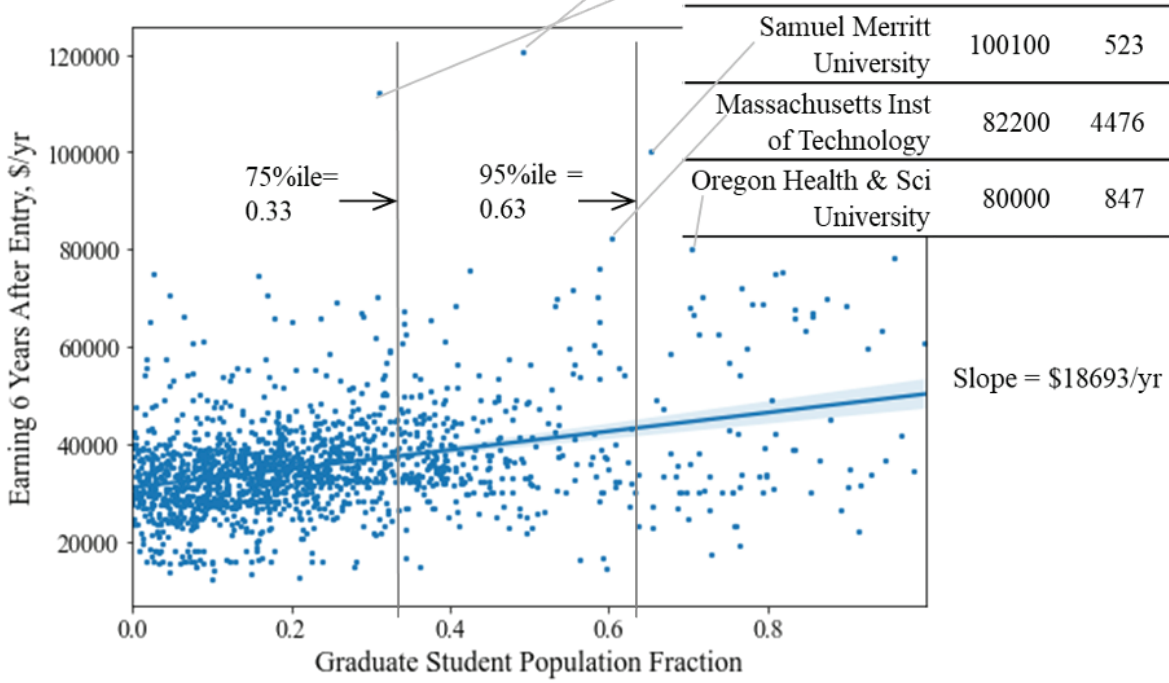

Figure 1. Colleges whose graduate student ratio is near 100% (i.e. "near-totally graduate or professional" colleges) produce alumni with roughly 60% higher earnings than colleges whose graduate student proportion is near 0 (i.e. "near-totally undergraduate" colleges).

(MD_EARN_WNE_P6) as a function of *graduate student population fraction* at each college, defined in Pandas syntax as

```
df_clean['Grad_population'] = df_clean.GRADS / (df_clean.UGDS + df_clean.GRADS)
```
(2)

	College Name	Earning, $/yr	Undergrads	Grads
1	St. Louis College of Pharmacy	120400	693	668
2	Albany Coll of Pharm&Health Sci	112100	1076	483
3	Samuel Merritt University	100100	523	979
4	Massachusetts Inst of Technology	82200	4476	6807
5	Oregon Health & Sci University	80000	847	2014
6	Louisiana State U Health Sci Ctr	78200	35	835
7	Duke University	76300	6480	9230
8	Mass Coll of Pharma & Health Sci	75700	3944	2908
9	SUNY Downstate Medical Ctr	75300	338	1521
10	Maine Maritime Academy	75200	1031	29
11	Roseman U of Health Sciences	74900	269	1135
12	West Coast U - Los Angeles	74600	1395	264
13	Calif State U Maritime Academy	73100	1047	NaN
14	Loma Linda University	72000	1039	3411
15	University of Pennsylvania	71600	10678	13258
16	Rose-Hulman Inst. of Technology	70700	2208	108
17	Kettering [GM] University	70700	1689	347
18	Babson College	70400	2107	942
19	Stanford University	70400	7018	9944
20	Harvard University	70300	7236	18453
21	U Maryland Baltimore	70000	786	5484
22	Carnegie Mellon University	69800	5819	6699
23	Colorado School of Mines	69200	4383	1506
24	Thomas Jefferson University	69000	705	2715
25	The U of Texas Medical Branch	68800	708	2503

Table 2. Highest-earners-producing colleges give high proportions of graduate degrees. Colors indicate the colleges' prime field of study. Blue = Health Professions; Red = Engineering or Transportation; Green = Business. Turquoise numbers denote the undergraduate population that is smaller than the graduate population.

Table 3 shows the statistical summary from the linear regression analysis. Earning is positively correlated with the graduate student population fraction. The regression line intercepts the MD_EARN_WNE_P6 axis on the left (i.e., Grad_population = 0) at $31,305/yr. We call that intercept E6_ugds_mean. At the high extreme (Grad_population = 100%), the regression line intercepts the MD_EARN_WNE_P6 axis at $49,998/yr. So the slope of the line is ($49,998/yr - $31,305/yr) / 1 = $18,693/yr. The above numbers are obtained from the straight regression line among widely scattered data points. The correlation goodness of fit is somewhat low (R = 0.33). However, Table 3 is the best linear estimate that correlates alumni earning (MD_EARN_WNE_P6) with the Grads population.

Regression variable	Interpretation	Value	Unit
y at ($x = 0$)	Average earning of Bachelor's	31305	$/year
y at ($x = 1$)	Average earning of Masters and above	49998	$/year
Diff. between above	Graduate Earning Advantage	18693	$/year
$y\,(x = 1)\,/\,y\,(x = 0)$	Graduate Boost Factor (GBF)	1.615	None
R	Goodness of fit	0.33	None

Table 3. Regression line shows that Earning is positively correlated with Graduate Population fraction.

The estimate means that, on average, colleges with 100% graduate students produce alumni with roughly $19,000 (61%) higher earnings than colleges with 100% undergraduate students. To normalize the impact of graduate degree proportion to the alumni earning analysis, we introduce a concept called *Graduate Boost Factor (GBF)* which is the ratio of a college alumni's earning if the college had 100% graduate students to the college's alumni earning if the college had 0% graduate students:

$$\text{GBF} = (\text{Bachelors\_Earning} + \text{Grad\_slope}) / \text{Bachelors\_Earning} \quad (3)$$

In this analysis, GBF = 1.615. (For example, if Thunderbird School of Global Management (Grad_population = 100%) had only undergraduate students (Grad_population = 0%), then its MD_EARN_WNE_P6 would be $87400/1.615 = $54158.)

Colleges that award a large proportion of graduate degrees report higher alumni earnings, which is misleading to undergraduate program applicants. This article is about choosing colleges that give Bachelor's degrees. Thus, "Bachelor-Equivalent earning" is more important in their decisions than the average earning MD_EARN_WNE_P6, which is reported in the IPEDS database. "Bachelor-Equivalent earnings" are not listed in the database. Thus, we need to estimate "Bachelor-Equivalent Earning" from MD_EARN_WNE_P6, using the following algebra.

Assume that earning MD_EARN_WNE_P6 is an average of Bachelors_Earning and "100% Graduate" earning (E6_GRADS), each weighted by the proportions of Bachelor population fraction and Graduate population fraction:

$$\text{MD\_EARN\_WNE\_P6} = \text{Bachelors\_Earning} * (1 - \text{Grad\_population}) + \text{Graduate\_Earning} * \text{Grad\_population} \quad (4)$$

Also, assume that Graduate earning is equal to Bachelor's earning times graduate boost factor GBF:

$$\text{Graduate\_Earning} = \text{Bachelors\_Earning} * \text{GBF} \quad (5)$$

From (4) and (5), we calculate the Bachelor's earning of each college by implementing:

$$\text{Bachelors\_Earning} = \text{MD\_EARN\_WNE\_P6} / (\text{GBF} * \text{Grad\_population} + 1 - \text{Grad\_population}) \quad (6)$$

Thus, we now have a method to estimate Bachelors' earnings from College Scorecard's MD_EARN_WNE_P6 and Grad population. After applying the above code lines, the list of the few very top colleges with the highest Bachelor's earnings is shown in Table 4 (Colors indicate the colleges' prime field of study, mentioned in the note in Table 2). After considering graduate degree earnings, the top highest-earners-producing colleges seem to be colleges specializing in Health professions (Rank numbers shown in blue), Engineering/Computer Science/Technology (Rank numbers shown in red), or Business. The few colleges specializing in Marine Transportation are lumped into the Engineering category because of the small number.

	College Name	BS Earn, $/yr	Median_P6 $/yr	Grad Population
1	Albany Coll of Pharmacy& HealthSci	94170	112100	31%
2	St. Louis College of Pharmacy	92499	120400	49%
3	Maine Maritime Academy	73957	75200	3%
4	Samuel Merritt University	71471	100100	65%
5	Rose-Hulman Institute of Technology	68730	70700	5%
6	West Coast University-Los Angeles	67954	74600	16%
7	United States Merchant Marine Academy	64295	65200	2%
8	Kettering University	63997	70700	17%
9	Massachusetts Maritime Academy	63776	66300	6%
10	MCPHS University	60040	75700	42%
11	Massachusetts Institute of Technology	59967	82200	60%
12	Colorado School of Mines	59802	69200	26%
13	Rensselaer Polytechnic Institute	59528	66100	18%
14	Babson College	59166	70400	31%
15	Milwaukee School of Engineering	58269	61000	8%
16	Resurrection University	58127	65300	20%
17	SUNY Maritime College	58038	61200	9%
18	Bentley University	57437	65800	24%
19	Bucknell University	57123	57700	2%
20	Chamberlain University-Illinois	56989	67100	29%
21	Lehigh University	56184	66200	29%
22	Bryant University	56177	57600	4%
23	Duke University	56059	76300	59%
24	Oregon Health & Science University	55842	80000	70%
25	Worcester Polytechnic Institute	55768	67500	34%
26	Claremont McKenna College	55306	55900	2%

27	University of the Sciences	54691	68400	41%
28	Oregon Institute of Technology	53881	54400	2%
29	Cornell University	53530	64800	34%
30	University of Pennsylvania	53417	71600	55%
31	Georgia Inst Tech - Main Campus	53210	65500	38%
32	Carnegie Mellon University	52525	69800	54%

Table 4. Health professions (Blue) and Engineering/Computer Science/Technology (Red) give highest earnings.

THE MAJOR IS MORE IMPORTANT THAN THE COLLEGE NAME

Even after adjusting for graduate degree earnings, the top highest-earners-producing colleges seem to be colleges with high proportions of students in Health professions, Engineering (including Computer Science and Information Technology), Transportation of Materials, and Business. To test this conjecture, the author uses Data Visualization with Python Seaborn library. Figure 2 shows colleges with the top 25% (about 350) highest Bachelors' earnings (descending order from top to bottom). On the horizontal axis are 31 Fields of Study in the IPEDS database. Figure 2 suggests that the highest-earners-producing colleges give many of their degrees in just a few fields of study below:

1. Health professions (e.g., nursing, dental assistance, medical technicians). Note that the earnings considered here are Bachelor's earnings, thus excluding MD and Ph.D. earnings. Still, these top colleges produce alumni with very high earnings.
2. Engineering, which includes Computer Science and Information Technology since many Computer Science departments are part of a college of Engineering.
3. Business
4. Social Science
5. Transportation of Materials. Only a handful of colleges have this field of study as their largest. But most of those colleges produce alumni with remarkably high earnings.

The brightness of the rectangular symbols denotes the percentage of students at the college who are in the field of study. White/yellow is the brightest color, denoting that nearly 100% of the students at the college are in one major. Orange denotes a lower proportion than yellow, but still very high (around 80%). Red is a little less bright (meaning a little lower) than orange. Purple is lower than red, followed by dark purple, blue, etc. Black means near-zero.

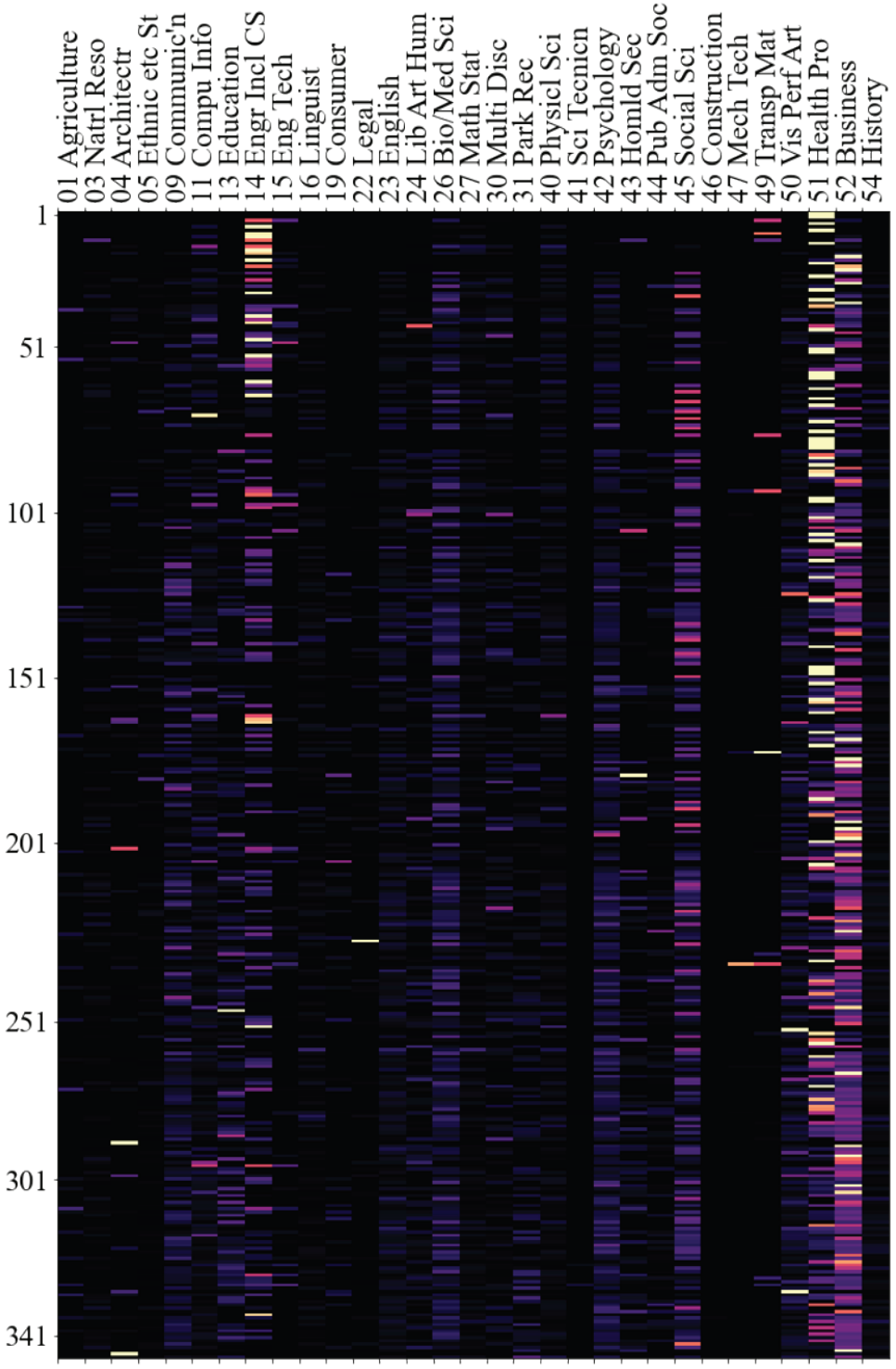

Figure 2. Highest-Earners-Producing colleges give degrees in a few fields of study in common.

Some fields of study are most common in the highest-earners-producing colleges because they are the most popular fields for all other schools too. According to the National Center for Education Statistics (*Most Popular Majors,* 2020), "Of the 1,956,000 Bachelor's degrees conferred in 2016–17, the greatest numbers of degrees were conferred in the fields of business (381,000), health professions and related programs (238,000), social sciences and history (159,000), psychology (117,000), biological and biomedical sciences (117,000), engineering (116,000), communication, journalism, and related programs (94,000), and visual and performing arts (91,000)". Among the 400 highest-earners-producing colleges, Business appears in most places, especially in ranks between 100 and 300. However, the most dominant fields in the top 100 appear to be Health Professions and Engineering. Note that *Most Popular Majors* (2020) actually discusses fields of study. Majors, as will be discussed later, are finer categories than fields of study.

To examine the above conjecture closer, Figure 3 shows the top 80 highest-earners-producing colleges, with only nine of the fields of study that these colleges teach. Lighter colors denote higher proportions of degrees awarded in the field of study. The colleges are shown from top to bottom in descending order of Bachelors' earnings. Figure 3 reveals that Biological/Biomedical Sciences is also a common field of study at highest-earners-producing colleges.

Figure 3. Top-80 Highest-Earners-Producing colleges teach mainly 1)Medical Profession; 2)Engineering including Computer Science/Technology; 3)Business; 4) Social Science; 5)Maritime Transportation; 6. Biological/Biomedical Sciences, and 7) Computer technology (IT, Cyber).

Going back to the top quartile (roughly 400) colleges in terms of earnings, Fig. 2 suggests that:

1. Health professions are the most widely taught, from the very top highest-earners-producing colleges all the way through rank 400 (and probably beyond).
2. Engineering is taught mainly at the very top 80 highest-earners-producing colleges, getting less common from there down.
3. Business and social science are widely taught everywhere throughout the 400 colleges.

Among the top-quartile-earnings colleges, Figure 4 shows that the very few top earners are colleges that have 100% of their students in Health Professions. In general, colleges with a high proportion of Health Professions students produce high Bachelor's earnings. Also among the top-quartile-earnings colleges, Figure 5 shows that colleges with a high proportion of Engineering students produce high Bachelor's earnings. Appendix E shows that proportion of Business students does not affect alumni earning significantly.

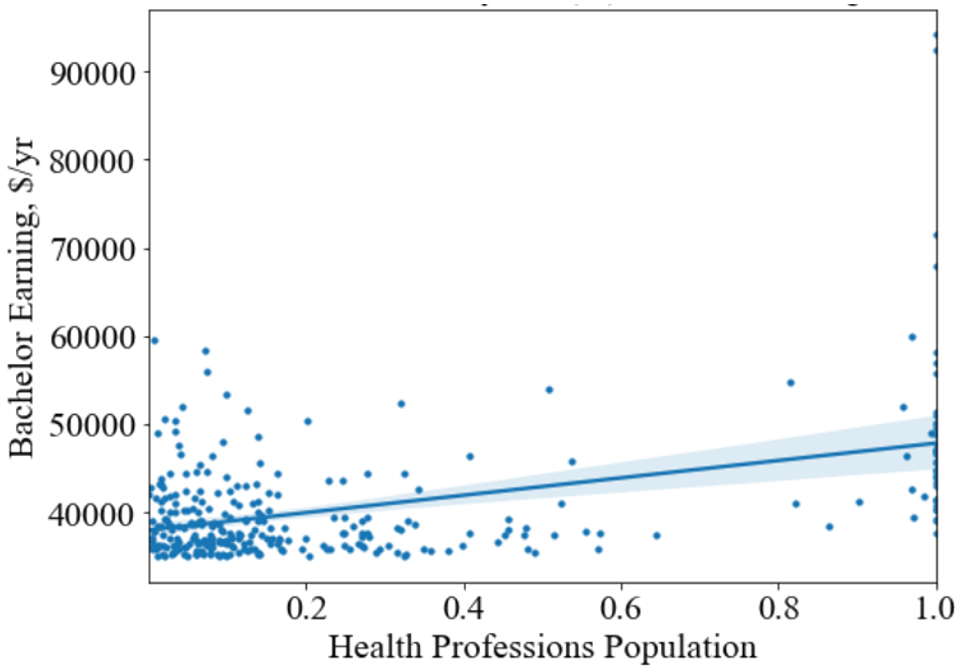

Figure 4. In general, colleges with a high proportion of Health Professions students produce high Bachelor's earnings. In particular, colleges that produce top earners have 100% of their students in Health Professions.

The hypothesis from Figure 5 is: The field of study is what makes college graduate alumni with high earnings. To investigate this hypothesis, the author refers to a report from Georgetown University (Carnevale et al, 2015), henceforth called "The Georgetown Report". Among other conclusions, the Georgetown Report says that a Bachelor's degree results in lifetime earnings of $1 million higher than a high school diploma. However, a Bachelor's degree in a high-paying major results in lifetime earnings of $3.4 million higher than a Bachelor's degree in a low-paying major. Thus, the popular question "How do we choose a college?" is far less

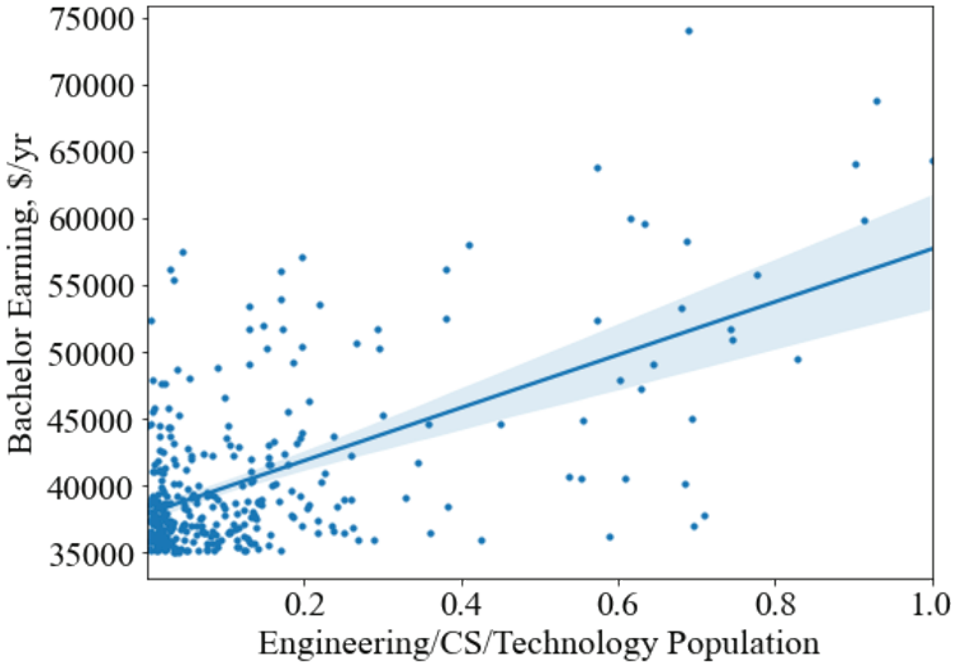

Figure 5. Colleges with a high proportion of Engineering/Computer Science students generally produce high Bachelors' earnings.

important than the better question: "How do we choose a college major?" Torpey (2003) can help answer the latter question, and the analysis below will answer both.

The Georgetown Report analyzes hundreds of college majors, which have an advantage over the College Scorecard for choosing a college major. The College Scorecard databases have only 38 fields of study because they "are easier for prospective students to understand and because combining six-digit CIP codes together leads to larger cell sizes, which in turn leads to fewer data points that need to be privacy-suppressed" (*College Scorecard Data by Field of Study*, 2020). In gathering and reporting information, the National Center for Education Statistics has used most of the Fields of Study since 1970 or earlier (*Digest of Education Statistics (Fields of Study)*, 2019). Some of those 38 fields have all but disappeared or evolved far beyond their names. For example, in 1970-1971, Library Studies had 1013 new college graduates. In 2017-2018, it had 81, while Business had 386,201 new college graduates. (Health Professions had 244,909. Engineering, 121,956.) Other Fields of Study are also so small that they should be merged. In 2017-2018, Communication Studies had 4231 new graduates; Legal Professions and Studies, 4239; Military Technologies and Applied Sciences, 655; Precision Production, 45; and Transportation and Materials Moving, 4924. Therefore, today the *college major* is more relevant than the field of study discussed above. US colleges award degrees in hundreds of college majors; College majors have much finer granularity than the 38 Fields of Study. Most importantly, every college applicant needs to plan for, or often decide, which major—not field of study—she or he will pursue a degree in. The Georgetown report shows average earnings by major in Table 5 below. Outside Pharmacy, the highest paying majors are in Engineering (including Computer Science/Technology). Other Health Professions majors besides Pharmacy also result in high earnings (Carnevale et al., 2015).

2014-2015 Ranking	Median, $/yr	25%ile, $/yr	75%ile, $/yr
Petroleum Engineering	120000	82000	189000
Pharmacy/Pharm Sci/Pharm Admin	105000	83000	120000
Math and Computer Science	98000	75000	134000
Aerospace Engineering	87000	60000	115000
Chemical Engineering	86000	60000	120000
Electrical Engineering	85000	60000	110000
Naval Architecture and Marine Eng	82000	44000	120000
Mechanical Engineering	80000	59000	105000
Metallurgical Engineering	80000	50000	106000
Mining and Mineral Engineering	80000	52000	125000

Table 5. Outside of Pharmacy, the top ten highest-paying majors are all in Engineering (including Computer Science and IT)(Carnevale et al., 2015).

College major is more important than the college name. Legendary elite colleges charge high tuition regardless of major or alumni earning. To get a good return on investment, a college applicant should first know (or at least make an educated guess of) which major he or she should pursue. Only then should he or she choose the colleges to apply to. To choose colleges to study the predetermined major, tuition must be considered very seriously. As exemplified in Figure 1, colleges with the highest tuition do not necessarily produce alumni with the highest earnings. The converse is also true. Table 6 shows a handful of rather extreme examples to drive the above point home. At the Bachelor's level, many other colleges produce alumni with equal or higher earnings than legendary elite colleges. (However, at the graduate school level, the elite colleges do produce alumni with very high earnings. See Appendix K for examples.)

College Name	Tuition, $/yr	Major	BA/BS Start Earning $/yr
Columbia U	61850	Architecture	47900
U Penn	57770	Psychology	52900
Yale U	55500	Sociology	47900
Texas A&M U[1)]	11232	Petroleum Engineering	111000
New Mexico Tech[2)]	8156	Computer & Info Sci	73300

Table 6. The major determines earning far more than the tuition – a few examples.
[1)] Out-of-state $37,726/yr; [2)] Out-of-state $23,524/yr; All values are from 2019.

As discussed above, the handful of colleges that produce top earners are colleges that have almost 100% of their students in Health Professions. Financially, it would be wise to choose a major in Health Professions even at the undergraduate level for students. If they do so, Table 7 gives them an idea of which "Bachelor's colleges" to apply to. Engineering is another top-earning profession, including Computer Science. In further analysis in this paper, Computer Information, Engineering Technology, and Transportation are lumped into Engineering. If a student is interested in Engineering, Table 8 gives an idea of the colleges that

produce the highest Bachelor's earners. A little caveat: a few colleges in that table have fewer than 20% of their students in Engineering. Therefore, the high earners they produce might not be their engineers but other professionals including health professionals.

Rank	College Name	BS Earn, $/yr	MD_EARN _WNE_P6, $/yr	HealthPro Fraction %
1	Albany College of Pharmacy and Health Sciences	94170	112100	100
2	St. Louis College of Pharmacy	92499	120400	100
3	Samuel Merritt University	71471	100100	100
4	West Coast University-Los Angeles	67954	74600	100
5	MCPHS University	60040	75700	97
6	Resurrection University	58127	65300	100
7	Chamberlain University-Illinois	56989	67100	100
8	Oregon Health & Science University	55841	80000	100
9	University of the Sciences	54691	68400	81
10	Oregon Institute of Technology	53881	54400	51
11	Excelsior College	52299	54700	32
12	AdventHealth University	52071	54300	96
13	Bellin College	51455	55600	100
14	Mount Carmel College of Nursing	50959	55500	100
15	SUNY Downstate Medical Center	50105	75300	100
16	Roseman University of Health Sciences	50039	74900	100
17	Research College of Nursing	49564	59400	100
18	Louisiana State Uni Health Sci Center-Shreveport	49187	78200	100
19	Loma Linda University	48944	72000	99
20	Barnes-Jewish College Goldfarb School of Nursing	48746	53900	100
21	Texas Tech University Health Sciences Center	47704	68300	100
22	American University of Health Sciences	47275	48100	100
23	Saint Anthony College of Nursing	47037	54100	100
24	Saint Luke's College of Health Sciences	47031	52200	100
25	Blessing Rieman Coll of Nursing & Health Sci	46838	49000	100
26	The University of Texas Medical Branch	46516	68800	100
27	Mount Saint Mary's University	46471	51900	41
28	Thomas Jefferson University	46374	69000	96
29	Kettering College	45853	48800	100
30	Molloy College	45768	53100	54
31	University of Maryland Baltimore	45527	70000	100
32	MGH Institute of Health Professions	44887	67900	100

Table 7. Bachelor's degree highest-earner producing colleges in Health Professions. "BS" denotes all types of Bachelor's degrees. Earnings are the college's alumni earning six years after enrollment. "BS Earning" is estimated using Equation (6). Average Earning is from the College Scorecard database. Health Pro Fraction denotes how many percent of the college's students are in Health Professional majors.

Rank	College Name	BS Earn, $/yr	MD_EARN _WNE_P6, $/yr	Eng or CS Fraction %
1	Maine Maritime Academy	73956	75200	69
2	Rose-Hulman Institute of Technology	68730	70700	93
3	United States Merchant Marine Academy	64295	65200	100
4	Kettering University	63996	70700	90
5	Massachusetts Maritime Academy	63776	66300	57
6	Massachusetts Institute of Technology	59966	82200	62
7	Colorado School of Mines	59801	69200	91
8	Rensselaer Polytechnic Institute	59527	66100	63
9	Milwaukee School of Engineering	58268	61000	69
10	SUNY Maritime College	58037	61200	41
11	Bucknell University	57122	57700	20
12	Lehigh University	56183	66200	38
13	Duke University	56058	76300	17
14	Worcester Polytechnic Institute	55767	67500	78
15	Oregon Institute of Technology	53881	54400	17
16	Cornell University	53530	64800	22
17	Georgia Inst of Tech - Main Campus	53210	65500	68
18	Carnegie Mellon University	52525	69800	38
19	Clarkson University	52339	57700	57
20	University of Notre Dame	51994	61800	15
21	Stanford University	51753	70400	29
22	Stevens Institute of Technology	51693	68600	74
23	Wentworth Institute of Technology	51691	53300	17
24	Missouri University of Science and Technology	50928	58700	75
25	Cal Poly University-San Luis Obispo	50645	52100	27
26	Princeton University	50316	60800	20
27	Manhattan College	50313	54200	29
28	University of Portland	50279	53800	15
29	South Dakota School of Mines and Technology	49467	53200	83
30	Santa Clara University	49209	61100	19
31	Michigan Technological University	49014	55200	65
32	DigiPen Institute of Technology	47912	50400	60

Table 8. Bachelor's degree highest-earners-producing colleges in Engineering/Computer Science. "BS" denotes all types of Bachelor's degrees. Earnings are the college's alumni earning six years after enrollment. "BS Earning" is estimated using Equation (6). Average Earning is from the College Scorecard database. Eng or CS Fraction denotes how many percent of the college's students are in Engineering/Computer Science majors.

HIGH-EARNERS-PRODUCING COLLEGES TEND TO CHARGE HIGH TUITION

Besides earnings, tuition is an important consideration in choosing colleges to apply to, since college tuitions today are almost the same magnitude as whole full-time salaries. Figure 6 shows the distribution of tuition based on IPEDS Scorecard data (Appendix F) after adjusting for undergraduate programs using Eq. (6). Linear regression analysis estimates a "Gradu-

ate Tuition Factor" (GTF) of 2.1. The coefficient of correlation R = 0.32. After that adjustment, Bachelor's tuitions are shown as distributions in Figure 6 based on whether the colleges are public, private nonprofit, or private for-profit. The horizontal axis is the bins (tuition ranges from $0 to $999, $1,000 to $1,999, $2,000 to $2,999, etc). The vertical axis is the number of colleges corresponding to each bin. Figure 6 shows that, generally, public colleges charge far lower tuition than private colleges. Private for-profit colleges do not seem to charge more than private nonprofit colleges. In fact, the most expensive colleges for Bachelor's degrees are private nonprofit. The following may help in reading the overlapping distributions in Figure 6: Public tails off around $20,000/yr; Private Nonprofit tails off at over $40,000/yr.

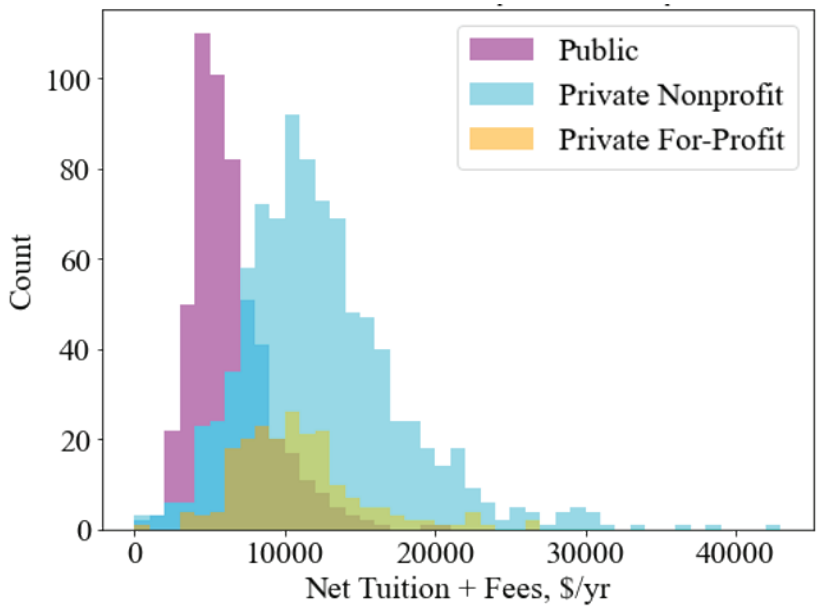

Figure 6. Distribution of Undergraduate Tuition. Generally, public colleges charge far less than private colleges.

The tuitions (including fees) listed in the Scorecard database are average values. The variable TUITFTE in the College Scorecard database is an average tuition that does not apply to most students. Each college applicant's situation determines the real tuition they will have to pay. Attending a public college within their state will likely cost far less (in tuition alone) than attending a private college or an out-of-state public college. Most colleges give financial aid to students from low-income families, some even to families with income over $100,000/year. Students from higher-income families may have to pay far more in tuition than average. A very expensive Ivy League college may offer the best deal to a highly qualified student from a low-income family with the potential for merit-based scholarships. Tuition is the most widely varying, complicated, and least certain variable in the analyses in this paper. Although very important, the discussion on tuition in this paper is at the "macro-economic" level and not for choosing a college to attend.

Figure 7 shows that more expensive colleges tend to produce alumni with higher earning on average. Zero tuition corresponds to an earning of $ 25,677/yr. Every $1,000 increment of tuition corresponds to roughly $540 increment in earnings. The linear fit has considerable scatter (R = 0.36). Tuitions of the very top high-earners-producing colleges vary

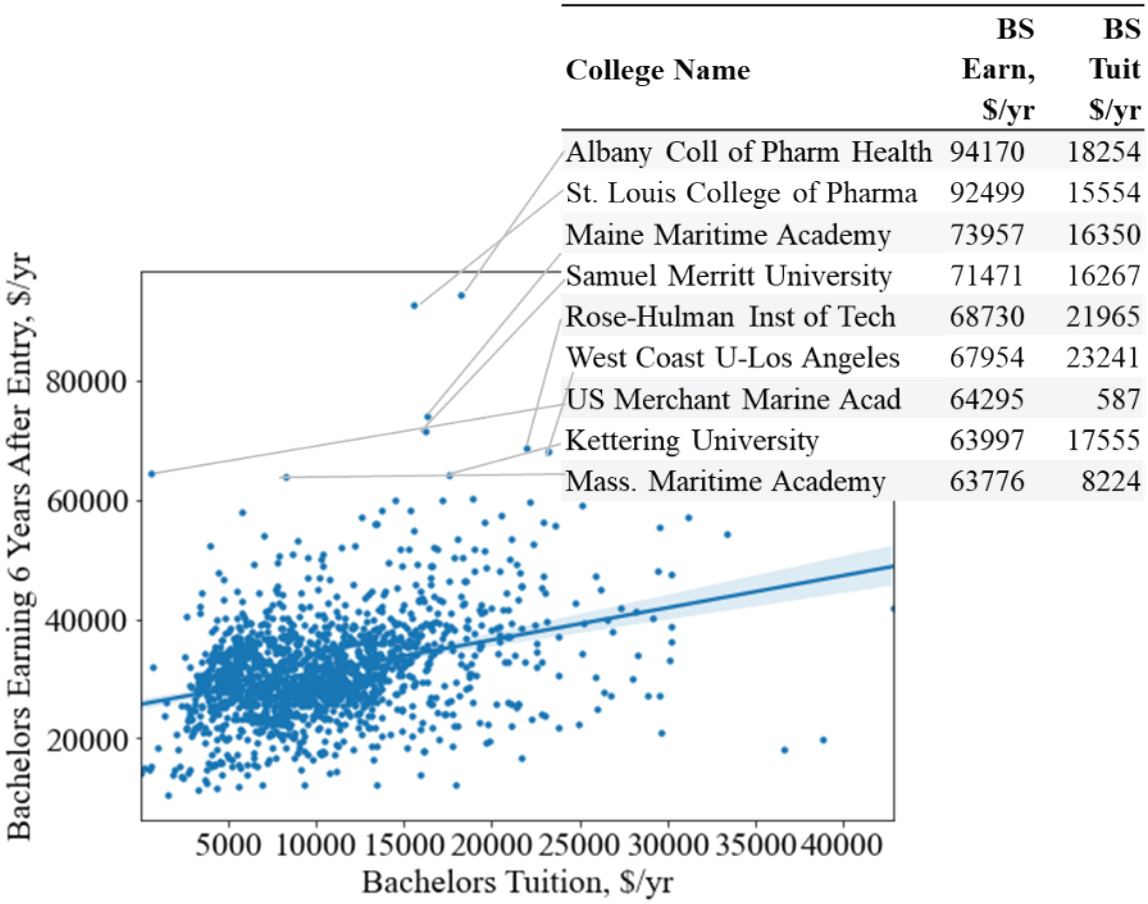

College Name	BS Earn, $/yr	BS Tuit $/yr
Albany Coll of Pharm Health	94170	18254
St. Louis College of Pharma	92499	15554
Maine Maritime Academy	73957	16350
Samuel Merritt University	71471	16267
Rose-Hulman Inst of Tech	68730	21965
West Coast U-Los Angeles	67954	23241
US Merchant Marine Acad	64295	587
Kettering University	63997	17555
Mass. Maritime Academy	63776	8224

Figure 7. Bachelor's earning versus Bachelors' tuition: High-earners-producing colleges tend to charge high tuition in general. However, the very top highest-earners-producing colleges, listed in the inset, do not charge very high tuition.

widely. However, they tend to be not the highest. Caveat: the most expensive colleges are not the highest earners producers. In fact, the three rightmost dots in Fig. 7 pertain to the lowest-earners producing colleges in Table 1. Another caveat: Although private for-profit colleges generally charge more than public colleges, they produce alumni with lower earnings than public or private non-profit colleges (Fig. 8).

ALUMNI OF HIGHEST-EARNERS-PRODUCING-COLLEGES DO NOT TAKE HIGH STUDENT LOANS IN GENERAL

Most college students have student loan debt, with no college in the US reporting zero student debt. In the College Scorecard database, the variable GRAD_DEBT_MDN is the median student loan debt accumulated at the college by all student borrowers of federal loans who graduate in a given fiscal year, measured at graduation. Figure 9 shows the distribution of colleges' median student debts in 2018 for 1977 four-year colleges in the US. (We use 2018 debt data because they were College Scorecard's latest at the time this analysis was done.) The horizontal axis is the bins or debt ranges. The vertical axis is the number of colleges corresponding to each debt range. Only Bachelors' debts are included, and private debts are

excluded as the US Department of Education collects data on federal debts only. No debts are in the names of the parents of the undergraduates.

Our data show that students at private for-profit colleges are the highest debtors. At two such colleges, the median debt at graduation in 2018 was $47,000. So 50% of their graduating students owed more than that. Ninety-two and 88 percent of undergraduates at those two colleges took federal loans. The College Scorecard database does not yet have their alumni earning information. Because 1453 colleges (outside of 1977 in this analysis) did not report

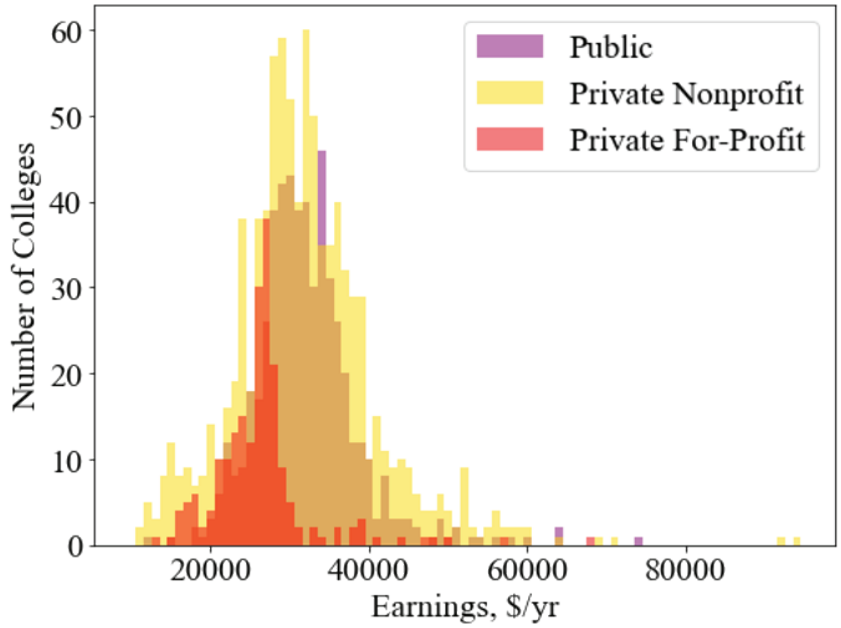

Figure 8. Distribution of Bachelor's earnings: Private for-profit colleges tend to produce alumni with low earnings.

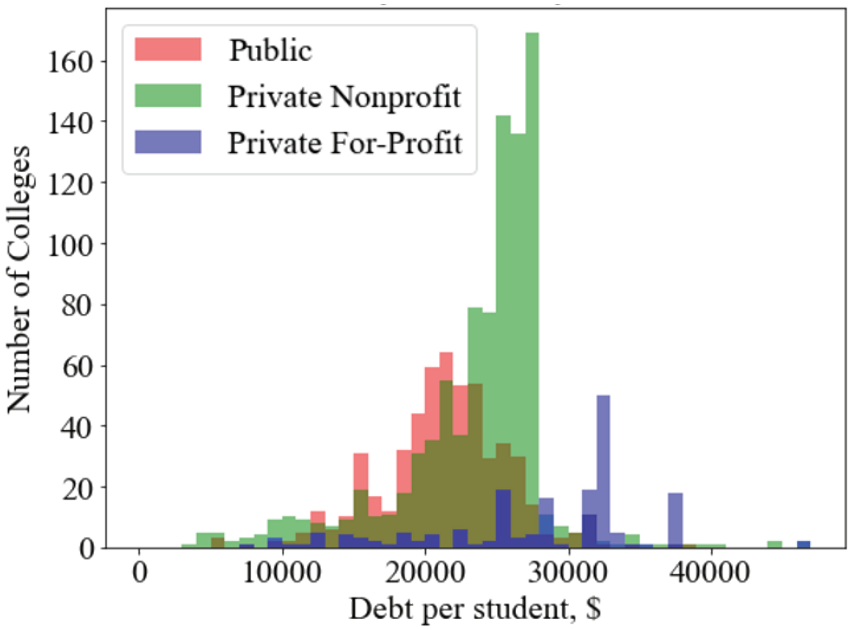

Figure 9. Distribution of Alumni Debt. Generally, alumni of public colleges accumulate less debt than alumni of private colleges.

GRAD_DEBT_MDN, it is quite likely that many colleges produced higher median debts than $47,000.

Figure 10 shows that there is no correlation between debt and earning. The data are from years 2014-2015, the latest year that earning data are available. The slope of the line is -0.07; and the correlation coefficient is -0.002. Therefore, the plot is pure random scatter for all practical purposes. The complete absence of correlation between debt and earning means that colleges whose students have a lot of debt do not produce alumni with high earnings. Alumni of these colleges often take on large debts without gaining the resources to pay them off in the future. Before enrolling or applying to a college, students should consider the average student debt at that college.

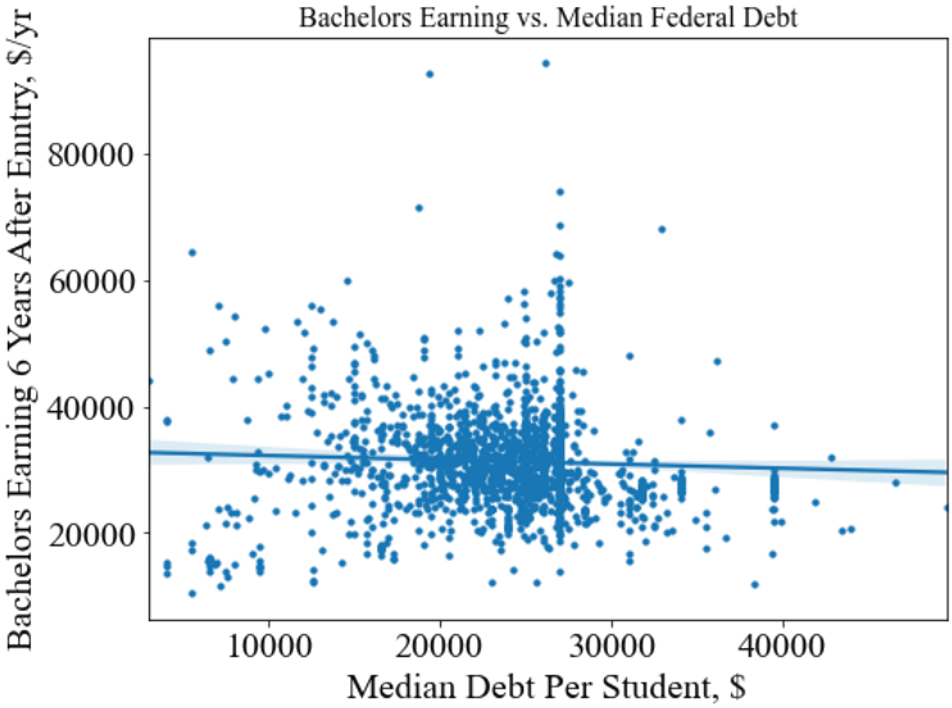

Figure 10. Bachelor's earning versus alumni debt: Alumni of colleges with higher debt do not earn a higher salary.

HIGHEST-EARNERS-PRODUCING COLLEGES REQUIRE HIGH SAT SCORES BUT HAVE REASONABLE ADMISSION RATES

Analyses above revealed that highest-earners-producing colleges are not always the most expensive. We will now analyze if they are the most selective. Table 9 suggests that many highest-earners-producing colleges have reasonable admission rates and SAT scores. Regression analysis shown in Figure 11 shows that Bachelor's earning is correlated with combined SAT scores. At the low extreme, a 75th percentile SAT score of 800 corresponds to a Bachelor's earning of $21,949/yr. Every 100-point increase in the SAT score corresponds to an earnings increase of $2,872/yr. At the high extreme, a 75th percentile SAT score of 1600 (perfect score) corresponds to an earning of $45,723/yr. The top 10 highest-earners-producing colleges have 75th percentile combined SAT scores between 1130 and 1400. Among all reported SAT scores, the median is 1150, and 1246 is the upper quartile. In conjunction with SAT scores, Appen-

dix J shows that most high-earners-producing colleges do not have low admission rates. The admission rates to the 10 highest-earners-producing colleges are between 25% and 89%, mostly above 58%. These admission rates are far more generous than the admission rates to legendary colleges like the Ivy League colleges, or Massachusetts Institute of Technology where the admission rate is 8%. (Its 75th percentile SAT is 1570.)

Rank	College Name	BS Earn, $/yr	BS Tuit $/yr	SAT 75%ile	Admit Rate %
1	Albany College of Pharmacy and Health Sci	94170	18254	1260	67
2	St. Louis College of Pharmacy	92499	15554	1330	
3	Maine Maritime Academy	73957	16350	1130	79
4	Samuel Merritt University	71471	16267		
5	Rose-Hulman Institute of Technology	68730	21965	1400	59
6	West Coast University-Los Angeles	67954	23241		25
7	United States Merchant Marine Academy	64295	587		
8	Kettering University	63997	17555	1310	72
9	Massachusetts Maritime Academy	63776	8224	1190	62
10	MCPHS University	60040	18952	1190	84
11	Massachusetts Institute of Technology	59967	17152	1570	8
12	Colorado School of Mines	59802	14513	1400	36
13	Rensselaer Polytechnic Institute	59528	22181	1490	38
14	Babson College	59166	25090	1370	26
15	Milwaukee School of Engineering	58269	13768	1260	69
16	Resurrection University	58127	15362		
17	SUNY Maritime College	58038	5810	1190	53
18	Bentley University	57437	20489	1330	46
19	Bucknell University	57123	31201	1400	31
20	Chamberlain University-Illinois	56989	12589		66
21	Lehigh University	56184	19598	1410	34
22	Bryant University	56177	22952		75
23	Duke University	56059	13488	1550	11
24	Oregon Health & Science University	55842	13304		
25	Worcester Polytechnic Institute	55768	23627		44
26	Claremont McKenna College	55306	29500	1520	11
27	University of the Sciences	54691	15543	1260	58
28	Thunderbird School of Global Management	54158	33374		
29	Oregon Institute of Technology	53881	7051	1150	60
30	Cornell University	53530	18007	1510	14
31	University of Pennsylvania	53417	21153	1550	10
32	Georgia Institute of Tech - Main Campus	53210	8973	1490	33
33	Carnegie Mellon University	52525	22402	1540	25

Table 9. Bachelor's highest-earners-producing colleges require high SAT scores, but are not necessarily very hard to get into. "BS" denotes all types of Bachelor's degrees. Earnings are the college's alumni earning six years after enrollment. "BS Earning" is estimated using Equation (6). SAT 75%ile is the 75th percentile SAT total score. All data are from the College Scorecard database.

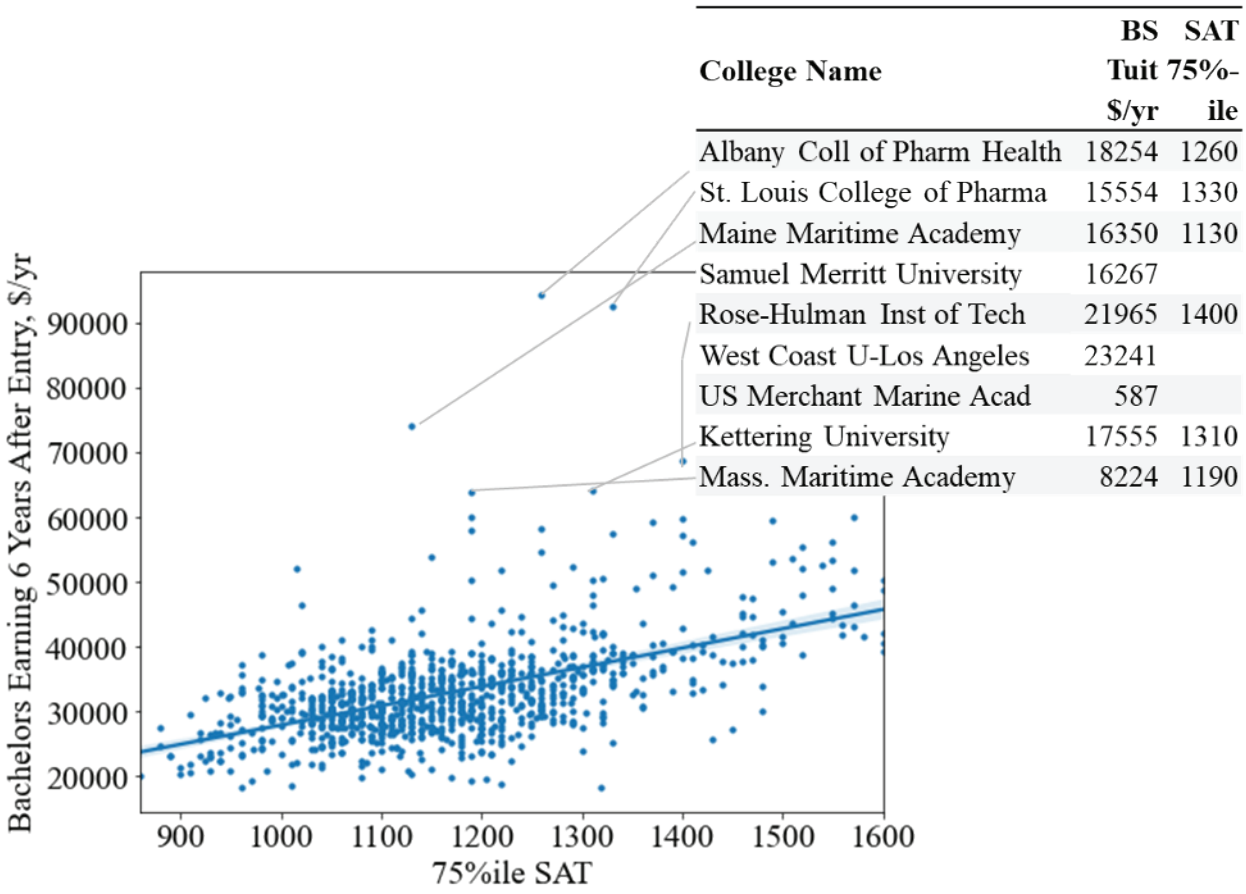

College Name	BS Tuit $/yr	SAT 75%-ile
Albany Coll of Pharm Health	18254	1260
St. Louis College of Pharma	15554	1330
Maine Maritime Academy	16350	1130
Samuel Merritt University	16267	
Rose-Hulman Inst of Tech	21965	1400
West Coast U-Los Angeles	23241	
US Merchant Marine Acad	587	
Kettering University	17555	1310
Mass. Maritime Academy	8224	1190

Figure 11. Bachelor's earning plotted against 75th percentile SAT score. High-earners-producing colleges tend to require high SAT scores.

As the last step of this study, the author has created a list of the top-quartile (25% = about 400) highest-earners-producing colleges for Bachelor's degrees, with their 1) Median Bachelor's earning at six years after enrollment; 2) Field of Study with most students; 3) Total SAT Score at 75th percentile; 4) Admission Rate; 5) Bachelor's Tuition (including fees); and 6) Median Debt. A college applicant can narrow down the list further by specifying his/her choice of major. The *List of Colleges with Highest Bachelor Alumni Earnings* (2020) will be maintained on the College Analytica website. Appendices G, H, I, and J show more information admission competitiveness and student debts. Appendix J lists the colleges with the highest bachelor's earnings. Figure 12 illustrates the earnings versus tuition confirming the conclusion from early in this paper: The very top high-earners-producing colleges have large proportions of their students in Health Professions or Engineering. Many high-earners-producing colleges are big on business, which is the most popular major, with more alumni per year than Health Professions and Engineering combined.

The IPEDS database used in this analysis is from the years 2014-2015 because those are the years for which earning data are available. For relative comparisons among colleges, the earning data are very useful. However, the absolute values are old and need to be updated. For the latest earning information, refer to US News and World Report's College Compass (premium/paid subscription). From that website, the part that gives median starting salaries

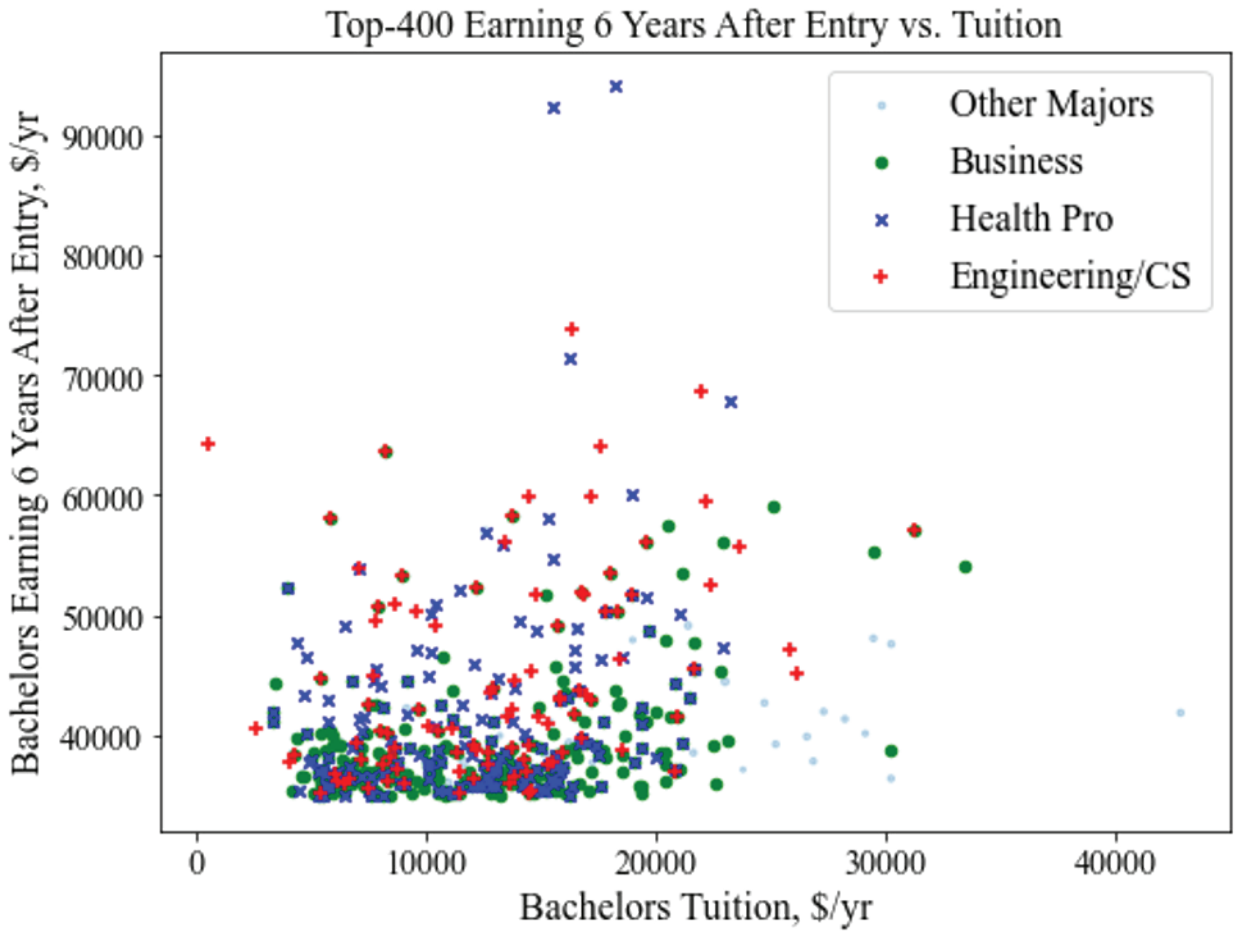

Figure 12. Bachelor's earning plotted against tuition, for the top quartile (25% = 400) high-earners-producing colleges. Green o symbol means Business > 10%; Blue x means Health Profession > 10%; Red + means Engineering/Computer Science > 10% of undergrad population at the college.

by major does not say whether the starting salaries are those of Bachelors or graduate degree holders. Therefore, the starting salary information may have to be adjusted to account for the proportion of graduate students at each college. Use Eq. (6) to estimate Bachelors' earnings. As this research shows, colleges with high graduate student population proportions produce alumni with higher earnings than Bachelor's earning. Also, College Compass earning data are based on self-reported survey entries, unlike the IPEDS data that are based on tax returns and information required by student loan providers.

CONCLUSIONS

Data science and the US Department's College Scorecard database enable students to choose colleges based on college alumni's earnings. The most expensive or famous colleges do not necessarily produce alumni with the highest earnings. The highest-earners-producing colleges produce alumni who get the highest salaries, to a large extent because those colleges give a large proportion of their degrees in graduate or professional degrees (MD, JD/Law, Ph.D., MS, etc.). Therefore, the earnings reported by each college are skewed rather heavily by the college's graduate population fraction. Colleges that award a large proportion of graduate

degrees report higher alumni earnings, which are misleading to applicants to undergraduate programs. To correct for the graduate degree effect, we introduced the concept of "Graduate Boost Factor" (GBF) which enables us to estimate the earnings of each college's Bachelor's alumni based on the percentage of graduate students at that college.

Even after accounting for GBF, highest-earners-producing colleges give many degrees in just a few fields of study (as defined by the US Department of Education):

1. Health professions (e.g., nursing, dental assistance, medical technicians). Note that the earnings considered here are Bachelor's earnings, thus excluding MD and Ph.D. earnings. Still, these top colleges produce alumni with very high earnings.
2. Engineering, including Computer Science and technology
3. Business
4. Maritime Transportation. (These include only a handful of colleges. But their earnings are remarkably high).

College majors are a finer granularity than the fields of study. A college major is more important than the college name. Notable elite colleges charge high tuition regardless of major or alumni earning.

To choose colleges to study the predetermined major, tuition must be considered very seriously. Public colleges charge significantly less tuition than private colleges. High-earners-producing colleges tend to charge higher tuition than other colleges. Colleges with the highest tuition do not necessarily produce alumni with the highest earnings. Colleges with the lowest tuition do not necessarily produce alumni with low earnings.

High-earners-producing colleges tend to require higher SAT scores. However, admission rates to most of those colleges seem to be reasonable. The few colleges with low admission rates (the most extreme is 1 in 19 applicants) that are high-earners-producing colleges are top-tier elite colleges. However, at the Bachelor's level, many other colleges produce alumni with equal or higher earnings than those elite colleges. At the graduate school level, the elite colleges do produce alumni with very high earnings (Appendix K).

All colleges report significant amounts of student loan debt. Bachelor's alumni with larger college debts do not earn more than those with smaller debts. Private for-profit colleges incur huge student loan debts and produce alumni with lower earnings in general. College loan debts are so large that they are one of the top economic problems in the U.S.

The US Department of Education's College Scorecard database is very useful in revealing important information for choosing colleges to apply to and to attend. Ten years ago, there was no simple way to perform college cost-benefit analysis and reach the above conclusions. Python data science library Pandas and visualization library Seaborn (which uses and supplements Matplotlib) facilitated the analysis tremendously. Future work will incorporate machine learning to help students choose a major and the colleges that will give them the best financial value.

AUTHOR INFORMATION

Corresponding Author

*Mario Sumali, swimsuper12@gmail.com

ACKNOWLEDGMENTS

The author is grateful for the guidance of Ms. Yolanda Lozano, Computer Science teacher at La Cueva High School. The author also thanks Mr. Duncan Lee of MIT and Dr. Ronghua Wang of Intel for their valuable reviews and guidance.

REFERENCES

Carnevale, A.P.; Cheah, B.; Hanson, A. *Economic Value of College Majors*. Georgetown University Center for Education and The Workforce: Washington, DC, 2015; https://repository.library.georgetown.edu/bitstream/handle/10822/1050288/The-Economic-Value-of-College-Majors-Full-Report-web-FINAL.pdf?sequence=1&isAllowed=y

College Scorecard Data by Field of Study; Technical Documentation; United States Department of Education. Washington, DC, 2021; https://collegescorecard.ed.gov/assets/FieldOfStudyDataDocumentation.pdf

Digest of Education Statistics (Fields of Study); National Center for Education Statistics (NCES), 2019; https://nces.ed.gov/programs/digest/d19/tables/dt19_322.10.asp

Friedman, Z. *Student Loan Debt Statistics In 2020: A Record $1.6 Trillion*; Forbes, Feb. 3, 2020; https://www.forbes.com/sites/zackfriedman/2020/02/03/student-loan-debt-statistics/#d38db5e281fe

List Of Colleges With Highest Bachelor Alumni Earnings; College Analytica website; collegeanalytica.com.

Most Popular Majors; Fast Facts; National Center for Education Statistics (NCES), 2020; https://nces.ed.gov/fastfacts/display.asp?id=37

Seeger, J. *A Starter Guide to College for Clueless Students & Parents: For a State College or the Ivy League, Here's What You Need to Know*; Starter Guides LLC, 2018; ISBN 0999586025, 344p.

Torpey, E.M. *The Class of 1993: Earnings and occupations by college majors, 1 and 10 years after graduation*; Occupational Outlook Quarterly, Summer 2008; https://www.bls.gov/careeroutlook/2008/summer/art02.pdf

US News And World Report College Compass Premium Subscription; https://premium.usnews.com/best-colleges

APPENDIX A: LIST OF VARIABLES

From IPEDS full documentation, the author used the following variables in the analysis:

1. INSTNM: The institution's name, as reported in IPEDS.
2. TUITFTE: The net tuition revenue per full-time equivalent (FTE) student uses tuition revenue minus discounts and allowances, and divides that by the number of FTE undergraduate and graduate students.
3. MD_EARN_WNE_P6: 6_yrs_after_entry.median [working_not_enrolled.]
4. MD_EARN_WNE_P10: 10_yrs_after_entry.median [working_not_enrolled.]
5. PCT75_EARN_WNE_P6: The variable in the IPEDS database is called 6_yrs_after_entry.working_not_enrolled.earnings_percentile.75
6. PCT25_EARN_WNE_P6: 6_yrs_after_entry.working_not_enrolled.earnings_ percentile.25
7. PCT75_EARN_WNE_P10: 10_yrs_after_entry.working_not_enrolled.earnings_ percentile.75
8. PCT25_EARN_WNE_P10: 10_yrs_after_entry.working_not_enrolled.earnings_ percentile.25
9. UGDS: Number of degree/certificate-seeking undergraduates enrolled in the fall, as reported in the IPEDS Fall Enrollment component.
10. GRADS: Number of graduate students.
11. CONTROL: Governance structure: public, private nonprofit, or private for-profit.
12. PCIP01: Percentage of degrees awarded in Agriculture, Agriculture Operations, And Related Sciences. (program_percentage.agriculture in IPEDS database)
13. PCIP03: Percentage in Natural Resources And Conservation
14. PCIP04: Percentage in Architecture And Related Services
15. PCIP05: Percentage Area, Ethnic, Cultural, Gender, and Group Studies
16. PCIP09: Percentage Communication, Journalism, and Related Programs
17. PCIP10: Communications Technologies/Technicians and Support Services
18. PCIP11: Percentage in Computer and Information Sciences and Support Services
19. PCIP12: Percentage Personal and Culinary Services
20. PCIP13: Percentage Education
21. PCIP14: Percentage of degrees awarded in Engineering
22. PCIP15: Percentage Engineering Technologies and Engineering-Related Fields
23. PCIP16: Percentage Foreign Languages, Literatures, and Linguistics
24. PCIP19: Percentage Family and Consumer Sciences/Human Sciences
25. PCIP22: Percentage Legal Professions and Studies

26. PCIP23: Percentage English Language and Literature/Letters
27. PCIP24: Percentage Liberal Arts and Sciences, General Studies and Humanities
28. PCIP25: Percentage Library Science
29. PCIP26: Percentage Biological and Biomedical Sciences
30. PCIP27: Percentage Mathematics and Statistics
31. PCIP29: Percentage Military Technologies and Applied Sciences
32. PCIP30: Percentage Multi/Interdisciplinary Studies
33. PCIP31: Percentage Parks, Recreation, Leisure, and Fitness Studies
34. PCIP38: Percentage Philosophy and Religious Studies
35. PCIP39: Percentage Theology and Religious Vocations
36. PCIP40: Percentage Physical Sciences
37. PCIP41: Percentage Science Technologies/Technicians
38. PCIP42: Percentage Psychology
39. PCIP43: Pct Homeland Security, Law Enforcement, Firefighting and Related Protective Services
40. PCIP44: Percentage Public Administration and Social Service Professions
41. PCIP45: Percentage Social Sciences
42. PCIP46: Percentage Construction Trades
43. PCIP47: Percentage Mechanic and Repair Technologies/Technicians
44. PCIP48: Percentage Precision Production
45. PCIP49: Percentage Transportation and Materials Moving
46. PCIP50: Percentage Visual and Performing Arts
47. PCIP51: Percentage of degrees awarded in Health Professions and Related Programs
48. PCIP52: Percentage Business, Management, Marketing, and Related Support Services
49. PCIP54: Percentage History
50. ADM_RATE_ALL: Number of admitted undergraduates divided by the number of undergraduates who applied.
51. SATVR25, SATVR75, SATMT25, SATMT75, ACTCM25, ACTCM75:
    The files include the 25th and 75th percentiles of SAT reading (SATVR* for _25 and _75), writing (SATWR* for _25 and _75), math (SATMT* for _25 and _75)
52. COSTT4_A: Average annual cost of attendance includes tuition and fees, books and supplies, and living expenses for all full-time undergraduate.
53. TUITIONFEE_OUT: Tuition + fees, for out-of-state undergraduates.
54. TUITIONFEE_IN:Tuition + fees, for in-state undergraduates.
55. DEBT_MDN: median loan debt accumulated at the institution by all student

borrowers of federal loans who separate (i.e., either graduate or withdraw) in a given fiscal year.

56. PCTFLOAN: The share of undergraduate students who received federal loans.
57. LOAN_COMP_ORIG_YR4_RT: Percent of students who received a federal loan at the institution and who completed in 4 years at original institution
58. HIGHDEG: Highest award identifies the highest award level conferred at the institution.
59. PREDDEG: Predominant undergraduate award identifies the type of award that the institution primarily confers.

APPENDIX B: KEY LINES IN THE CODE

```
df_clean = df_clean[df_clean['UGDS'].notnull()]  #Excludes col-
leges that give no Bachelor's degrees.
df_clean = df_clean[(df_clean['HIGHDEG'] == 'Graduate')]
df_clean = df_clean[df_clean['MD_EARN_WNE_P6']!= 'PrivacySup-
pressed']
df_clean = df_clean[df_clean['MD_EARN_WNE_P6'].notnull()]
df_clean['MD_EARN_WNE_P6'] = df_clean['MD_EARN_WNE_P6'].as-
type(int)
df_clean['MD_EARN_WNE_P6'] = pd.to_numeric(df_clean['MD_EARN_WNE_
P10'], errors='coerce')
# Do above to all variables that need to be converted to numeric
sns.regplot(data = df_clean, x = 'Grad_population', y = 'MD_EARN_
WNE_P6', fit_reg = True, scatter_kws = {'alpha':1, 's': 5})
GBF = (E6_ugds_mean + Grad_slope*1) / E6_ugds_mean
df_clean['Bachelor_MD_EARN_WNE_P6'] = df_clean.MD_EARN_WNE_P6 / (
GBF * df_clean.Grad_population + df_clean.Grad_population)

GTF = (Tuitn_ugds_mean + Grad_tslope) / Tuitn_ugds_mean
print('Graduate Tuition Factor GTF = ', GTF)

#Plot color chart
img = plt.pcolormesh(df_PCIP, cmap=cmap, vmin=0.0002, vmax=0.6)

#Linear Regression with Seaborn
sns.regplot(data = Hi_earn_6[Hi_earn_6.PCIP51>0], x = 'PCIP51', y
= 'Bachelor_MD_EARN_WNE_P6',
            fit_reg = True, scatter_kws = {'alpha':1, 's': 10})
```

APPENDIX C: EXCLUSIVELY GRADUATE OR PROFESSIONAL COLLEGES

Rank	College Name	Earning, $/yr	UGDS	GRADS
1	Philadelphia Coll of Osteopathic Medicine	127400	NaN	2806
2	Western University of Health Sciences	108100	NaN	3842
3	Salus University	100400	NaN	1124
4	Southern College of Optometry	99300	NaN	527
5	A T Still University of Health Sciences	99000	NaN	3226
6	Illinois College of Optometry	96000	NaN	638
7	University of California-San Francisco	95400	NaN	3170
8	Northeast Ohio Medical University	91700	NaN	893
9	Brooklyn Law School	89300	NaN	1141
10	Midwestern University-Glendale	87500	NaN	3146
11	Midwestern University-Downers Grove	87500	NaN	2917
12	U of California-Hastings College of Law	86100	NaN	1003
13	Marshall B Ketchum University	83300	NaN	427
14	Southwestern Law School	74100	NaN	1106
15	New York Law School	72400	NaN	1029
16	New York Medical College	70300	NaN	1482
17	Albany Medical College	68800	NaN	823
18	CUNY School of Law	68500	NaN	325
19	Icahn School of Medicine at Mount Sinai	68400	NaN	1074
20	Rosalind Franklin U of Medicine and S...	68100	NaN	2191
21	California Western School of Law	67400	NaN	781
22	Rensselaer at Hartford	66100	NaN	191
23	WV School of Osteopathic Medicine	65800	NaN	815
24	Weill Cornell Medical College	64800	NaN	1023
25	New England Law-Boston	64600	NaN	871
26	Meharry Medical College	63500	NaN	802
27	U of Massachusetts Medical School Wor...	63500	NaN	1103
28	Albany Law School	61100	NaN	475
29	Mayo Clinic Coll of Medicine and Science	60300	NaN	228
30	Mayo Clinic Grad School of Biomed Sci	60300	NaN	291
31	Teachers College at Columbia University	60000	NaN	5011
32	Brite Divinity School	46900	NaN	196
33	Widener U-Commonwealth Law School	45300	NaN	330
34	Roger Williams University School of Law	42600	NaN	370
35	U of New Hampshire-School of Law	42400	NaN	271
36	New York Chiropractic College	42300	NaN	965
37	Bethel Seminary-San Diego	41100	NaN	176
38	Bethel Seminary-St Paul	41100	NaN	459
39	Penn State University-College of Medicine	40100	NaN	842
40	Penn State University-Penn State Great...	40100	NaN	469

41	Penn State University-Dickinson Law	40100	NaN	153
42	Asbury Theological Seminary	39000	NaN	1470
43	Saint Vincent Seminary	37700	NaN	45
44	LIU Hudson at Rockland	33900	NaN	239
45	LIU Hudson at Westchester	33900	NaN	158
46	Antioch University-New England	33500	NaN	705
47	Trinity Law School	32300	NaN	193
48	Western State Coll of Law at Argosy U	30300	NaN	353
49	Evangel U - Assemblies of God Theolog...	30300	NaN	327
50	University of the D.C.-David A...	29100	NaN	312
51	National American U-Harold D. Bucking...	28200	NaN	358
52	Southern University Law Center	27300	NaN	644

APPENDIX D: DISTRIBUTION OF MEDIAN EARNINGS AT SIX YEARS AFTER ENROLLMENT, FOUR-YEAR COLLEGES ONLY

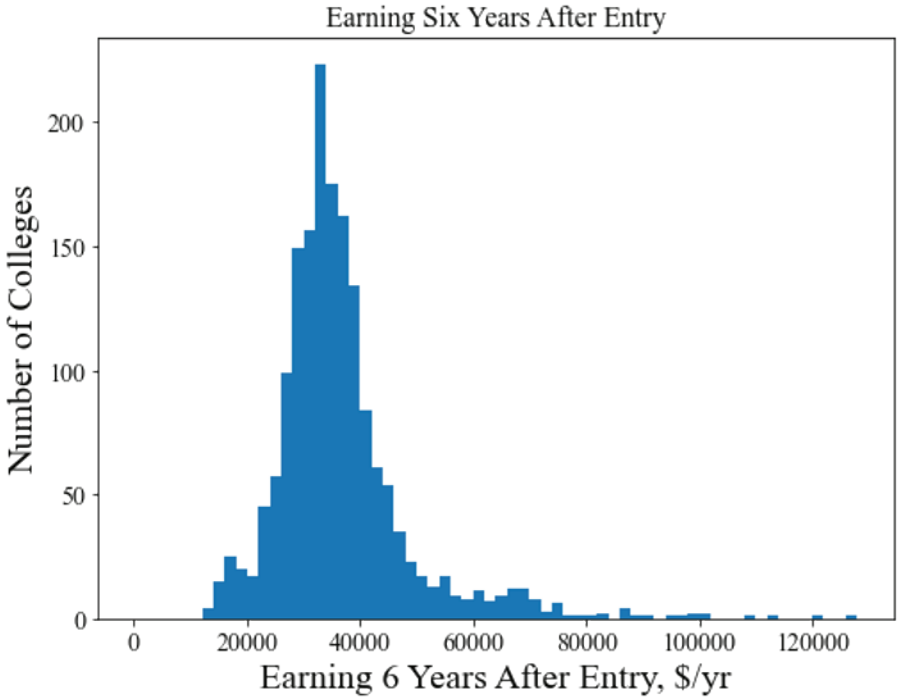

APPENDIX E: BACHELOR'S EARNINGS NOT CORRELATED WITH PROPORTION OF BUSINESS MAJORS.

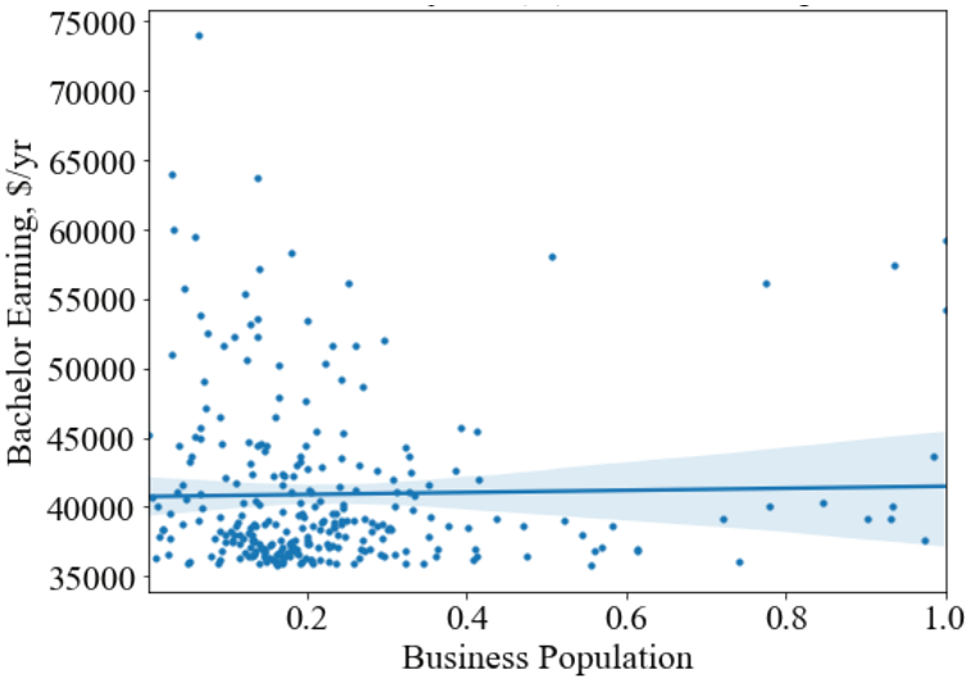

APPENDIX F. DISTRIBUTION OF TUITIONS, NOT ADJUSTED FOR GRADUATE SCHOOL TUITIONS.

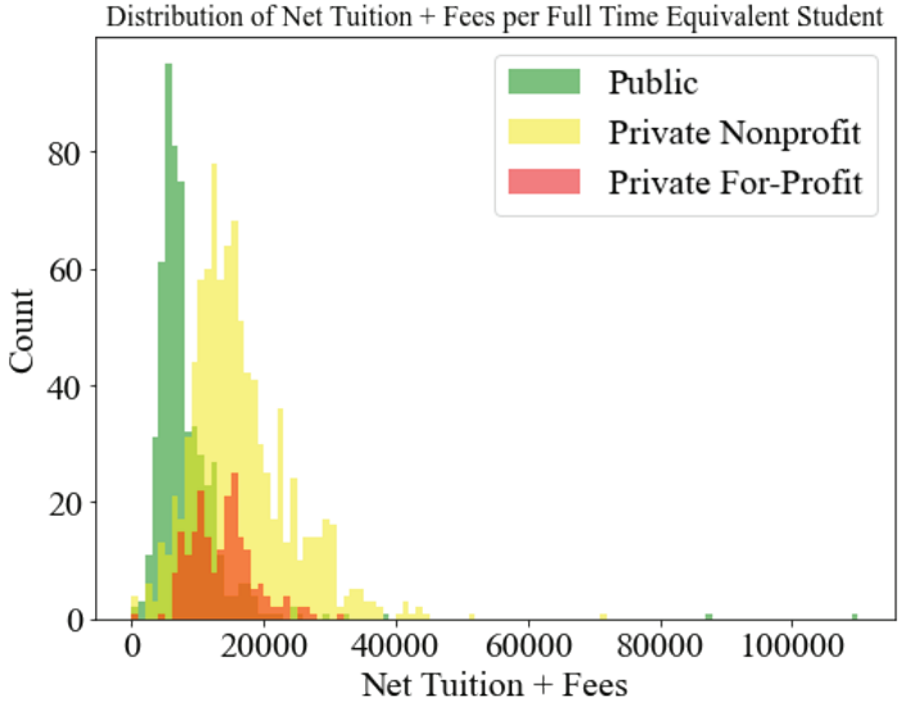

APPENDIX G: ADMISSION COMPETITIVENESS AND DEBTS

Rank	College Name	Bach Earn, $/yr	SAT Math 75%ile	SAT Verbl 75%ile	Admit rate 1/n	Bach Tuit $/yr	Median Debt
1	Albany Coll of Pharmacy and Health Sciences	94170	610	650	1.48	18254	23222
2	St. Louis Coll of Pharmacy	92499	620	710		15554	17500
3	Maine Maritime Academy	73957	550	580	1.27	16350	27000
4	Samuel Merritt University	71471				16267	18750
5	Rose-Hulman Inst of Tech	68730	660	740	1.70	21965	25500
6	West Coast University-L.A Angeles	67954			3.92	23241	25000
7	US Merchant Marine Academy	64295				587	5500
8	Kettering University	63997	650	660	1.40	17555	18976
9	Massachusetts Maritime Academy	63776	570	620	1.62	8224	22050
10	MCPHS University	60040	570	620	1.19	18952	25000
11	MIT	59967	770	800	12.69	17152	13000
12	Colorado School of Mines	59802	680	720	2.74	14513	22000
13	Rensselaer Polytechnic Institute	59528	720	770	2.67	22181	26001
14	Babson College	59166	660	710	3.80	25090	26000
15	Milwaukee School of Eng	58269	580	680	1.46	13768	25000
16	Resurrection University	58127				15362	20000
17	SUNY Maritime College	58038	580	610	1.90	5810	20157
18	Bentley University	57437	640	690	2.17	20489	25821
19	Bucknell University	57123	680	720	3.26	31201	26467
20	Chamberlain University-Illinois	56989			1.51	12589	17294
21	Lehigh University	56184	670	740	2.92	19598	22250
22	Bryant University	56177			1.33	22952	25279
23	Duke University	56059	760	790	8.76	13488	6500
24	Oregon Health & Science University	55842				13304	10939
25	Worcester Polytechnic Institute	55768			2.28	23627	27000
26	Claremont McKenna College	55306	750	770	9.29	29500	11500
27	University of the Sciences	54691	610	650	1.73	15543	26935
28	Thunderbird School of Global Management	54158				33374	8000
29	Oregon Inst of Technology	53881	560	590	1.67	7051	15917

30	Cornell University	53530	740	770	7.05	18007	10912
31	University of Pennsylvania	53417	770	780	9.64	21153	12018
32	Georgia Tech - Main Campus	53210	720	770	3.00	8973	20500
33	Carnegie Mellon University	52525	740	800	4.07	22402	24827

APPENDIX H: CORRELATION BETWEEN EARNING AND COLLEGES' REJECTION RATE

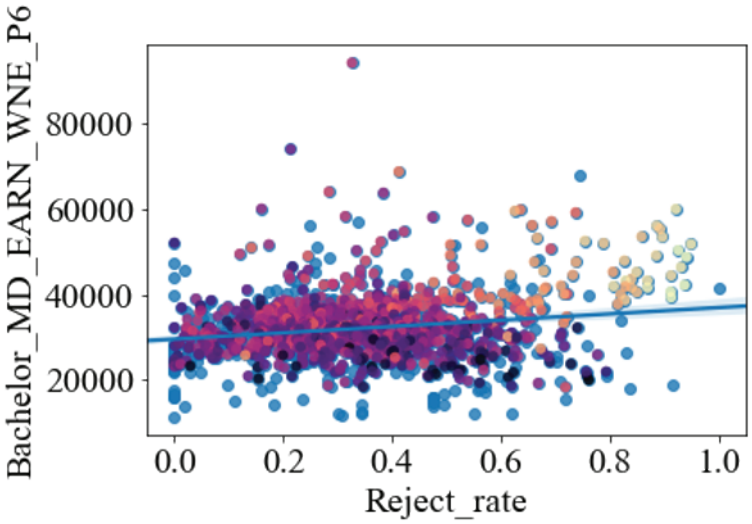

- Lighter dots correspond to higher SAT scores
- About a thousand colleges admit almost 100% of applicants.
- A little over 100 colleges admit 1 in every 2 applicants.
- If you are top 1/10 applicant, then at least 99% of US colleges would admit you.
- Nine schools have admission rates lower than 1/11.
- The lowest admission rate, Stanford admits only 1 student per 19 applicants.

APPENDIX I: GRADUATE POPULATION PROPORTION HAS NO EFFECT ON DEBT

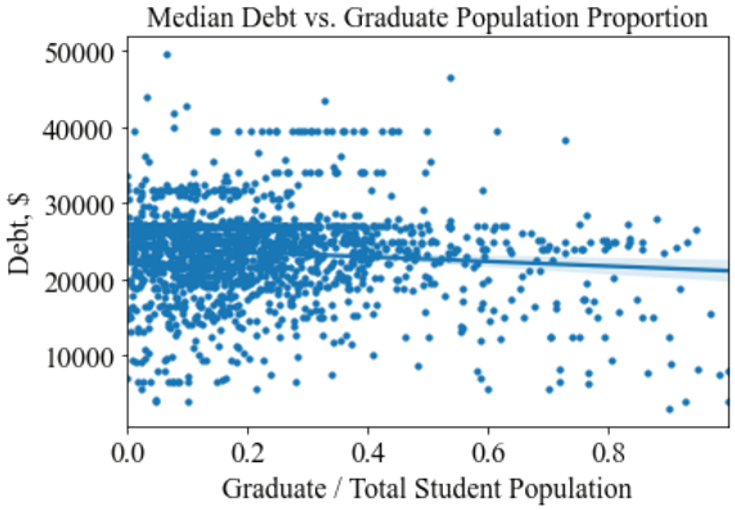


```
Grad_Dslope =  283.2
Debt_ugds_mean =  14821
R =  0.0169
Graduate Debt Factor GDF =  1.02
```

APPENDIX J: HIGHEST-EARNERS-PRODUCING COLLEGES

#	College Name	Bach Earn, $/yr	Largest Field	SAT Total 75%ile	Admit rate 1/n	Bach Tuit $/yr	Median Debt
1	Albany College of Pharmacy and Health Sciences	94170	Health Pro	1260	1.48	18254	23222
2	St. Louis Coll of Pharmacy	92499	Health Pro	1330		15554	17500
3	Maine Maritime Academy	73957	Engineer-ing/CS	1130	1.27	16350	27000
4	Samuel Merritt University	71471	Health Pro			16267	18750
5	Rose-Hulman Inst of Tech	68730	Engineer-ing/CS	1400	1.70	21965	25500
6	West Coast University-L.A Angeles	67954	Health Pro		3.92	23241	25000
7	US Merchant Marine Academy	64295	Engineer-ing/CS			587	5500
8	Kettering University	63997	Engineer-ing/CS	1310	1.40	17555	18976
9	Massachusetts Maritime Academy	63776	Engineer-ing/CS	1190	1.62	8224	22050
10	MCPHS University	60040	Health Pro	1190	1.19	18952	25000
11	MIT	59967	Engineer-ing/CS	1570	12.69	17152	13000
12	Colorado School of Mines	59802	Engineer-ing/CS	1400	2.74	14513	22000

13	Rensselaer Polytechnic Institute	59528	Engineering/CS	1490	2.67	22181	26001
14	Babson College	59166	Business	1370	3.80	25090	26000
15	Milwaukee School of Engineering	58269	Engineering/CS	1260	1.46	13768	25000
16	Resurrection University	58127	Health Pro			15362	20000
17	SUNY Maritime College	58038	Business	1190	1.90	5810	20157
18	Bentley University	57437	Business	1330	2.17	20489	25821
19	Bucknell University	57123	Social Sci	1400	3.26	31201	26467
20	Chamberlain University-Illinois	56989	Health Pro		1.51	12589	17294
21	Lehigh University	56184	Engineering/CS	1410	2.92	19598	22250
22	Bryant University	56177	Business		1.33	22952	25279
23	Duke University	56059	Social Sci	1550	8.76	13488	6500
24	Oregon Health & Science University	55842	Health Pro			13304	10939
25	Worcester Polytechnic Institute	55768	Engineering/CS		2.28	23627	27000
26	Claremont McKenna College	55306	Social Sci	1520	9.29	29500	11500
27	University of the Sciences	54691	Health Pro	1260	1.73	15543	26935
28	Thunderbird School of Global Management	54158	Business			33374	8000
29	Oregon Inst of Technology	53881	Health Pro	1150	1.67	7051	15917
30	Cornell University	53530	Engineering/CS	1510	7.05	18007	10912
31	University of Pennsylvania	53417	Business	1550	9.64	21153	12018
32	Georgia Tech - Main Campus	53210	Engineering/CS	1490	3.00	8973	20500
33	Carnegie Mellon University	52525	Engineering/CS	1540	4.07	22402	24827

APPENDIX K: HIGHEST-EARNERS-PRODUCING GRADUATE SCHOOLS FOR 75TH PERCENTILE EARNERS 10 YEARS AFTER UNDERGRADUATE ENTRY

#	INSTNM	EARN 75_P10	TUITFTE	Adm rate 1/n	EngCS Tech Prop
1	Harvard University	166800	30239	16.8	0.09
2	MIT	164900	28992	12.7	0.62
3	Stanford University	164000	24668	19.6	0.29
4	Yale University	153300	15008	15.9	0.08
5	University of Pennsylvania	151600	34560	9.6	0.13
6	Maine Maritime Academy	150200	16862	1.3	0.69
7	California Institute of Technology	142400	16533	11.3	0.54
8	Columbia U in the City of New York	137600	33371	14.4	0.21
9	Dartmouth College	136800	29358	8.7	0.13
10	Duke University	134500	22556	8.8	0.17
11	Princeton University	132100	13255	13.4	0.20
12	Carnegie Mellon University	125400	36119	4.1	0.38
13	Massachusetts Maritime Academy	124300	8830	1.6	0.57
14	Cornell University	120500	25066	7.0	0.22
15	Tufts University	119000	29681	5.8	0.14
16	Colorado School of Mines	118300	18760	2.7	0.91
17	University of Notre Dame	118300	22629	4.7	0.15
18	Cali State Univ Maritime Academy	117400	7649	1.5	0.55
19	University of the Pacific	116500	30355	1.8	0.15
20	DigiPen Institute of Technology	115000	20838	1.5	0.60
21	University of Southern California	113200	30675	5.5	0.12
22	Lehigh University	112600	26103	2.9	0.38
23	SUNY Maritime College	110300	6399	1.9	0.41
24	Northwestern University	109800	28395	7.6	0.16
25	Case Western Reserve University	109600	22634	2.6	0.36


NMAS
NEW MEXICO
ACADEMY OF SCIENCE